

Borane-Catalyzed Double Sila-Friedel-Crafts Reaction for the Synthesis of Silacycles

董, 亜芳

<https://hdl.handle.net/2324/4772311>

出版情報 : Kyushu University, 2021, 博士 (理学), 課程博士
バージョン :
権利関係 :

**Borane-Catalyzed Double Sila-Friedel–Crafts Reaction
for the Synthesis of Silacycles**

By
Yafang Dong

A dissertation submitted to the graduate faculty
for the degree of
DOCTOR OF PHILOSOPHY

Major: Organic Chemistry
Program of Study Committee:
Interdisciplinary Graduate School of Engineering Sciences
Institute for Materials Chemistry and Engineering

Supervisor:
Prof. Dr. Yoichiro Kuninobu

Kyushu University
Yafang Dong
2021/08

CONTENTS

ABSTRACT	1
Chapter 1 Introduction of C(sp ²)-H Silylation and Its Application.....	5
1.1 Transition Metal-Catalyzed Silylation of C-H Bonds	6
1.2 Sila-Friedel-Crafts Reaction.....	13
1.3 Applications of C-H Silylation	22
1.4 Silacyclic Compounds.....	26
1.5 Purpose, Importance, and Design of My Researches	29
Chapter 2 Lewis Acid-Catalyzed Synthesis of Silafluorene Derivatives from Biphenyls and Dihydrosilanes via a Double Sila-Friedel-Crafts Reaction	31
2.1 Introduction.....	31
2.2 Results and Discussion.....	37
2.3 Conclusion	49
2.4 Experimental Section.....	50
Chapter 3 Synthesis of Six-membered Silacycles by Borane-Catalyzed Double Sila-Friedel- Crafts Reaction	69
3.1 Introduction	69
3.2 Results and Discussion	73
3.3 Conclusion.....	79
3.4 Experimental Section.....	80
Chapter 4 Facile Synthesis of Tribenzosilolepins from Terphenyls and Dihydrosilanes by Double Sila-Friedel-Crafts Reaction	87
4.1 Introduction	87
4.2 Results and Discussion	90
4.3 Conclusion.....	102
4.4 Experimental Section.....	103

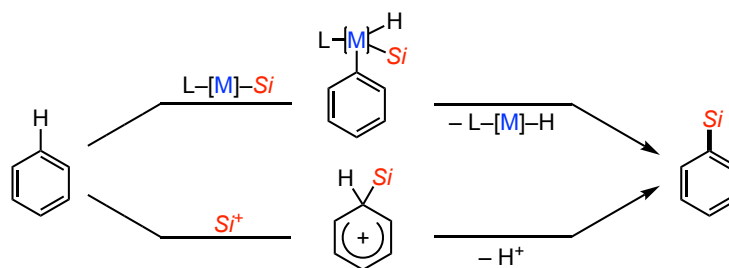
Chapter 5 Conclusion	113
Supporting Information	117
References	161
Publication List	169
Acknowledgments	171

ABSTRACT

This dissertation focuses on the investigation of sila-Friedel–Crafts reaction for the synthesis of silacyclic compounds. The direct synthesis of silacycles is challenging because it generally relies upon the lithiation of the corresponding dihalogenated substrates and sequential reaction of the dilithiated intermediates with dichlorosilanes. However, these reactions have some problems, such as the waste of stoichiometric reagents, the tolerance of functional groups, and the difficulty in the synthesis of multi-substituted starting materials. Hence, the efficient and versatile synthetic methods of silacyclic compounds are still desirable.

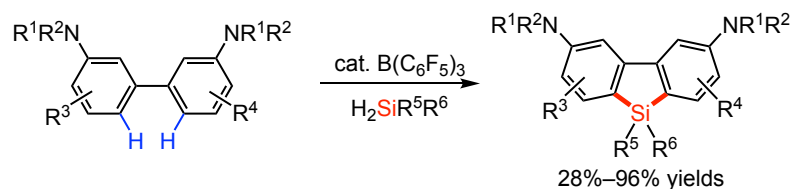
Recently, Kuninobu and other research groups reported iridium- or rhodium-catalyzed intramolecular C–H silylations for the synthesis of silafluorenes, phenazasilines, and silepins. The intra- and intermolecular sila-Friedel–Crafts reaction is appearing as an efficient tool to construct C–Si bonds. Inspired by the intermolecular sila-Friedel–Crafts reaction of aniline derivatives with hydrosilanes, I envisioned that double sila-Friedel–Crafts reactions between biphenyls/biaryl derivatives/terphenyls and dihydrosilanes are ideal and efficient synthetic methods of highly substituted silacyclic compounds.

In Chapter 1, C(sp²)–H silylation for organosilanes and its applications to the synthesis of π -conjugated molecules is introduced. Here, I briefly survey the progress of research activities regarding transition metal-catalyzed C(sp²)–H silylation and sila-Friedel–Crafts reactions.

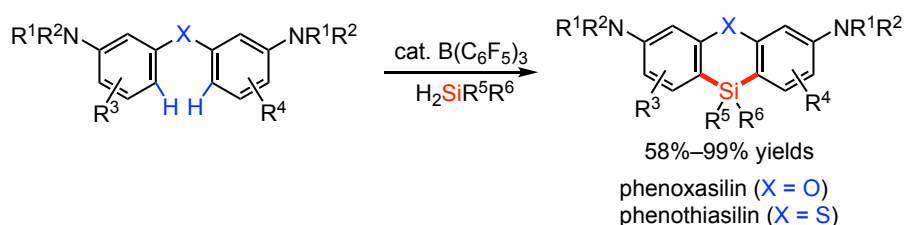


Chapter 2 describes the silafluorene synthesis from amino-substituted biphenyls and dihydrosilanes through a borane-catalyzed double sila-Friedel–Crafts reaction. This reaction system is suitable for the synthesis of multisubstituted silafluorenes, spirozilabifluorenes, and

silicon-bridged terphenyl compounds, which are not readily obtained using traditional synthetic methods. Besides, the transformation of the amino groups in those silafluorene derivatives into other substituents was achieved by the cross-coupling reaction between ammonium salts and Grignard reagents.

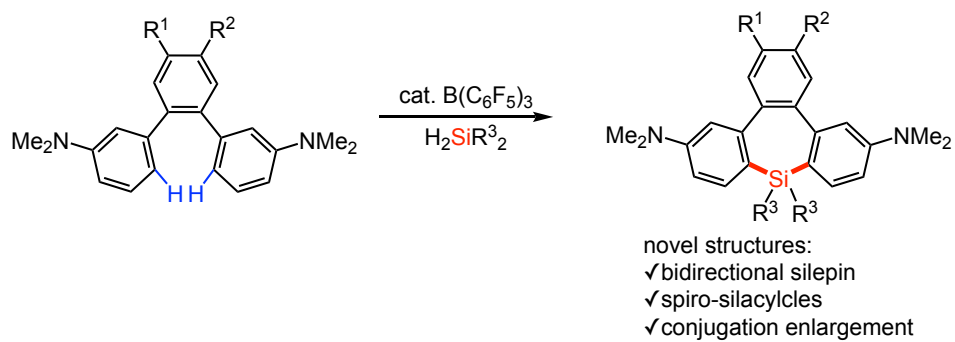


In Chapter 3, the synthesis of six-membered silacycles, including phenoxasilin and phenothiasilin derivatives is detailed. The borane-catalyzed double sila-Friedel–Crafts reaction of amino group-containing diaryl ethers and dihydrosilanes afforded phenoxasilin derivatives with moderate to excellent yields. Diaryl thioethers was also converted to the corresponding six-membered silacyclic products under the optimal conditions. In addition, the gram-scale synthesis of a selected phenoxasilin and the conversions of amino groups were investigated.



Chapter 4 focuses on the synthesis of seven-membered silacycles, tribenzosilepin derivatives. During the investigation for the synthesis of a silafluorene derivative using a terphenyl substrate, the corresponding tribenzosilepin was obtained in 87% yield. The optimal reaction system was applied to the synthesis of other silepin derivatives with different substituents on the center benzene ring or using other hydrosilane reagents, such as dimethylamino-, difluoro-, naphthalene backbone-containing silepin and 5-silaspiro[4.6]silepin. Besides, a bidirectional reaction forms bissilepin compound. The transformation of the amino groups in tribenzosilepin

derivatives to aryl groups and the enlargement of the π -system in tribenzosilepin were realized. The optical properties of some selected tribenzosilepin derivatives were investigated by UV/Vis absorption and photoluminescence spectroscopy.



Chapter 1

Introduction of C(sp²)-H Silylation and Its Application

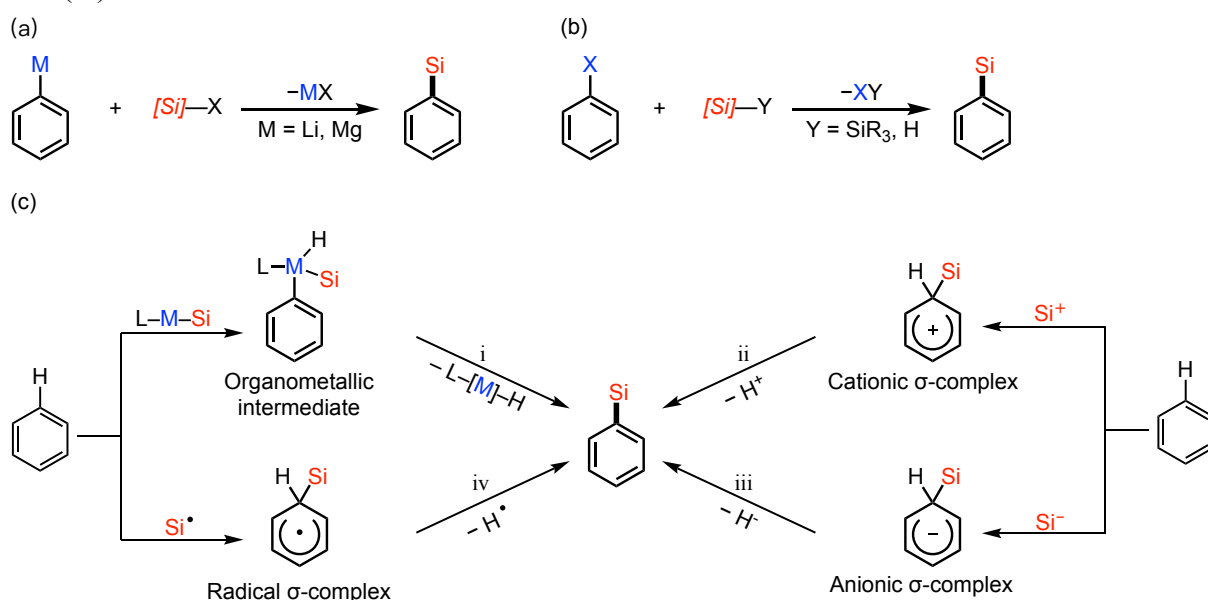
Silicon-containing molecules are of great research interests with extensive applications in several research areas, such as materials science, medicinal chemistry, and complex molecule synthesis. C-Si bond formation by direct C-H functionalization is a modern synthetic approach towards the synthesis of valuable compounds. C-H functionalization offers a high step and atom economy in contrast to conventional procedures using reaction partners, which are prefunctionalized, at least, once. In this chapter, I briefly survey the progress of research activities regarding silylation of C(sp²)-H bonds, especially transition metal-catalyzed silylation and sila-Friedel-Crafts reactions.

Traditional C-Si bond formation often relies on prefunctionalized substrates and typically employs organometallic reagents, such as Grignard and organolithium reagents, as nucleophiles and silicon halides or alkoxides as electrophiles (Scheme 1.1a).^[1] The limitations of this method are multi-steps synthesis of substrates and the incompatibility of Grignard and organolithium reagents with functional groups, such as carboxyl, hydroxyl, sulfhydryl, amine, and amide groups. Meanwhile, considerable amounts of wastes are produced during the prefunctionalization and C-Si bond formation. Besides, the transition metal complex-catalyzed cross-coupling reactions between organohalide reagents and hydrosilanes give organosilanes (Scheme 1.1b).^[2] Even though it is possible to get rid of the incompatibility of Grignard and organolithium reagents with functional groups, this approach still requires the prefunctionalization, and the regioselectivity of silylation is determined by the halogenation step.

Hence, the direct and regioselective silylation of C-H bonds for the synthesis of organosilanes is fascinating as it can convert C-H bonds into the corresponding C-Si bonds without requirement of the prefunctionalization of substrates. In 1982, the first example of C-H silylation (unselective silylation of neat benzene accompanied by silane redistribution) was reported by Curtis and Epstein.^[3] Over the years, significant efforts have been made to address

this synthetic challenge (Scheme 1.1c). The resulting strategies can be categorized into four fundamentally different reaction classes: (i) Transition metal-catalyzed C–H silylation, (ii) electrophilic aromatic substitution ($S_{\text{E}}\text{Ar}$), (iii) nucleophilic substitution, and (iv) homolytic aromatic substitution ($S_{\text{H}}\text{Ar}$). Here I describe transition metal-catalyzed C–H silylation and sila-Friedel–Crafts reactions, which are related to Chapters 2–4.

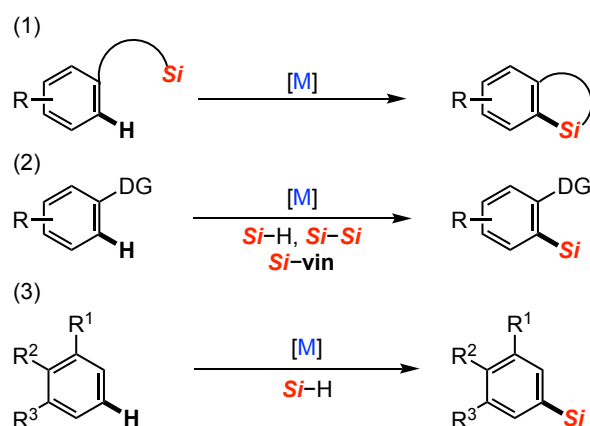
Scheme 1.1. Methods for the synthesis of organosilicon compounds. (a) Traditional synthesis of organosilanes using prefunctionalized substrates. (b) Transition metal-catalyzed cross-coupling reactions. (c) Synthesis of organosilanes by direct C–H silylation: (i) transition metal-catalyzed C–H silylation, (ii) electrophilic aromatic substitution, (iii) nucleophilic substitution, and (iv) radical aromatic substitution.



1.1 Transition Metal-Catalyzed Silylation of C–H Bonds

During the past few decades, great success has been achieved in the field of direct C–H bond silylation catalyzed by transition metals. Various transition metal compounds, such as iridium, ruthenium, and rhodium complexes, can be used as catalysts for C–H silylation. As introduced in the review by Hartwig,^[4] examples of transition metal-catalyzed C–H silylation can be divided into three classes: (1) Intramolecular, (2) directed intermolecular, and (3) undirected intermolecular manners (Scheme 1.2).

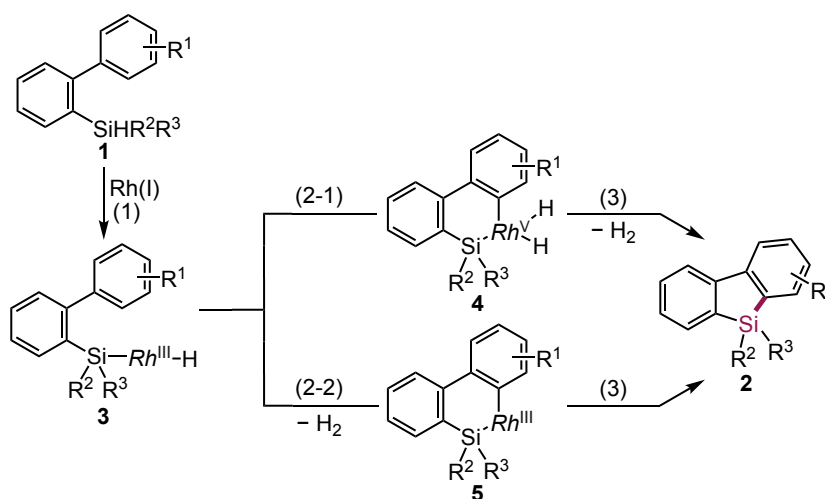
Scheme 1.2. Transition metal-catalyzed C–H silylation reactions.



1.1.1 Intramolecular C–H Silylation

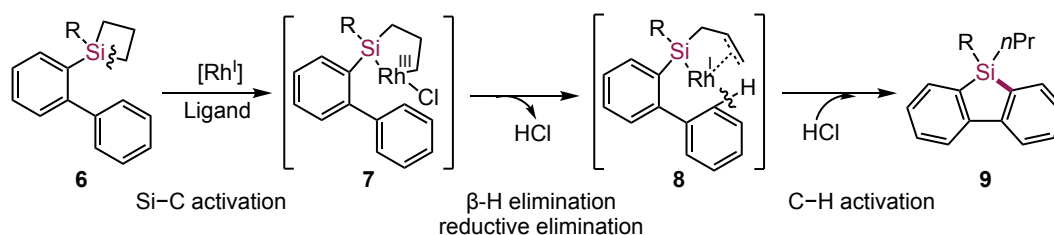
Kuninobu and co-workers reported a rhodium-catalyzed intramolecular silylation via the cleavage of Si–H and C–H bonds of biphenylhydrosilanes **1** for the synthesis of silafluorene derivatives **2** (Scheme 1.3).^[5] The reaction proceeds via (1) Si–H bond activation by oxidative addition of a hydrosilane to the metal center (intermediate **3**); (2-1) sequential oxidative addition (intermediate **4**); or (2-2) σ -bond metathesis (intermediate **5**), and (3) formation of silafluorenes **2** from the intermediates (**4** and/or **5**) by reductive elimination.

Scheme 1.3. Rhodium-catalyzed intramolecular silylation via cleavage of Si–H and C–H bonds.



Sequential C–Si/C–H bond activation of silacyclobutanes **6** under Rh^I catalysis afforded a series of silafluorenes **9** in high yields and with high regioselectivities.^[6] The proposed catalytic cycle involves an endocyclic β-hydride elimination of five-membered metallacycles **7** and reductive elimination to give Si–Rh^I species **8**, which is capable of C–H activation and successive reductive elimination to produce silafluorenes **9** (Scheme 1.4).

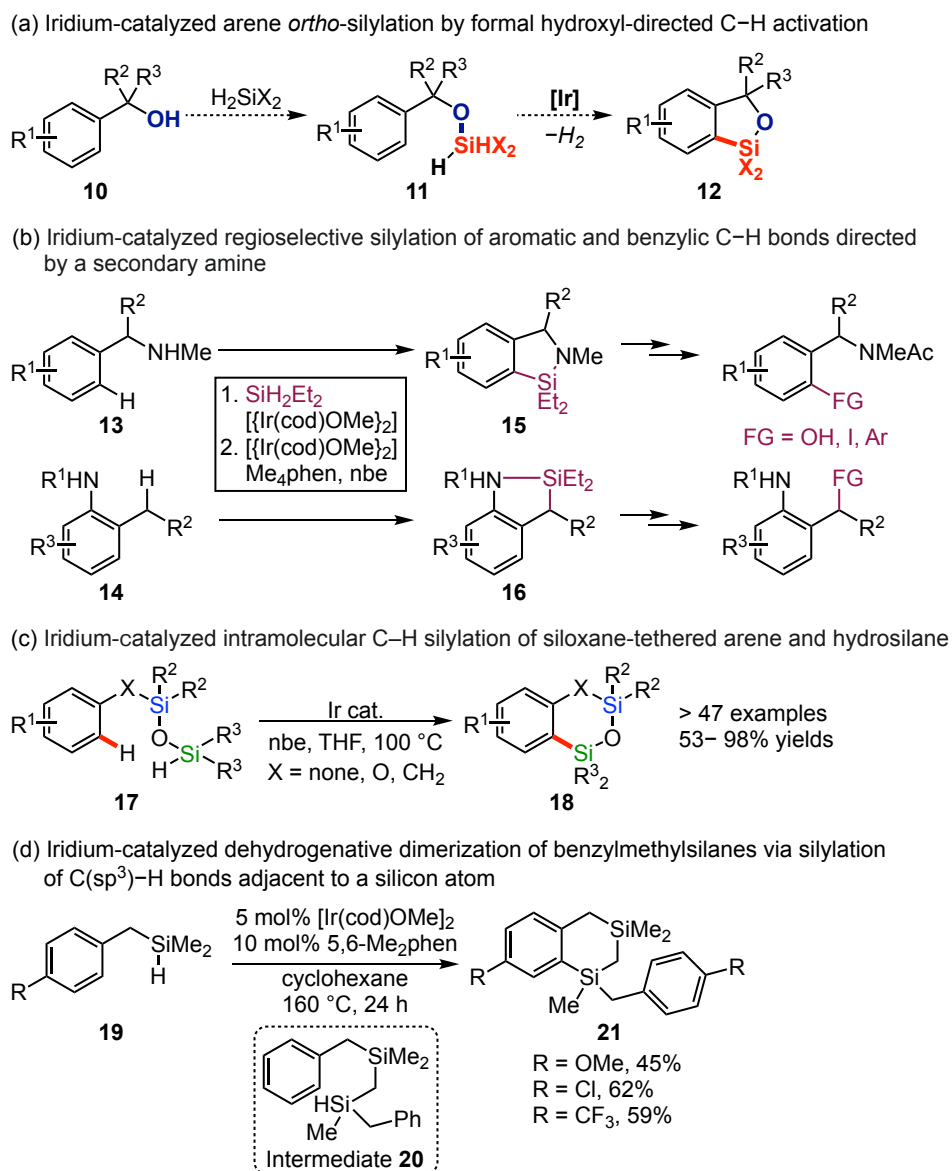
Scheme 1.4. Rhodium-catalyzed intramolecular C–H silylation via the cleavage of C–Si bond of silacyclobutanes.



Intramolecular C–H silylation of arenes with hydrosilanes afforded the corresponding silacyclic compounds. This strategy, however, requires tethering a suitable hydrosilyl group to the arene substrates. Silylation of alcohols **10** (Scheme 1.5a),^[7] amines **13** and **14** (Scheme 1.5b),^[8] and silanols **17** (Scheme 1.5c),^[9] or hydrosilylation of carbonyl groups^[7] achieved by Si–C or Si–heteroatom bond formation, which give silane-tethered arenes **11** and **17** including one free Si–H bond (Scheme 1.5). The following Si–H/C–H dehydrogenative silylation proceeds through a cyclometalated intermediate, furnished the C–Si bond in the products **12**, **15**, **16**, and **18**. Those method can avoid undesirable double silylation.

Regarding the above-reactions, the iridium-catalyzed dehydrogenative dimerization of benzylmethylsilanes **19** via site-selective silylation of two different types of C–H bonds: selective C(sp³)–H bond of the methyl group forms hydrosilane **20** and *ortho*-C(sp²)–H bond activation of the benzyl group convert **20** into disilane **21** (Scheme 1.5d).^[10] The α-effect of the silicon atom is the key to controlling the reactivity and selectivity of C–H bond activation.

Scheme 1.5. Intramolecular silylation of aryl C–H bonds in benzyl silyl ethers, amines, and silanols.

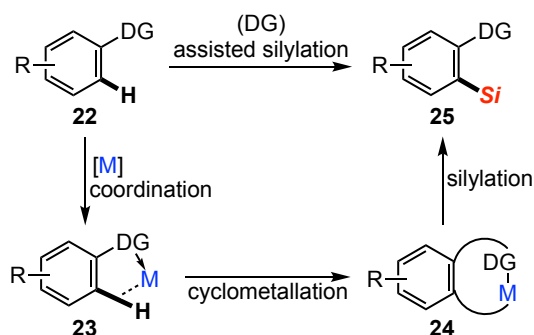


1.1.2 Intermolecular C–H Silylation

The C–H silylation assisted by a directing group can be faster than undirected reactions and can occur with high regioselectivity. C–H bond activation by the coordination of a directing group of **22** to a metal catalyst forms cyclometalated species **24** (Scheme 1.6). This directed silylation of C–H bonds produce only *ortho*-functionalized products **25** with excellent regioselectivity. When two *ortho*-C–H bonds exist, C–H silylation can occur at both *ortho*-positions. A wide variety of directing groups have been developed for C(sp²)–H silylation: that

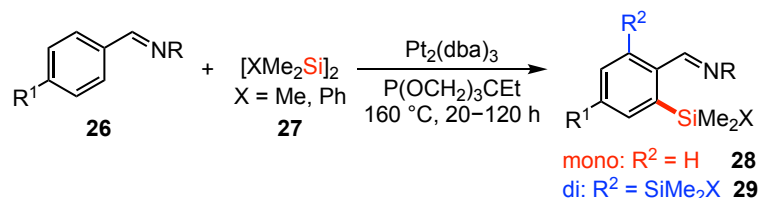
is, imino,^[11] amide,^[12] ester,^[12a,13] ketone,^[12a] and amino,^[14] and even the unusual alkoxy^[15] groups have been used as directing groups for C–H silylation.

Scheme 1.6. Directing group-assisted intermolecular silylation.



The first directed C–H silylation of aromatic imines **26** catalyzed by the combination of $\text{Pt}_2(\text{dba})_3$ and $\text{P}(\text{OCH}_2)_3\text{CEt}$ using the imino group as the directing group and disilanes **27** as the silicon source produced mixtures of mono- and di-silylated products **28** and **29** (Scheme 1.7).^[11a]

Scheme 1.7. Imine-directed C–H silylation of arenes.



The ruthenium-catalyzed *ortho*-C–H silylation of arylboronic acids **30** modified to contain 2-pyrazol-5-ylaniline **31** as the directing group.^[16] The key feature of the directing group is the ease of its installation and removal (Scheme 1.8a). 2-Pyrazol-5-ylaniline **31** can be easily attached to boron atom via condensation with boronic acid **30**. The silylation of the formed product **32** with triethylhydrosilane affords the *o*-silylation product **33**. The detachment of the directing group can be realized by the treatment of the reaction mixture with pinacol and TsOH.

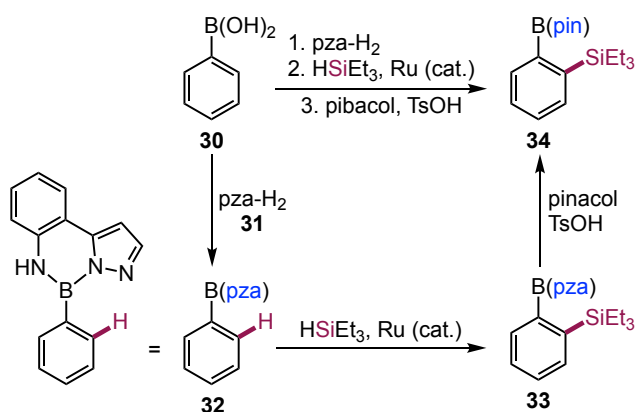
The half-sandwich scandium alkyl complexes catalyzed *ortho*-selective C–H silylation of various alkoxy-substituted aromatic compounds **35** without the requirement of a hydrogen

acceptor to achieve high conversion (Scheme 1.8b).^[15] This scandium-based *ortho*-selective silylation is mainly due to the oxophilicity of early transition metals. The *ortho*-C–H bond activation of alkoxy compound through assistance of the interaction between the alkoxy group and the Sc atom affording the 2-anisyl complex with release of H₂. The σ -bond metathesis reaction between the complex and phenylsilane would yield the silylated product **36**. The coordination of the alkoxy group to the metal center could be the rate-determining step of this catalytic process.

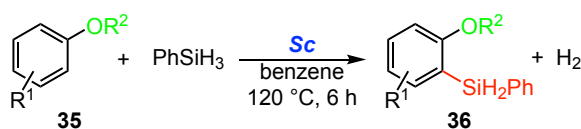
An ruthenium(II)-catalyzed intermolecular *ortho*-selective C–H silylation of 2-aryloxazoles **37** was also reported (Scheme 1.8c).^[17] For Ru(II)–OAc-catalytic C–H bond activation, the use of OAc[−] as the co-catalyst to the Ru center promoted the cleavage of the *ortho*-C–H bond to afford the *o*-silylated oxazoles **38**.

Scheme 1.8. Transition metal-catalyzed intermolecular C–H silylation assisted by directing groups.

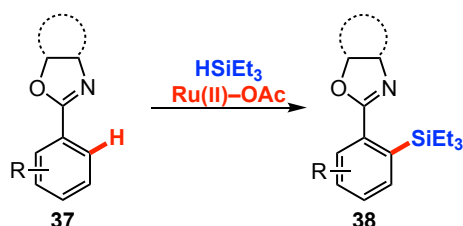
(a) *ortho*-silylation of arylboronic acids directed by a temporary directing group



(b) Sc-catalyzed silylation of aryl C–H bonds

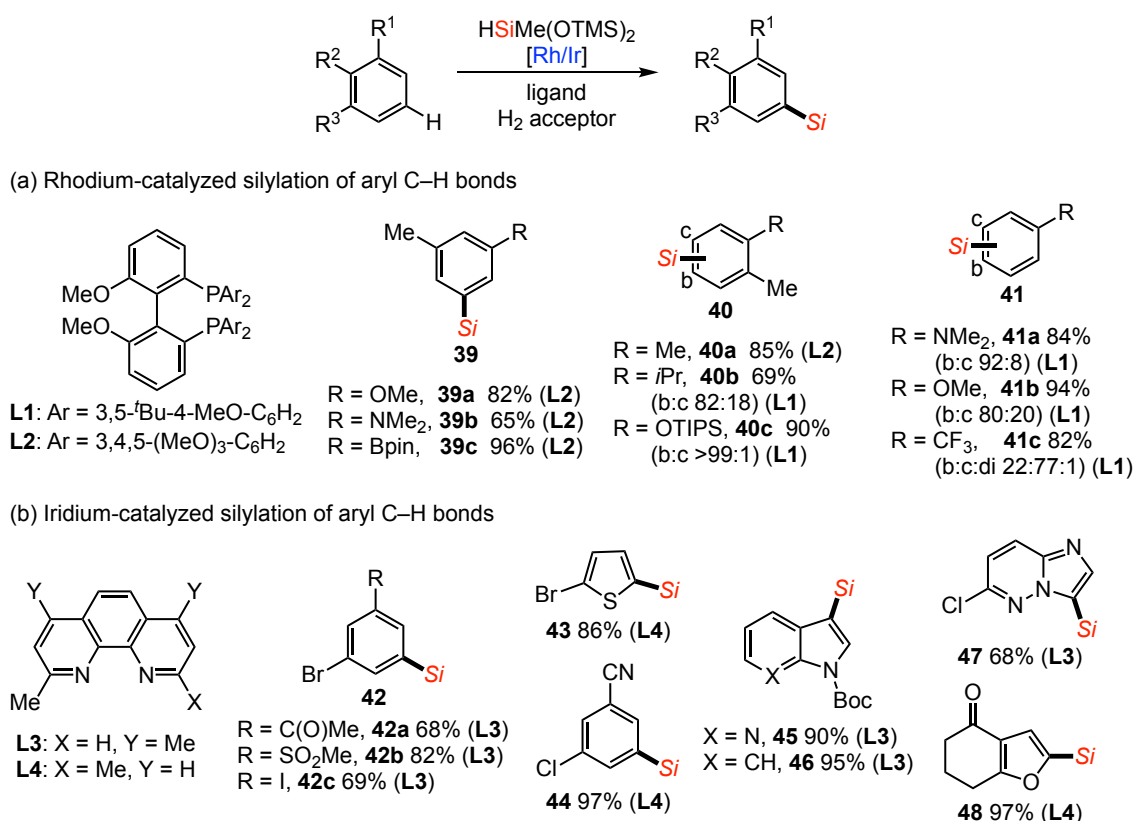


(c) Ru(II) catalyzed synthesis of silylated oxazoles via C–H silylation and dehalogenation



Transition metal-catalyzed intermolecular C–H silylation assisted by directing groups is predominant with *ortho*-positions. However, the *meta*-^[18] and even *para*-^[19] positions were also disclosed. The designed elongated tether enables cyclometalation at the remote reaction sites. Without directing groups, rhodium-catalyzed intermolecular C–H silylation of unactivated arenes that manifests very high regioselectivity through the steric effects of substituents *meta* to the potential reaction sites (Scheme 1.9a).^[20] Iridium-catalyzed intermolecular C–H silylation of arenes, which are the limiting substrates, exhibited high regioselectivity controlled by the steric effect (Scheme 1.9b).^[21] Compared to the rhodium-catalyzed silylation of an aryl C–H bond, the iridium-catalyzed C–H silylation proceeded using a variety of heteroarenes and showed a much broader functional group tolerance. However, the reaction requires higher temperatures than the rhodium-catalyzed C–H silylation, and the regioselectivities of the reactions were low in the case of unsymmetrical 1,2-disubstituted arenes.

Scheme 1.9. Intermolecular C–H silylation of arenes without directing groups.

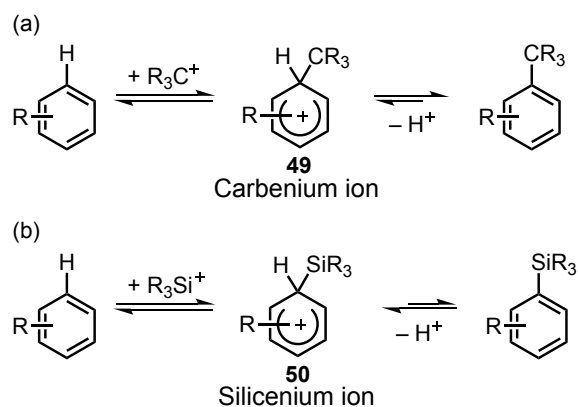


The silylation of C(sp²)–H bonds adjacent to a heteroatom, such as boron, nitrogen, sulfur, or oxygen atom, were also reported.^[22] So far great success has been achieved in the silylation of C–H bonds under transition metal catalysis. Various transition metals, such as Ir, Ru, Rh, and Pt, have been used as catalysts for C–H silylation. The reaction efficiency has been greatly improved in terms of the substrate diversity, reaction temperature, reaction time, stoichiometry of arenes and the regioselectivity of the C–H silylation.

1.2 Sila-Friedel–Crafts Reaction

Electrophilic aromatic substitution is an efficient way for silylation of C–H bonds, which proceeds via the formation of cationic σ -complexes **49** and **50** (Wheland intermediates), which are rearomatized by proton release. Similar with Friedel–Crafts alkylation, the difficulty of this reaction lies in the reversibility (Scheme 1.10).^[23] In the case of Friedel–Crafts silylation, the silicenium ion **50** is substantially stabilized by a pronounced β -silicon effect, thereby facilitating proton capture at the *ipso*-position of arylsilanes (Scheme 1.10b).

Scheme 1.10. Reversibility of Friedel–Crafts alkylation and silylation.

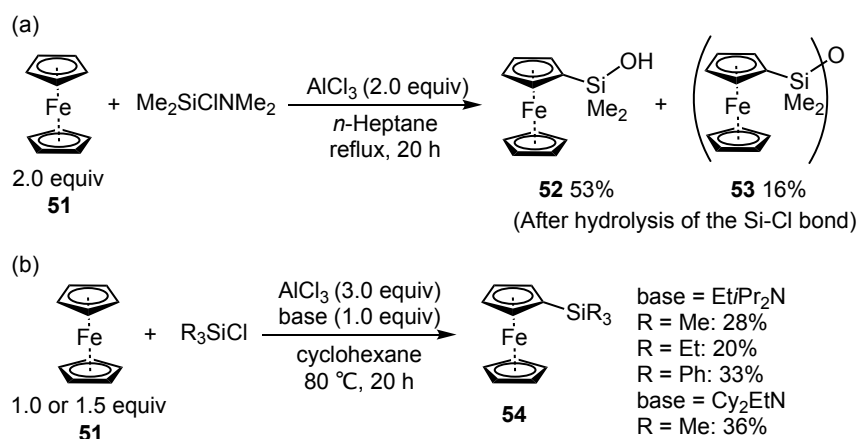


1.2.1 Stoichiometric Sila-Friedel–Crafts Reaction

Early sila-Friedel–Crafts reactions were based on the traditional procedures for Friedel–Crafts alkylation. In these reactions, chlorosilanes have been used as the silylation reagents together with strong main-group Lewis acids as promoters (Scheme 1.11a).^[24] In sila-Friedel–Crafts reactions, proton must be effectively removed from the reaction mixture to suppress the

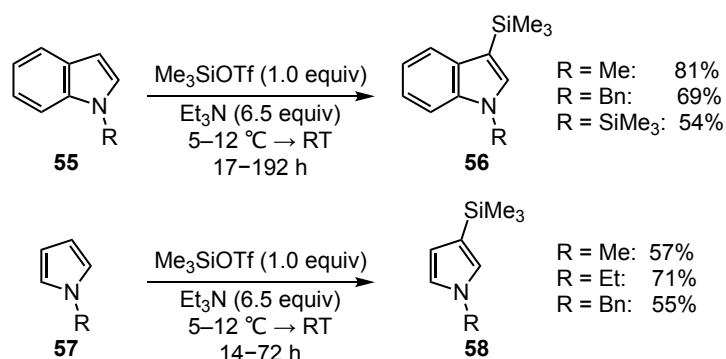
backward reaction and shift the equilibrium to the product side. An apparent solution to solve the problem is the addition of an excess amount of a base. With nucleophilic benzenoids ferrocene **51**, Olah and co-workers accomplished the sila-Friedel–Crafts reaction with AlCl_3 as an activating reagent, but the yields of silylated products **54** were low, and stoichiometric amount of a base was needed to suppress protodesilylation (Scheme 1.11b).^[25]

Scheme 1.11. Sila-Friedel–Crafts reactions of ferrocene with silicon electrophiles.



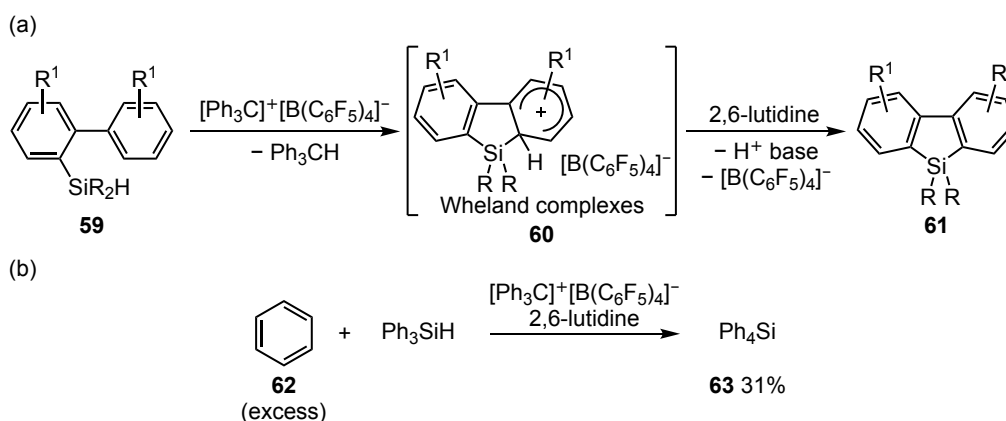
By using other electron-rich heteroarenes, such as indoles **55** and pyrroles **57** as nucleophiles, Simchen and Frick achieved sila-Friedel–Crafts reactions with a neutral silicon electrophile (Me_3SiOTf). The reverse reaction was also avoided by the addition of an excess amount of Et_3N as the proton-trapping base (Scheme 1.12).^[26]

Scheme 1.12. Sila-Friedel–Crafts reaction of indoles and pyrroles with a neutral silicon electrophile.



The intramolecular sila-Friedel–Crafts reaction was achieved by Kawashima and coworkers a few decades later. In this reaction, they used biphenyl hydrosilanes **59** as substrates, $[\text{Ph}_3\text{C}]^+[\text{B}(\text{C}_6\text{F}_5)_4]^-$ as a hydride abstraction reagent, and 2,6-lutidine as a base, to afford dibenzosiloles **61** in excellent yields (Scheme 1.13).^[27] They also extended this reaction to an intermolecular reaction with benzene **62** and triphenylsilane, which gave the corresponding tetraphenylsilane **63** in 31% yield.

Scheme 1.13. (a) Intramolecular Friedel–Crafts silylation of a dimethyl-substituted hydrosilane; (b) intermolecular reaction of benzene with triphenylsilane.



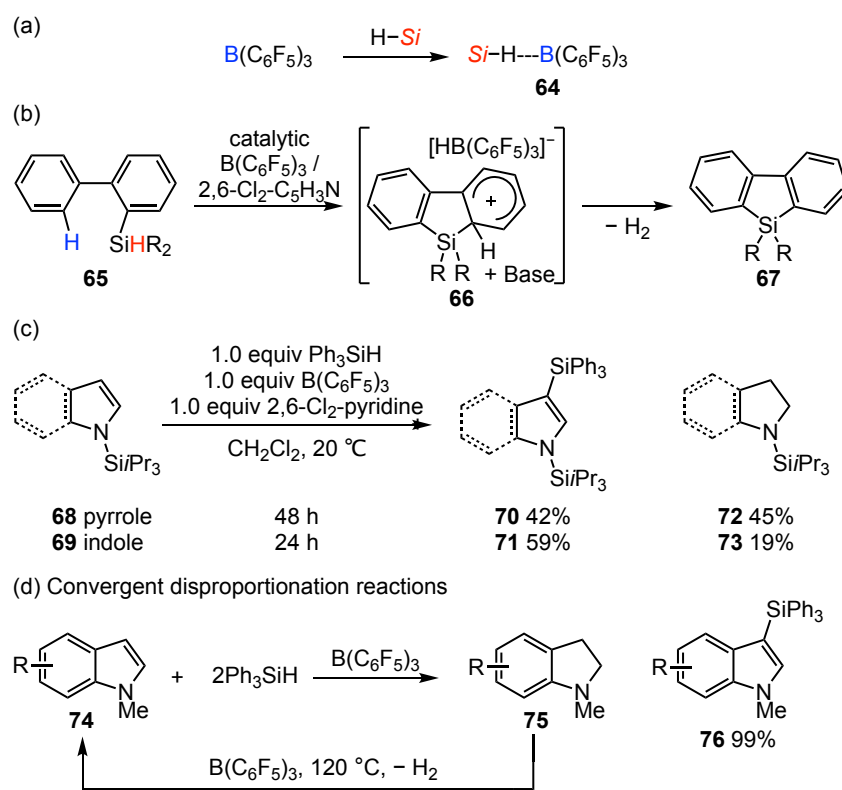
In the above-mentioned sila-Friedel–Crafts reactions, several kinds of bases are used for proton removal from the reaction mixture to suppress the reverse reaction. However, the resulting acid–base adduct might be still too acidic to prevent the product decomposition. Key to success for recent methodologies is the conversion of proton into dihydrogen gas, which irreversibly escapes from the reaction mixture.

1.2.2 Catalytic Sila-Friedel–Crafts Reaction

Tris(pentafluorophenyl)borane ($\text{B}(\text{C}_6\text{F}_5)_3$) is a convenient and commercially available Lewis acid with a comparable strength to BF_3 , but without the problem associated with reactive B–F bonds.^[28] $\text{B}(\text{C}_6\text{F}_5)_3$ activates H–SiR₃ via the formation of a weak adduct **64** (Scheme 1.14a).^[29] The adduct **64** enhanced the electrophilicity of the silicon atom, promoting the nucleophilic attack of the aromatic substrates. A reaction of $\text{B}(\text{C}_6\text{F}_5)_3$ -activated hydrosilanes with

heteroarenes **65** by the sila-Friedel–Crafts reaction was achieved firstly by Ingleson’s group (Scheme 1.14b).^[30] In the presence of $B(C_6F_5)_3$, the dehydrosilylation of heteroarenes favored by the addition of a weak base, produced H_2 as a byproduct. However, the generation of H_2 from dehydrosilylation also permits the potentially competitive frustrated Lewis pair (FLP) mediated hydrogenation as an additional reaction pathway (Scheme 1.14c). Electrophilic silylation of 5-membered *N*-heterocycles **68** and **69**, such as pyrroles and indoles, in the presence of $B(C_6F_5)_3/R_3SiH$ occurred at the C3-position in moderate yields. The competing hydrogenation proceeded to give **72** and **73**, with no hydrosilylation was observed in either case.^[31]

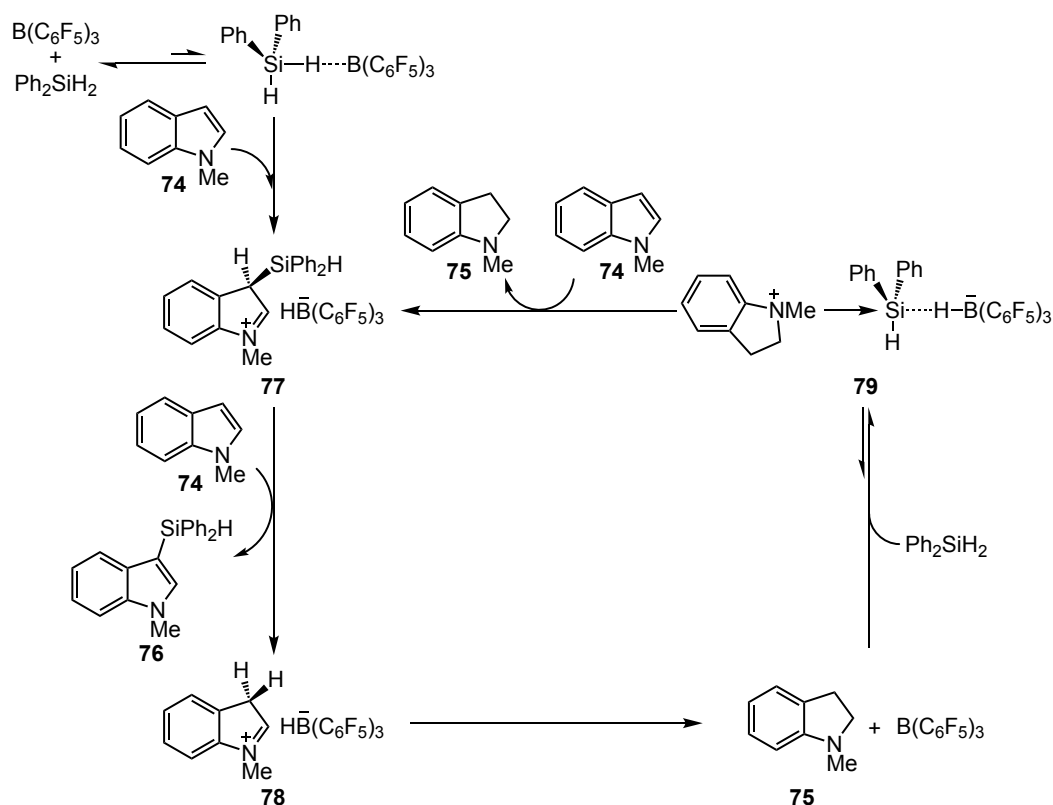
Scheme 1.14. $B(C_6F_5)_3$ -mediated and -catalyzed sila-Friedel–Crafts reaction.



Zhang and coworkers avoided the side hydrosilylation and hydrogenation of indoles in S_EAr reaction by $B(C_6F_5)_3$ -catalyzed convergent disproportionation (Scheme 1.14d)^[32] or by using $Al(C_6F_5)_3$ as a catalyst.^[33] In those cases, indolines **75** were continuously converted back to indoles **74**, and the disproportionation reaction afforded C3-silylated indoles **76** and indolines

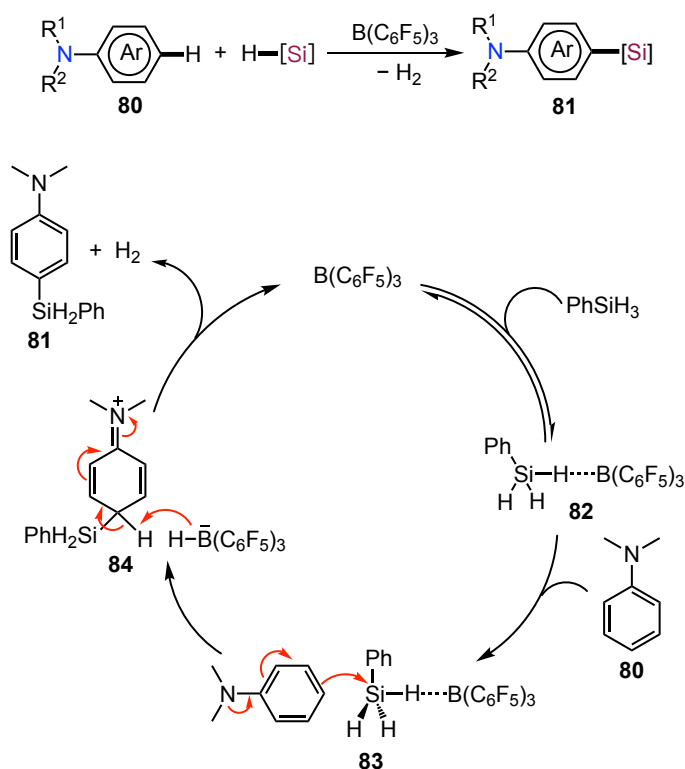
74 for the next catalytic cycle, and thus, C3-selective silylated products **76** were obtained in up to 99% yield (Scheme 1.15).

Scheme 1.15. Possible mechanism for $B(C_6F_5)_3$ -catalyzed disproportionation reaction of indoles.



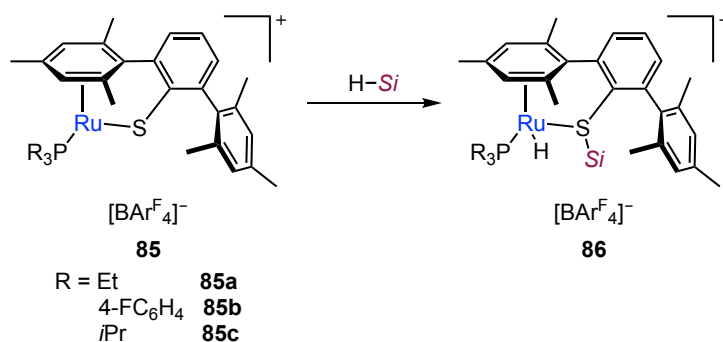
Hou and coworkers developed intermolecular *para*-selective sila-Friedel–Crafts reactions of *N,N*-disubstituted anilines **80** with hydrosilanes catalyzed by $B(C_6F_5)_3$ (Scheme 1.16).^[34] The reaction starts from the activation of hydrosilane by the coordination of $B(C_6F_5)_3$ to the hydridic Si–H bond, which forms an weak adduct **82**. Then, nucleophilic attack of the *para*-carbon atom of an electron-rich *N,N*-dimethylaniline to the electropositive silicon center of the adduct from the back side produce an ion-pair intermediate **84**. Release of H_2 yielded the silylated product **81** along with regeneration of $B(C_6F_5)_3$. The formation of H_2 (at 4.67 ppm) was observed by 1H NMR of the reaction of *N,N*-dimethylaniline with diphenylsilane in C_6D_5Cl .

Scheme 1.16. Boron-catalyzed sila-Friedel–Crafts reaction with hydrosilanes.



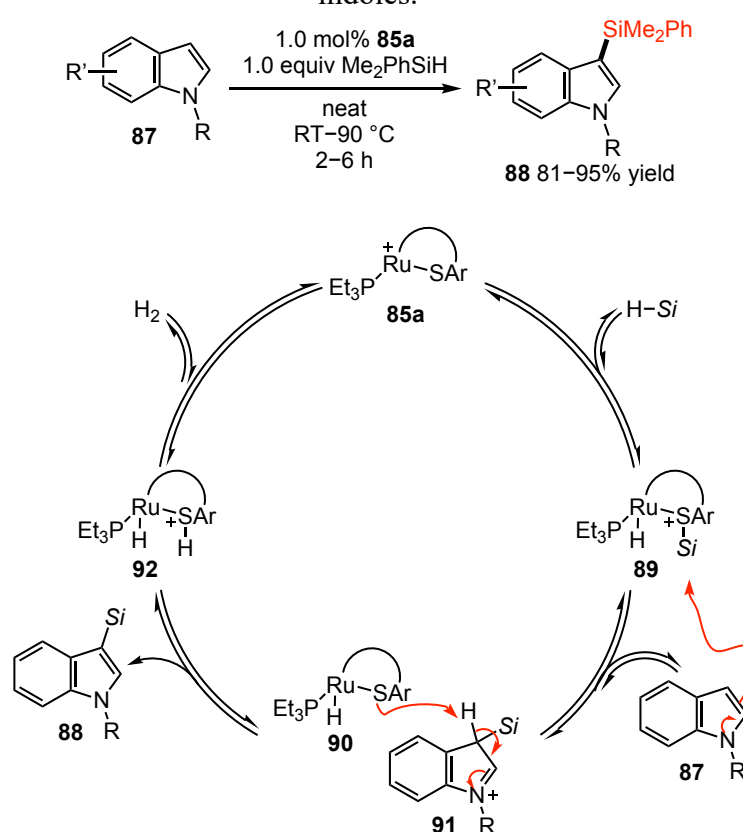
Cooperative Si–H bond activation at Lewis acidic metal centers is an entry into catalysis with electrophilic silylation reagents for sila-Friedel–Crafts reaction.^[35] Ruthenium thiolate complexes **85** (Ohki–Tatsumi complexes), were used for Si–H bonds activation in sila-Friedel–Crafts reactions (Scheme 1.17).^[36–38] In this case, the Si–H bond is heterolytically split by the Ru–S bond of the coordinatively unsaturated cationic ruthenium(II) complex **85**, forming a sulfur-stabilized silicon electrophile. The Wheland intermediate of the subsequent Friedel–Crafts-type process is assumed to be deprotonated by the sulfur atom without addition of a base.

Scheme 1.17. Cooperative Si–H bond activation.



The very first catalytic cooperative Si–H bond activation for sila-Friedel–Crafts reaction paves the way for C3-selective C–H functionalization of indoles and pyrroles by electronic control (not by conventional steric control) (Scheme 1.18).^[36] The proposed catalytic cycle includes cooperative Ru–S-catalyzed Si–H bond activation and regioselective sila-Friedel–Crafts reaction of indoles. Initial coordination of the Si–H bond to the vacant ruthenium(II) site merges into the reversible heterolytic Si–H bond cleavage by the polar Ru–S bond. The silicon-substituted sulfonium ion **89** is then transferred onto nucleophilic indole **87**, yielding Ru–H complex **90** and σ -complex **91**. Proton abstraction from the formed Wheland intermediate was facilitated by the weakly basic sulfur atom to give silylated indole products **88**.

Scheme 1.18. Ruthenium(II) thiolate complex-catalyzed dehydrogenative silylation of indoles.



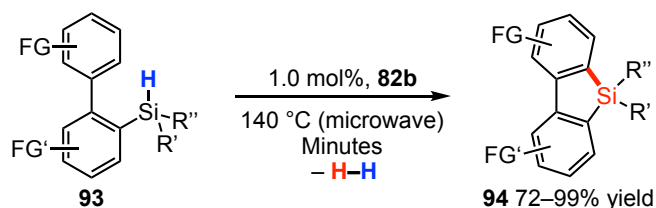
The ruthenium catalyst can be applied to the synthesis of dibenzosiloles functionalized at both benzene cores **93** (Scheme 1.19a). The intramolecular sila-Friedel–Crafts reaction

proceeded via the formation of a sulfur-stabilized silicon cation, generated catalytically from the hydrosilane precursor.^[37]

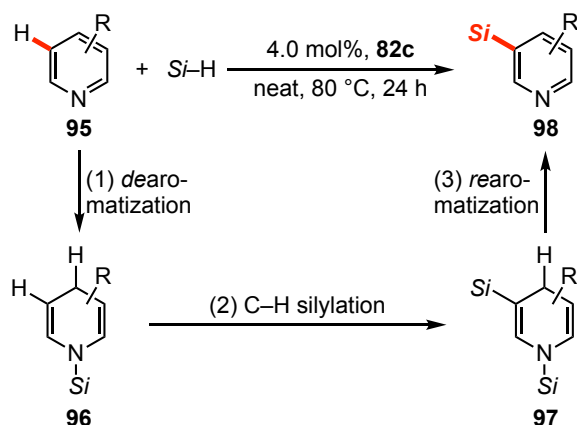
In the presence of the ruthenium catalyst, reactions of 2- and 3-substituted pyridines **95** with hydrosilanes also yielded the corresponding 5-silylated pyridines **98** (Scheme 1.19b). This formal silylation of an aromatic C–H bond is the result of a three-step sequence, consisting of (1) a 1,4-selective hydrosilylation of pyridine (dearomatization), (2) a dehydrogenative C–H silylation of the enamine intermediate **96**, and (3) the retro-hydrosilylation of *N*-silylated 1,4-dihydropyridine **97** (rearomatization). The key intermediates, *N*-silylated 1,4-dihydropyridines **96** and 1,5-silylated 1,4-dihydropyridine **97** were detected by ¹H NMR spectroscopy and prepared through the individual steps. The complex interplay of the electrophilic silylation, hydride transfer, and proton abstraction is promoted by a single catalyst.^[38]

Scheme 1.19. Sila-Friedel–Crafts reaction involving cooperative Si–H bond activation.

(a) Sila-Friedel–Crafts reaction to dibenzosiloles functionalized at both benzene cores



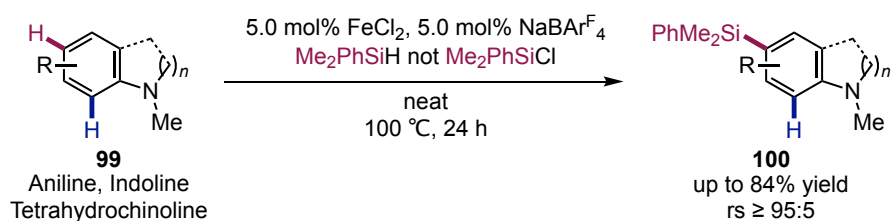
(b) Sila-Friedel–Crafts reaction of pyridines enabled by temporary dearomatization



Oestreich and coworkers found that the Lewis acid, which is generated in situ from base metal salts and NaBAr^F (Ar^F = 3,5-bis(trifluoromethyl)phenyl), promoted the sila-Friedel–Crafts reaction of electron-rich arenes **99**, such as *N,N*-disubstituted anilines, pyrroles, and

indoles, with hydrosilanes (Scheme 1.20). The sila-Friedel–Crafts reaction was optimized for $\text{FeCl}_2/\text{NaBAR}^{\text{F}}$ where the addition of a base is not needed to absorb the released proton.^[39] Along this reaction, Tsuchimoto achieved Zn-pyridine-nitrile system-catalyzed constructing of N(indolyl)–Si bond in a dehydrogenative fashion.^[40]

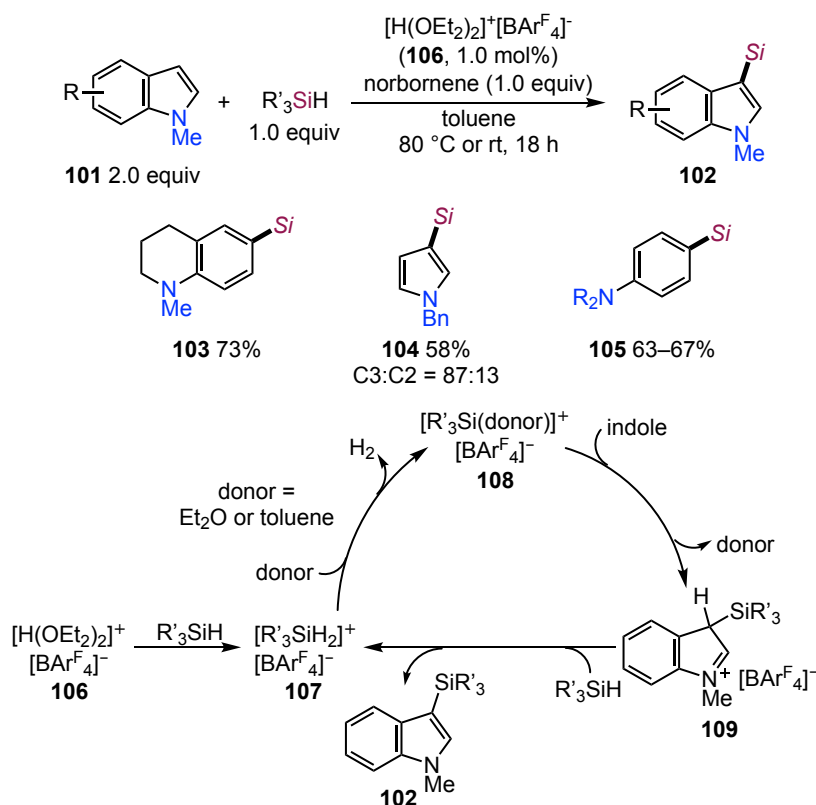
Scheme 1.20. Intermolecular sila-Friedel–Crafts reaction of electron-rich arenes initiated by base metal salts.



Sila-Friedel–Crafts reaction initiated by Brønsted acid-promoted generation of electrophilic silicon cation from hydrosilanes was presented by Oestreich and coworkers.^[41] Protonation of the hydrosilane followed by elimination of dihydrogen is key to generate the stabilized silylium ion and to remove the proton released from the Wheland intermediate. Brookhart's acid **106** is strong enough to protonate the hydrosilane to give a pentacoordinate siliconium ion **107**. That intermediate release dihydrogen to afford the silylium ion **108** which is stabilized by Et_2O or toluene. Et_2O introduced with Brookhart's acid $[\text{H}(\text{OEt}_2)_2]^+[\text{BARF}_4]^-$ (**106**) acts as the stabilizing donor, however, toluene solvent will competent this job if ether cleavage occurs in the reaction process. Then nucleophilic attack of the electron rich indole to the cationic silicon electrophile **108** occur affording Wheland complex **109**. The Wheland complex **109** is a strong Brønsted acid to directly protonate another hydrosilane molecule, and then the catalytic cycle closes along with the formation of the C3-silylated indole **102**.

Alkyl substitution at the *ortho*-position to the amino group was tolerated in 1-methyl-1,2,3,4-tetrahydroquinoline **103**. In the case of the pyrrole substrate, the silylated product **104** in moderate yield with regioselectivity (C3:C2 = 87:13). *N,N*-Disubstituted aniline gave the desired silylated product **105** in good yield with highly regioselectivity.

Scheme 1.21. Brønsted acid-mediated formation of stabilized silylium ions for catalytic silylation–Friedel–Crafts reaction.



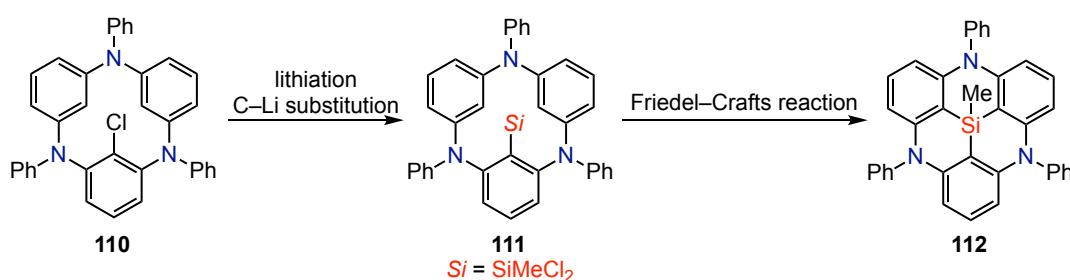
1.3 Applications of C(sp²)–H Silylation

Heteroatom-containing π -conjugated systems have been one of the exciting subjects in the last few decades because electronic tuning by main group elements enables π -electron systems to acquire intriguing photophysical and electronic properties. Heteroatom-containing triangulenes, heteroatom-containing ladder-type π -conjugated molecules, heteroatom-porphyrin π -conjugate systems, and trisilasumanene are well-known. Based on the great success of the above-mentioned C(sp²)–H silylation, the synthesis of silicon-containing π -conjugated molecules were demonstrated.

Hatakeyama and coworkers have developed a method for the divergent synthesis of silicon-centered 4,8,12-triazatriangulene **112**, with the key step to efficiently incorporate a silicon atom into the macrocyclic precursor **111** through electrophilic substitution of C–Li bond and Friedel–Crafts-type reaction (Scheme 1.22).^[42] The bowl-shaped structure of the compound was revealed by X-ray crystallography. Spectroscopic characterization of the compound revealed

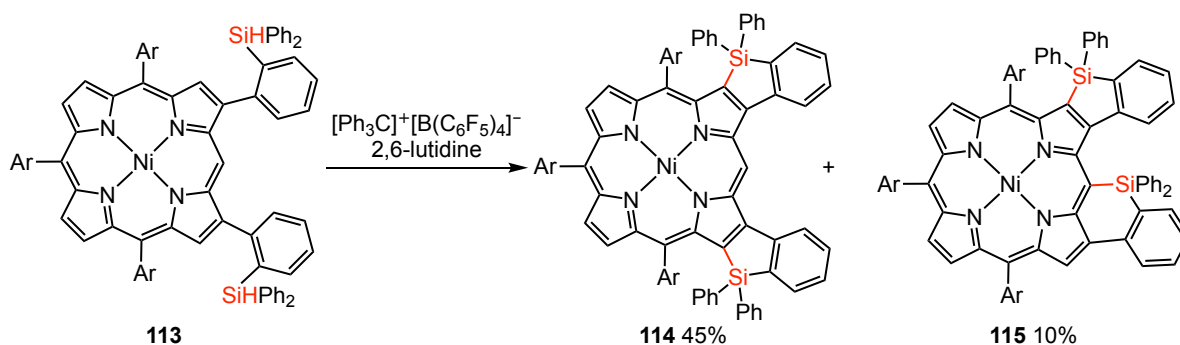
that its UV/Vis spectra showed strong absorption band, which is corresponding to a $\pi-\pi^*$ transition with maximum wavelength at $\lambda = 335$ nm, while the fluorescence spectra showed weak emission bands at $\lambda = 383$ nm ($\Phi_F = 0.09$).

Scheme 1.22. Synthesis of silicon-centered 4,8,12-triazatriangulenes.



Porphyrin is an 18π aromatic macrocyclic compound that consists of four pyrrole units and four bridging carbon atoms in a planar conformation. Osuka *et al.* reported the synthesis of triphenylsilane-fused porphyrins by a synthetic protocol consisting of installation of a 2-(diphenylsilyl)phenyl group by Negishi coupling and subsequent intramolecular sila-Friedel-Crafts reaction initiated by a trityl cation and 2,6-lutidine (Scheme 1.23).^[43] Doubly fused Ni^{II}-porphyrin **114** showed the first oxidation and reduction potentials at 0.47 and -1.77 V, respectively, leading to a HOMO-LUMO gap of 2.24 eV. The absorption spectra of doubly fused Ni^{II}-porphyrin showed peaks (λ_{max}) at 444 and 555 nm.

Scheme 1.23. Triphenylsilane-fused porphyrins.

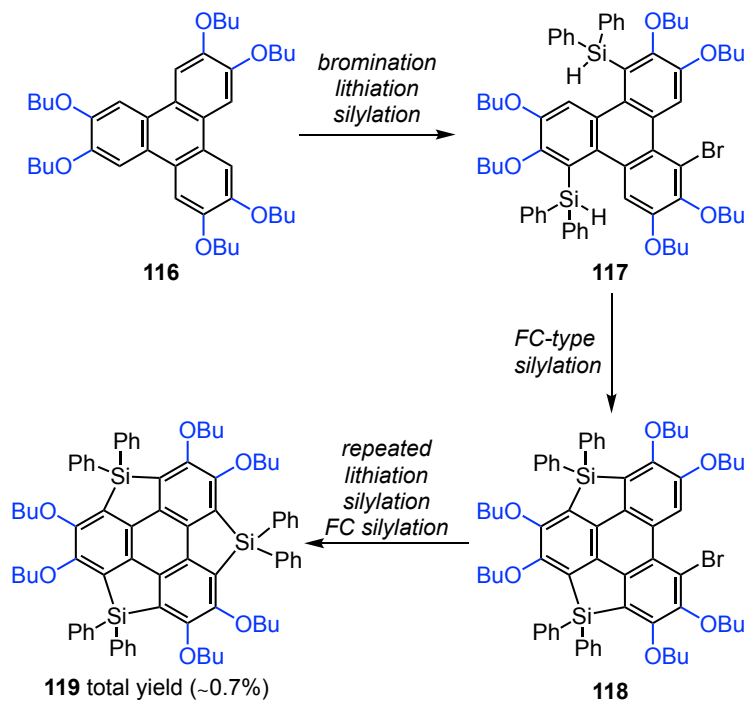


Trisilasumanene has attracted much attention as both a sumanene analogue and a novel π -extended silole derivative.^[44] Kawashima *et al.* reported the first synthesis of silasumanene **119** from 2,3,6,7,10,11-hexabutoxytriphenylene (**116**) through bromination followed by repeated lithiation/silylation/sila-Friedel–Crafts reaction (Scheme 1.24a).^[27a] X-ray structural analysis of the trisilasumanene **119** indicated that the main framework was almost planar. UV-vis absorption spectrum of trisilasumanene **119** showed an intense absorption band ($\lambda_{\text{max}} = 299 \text{ nm}$), and a weak absorption band in the longer-wavelength region ($>350 \text{ nm}$). The emission spectrum showed a blue fluorescence in dichloromethane solution ($\lambda_{\text{max}} = 427 \text{ nm}$) and in the solid state ($\lambda_{\text{max}} = 447 \text{ nm}$).

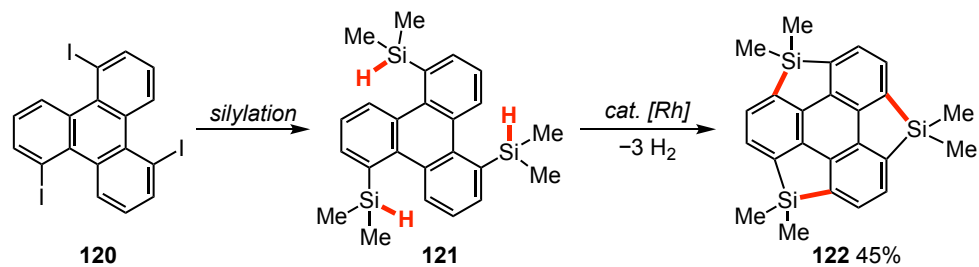
Afterward, Xu and coworkers have succeeded in the synthesis of pristine all-methyl substituted silasumanene **122** using a threefold rhodium-catalyzed cyclo-dehydrogenation of Si–H and C–H bonds as the key step.^[45] This three-step procedure from readily available starting materials **120** provides a shortcut to homogeneous methyl or isobutyl substituted silicon-containing sumanenes without substituents on their peripheral carbons, which are difficult targets through known methods. This work demonstrated the power of the transition metal-catalyzed cyclodehydrogenative reactions for the synthesis of polycyclic aromatic hydrocarbons and their heteroanalogues (Scheme 1.24b).

Scheme 1.24. Synthesis of trisilasumanene.

(a) Synthesis of trisilasumanene: stepwise process



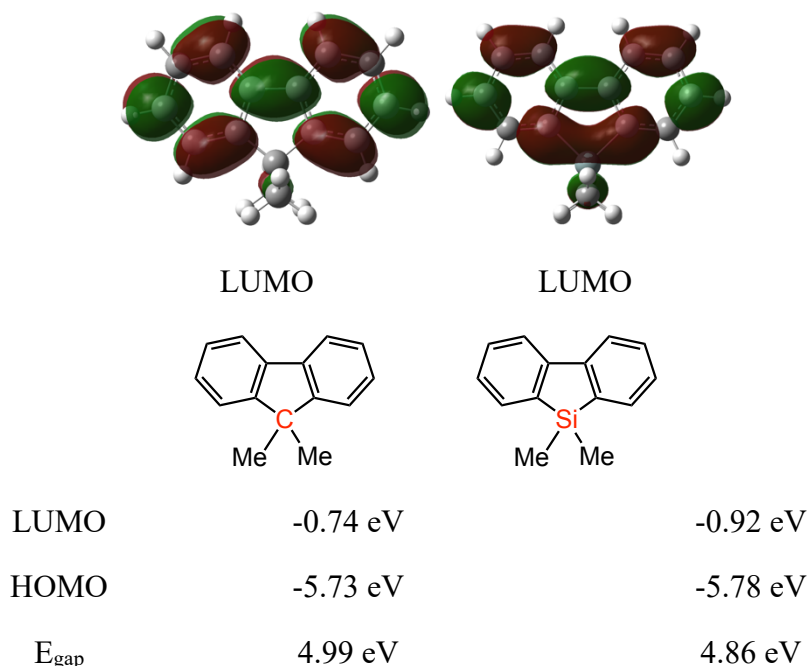
(b) Three-fold Rh-catalyzed cyclodehydrogenation



1.4 Silacyclic Compounds

Silicon-containing π -conjugated compounds exhibit characteristic optical and electronic properties due to the particular interactions between Si and the π -system. For example, DFT calculations show that the LUMO level of silafluorene (-0.92 eV) is significantly lower than that of fluorene (-0.74) due to $\sigma^*-\pi^*$ conjugation (Scheme 1.25).^[46] As the energy gap of organosilicon compounds between the HOMO and LUMO is tuned, red- or blue-shift emerges in conjugated materials. The addition of silicon atom(s) to aromatic molecules induces hyperconjugation between the σ orbital of the silicon atom(s) and the aromatic π orbital. UV-vis absorption and fluorescence spectra are red-shift and the molecule's absorption coefficient and fluorescence intensity increase owing to the $\sigma-\pi$ conjugation. These effects are evident in dibenzosilole, a five-membered ring molecule that contains silicon.^[47]

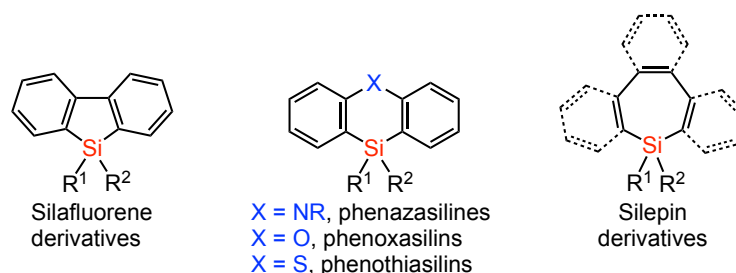
Scheme 1.25. Structures of fluorene and silafluorene and their DFT calculations at B3LYP/6-31G(d) level.



The silacyclic compounds, such as silafluorene derivatives, silicon and heteroatom-bridged six-membered biaryls (phenazasilines, phenoxasilins, and phenothiasilins) and silepin

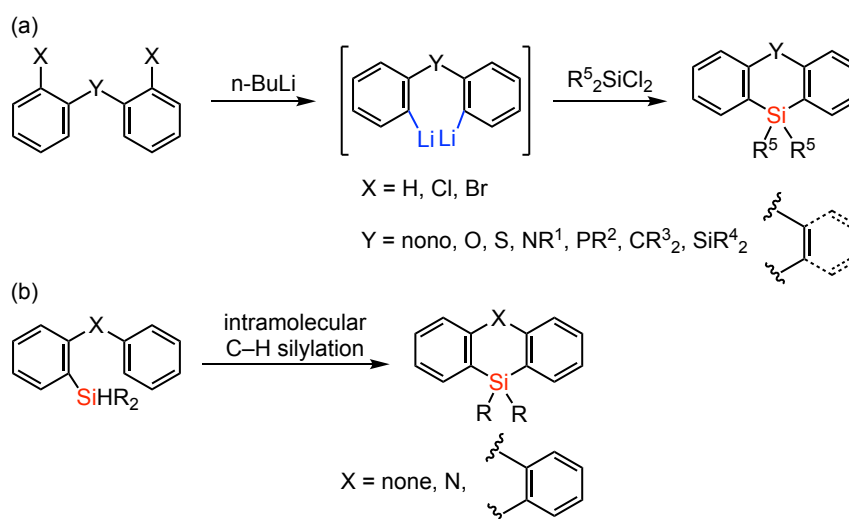
derivatives (Scheme 1.26), are promising for optoelectronic devices, except for their synthetic difficulties.^[48]

Scheme 1.26. Structures of silacyclic compounds.



Even though the synthesis of silicon-containing compounds by $\text{C}(\text{sp}^2)\text{-H}$ silylation has been widely studied, the existing strategies for the synthesis of the above silacyclic compounds are limited to the traditional reaction between dilithiated intermediates with dichlorosilanes (Scheme 1.27a)^[48-53] or intramolecular silylation from silyl-substituted arenes (Scheme 1.27b).^[5,6,27,30,47,54]

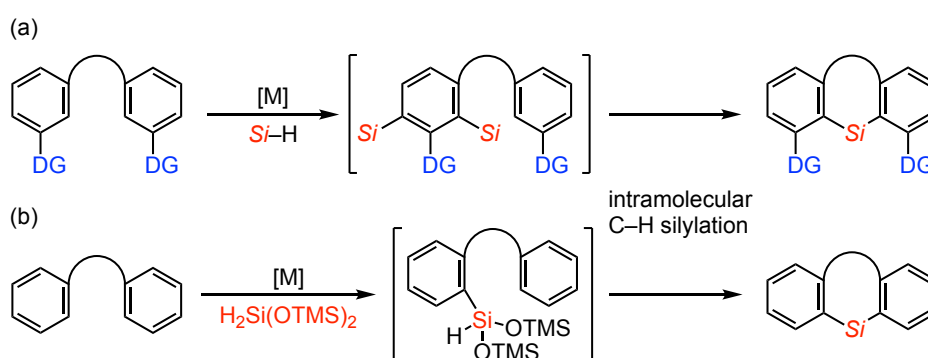
Scheme 1.27. Current synthetic methods for synthesis of silacycles.



Furthermore, the application of those synthetic methods for construction of π -system are relatively less developed. I assumed that a simple synthesis of silacyclic compounds can be feasible by direct intermolecular C–H silylation, especially sila-Friedel–Crafts reaction,

considering the advantages and the disadvantages of transition metal-catalyzed intermolecular C(sp²)–H silylation. In the case of the transition metal-catalyzed directed intermolecular C(sp²)–H silylation, *ortho*-selective C(sp²)–H silylation can be achieved using a directing group but C(sp²)–H silylation can occur at both *ortho*-positions if the substrate has two *ortho*-C–H bonds, which will be demerit of the construction of silacycles (Scheme 1.28a). There also have the problems of the attachment and detachment of a suitable directing group.^[4,11a] In addition, in the transition metal-catalyzed undirected intermolecular silylation, special silylation reagents, such as H₂Si(OTMS)₂, are required (Scheme 1.28b).^[20,21] It is also difficult to control the regioselectivity of the reaction to form the desired silacycles.

Scheme 1.28. Construction of silacycles by transition metal-catalyzed C–H silylation.



In contrast, the reported intramolecular sila-Friedel–Crafts reactions for the synthesis of silafluorene derivatives^[27,30] and the intermolecular sila-Friedel–Crafts using a hydrosilane reagent^[34] could avoid the above problems, and silylated products can be obtained regioselectivity without using directing groups.

1.5 Purpose, Importance, and Design of My Researches

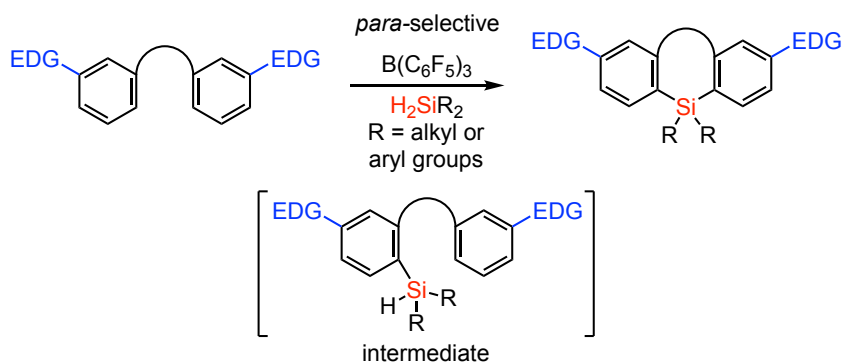
The purpose of this research project is the synthesis of five-, six-, and seven-membered silacyclic compounds by a direct synthetic route from biaryls and dihydrosilanes. The synthesis of the silacyclic compounds is important because of their potential applications, such as optoelectronic devices.

Based on the above studies on sila-Friedel–Crafts reactions, the electron-rich arenes or heteroarenes were required as substrates, especially in the intermolecular reactions.^[55] Concerning about the intermolecular *para*-selective sila-Friedel–Crafts reactions of *N,N*-disubstituted anilines with hydrosilanes, I designed the substrates with strong electron-donating groups, such as amino groups, at the *para*-position from the reaction sites.

Tris(pentafluorophenyl)borane $B(C_6F_5)_3$ is a commercially available, air-stable and water-tolerant Lewis acid.^[56] $B(C_6F_5)_3$ has a strong Lewis acidity similar to that of BF_3 due to the electron-withdrawing nature of the three pentafluorophenyl rings.^[57] $B(C_6F_5)_3$ is less prone to hydrolysis than BF_3 .^[58] The steric bulkiness of the perfluorinated phenyl rings additionally makes $B(C_6F_5)_3$ an ideal Lewis acid for frustrated Lewis pair chemistry.^[59] $B(C_6F_5)_3$ has often been used in the field of main-group Lewis acid and metal-free catalysis.^[60] Other Lewis acid catalysts reported in sila-Friedel–Crafts reactions, such as trityl cation ($[Ph_3C]^+[B(C_6F_5)_4]^-$), ruthenium thiolate complexes, base-metals, and Brønsted acid, have some problems: addition of stoichiometric amounts, limited tolerance of hydrosilane reagents, and harsh reaction conditions.

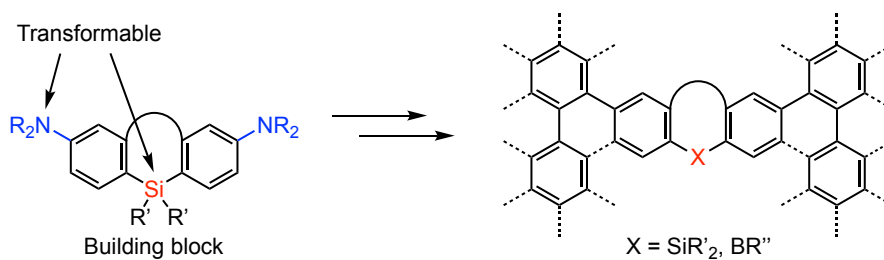
Herein, I designed the $B(C_6F_5)_3$ -catalyzed double sila-Friedel–Crafts reaction as ideal and efficient synthetic methods of silacyclic compounds (Scheme 1.29).

Scheme 1.29. Boron-catalyzed double sila-Friedel–Crafts reactions for the synthesis of silacyclic compounds.



First of all, I planned to investigate $\text{B(C}_6\text{F}_5)_3$ -catalyzed double sila-Friedel–Crafts reaction for the synthesis of silafluorene derivatives from amino-substituted biphenyls and dihydrosilanes. I hypothesized that the reaction system could be useful for the direct synthesis of silacycles, especially multisubstituted ones, which are not readily obtained by conventional synthetic routes. In addition, I expected to realize the construction of extended π -conjugated systems based on the introduction of amino groups as transformable directing groups on the silacycles (Scheme 1.30).^[61]

Scheme 1.30. Design of construction of π -conjugated systems.



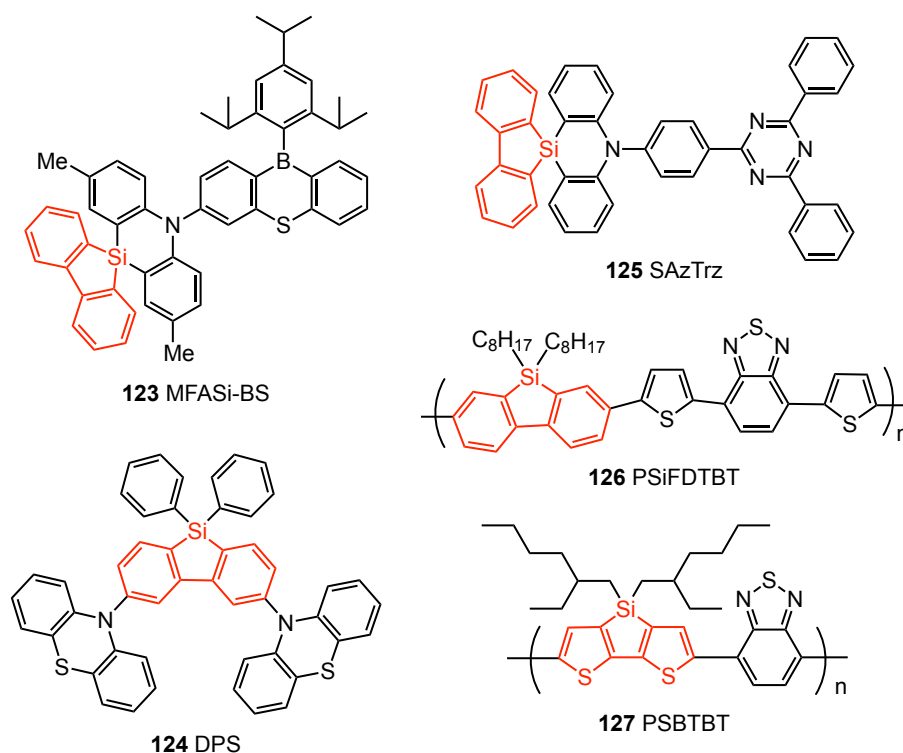
Chapter 2

Lewis Acid-Catalyzed Synthesis of Silafluorene Derivatives from Biphenyls and Dihydrosilanes via a Double Sila-Friedel–Crafts Reaction

2.1 Introduction

9-Silafluorene (dibenzosilole), a silole embedded in a biphenyl framework, has recently received much attention due to its great potential applications for organic electroluminescent compounds (**123**),^[62] organic light emitting materials (**124**, **125**),^[63] field effect transistors (**126**, **127**),^[64] and photovoltaics (Scheme 2.1).^[65] Hence, several approaches for the construction of the silafluorene structure have been developed.

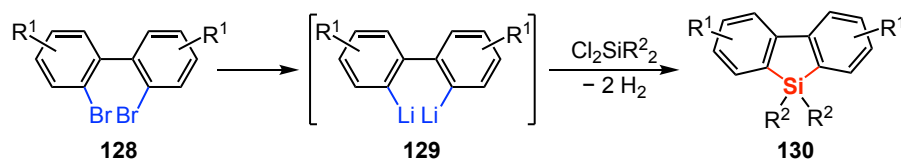
Scheme 2.1. Examples of silafluorene derivatives as functional molecules.



One of the common synthetic methods is dilithiation of 2,2'-dibromobiphenyls and sequential transmetalation of dilithiated biphenyls **129** with dichlorosilanes (Scheme 2.2).^[49] Even though the method is practical, several limitations remain: (1) multiple-steps synthesis is necessary; (2)

functional groups which react with organolithium reagents cannot be used; and (3) the synthesis of multi-substituted silafluorene derivatives is not readily achieved due to the difficulty of the preparation of their multi-substituted dibromobiphenyl precursors. Therefore, a direct synthesis of multi-substituted silafluorenes is desirable.

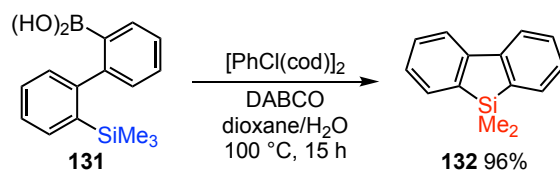
Scheme 2.2. Transformation of organometallic biphenyls with dichlorosilanes.



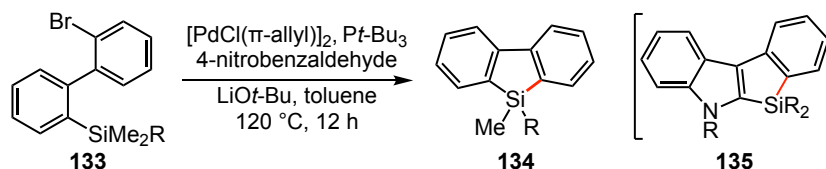
Transition metal-catalyzed synthetic methods have been developed to synthesize diverse silafluorene derivatives under mild conditions (Scheme 2.3).^[66] In 2009, Chatani and co-workers reported a rhodium-catalyzed synthesis of benzosilole **132** via the cleavage of a C–Si bond of **131** (Scheme 2.3a).^[66a] In 2011, Xi's group developed a new process involving palladium-catalyzed selective cleavage of the C(sp³)–Si bond in a trialkylsilyl group of **133** and consequent intramolecular C(sp²)–Si bond forming process. This reaction provided the first efficient synthesis of benzosilolo[2,3-*b*]indoles **135**, which represent a new type of silicon-bridged polyheteroarene (Scheme 2.3b).^[66b] In 2008, Hiyama *et al.* described a palladium-catalyzed intramolecular direct arylation of readily available 2-(arylsilyl)aryl triflates **136** as versatile synthetic route to silafluorenes. Key to this success is the installation of bulky substituents on the silicon atom and the use of Et₂NH as a base (Scheme 2.3c).^[66c] The effects of the bulkier substituents may be rationalized as the Thorpe–Ingold effect or *gem*-dialkyl effect from these groups positioned the two phenyl groups closer together, and suppressed the decomposition of silafluorene.

Scheme 2.3. Transition metal-catalyzed synthesis of silafluorene derivatives.

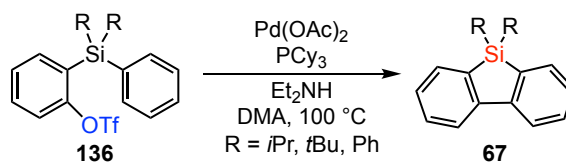
(a) Rhodium-catalyzed cyclization reaction of boronic acids via Me-Si bond cleavage



(b) Pd-catalyzed selective cleavage of a $\text{C}(\text{sp}^3)\text{-Si}$ bond and consequent intramolecular $\text{C}(\text{sp}^2)\text{-Si}$ coupling reaction

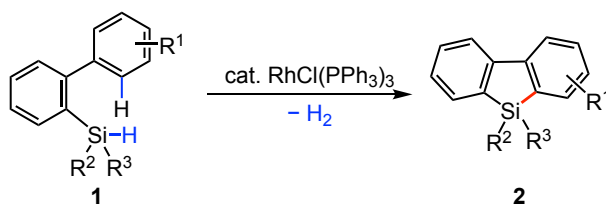


(c) Palladium-catalyzed intramolecular coupling of 2-(arylsilyl)aryl triflates



The silylation of C–H bonds is an attractive protocol because for the reactions do not require the prefunctionalization of arene substrates.^[4] Rhodium-catalyzed double activation of Si–H and C–H bonds is an effective strategy for the synthesis of silafluorene derivatives.^[5] Our group successfully developed the synthesis of silafluorenes from biarylhydrosilanes **1** (Scheme 2.4). The reaction proceeded by double activation of Si–H and C–H bonds via dehydrogenation. The dehydrogenation reaction does not require oxidants, such as molecular oxygen.^[5a] Our group also realized the synthesis of a spiro-silafluorene derivative from a bis(biphenyl)silane by double dehydrogenative cyclization using the rhodium catalyst. This reaction was applied to the synthesis of chiral spiro-silafluorene derivatives using a rhodium catalyst with a chiral phosphine ligand ($[\text{RhCl}(\text{cod})]_2 + (R)\text{-binap}$).^[5b] Several other transition metal-catalyzed synthetic methods to prepare silafluorenes have also been reported.^[67]

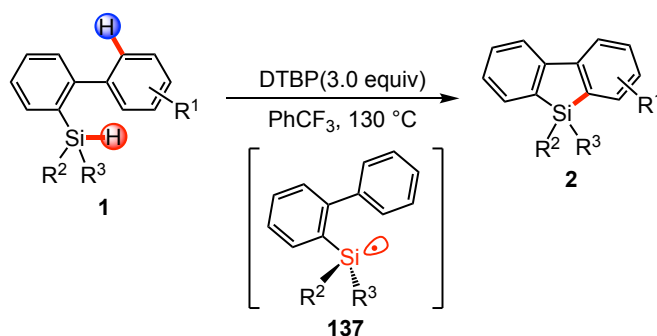
Scheme 2.4. Rhodium-catalyzed direct intramolecular aromatic C–H silylation.



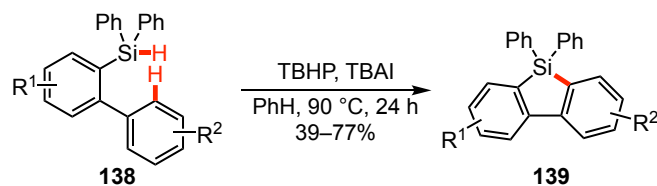
Silyl radical-based strategy for the synthesis of silafluorenes via direct C–H bond cleavage of arylsilanes without the aid of transition metals, acids, or bases were also disclosed (Scheme 2.5).^[68] A direct and efficient strategy employing aryl silyl radical intermediates **137** towards the synthesis of silafluorenes and silaindenes was introduced by Li and co-workers. These reactions start from readily available arylhydrosilanes **1**, furnish the products **2** via direct Si–H and C–H cleavage pathways in one step (Scheme 2.5a).^[68a] Leifert and Studer developed a base-promoted homolytic aromatic substitution (BHAS) of 2-diphenylsilylbiaryls **138** for 9-silafluorenes. Cross dehydrogenative silylation occurred with tetrabutylammonium iodide (TBAI) as an initiator, *tert*-butylhydroperoxide (TBHP) as a stoichiometric oxidant (Scheme 2.5b).^[68b]

Scheme 2.5. Silyl radical-based strategy for the synthesis of silafluorenes via direct C–H bond cleavage.

(a) Synthesis of silafluorenes via silyl radicals from arylhydrosilanes



(b) 9-Silafluorenes via base-promoted homolytic aromatic substitution

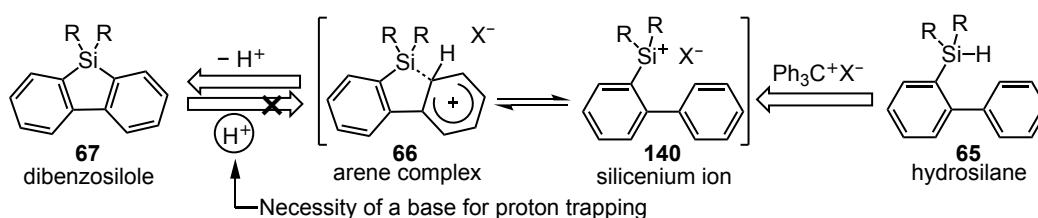


Recently, the intramolecular sila-Friedel–Crafts reaction of biphenylhydrosilanes for the synthesis of silafluorene derivatives has been developed (Scheme 2.6).^[27a,30,37] Kawashima and co-workers reported an intramolecular sila-Friedel–Crafts reaction for dibenzosilole derivatives (Scheme 2.6a).^[27a]

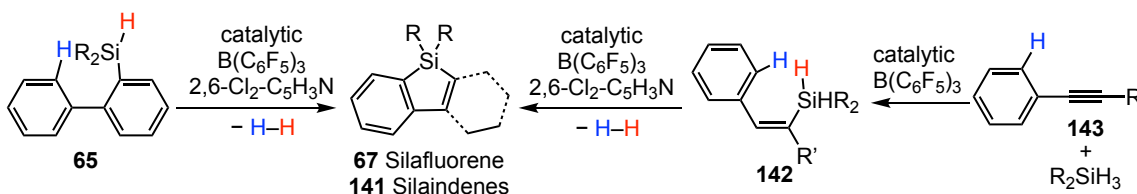
Ingleson *et al.* reported $B(C_6F_5)_3$ catalyst promoted the dehydrosilylation of 2-(HR₂Si)-biphenyls **65** in the presence of a weak base to form silafluorenes with the generation H₂. This synthetic system is applicable for the synthesis of silaindenes **141** from alkynes **143** by *trans*-hydrosilylation and sequential intramolecular sila-Friedel–Crafts reaction (Scheme 2.6b).^[30]

Scheme 2.6. Sila-Friedel–Crafts reaction for synthesis of silafluorenes.

(a) Strategy for intramolecular sila-Friedel–Crafts reaction



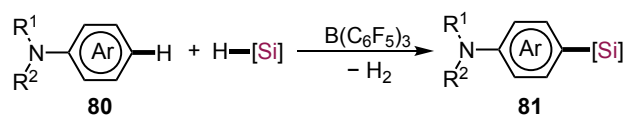
(b) $B(C_6F_5)_3$ -catalyzed synthesis of benzofused-siloles



The above-mentioned synthetic strategies have been limited to the intramolecular silylation for the synthesis of silafluorene derivatives. Although the intramolecular silylations produced the silafluorenes in good yields, this strategy requires tethering suitable silyl groups to the arene substrates, which limits the diversity of functional groups. Therefore, I assumed the intermolecular reaction of biphenyl as substrates and dihydrosilanes as silane sources is a promising protocol to provide silafluorene derivatives.

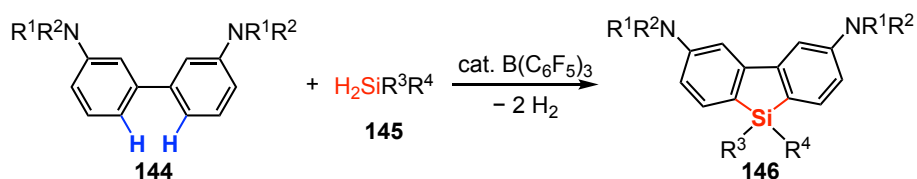
Hou's group reported the boron-catalyzed intermolecular sila-Friedel–Crafts reaction of aromatic amines with various hydrosilanes (Scheme 2.7).^[34]

Scheme 2.7. Boron-catalyzed aromatic sila-Friedel–Crafts reaction with hydrosilanes.



I then considered that it is feasible to synthesize silafluorene derivatives using a double sila-Friedel–Crafts reaction between electron-rich biphenyls and dihydrosilanes. Additionally, there is no example of the synthesis of silafluorenes, despite the report of ruthenium-catalyzed reaction of 2-phenylindoles and dihydrosilanes through successive sila-Friedel–Crafts reaction.^[69] Herein, I report a borane-catalyzed sila-Friedel–Crafts reaction between amino groups-substituted biphenyls **144** and dihydrosilanes **145** for the synthesis of silafluorene derivatives **146** (Scheme 2.8).^[70]

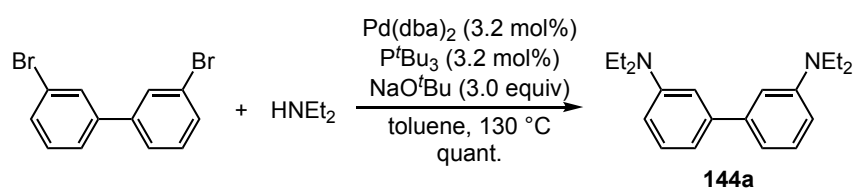
Scheme 2.8. This work: double sila-Friedel–Crafts reaction by single operation.



2.2 Results and Discussion

First, I started the feasibility studies of my synthetic approach using diaminobiphenyl **144a** and dihydrodiphenylsilane **145a** as model substrates (Table 2.1). Biphenyl **144a** was synthesized by palladium-catalyzed amination of 3,3'-dibromobiphenyl with HNEt₂ (Scheme 2.9).^[71]

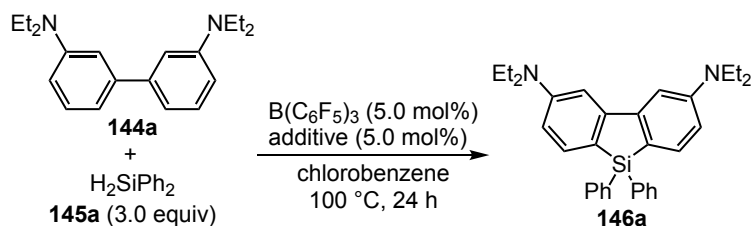
Scheme 2.9. Synthesis of biphenyl **144a**.



The double sila-Friedel–Crafts reaction of **144a** with **145a** using a catalytic amount of B(C₆F₅)₃ in chlorobenzene as a solvent at 100 °C for 24 h provided silafluorene **146a** in 73% yield (Table 2.1, entry 1). The result can be rationalized as that the electron-rich nature or that the tertiary amine itself may act as a base during the reaction, in a stepwise deprotonation/hydrogen release mechanism.^[72]

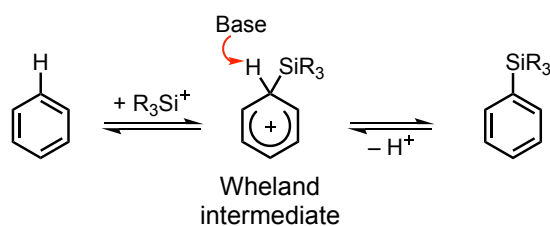
Due to the reversibility of sila-Friedel–Crafts reaction, the presence of a base is necessary to prevent the reverse protonation reaction of Wheland complex from occurring. Kawashima investigated the effectiveness of different bases in the sila-Friedel–Crafts reaction, no bases other than 2,6-lutidine worked well.^[27a,30] They rationalized that the bulkiness and basicity of 2,6-lutidine were important factors in this reaction. Based on the above-mentioned results, pyridines were examined as an additive (entries 2–4). When using pyridine as an additive, no reaction proceeded due to the deactivation of B(C₆F₅)₃ by the coordination of pyridine (entry 2). The yield of **146a** reached 89% using 5.0 mol% of 2,6-dichloropyridine (entry 3). In the presence of 7.5 mol% of 2,6-lutidine, **146a** was afforded in 93% yield (87% isolated yield, entry 5). The structure of the silafluorene **146a** was confirmed by ¹H and ¹³C NMR spectroscopy and HRMS spectrometry.

Table 2.1. Synthesis of silafluorene derivative **146a** from diaminobiphenyl **144a** and dihydrodiphenylsilane **145a**.



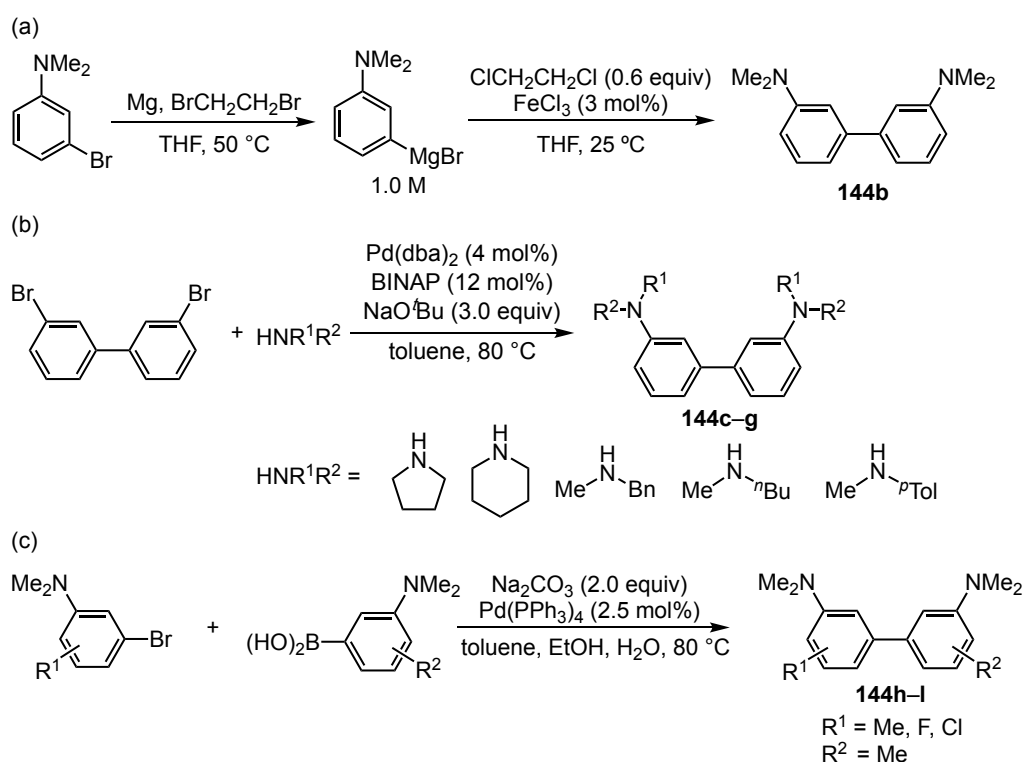
entry	additive	yield (%) ^b
1	none	73
2	pyridine	0
3	2,6-dichloropyridine	80
4	2,6-lutidine	89
5	2,6-lutidine ^a	93 (87) ^c

^a7.5 mol%. ^bDetermined by ¹H NMR. ^cIsolated yield.



Compound **144b** was synthesized by an iron-catalyzed homo-coupling of 3-(*N,N*-dimethylamino)phenyl magnesium bromide (Scheme 2.10a).^[73] Biphenyls **144c–144g** were synthesized by Pd/BINAP-catalyzed amination of dibromobiphenyl (Scheme 2.10b).^[74] Biphenyls **144h–144n** were synthesized by the Suzuki-Miyaura cross-coupling reaction of functionalized anilines with arylboronic acids (Scheme 2.10c).^[75] The details of the reaction conditions and spectral data were shown in the experimental section.

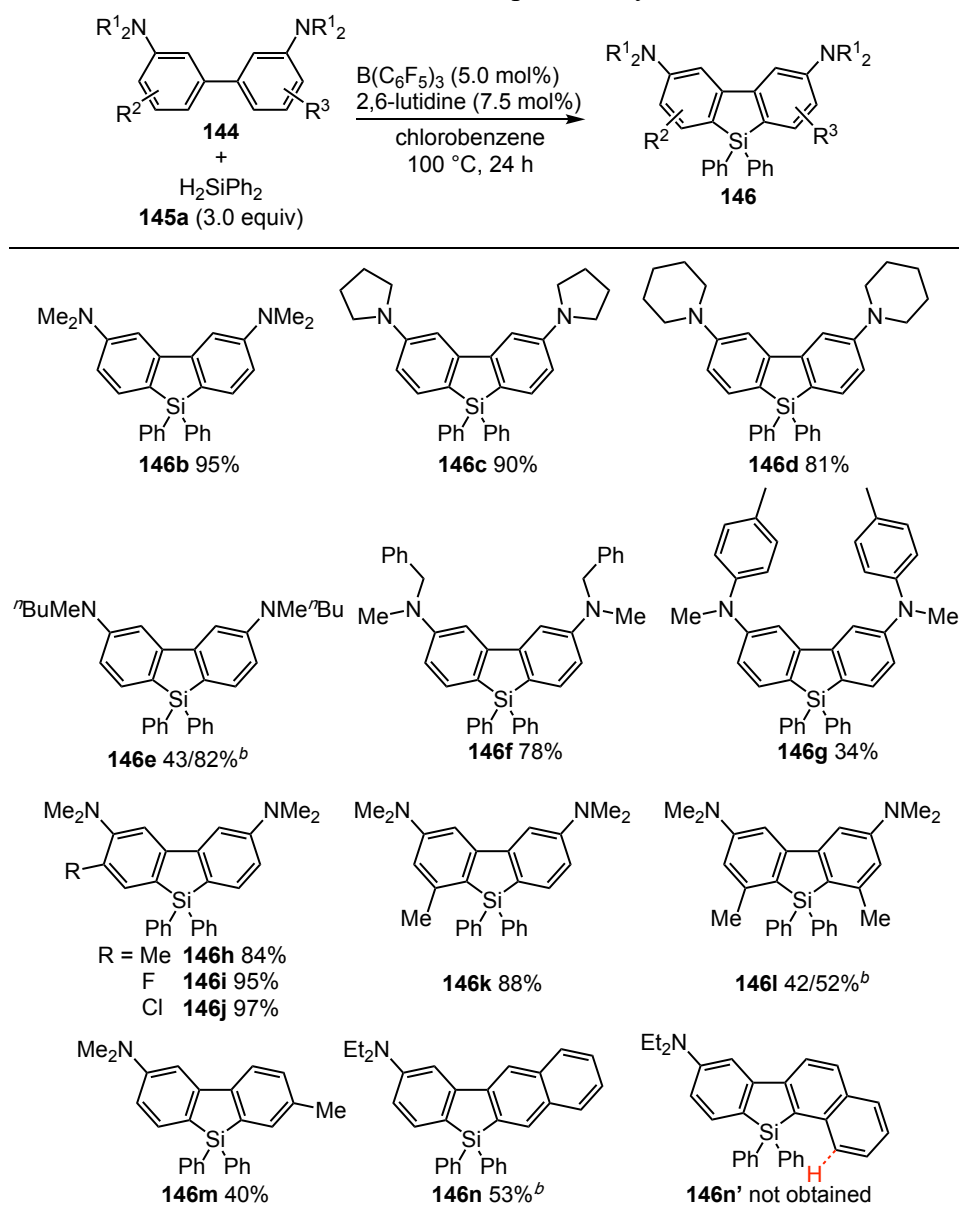
Scheme 2.10. Synthesis of biphenyls (a) **144a**, (b) **144c–144g**, and (c) **144h–l**.



The substrate scope of biaryls was then investigated under the optimized reaction conditions (Scheme 2.11). Silafluorene derivatives **146b–d** containing dimethylamino groups or cyclic *N,N*-dialkylamino groups, pyrrolidine and piperidine were obtained in 81–95% yields from the corresponding biphenyls **144b–d**. *N*-*n*-butyl-*N*-methylamino group-substituted biphenyl **144e** afforded silafluorene **146e** in 43% yield. By increasing the reaction temperature to 140 °C, the yield of **146e** was increased to 82%. Silafluorene **146f** was formed in 78% yield using *N*-benzyl-*N*-methylamino group-substituted biphenyl **144f**, while *N*-*p*-tolyl-*N*-methylamino group-substituted biphenyl **144g** gave silafluorene **146g** in 34% yield. It is probably because nucleophilicity of aromatic rings is decreased by the introduction of *p*-tolyl groups on amino groups. In addition, there is also the steric effect of the tolyl groups compared with other substituents of the amino groups. The conventional synthetic methods of multi-substituted silafluorene derivatives are not easily applied for preparing their multi-substituted substrates. In contrast, the readily prepared trisubstituted biphenyls **144h–k** were transformed to the silafluorene derivatives **146h–k** in good to excellent yields. Furthermore, tetrasubstituted silafluorene **146l** was afforded in 42% yield. The yield was improved to 52% at 140 °C. Mono-

aminobiphenyls **144m** and **144n** are also good substrates to afford their corresponding silafluorenes **146m** and **146n** in 40% and 53% yields, respectively. The naphthyl substituted substrate **144n** selectively gave silafluorene **146n** without the formation of **146n'**, probably due to the electronic effect on the naphthalene moiety and the steric hindrance between the hydrogen atom at the *peri*-position of the naphthalene moiety and phenyl groups on the silicon atom in the intramolecular silylation step.

Scheme 2.11. Substrate scope of biaryls **144**.^a



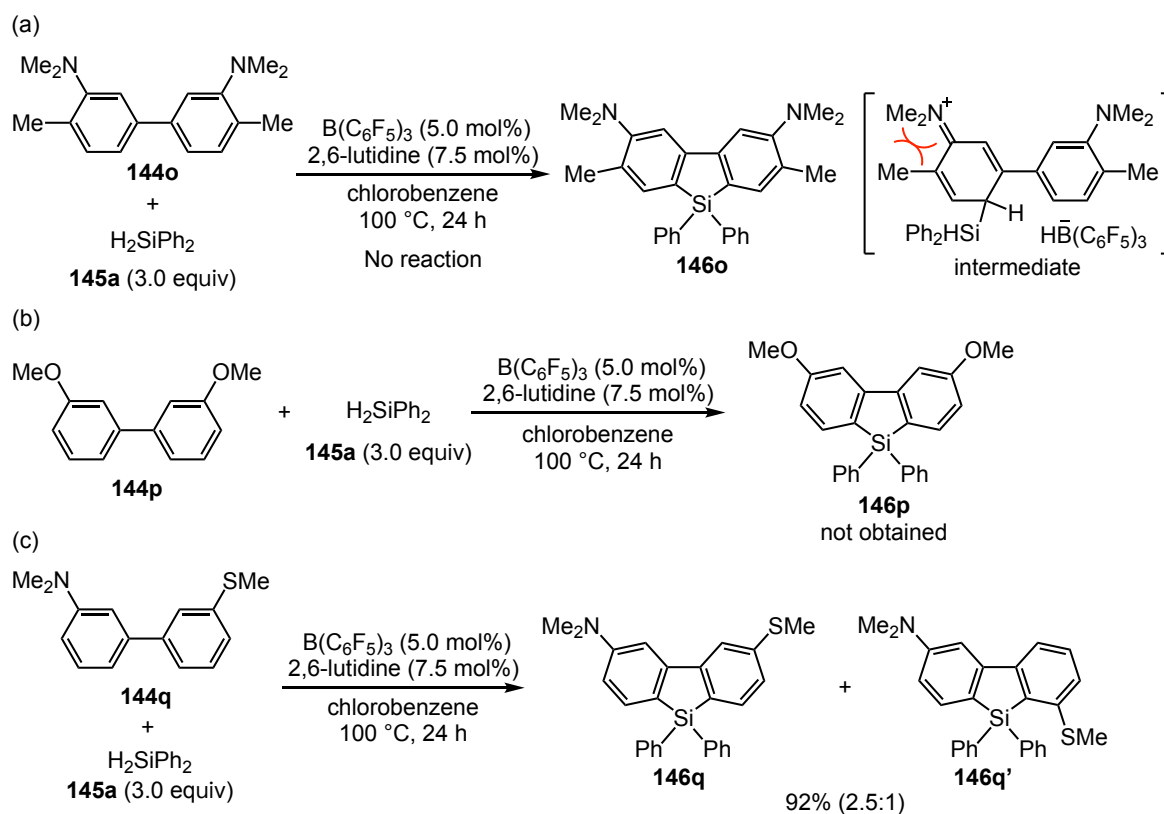
Reaction conditions: biphenyls (0.25 mmol), hydrosilane (0.75 mmol), $B(C_6F_5)_3$ (5.0 mol%), 2,6-lutidine (7.5 mol%) in chlorobenzene (0.5 mL) under N_2 at 100 °C for 24 h. ^aIsolated yield. ^b140 °C.

In contrast to **144l**, no desired compound was obtained in the case of tetrasubstituted biphenyl **144o**, and the substrate was completely recovered under the aforementioned reaction conditions. It is probably due to the steric hindrance of *ortho*-methyl group during the first nucleophilic attack step, that is, the silylated intermediate does not form (Scheme 2.12a).

This catalytic system was not able to facilitate the sila-Friedel–Crafts reaction of biphenyl **144p** containing methoxy groups instead of amino groups (Scheme 2.12b).^[76a] After the reaction, the substrate did not remain and a byproduct was obtained. The reaction detail and the structure of the byproduct were discussed in the experimental section.

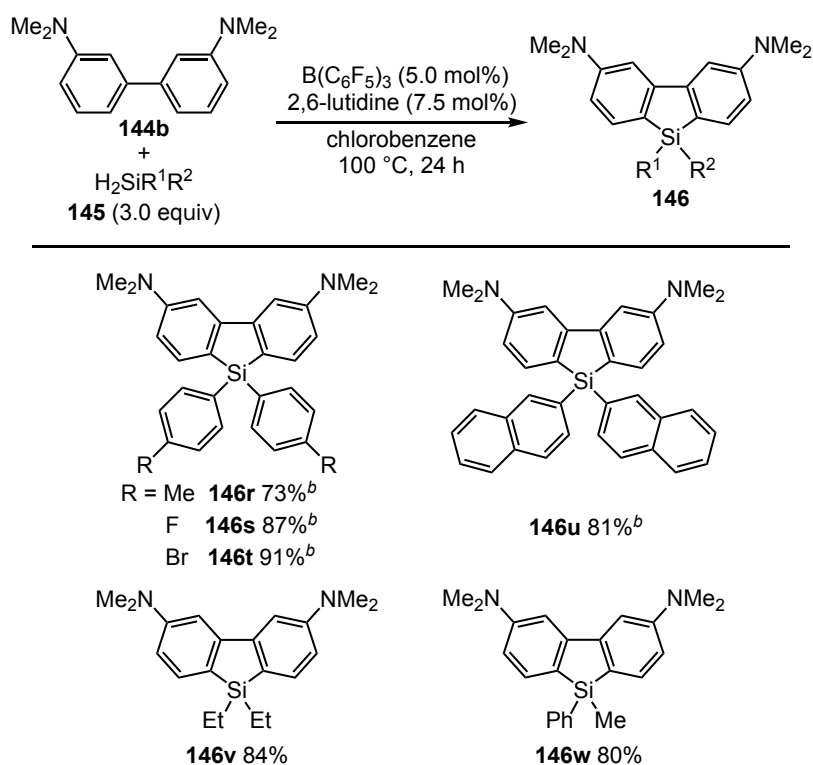
When one of the amino groups was replaced with a methylthio group, the reaction between **144q** and **145a** afforded a mixture of silylated products **146q** and **146q'** in 92% yield (ratio = 2.5:1) under the optimal reaction conditions (Scheme 2.12c). These results revealed that the amino groups are essential for regioselective synthesis of silafluorene derivatives by the double sila-Friedel–crafts reaction.

Scheme 2.12. Substrate scope of **146o**, **146p** and **146q**.



Subsequently, the scope of dihydrosilanes **145** was investigated (Scheme 2.13). Diaryldihydrosilanes bearing electron-donating or -withdrawing groups gave silafluorene derivatives **146r**, **146s**, and **146t** in 73%, 87%, and 91% yields, respectively, without loss of the halogen atoms. Silafluorene **146u** was obtained using di(2-naphthyl)silane **145e** in high yield. Phenylmethylsilane and diethyldihydrosilane were also transformed into silafluorene derivatives **146v** and **146w** in high yields.

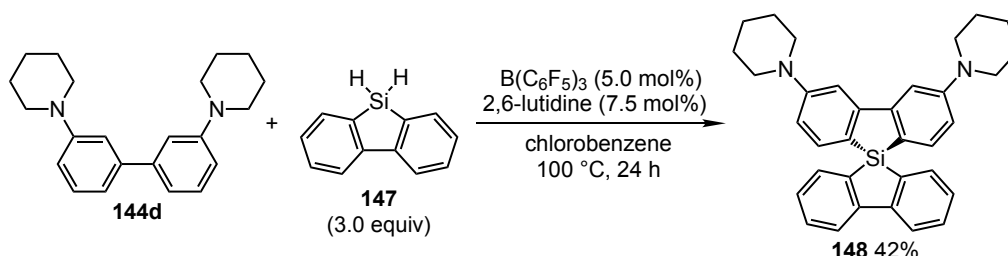
Scheme 2.13. Substrate scope of dihydrosilanes **145**.^a



^aisolated yield. ^b140 °C.

Spirosilabifluorenes are attractive scaffolds for organic optoelectronic materials.^[5b,67a] The introduction of a “spiro” linkage into organic compounds contributes to many advantageous properties, such as high thermal stabilities, facile processability, and high luminescence quantum efficiencies.^[77] It is notable that a spiro-silabifluorene derivative **148** was synthesized from biphenyl **144d** and 9,9-dihydro-5-silafluorene **147** in 42% yield (Scheme 2.14).

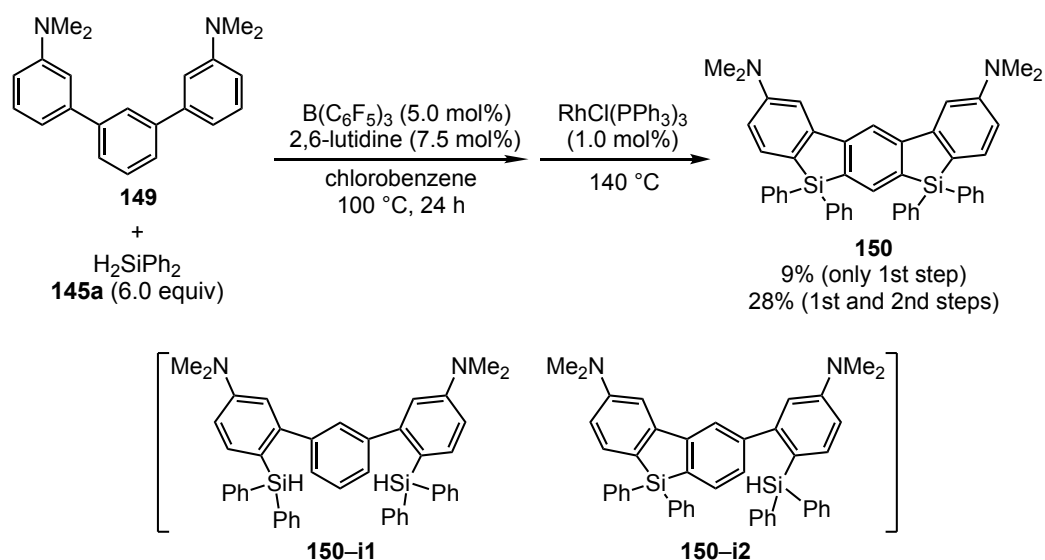
Scheme 2.14. Synthesis of spiro-silabifluorene derivative **148**.



Silicon-bridged terphenyl compounds have attracted much attention due to their optoelectronic properties. Although silicon-bridged *para*-terphenyl compounds are well

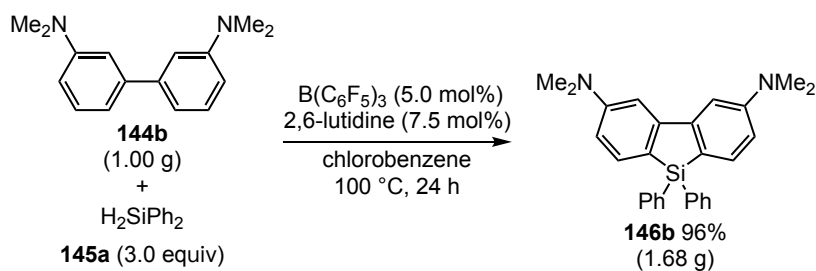
known,^[5a,55a,27a,78] examples of the synthesis of silicon-bridged *meta*-terphenyl compounds are quite rare.^[79] Hence, I investigated the synthesis of a silicon-bridged *meta*-terphenyl compound using the synthetic condition. A quadruple sila-Friedel–Crafts reaction of *meta*-terphenyl derivative **149** with diphenylsilane **145a** afforded silicon-bridged *meta*-terphenyl compound **150** in only 9% yield (Scheme 2.15). After the reaction, the signals at 5.5 ppm and 5.6 ppm were observed in the ¹H NMR of the crude products, which could be assigned as hydrogens of hydrosilyl groups of a mixture of intermediates **150-i1** and **150-i2** (Scheme 2.15). This result indicates that the intramolecular sila-Friedel–Crafts reaction on the central benzene ring did not proceed effectively. Therefore, after the intermolecular borane-catalyzed sila-Friedel–Crafts reaction, a successive rhodium-catalyzed intramolecular C–H silylation^[8] was carried out. As a result, the yield of **150** was improved to 28%.

Scheme 2.15. Synthesis of silicon-bridged terphenyl molecule **150**.



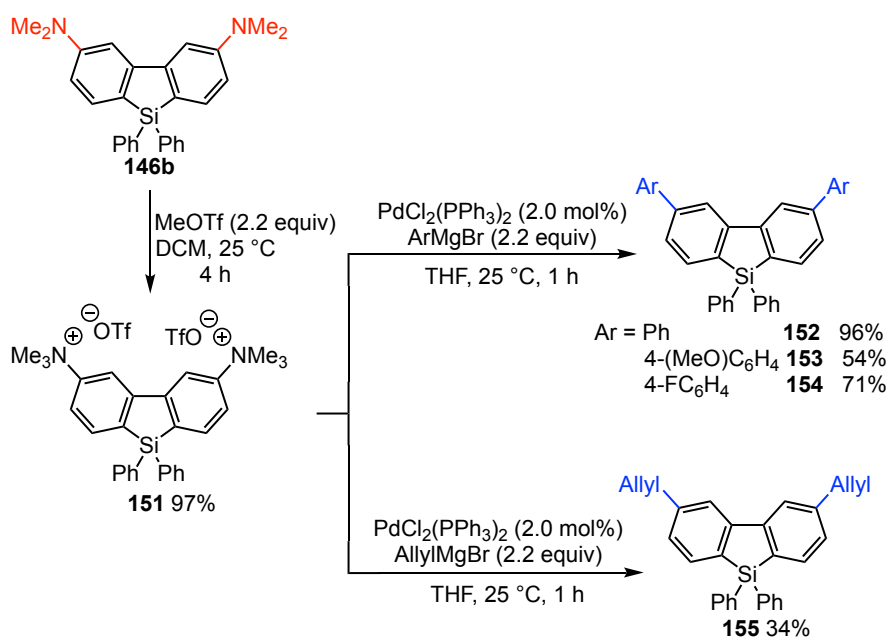
To demonstrate the practicability of this protocol, a gram-scale synthesis of silafluorene **146b** was performed (Scheme 2.16). Treatment of 1.00 g of biphenyl **144b** with 2.33 g of dihydrodiphenylsilane **145a** in the presence of catalytic amounts of $\text{B(C}_6\text{F}_5)_3$ and 2,6-lutidine in chlorobenzene afforded 1.68 g of silafluorene **146b** in 96% yield, which are comparable to the yield in the smaller scale (0.250 mmol) reaction of **144b** with **145a** (87%).

Scheme 2.16. Gram-scale synthesis of silafluorene derivative **146b**.



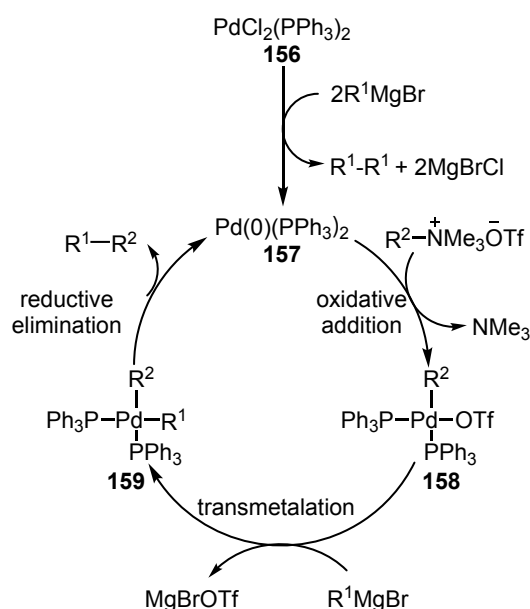
The dimethylamino (Me_2N) group is the most versatile functional group capable of highly efficient and site-selective directed aromatic functionalizations.^[61] The amino groups on the silafluorene derivatives can be converted into other functional groups (Scheme 2.17).^[80] Initially, the amino groups in **146b** were converted into their ammonium salts upon treatment with MeOTf and gave **151** in 97% yield. The activated compound **151** was then treated with a Grignard reagent PhMgBr in the presence of a palladium catalyst $PdCl_2(PPh_3)_2$ to give the cross-coupling product **152** in 96% yield. Other Grignard reagents including 4-(MeO) C_6H_4 MgBr, 4- FC_6H_4 MgBr and $(CH_2=CH-CH_2)MgBr$ also gave the corresponding silafluorenes **153–155** in moderate to good yields.

Scheme 2.17. Conversions of amino groups.



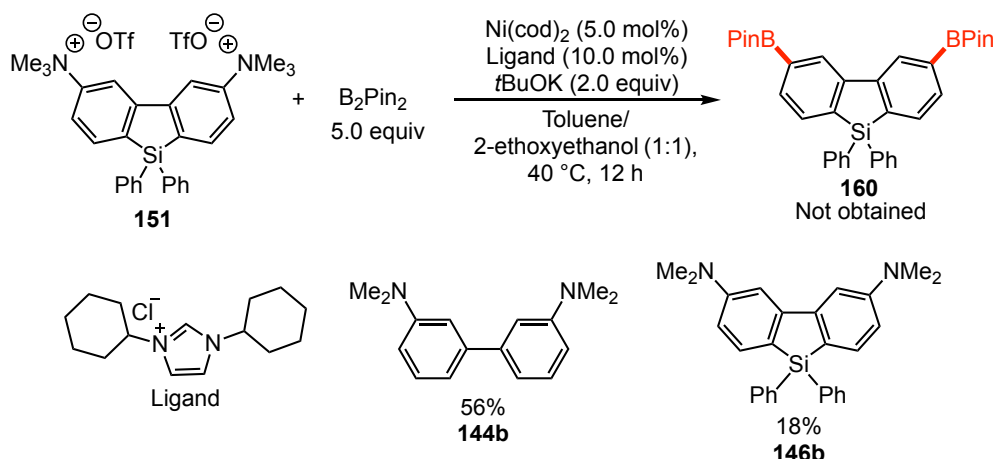
A possible catalytic pathway for the above palladium catalyzed cross coupling of aryltrimethylammonium triflates with aryl Grignard reagents was shown in Scheme 2.18. First of all, Pd(II) (**156**) was converted to Pd(0) (**157**) by reductive elimination with Grignard reagent. The resulting electron-rich Pd(0) catalyst **157** inserts into the ArNMe₃⁺OTf⁻ to form an oxidative addition species L₂Pd(OTf)Ar (**158**) and release NMe₃. Subsequent transmetalation with the Grignard reagent forms a hetero-organometallic intermediate **159**. Finally, reductive elimination of **159** forms a carbon–carbon bond and along with regeneration of the Pd(0) complex (**157**).

Scheme 2.18. Proposed mechanism for the palladium-catalyzed cross-coupling of aromatic ammonium salts with Grignard reagents



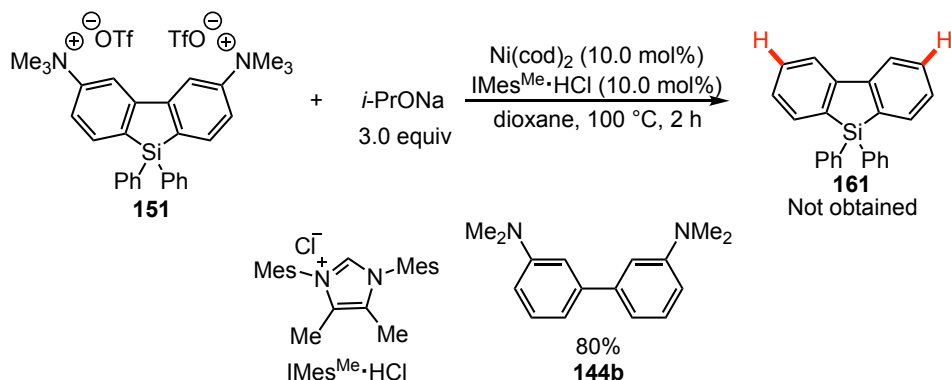
Organoboron compounds are one of the most diverse classes of reagents in organic synthesis, providing access to a mass of valuable and essential transformations.^[81] Therefore, nickel-catalyzed borylation of ammonium salt **151** was conducted. The reaction gave biphenyl **144b** (56%) and silafluorene **146b** (18%) instead of organo-boronates **160** as products (Scheme 2.19).^[82]

Scheme 2.19. Attempt of nickel-catalyzed borylation.



The common reductive deamination is carried out by catalytic hydrogenation with H_2 under transition metal catalysis. Nickel-catalyzed C–N bond reduction of aromatic ammonium triflate **151** using sodium isopropoxide as a reducing agent gave only desilylated product **144b** in 80% yield (Scheme 2.20).^[83]

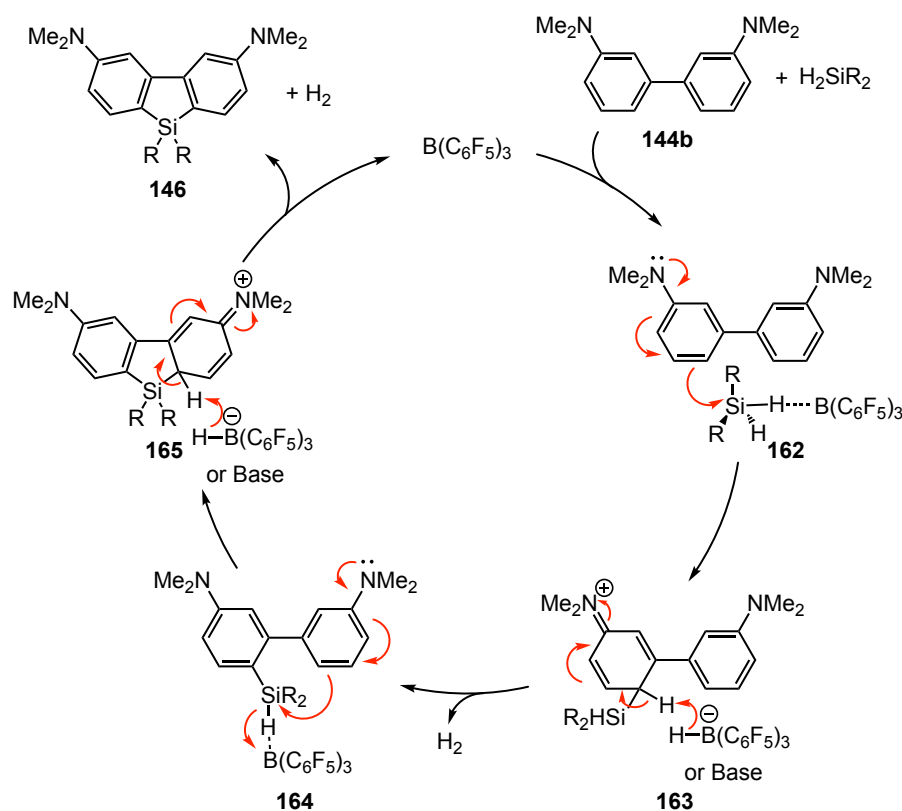
Scheme 2.20. Attempt of nickel-catalyzed C–N bond reduction.



A possible reaction pathway for the boron-catalyzed double sila-Friedel–Crafts reaction is proposed in Scheme 2.21 on the basis of previous studies of Si–H bond activation.^[30,34] The reaction starts from the activation of dihydrosilane by $\text{B}(\text{C}_6\text{F}_5)_3$ through a $\text{B}\cdots\text{H}$ interaction to form the weak adduct **162**. Nucleophilic attack of the *para*-carbon of the electron rich *N,N*-dimethylaniline at the electropositive silicon center in **162** from the back side generates ion-pair intermediate **163**. Re-aromatization of **163** along with the release of H_2 is promoted by the

abstraction of proton by hydroborate or a base. Nucleophilic attack of the other electron rich *N,N*-dimethylaniline at the electropositive silicon center in **164** generates ion-pair intermediate **165**. Release of one more molar of H₂ from **165** give desired silafluorene **146**. The formation of H₂ (at 4.49 ppm) was observed by ¹H NMR of the reaction of biphenyl **144b** with dihydrodiphenylsilane **145a** in toluene-*d*₈ (see experimental section).

Scheme 2.21. Possible mechanism for boron-catalyzed synthesis of silafluorene derivatives from biphenyls and dihydrosilanes via a double sila-Friedel–Crafts reaction.



2.3 Conclusion

In conclusion, I developed the new synthetic method of silafluorene derivatives from diamino-substituted biaryls and dihydrosilanes via a borane catalyzed double sila-Friedel–Crafts reaction. This reaction is the first example of direct synthesis of silafluorenes from biaryls and dihydrosilanes. The silafluorene derivatives were formed in moderate to excellent yields, even on gram-scale. The synthesis of multi-substituted silafluorene derivatives from readily prepared biphenyl was also achieved. Spirosilabifluorenes and silicon-bridged terphenyl derivatives can be provided using the reaction system. Additionally, the transformation of the amino groups in the silafluorene derivatives into other substituents was demonstrated. This result will lead to the synthesis of silicon-containing π -conjugated molecules with large π -conjugated systems. I hope that the reported reaction will be useful and effective for the synthesis of various silafluorene derivatives.

2.4 Experimental Section

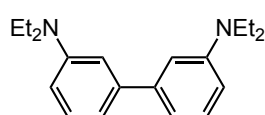
2.4.1 General

All reactions were carried out using standard Schlenk techniques under an inert atmosphere. All reagents were purchased from commercial sources and used without further purification unless otherwise noted. Silica gel column chromatography was carried using Silica gel 60 (Kanto Chemical, particle size: 40–50 μm or 63–210 μm). NMR spectra were recorded on JEOL JNM-ECA600 (600 MHz for ^1H NMR, 150 MHz for ^{13}C NMR), JEOL ECZ-400 (400 MHz for ^1H NMR, 100 MHz for ^{13}C NMR), JEOL JNM-LA400 (400 MHz for ^1H NMR, 100 MHz for ^{13}C NMR) spectrometers. Proton and carbon chemical shifts are reported relative to tetramethylsilane (TMS, δ 0.00 (^1H NMR, ^{13}C NMR)) or the residual solvent (CDCl_3 (δ 7.26 for ^1H NMR or δ 77.16 for ^{13}C NMR), CH_2Cl_2 (δ 5.32 for ^1H NMR or δ 53.84 for ^{13}C NMR), $\text{DMSO}-d_6$ (δ 2.49 for ^1H NMR or δ 39.60 for ^{13}C NMR)) used as an internal reference. HRMS were measured on a JEOL JMS-700 spectrometer. UV/vis absorption and photoluminescence (PL) spectra were measured with a V650 spectrophotometer (JASCO), and C9920-02 (Hamamatsu Photonics).

(3-(Dimethylamino)phenyl)boronic acid,^[84] di-*p*-tolylsilane,^[85a] bis(4-fluorophenyl)silane,^[85a] bis(4-bromophenyl)silane,^[85a] di(naphthalen-2-yl)silane^[85a], 9,9-dihydro-5-silafluorene,^[85b,c] 1,2-dibromo-4,5-diiodobenzene,^[86] Turbo Grignard reagents,^[87] 1-(hexyloxy)-3-iodobenzene,^[88] 3,4-dibromoaniline,^[89] 3,4-dibromo-*N,N*-dimethylaniline^[90] were prepared according to the literature procedures or modified procedures.

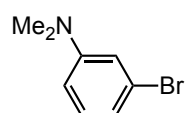
2.4.2 Synthesis and Characterization of Substrates

Biphenyl 144a



Compound **144a** was synthesized according to the reported method.^[71] Schlenk flask was charged with 3,3'-dibromobiphenyl (1.87 g, 6.00 mmol, 1.0 equiv), $\text{HN}(\text{Et})_2$ (878 mg, 12.0 mmol, 2.0 equiv), NaO^tBu (1.73 g, 18.0 mmol, 3.0 equiv), $\text{Pd}(\text{dba})_2$ (138 mg, 0.240 mmol, 4.0 mol%), P^tBu_3 (39.2 mg, 0.190 mmol, 3.2 mol%), and toluene (12 mL) under N_2 . The flask was immersed in an oil bath and heated to 130 $^\circ\text{C}$ with stirring overnight. The mixture was cooled to room temperature, filtered over Celite, and concentrated. The crude product was then purified by column chromatography (eluent: ethyl acetate) on silica gel to give **144a** as yellow solid (1.78 g, quant). ^1H NMR (400 MHz, CDCl_3) δ 7.26 (dd, $J = 8.0, 8.0$ Hz, 2H), 6.86–6.83 (m, 4H), 6.67 (dd, $J = 8.1, 2.3$ Hz, 2H), 3.40 (q, $J = 7.0$ Hz, 8H), 1.19 (t, $J = 7.0$ Hz, 12H); ^{13}C NMR (100 MHz, CDCl_3) δ 148.0, 144.0, 129.5, 114.9, 111.2, 110.6, 44.6, 12.8; HRMS(EI⁺) Calcd for $\text{C}_{20}\text{H}_{28}\text{N}_2$ ($[\text{M}]^+$) 296.2247, Found 296.2253.

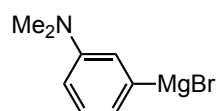
3-Bromo-*N,N*-dimethylaniline (S1)



Compound **S1** was synthesized according to the reported method.^[90] A mixture of aniline (10 mmol), iodomethane (22 mmol) and K_2CO_3 (22 mmol) in DMF (30 mL) was refluxed at 75 $^\circ\text{C}$. After completion of the reaction monitored by

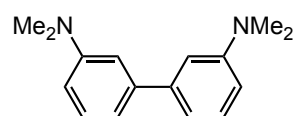
TLC, the mixture was poured into aqueous NaHCO₃ solution and extracted with ethyl acetate. The organic layer was washed with brine, dried over Na₂SO₄ and concentrated under vacuo. Purification by column chromatography on silica gel afford *N,N*-dimethylanilines (1.80 g, 90%). ¹H NMR (400 MHz, CDCl₃) δ 7.08 (dd, *J* = 8.0, 8.0 Hz, 1H), 6.84–6.81 (m, 2H), 6.64–6.61 (m, 1H), 2.94 (s, 6H). The analytical data is in accordance with the previous report.^[91]

Compound S2^[92]



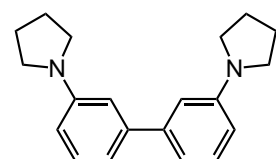
To an oven dried 25 mL two-necked round bottom flask equipped with a magnetic stir bar and a constant-pressure dropping funnel, activated magnesium turnings (460 mg, 18.9 mmol, 1.05 equiv) was added. The equipment was sealed with rubber septum, then heated with a heat gun under high vacuum for 5 minutes, evacuated, and back filled with nitrogen. After cooling to room temperature, to the funnel was added 1 M solution of 3-bromide-*N,N*-dimethylaniline (3.60 g, 18 mmol, 1.0 equiv) in THF (18 mL) by a syringe. The above solution was added dropwise at room temperature within 30 min. when 1 mL of the solution was added, 10 drops of 1,2-dibromoethane was added by a syringe to initiate the reaction. Upon addition, the flask was immersed in a preheated 50 °C oil-bath for 2 h. The prepared 3-(*N,N*-dimethylamino)phenyl magnesium bromide solution (1.0 M in THF) was stored in nitrogen atmosphere and used in the next step.

Biphenyl 144b



Compound **144b** was synthesized according to the reported method.^[73] A dried two-necked flask equipped with a magnetic stirrer was charged under nitrogen with a solution of FeCl₃ (29 mg, 0.18 mmol, 3.0 mol%) and 1,2-dichloroethane (356 mg, 3.6 mmol, 0.60 equiv) in 15 mL of THF. A solution of the 3-(*N,N*-dimethylamino)phenyl magnesium bromide **S2** in THF (1.0 M, 6 mmol) was added via a syringe. The color immediately changed to dark brown and the temperature increased. The resulting mixture was stirred at room temperature for 1 h then quenched with H₂O (10 mL). After extraction with CH₂Cl₂ (3 × 30 mL), the combined organic layers were dried over anhydrous Na₂SO₄ and concentrated under reduced pressure. The residue was purified by column chromatography (eluent: hexane/ethyl acetate = 20:1) on silica gel to give **144b** as yellowish oil (1.12 g, 78%). ¹H NMR (400 MHz, CDCl₃) δ 7.30 (dd, *J* = 8.0, 8.0 Hz, 2H), 6.96–6.94 (m, 4H) 6.76–6.73 (m, 2H), 3.00 (s, 12H); ¹³C NMR (100 MHz, CDCl₃) δ 151.0, 143.5, 129.4, 116.3, 112.1, 111.7, 40.9; HRMS(EI⁺) Calcd for C₁₆H₂₀N₂ ([M]⁺) 240.1621, Found 240.1622. The analytical data is in accordance with the previous report.^[93]

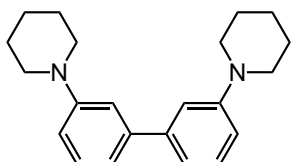
Biphenyl 144c



Compound **144c** was synthesized according to the reported method.^[74] A Schlenk flask was charged with 3,3'-dibromobiphenyl (624 mg, 2.00 mmol, 1.0 equiv), pyrrolidine (427 mg, 6.00 mmol, 3.0 equiv), NaO^tBu (577 mg, 6.00 mmol, 3.0 equiv), Pd(dba)₂ (46.0 mg, 0.08 mmol, 4.0 mol%), BINAP (149 mg, 0.240 mmol, 12 mol%), and toluene (4.0 mL) under N₂. The flask was immersed in an oil bath and heated to 80 °C with stirring overnight.

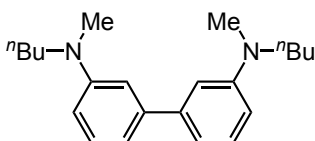
The mixture was cooled to room temperature, filtered over Celite, and concentrated. The crude product was then purified by column chromatography (eluent: ethyl acetate) on silica gel to give **144c** as yellowish solid (601 mg, quant). $^1\text{H NMR}$ (400 MHz, CDCl_3) δ 7.28 (dd, $J = 7.6$, 8.4 Hz 2H), 6.90 (d, $J = 7.3$ Hz, 2H), 6.79 (s, 2H), 6.57 (d, $J = 8.2$ Hz, 2H), 3.35 (t, $J = 6.4$ Hz, 8H), 2.04–2.01 (m, 8H); $^{13}\text{C NMR}$ (100 MHz, CDCl_3) δ 148.3, 143.7, 129.4, 115.1, 111.0, 110.7, 47.9, 25.6; HRMS(EI $^+$) Calcd for $\text{C}_{20}\text{H}_{24}\text{N}_2$ ($[\text{M}]^+$) 292.1934, Found 292.1938.

Biphenyl 144d



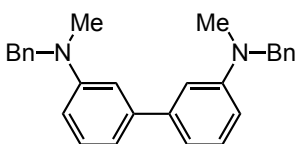
The same method as **144c**. 3,3'-dibromobiphenyl (624 mg, 2.00 mmol, 1.0 equiv), piperidine (427 mg, 6.00 mmol, 3.0 equiv), NaO^tBu (577 mg, 6.00 mmol, 3.0 equiv), $\text{Pd}(\text{dba})_2$ (46.0 mg, 0.0800 mmol, 4.0 mol%), BINAP (149 mg, 0.240 mmol, 12 mol%), and toluene (4.0 mL). **144d** was obtained as yellow solid (682 mg, quant). $^1\text{H NMR}$ (400 MHz, CDCl_3) δ 7.29 (dd, $J = 8.0$, 8.0 Hz, 2H), 7.13 (t, $J = 2.0$ Hz, 2H), 7.03 (dd, $J = 6.4$, 1.4 Hz, 2H), 6.92 (dd, $J = 8.1$, 2.0 Hz, 2H), 3.21 (t, $J = 5.7$ Hz, 8H), 1.74 (quint, 5.7 Hz, 8H), 1.60 (quint, $J = 5.7$ Hz, 4H); $^{13}\text{C NMR}$ (100 MHz, CDCl_3) δ 152.7, 143.1, 129.3, 118.7, 116.0, 115.5, 51.0, 26.1, 24.5; HRMS(EI $^+$) Calcd for $\text{C}_{22}\text{H}_{28}\text{N}_2$ ($[\text{M}]^+$) 320.2247, Found 320.2251.

Biphenyl 144e



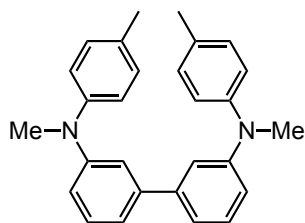
The same method as **144c**. 3,3'-dibromobiphenyl (624 mg, 2.00 mmol, 1.0 equiv), *N*-methylbutan-1-amine (419 mg, 4.80 mmol, 2.4 equiv), NaO^tBu (577 mg, 6.00 mmol, 3.0 equiv), $\text{Pd}(\text{dba})_2$ (46.0 mg, 0.0800 mmol, 4.0 mol%), BINAP (149 mg, 0.240 mmol, 12 mol%), and toluene (4.0 mL). The crude product was then purified by column chromatography (eluent: hexane/ethyl acetate = 10:1) on silica gel to give **144e** as yellow solid (289 mg, 46%). $^1\text{H NMR}$ (400 MHz, CDCl_3) δ 7.27 (dd, $J = 8.0$, 8.0 Hz, 2H), 6.89–6.87 (m, 4H), 6.68 (dd, $J = 8.5$, 2.5 Hz, 2H), 3.35 (t, $J = 7.5$ Hz, 4H), 2.97 (s, 6H), 1.61–1.55 (m, 4H), 1.36 (q, $J = 7.5$ Hz, 4H), 0.94 (t, $J = 7.3$ Hz, 6H); $^{13}\text{C NMR}$ (100 MHz, CDCl_3) δ 149.7, 143.7, 129.4, 115.4, 111.5, 111.0, 52.8, 38.6, 29.1, 20.6, 14.2; HRMS(EI $^+$) Calcd for $\text{C}_{22}\text{H}_{32}\text{N}_2$ ($[\text{M}]^+$) 324.2560, Found 324.2564.

Biphenyl 144f



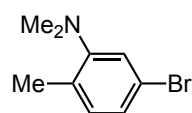
The same method as **144c**. 3,3'-dibromobiphenyl (624 mg, 2.00 mmol, 1.0 equiv), *N*-methylbenzylamine (582 mg, 4.80 mmol, 2.4 equiv), NaO^tBu (577 mg, 6.00 mmol, 3.0 equiv), $\text{Pd}(\text{dba})_2$ (46.0 mg, 0.0800 mmol, 4.0 mol%), BINAP (149 mg, 0.240 mmol, 12 mol%), and toluene (4.0 mL). The crude product was then purified further by column chromatography (eluent: hexane/ethyl acetate = 19:1) on silica gel (pretreated with 1% NEt_3 in hexane) to give **144f** as yellowish oil (740 mg, 94%). $^1\text{H NMR}$ (400 MHz, CDCl_3) δ 7.36–7.27 (m, 4H), 7.27–7.15 (m, 8H), 6.91–6.89 (m, 4H), 6.74–6.71 (m, 2H), 4.55 (s, 4H), 3.04 (s, 6H); $^{13}\text{C NMR}$ (100 MHz, CDCl_3) δ 150.0, 143.4, 139.1, 129.4, 128.6, 126.9, 126.9, 116.0, 111.7, 111.4, 56.9, 38.7; HRMS(EI $^+$) Calcd for $\text{C}_{20}\text{H}_{28}\text{N}_2$ ($[\text{M}]^+$) 392.2247, Found 392.2251.

Biphenyl 144g



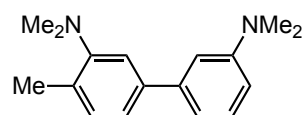
The same method as **144c**. 3,3'-dibromobiphenyl (624 mg, 2.00 mmol 1.0 equiv), *N*-methyl-*p*-toluidine (582 mg, 4.80 mmol, 2.4 equiv), NaO^tBu (577 mg, 6.00 mmol, 3.0 equiv), Pd(dba)₂ (46.0 mg, 0.0800 mmol, 4.0 mol%), BINAP (149 mg, 0.240 mmol, 12 mol%), and toluene (4.0 mL). The crude product was then purified by column chromatography (eluent: hexane/ethyl acetate = 20:1) on silica gel (pretreated with 1% NEt₃ in hexane) to give **144g** as a white solid (665 mg, 85%). ¹H NMR (400 MHz, CDCl₃) δ 7.36–7.27 (m, 4H), 7.27–7.15 (m, 8H), 6.90 (d, *J* = 6.8 Hz 2H), 6.89 (d, *J* = 2.0 Hz 2H), 6.72 (dd, *J* = 6.8, 2.0 Hz, 2H), 4.55 (s, 4H), 3.04 (s, 6H); ¹³C NMR (100 MHz, CDCl₃) δ 150.0, 143.4, 139.1, 129.4, 128.6, 126.93, 126.87, 116.0, 111.7, 111.4, 56.9, 38.7; HRMS(EI⁺) Calcd for C₂₈H₂₈N₂ ([M]⁺) 392.2247, Found 392.2252.

5-Bromo-*N,N*,2-trimethylaniline (S3)



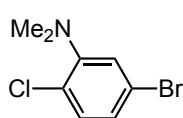
To a solution of 5-bromo-2-methylaniline (1.12 g, 6.00 mmol, 1.0 equiv) in dry DMF (30 mL) were added MeI (4.26 g, 30.0 mmol, 5.0 equiv) and NaH (720 mg, 18.0 mmol, 3.0 equiv; 60 wt% in mineral oil). After 1 h, the reaction was quenched with water (5 mL). Brine (25 mL) and Et₂O (25 mL) were added. The organic layer was separated, washed with brine (2 × 25 mL), dried over anhydrous MgSO₄, filtered and concentrated. The crude product was then purified by column chromatography (eluent: hexane/ethyl acetate = 20:1) on silica gel to give 5-bromo-*N,N*,2-trimethylaniline as colorless oil (964 mg, 75%). ¹H NMR (400 MHz, CDCl₃) δ 7.11 (d, *J* = 1.8 Hz, 1H), 7.06 (dd, *J* = 8.2, 1.8 Hz, 1H), 7.00 (d, *J* = 8.2 Hz, 1H), 2.68 (s, 6H), 2.26 (s, 3H); ¹³C NMR (100 MHz, CDCl₃) δ 154.2, 132.5, 130.9, 125.3, 121.8, 119.7, 44.1, 18.2; HRMS(EI⁺) Calcd for C₉H₁₂BrN ([M]⁺) 213.0148, Found 213.0152.

Biphenyl 144h



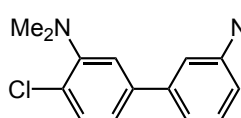
A mixture of (3-(dimethylamino)phenyl)boronic acid (330 mg, 2.00 mmol, 1.0 equiv), 5-bromo-*N,N*,2-trimethylaniline (428 mg, 2.00 mmol, 1.0 equiv), Na₂CO₃ (424 mg, 4.00 mmol, 2.0 equiv) and Pd(PPh₃)₄ (57.8 mg, 0.0500 mmol, 2.5 mol%) in a mixture of toluene (25 mL), water (4 mL) and ethanol (8 mL) was heated to 80 °C under nitrogen. After completion of the reaction monitored by TLC, the mixture was cooled to room temperature then diluted with water and EtOAc. The aqueous layer was extracted with EtOAc (3 × 30 mL). The combined organic phase was dried over MgSO₄ and concentrated under reduced pressure. The crude product was then purified by column chromatography (eluent: hexane/ethyl acetate 20:1) on silica gel to give **144h** (208 mg, 60%) as colorless oil. ¹H NMR (400 MHz, CDCl₃) δ 7.30 (dd, *J* = 8.0, 8.0 Hz, 1H), 7.25–7.19 (m, 3H), 6.93 (d, *J* = 7.8 Hz, 2H), 6.75–6.73 (m, 1H), 3.00 (s, 6H), 2.77 (s, 6H), 2.38 (s, 3H); ¹³C NMR (100 MHz, CDCl₃) δ 153.0, 151.1, 142.8, 140.9, 131.5, 131.1, 129.4, 121.6, 117.7, 116.0, 111.8, 111.6, 44.4, 40.9, 18.3; HRMS(EI⁺) Calcd for C₁₇H₂₂N₂ ([M]⁺) 254.1778, Found 254.1783.

5-Bromo-2-chloro-*N,N*-dimethylaniline (S4)



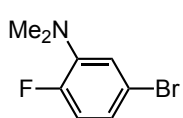
The same method as 5-bromo-*N,N*,2-trimethylaniline. 5-Bromo-2-chloroaniline (1.03 g, 5.00 mmol, 1.0 equiv), MeI (1.55 mL, 25.0 mmol, 5.0 equiv) and NaH (600 mg, 15.0 mmol, 3.0 equiv; 60 wt% in mineral oil) were used. The crude product was then purified by column chromatography (eluent: hexane/ethyl acetate = 20:1) on silica gel to give the desired compound as colorless oil (1.022 g, 87%). ¹H NMR (400 MHz, CDCl₃) δ 7.19 (d, *J* = 8.2 Hz, 1H), 7.15 (d, *J* = 2.3 Hz, 1H), 7.05 (dd, *J* = 8.2, 2.3 Hz, 1H), 2.81 (s, 6H); ¹³C NMR (100 MHz, CDCl₃) δ 151.7, 131.9, 127.1, 126.0, 123.4, 120.9, 43.7; HRMS(EI⁺) Calcd for C₈H₉BrClN ([M]⁺) 232.9601, Found 232.9609.

Biphenyl 144i



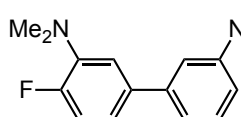
The same method as **144h**. A mixture of (3-(dimethylamino)phenyl)boronic acid (248 mg, 1.50 mmol, 1.0 equiv), 5-bromo-2-chloro-*N,N*-dimethylaniline (352 mg, 1.50 mmol, 1.0 equiv), Na₂CO₃ (318 mg, 3.00 mmol, 2.0 equiv) and Pd(PPh₃)₄ (43.3 mg, 0.0375 mmol, 2.5 mol%) in a mixture of toluene (20 mL), water (2 mL) and ethanol (4 mL) was heated to 80 °C under nitrogen. After completion of the reaction monitored by TLC, the mixture was cooled to room temperature then diluted with water and EtOAc. The aqueous layer was extracted with EtOAc (3 × 30 mL). The combined organic phase was dried over MgSO₄ and concentrated under reduced pressure. The crude product was then purified by column chromatography (eluent: hexane/ethyl acetate = 15:1) on silica gel to give **144i** (323 mg, 78%) as colorless oil. ¹H NMR (400 MHz, CDCl₃) δ 7.39 (d, *J* = 8.2 Hz, 1H), 7.31 (dd, *J* = 7.8, 8.4 Hz, 1H), 7.27 (s, 1H), 7.16 (dd, *J* = 8.0, 2.1 Hz, 1H), 6.91–6.86 (m, 2H), 6.76 (dd, *J* = 8.2, 1.8 Hz, 1H), 3.01 (s, 6H), 2.87 (s, 6H); ¹³C NMR (100 MHz, CDCl₃) δ 151.1, 150.5, 142.0, 141.8, 130.9, 129.6, 127.3, 122.2, 119.2, 115.8, 112.0, 111.5, 44.0, 40.8; HRMS(EI⁺) Calcd for C₁₆H₁₉ClN₂ ([M]⁺) 274.1231, Found 274.1236.

5-Bromo-2-fluoro-*N,N*-dimethylaniline (S5)



The same method as 5-bromo-*N,N*,2-trimethylaniline. 5-Bromo-2-fluoroaniline (1.52 g, 8.00 mmol, 1.0 equiv), MeI (5.68 g, 40.0 mmol, 5.0 equiv) and NaH (960 mg, 24.0 mmol, 3.0 equiv; 60 wt% in mineral oil) were used. The crude product was then purified by column chromatography (eluent: hexane/ethyl acetate = 20:1) on silica gel to give the desired compound as colorless oil (1.30 g, 74%). ¹H NMR (400 MHz, CDCl₃) δ 6.98–6.84 (m, 3H), 2.84 (s, 6H); ¹³C NMR (100 MHz, CDCl₃) δ 154.0 (*J*_{C-F} = 243.4 Hz), 142.1 (*J*_{C-F} = 9.6 Hz), 123.2 (*J*_{C-F} = 7.7 Hz), 121.1 (*J*_{C-F} = 2.9 Hz), 117.5 (*J*_{C-F} = 22.0 Hz), 116.8, 42.6 (*J*_{C-F} = 4.8 Hz); HRMS(EI⁺) Calcd for C₈H₉BrFN ([M]⁺) 216.9897, Found 216.9903.

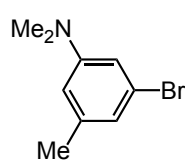
Biphenyl 144j



The same method as **144h**. A mixture of (3-(dimethylamino)phenyl)boronic acid (330 mg, 2.00 mmol, 1.0 equiv), 5-bromo-2-fluoro-*N,N*-dimethylaniline (436 mg, 2.00 mmol, 1.0

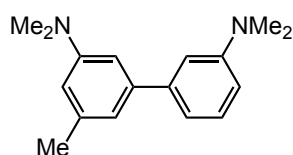
equiv), Na₂CO₃ (424 mg, 4.00 mmol, 2.0 equiv) and Pd(PPh₃)₄ (57.8 mg, 0.0500 mmol, 2.5 mol%) in a mixture of toluene (25 mL), water (4 mL) and ethanol (8 mL) was heated to 80 °C under nitrogen. After completion of the reaction monitored by TLC, the mixture was cooled to room temperature, then diluted with water and EtOAc. The aqueous layer was extracted with EtOAc (3 × 30 mL). The combined organic phase was dried over MgSO₄ and concentrated under reduced pressure. The crude product was then purified by column chromatography (eluent: hexane/ethyl acetate = 10:1) on silica gel to give **144j** (421 mg, 81%) as a colorless oil. ¹H NMR (400 MHz, CDCl₃) δ 7.30 (dd, *J* = 7.8, 8.4 Hz, 1H), 7.11–7.05 (m, 3H), 6.90–6.86 (m, 2H), 6.74 (dd, *J* = 8.2, 2.7 Hz, 1H), 3.01 (s, 6H), 2.90 (s, 6H); ¹³C NMR (100 MHz, CDCl₃) δ 154.9 (*J*_{C-F} = 244.4 Hz), 151.0, 142.2, 140.8 (*J*_{C-F} = 9.6 Hz), 138.90, 138.87, 129.5, 120.1 (*J*_{C-F} = 6.7 Hz), 117.7, 116.3 (*J*_{C-F} = 22.0 Hz), 116.0, 111.7, 43.0, 40.9; HRMS(EI⁺) Calcd for C₁₆H₁₉FN₂ ([M]⁺) 258.1527, Found 258.1531.

3-Bromo-*N,N*,5-trimethylaniline (S6)



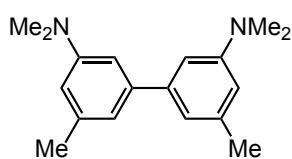
The same method as 5-bromo-*N,N*,2-trimethylaniline. 3-Bromo-5-methylaniline (1.12 g, 6.00 mmol, 1.0 equiv), K₂CO₃ (7.50 g, 54.0 mmol, 9.0 equiv), MeI (4.26 g, 30.0 mmol, 5.0 equiv) and DMF (15 mL). The crude product was then purified by column chromatography (eluent: hexane/ethyl acetate = 10:1) on silica gel to give the desired compound as a colorless oil (1.00 g, 78%). ¹H NMR (400 MHz, CDCl₃) δ 6.67–6.65 (m, 2H), 6.43 (s, 1H), 2.92 (s, 6H), 2.27 (s, 3H); ¹³C NMR (100 MHz, CDCl₃) δ 151.7, 140.5, 123.3, 120.2, 112.6, 111.9, 40.6, 21.8; HRMS(EI⁺) Calcd for C₉H₁₂BrN ([M]⁺) 213.0148, Found 213.0154.

Biphenyl 144k



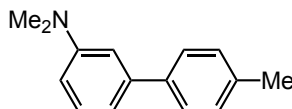
The same method as **144h**. A mixture of (3-(dimethylamino)phenyl)boronic acid (330 mg, 2.00 mmol, 1.0 equiv), 3-bromo-*N,N*,5-trimethylaniline (428 mg, 2.00 mmol, 1.0 equiv), Na₂CO₃ (424 mg, 4.00 mmol, 2.0 equiv) and Pd(PPh₃)₄ (57.8 mg, 0.0500 mmol, 2.5 mol%) in a mixture of toluene (25 mL), water (4 mL) and ethanol (8 mL) was heated to 80 °C under nitrogen. After completion of the reaction monitored by TLC, the mixture was cooled to room temperature then diluted with water and EtOAc. The aqueous layer was extracted with EtOAc (3 × 30 mL). The combined organic phase was dried over MgSO₄ and concentrated under reduced pressure. The crude product was then purified by column chromatography (eluent: hexane/ethyl acetate = 25:1) on silica gel to give **144k** (399 mg, 78%) as a colorless oil. ¹H NMR (400 MHz, CDCl₃) δ 7.29 (dd, *J* = 8.0, 8.0 Hz, 1H), 6.95–6.93 (m, 2H), 6.78–6.73 (m, 3H), 6.57 (s, 1H), 3.00 (s, 6H), 2.99 (s, 6H), 2.39 (s, 3H); ¹³C NMR (100 MHz, CDCl₃) δ 151.1, 151.0, 143.6, 143.5, 139.0, 129.3, 117.4, 116.3, 112.6, 112.1, 111.7, 109.5, 41.0, 40.9, 22.1; HRMS(EI⁺) Calcd for C₁₇H₂₂N₂ ([M]⁺) 254.1778, Found 254.1779.

Biphenyl 144l



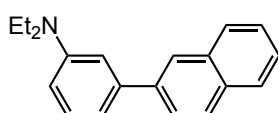
The same method as **144h**. A mixture of (3-(dimethylamino)-5-methylphenyl)boronic acid (269 mg, 1.50 mmol, 1.0 equiv), 3-bromo-*N,N*,5-trimethylaniline (321 mg, 1.50 mmol, 1.0 equiv), Na₂CO₃ (318 mg, 3.00 mmol, 2.0 equiv) and PdCl₂(PPh₃)₂ (26.3 mg, 0.0380 mmol, 2.5 mol%) in a mixture of toluene (15 mL), water (2 mL) and ethanol (4 mL) was heated to 80 °C under nitrogen. After completion of the reaction monitored by TLC, the mixture was cooled to room temperature then diluted with water and EtOAc. The aqueous layer was extracted with EtOAc (3 × 30 mL). The combined organic phase was dried over MgSO₄ and concentrated under reduced pressure. The crude product was then purified by column chromatography (eluent: hexane/ethyl acetate = 30:1) on silica gel to give **144l** (295 mg, 73%) as white solid. ¹H NMR (400 MHz, CDCl₃) δ 6.77–6.75 (m, 4H), 6.56 (s, 2H), 2.98 (s, 12H), 2.38 (s, 6H); ¹³C NMR (100 MHz, CDCl₃) δ 151.1, 143.6, 138.9, 117.4, 112.5, 109.6, 41.0, 22.1; HRMS(EI⁺) Calcd for C₁₈H₂₄N₂ ([M]⁺) 268.1934, Found 268.1939.

Biphenyl 144m



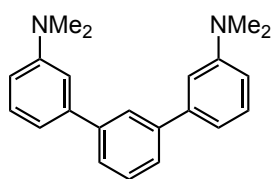
A mixture of 3-(*N,N*-dimethylamino)phenylboronic acid (330 mg, 2.00 mmol, 1.0 equiv), *p*-bromotoluene (342 mg, 2.00 mmol, 1.0 equiv), K₂CO₃ (829 mg, 6.00 mmol, 3.0 equiv) and Pd(PPh₃)₄ (57.8 mg, 0.0500 mmol, 2.5 mol%) in a mixture of water (1.4 mL) and dimethoxyethane (0.7 mL) was heated to 80 °C under nitrogen overnight. After cooled to room temperature, the mixture was diluted with water and EtOAc. The aqueous layer was extracted with EtOAc (3 × 30 mL). The combined organic phase was dried over Na₂SO₄ and concentrated under reduced pressure. The residue was dissolved in ethanol. Water was added and the mixture was evaporated to dryness. The crude product was then purified by column chromatography (eluent: hexane/ethyl acetate = 10:1) on silica gel (pretreated with 1% NEt₃ in hexane) to give **144m** (419 mg, 99%) as a colorless oil. ¹H NMR (400 MHz, CDCl₃) δ 7.51 (dt, *J* = 8.3, 1.9 Hz, 2H), 7.31 (t, *J* = 8.1 Hz, 1H), 7.25 (d, *J* = 8.3 Hz, 2H), 6.97–6.89 (m, 2H), 6.74 (dd, *J* = 8.1, 2.7 Hz, 1H), 3.01 (s, 6H), 2.40 (s, 3H); ¹³C NMR (100 MHz, CDCl₃) δ 151.0, 142.3, 139.5, 137.0, 129.5, 129.5, 127.3, 115.8, 111.6, 111.5, 40.9, 21.3; HRMS(MALDI⁺) Calcd for C₁₅H₁₇N ([M]⁺) 211.1356, Found 211.1362.

Biphenyl 144n



The same method as **144m**. ¹H NMR (400 MHz, CDCl₃) δ 8.02 (d, *J* = 0.7 Hz, 1H), 7.91–7.85 (m, 3H), 7.75 (dd, *J* = 8.2, 1.8 Hz, 1H), 7.52–7.45 (m, 2H), 7.33 (t, *J* = 8.0 Hz, 1H), 6.99–6.98 (m, 2H), 6.74–6.71 (m, 1H), 3.44 (q, *J* = 7.0 Hz, 4H), 1.23 (t, *J* = 6.9 Hz, 6H); ¹³C NMR (100 MHz, CDCl₃) δ 148.3, 142.5, 140.0, 135.7, 133.7, 132.7, 129.8, 128.3, 128.0, 127.7, 126.2, 126.1, 125.9, 125.8, 115.0, 111.1, 44.6, 12.8; HRMS(EI⁺) Calcd for C₂₀H₂₁N ([M]⁺) 275.1669, Found 275.1676.

*N*³,*N*³,*N*^{3'},*N*^{3'}-Tetramethyl-[1,1':3',1''-terphenyl]-3,3''-diamine **149**

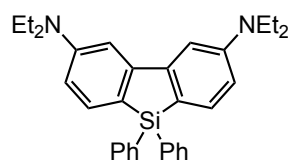


The same method as **144h**. A mixture of (3-(dimethylamino)phenyl)boronic acid (545 mg, 3.30 mmol, 2.2 equiv), 1,3-dibromobenzene (354 mg, 1.50 mmol, 1.0 equiv), Na₂CO₃ (795 mg, 7.50 mmol, 5.0 equiv) and Pd(PPh₃)₄ (87.0 mg, 0.0750 mmol, 5.0 mol%) in a mixture of toluene (15 mL), water (2 mL) and ethanol (4 mL) was heated to 80 °C under nitrogen. After completion of the reaction monitored by TLC, the mixture was cooled to room temperature, then diluted with water and EtOAc. The aqueous layer is extracted with EtOAc (3 × 30 mL). The combined organic phases are dried over MgSO₄ and concentrated under reduced pressure. The crude product was then purified further by column chromatography (eluent: hexane/ethyl acetate = 20:1) on silica gel to give **149** (354 mg, 75%) as a colorless oil. ¹H NMR (400 MHz, CDCl₃) δ 7.81 (t, *J* = 1.6 Hz, 1H), 7.58–7.55 (m, 2H), 7.48 (dd, *J* = 8.6, 7.0 Hz, 1H), 7.33 (t, *J* = 8.0 Hz, 2H), 7.01–6.97 (m, 4H), 6.77 (dd, *J* = 8.2, 2.3 Hz, 2H), 3.01 (s, 12H); ¹³C NMR (100 MHz, CDCl₃) δ 151.1, 142.8, 142.5, 129.6, 129.0, 126.7, 126.3, 116.1, 111.9, 40.9 (one carbon is missing); HRMS(EI⁺) Calcd for C₂₂H₂₄N₂ ([M]⁺) 316.1934, Found 316.1940.

2.4.3 General Procedure for Boron-catalyzed Double Sila-Friedel–Crafts Reaction^[34]

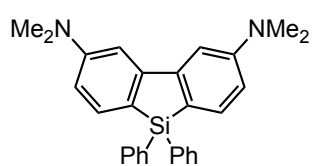
To a test tube with a screw cap equipped with a magnetic stir bar was charged biphenyl **144a** (74.1 mg, 0.250 mmol, 1.0 equiv) and tris(pentafluorophenyl)borane (B(C₆F₅)₃, 6.4 mg, 0.013 mmol, 5.0 mol%). The test tube was evacuated and filled with nitrogen. Chlorobenzene (0.50 mL) was added via syringe. Diphenylsilane **145a** (0.14 mL, 138 mg, 0.750 mmol, 3.0 equiv) and 2,6-lutidine (2.2 μL, 2.0 mg, 0.019 mmol, 7.5 mol%) were then added to the mixture. The test tube was closed with a cap. The reaction mixture was stirred at 100 °C (oil bath) for 24 h. After completion of the reaction, the mixture was cooled to room temperature. The resulting mixture was subjected to ¹H NMR spectroscopy. The crude NMR yields were calculated on the basis of 1,1,2,2-tetrachloroethane (26.4 μL, 42.0 mg, 0.25 mmol, 1.0 equiv). The desired silafluorene **146a** was obtained by column chromatography (eluent: hexane/ethyl acetate = 15:1) on silica gel in 87% isolated yield.

Silafluorene **146a**



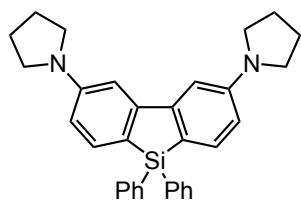
146a was obtained as white solid (104.1 mg, 87%). ¹H NMR (400 MHz, CDCl₃) δ 7.65 (d, *J* = 7.3 Hz, 4H), 7.57 (d, *J* = 8.2 Hz, 2H), 7.38–7.28 (m, 6H), 7.16 (s, 2H), 6.64 (d, *J* = 8.2 Hz, 2H), 3.45 (q, *J* = 7.1 Hz, 8H), 1.22 (t, *J* = 7.1 Hz, 12H); ¹³C NMR (100 MHz, CDCl₃) δ 150.8, 149.9, 135.6, 135.3, 134.8, 129.5, 127.9, 121.4, 111.5, 104.3, 44.6, 12.8; HRMS(EI⁺) Calcd for C₃₂H₃₆N₂Si ([M]⁺) 476.2642, Found 476.2647.

Silafluorene 146b



146b was obtained as white solid (1.68 g, 96%). ^1H NMR (400 MHz, CDCl_3) δ 7.67 (dd, $J = 8.0, 1.6$ Hz, 4H), 7.62 (d, $J = 8.1$ Hz, 2H), 7.43–7.28 (m, 6H), 7.26 (d, $J = 2.4$ Hz, 2H), 6.71 (dd, $J = 8.1, 2.4$ Hz, 2H), 3.08 (s, 12H); ^{13}C NMR (100 MHz, CDCl_3) δ 152.6, 150.5, 135.6, 134.9, 134.6, 129.6, 127.9, 122.7, 112.2, 105.0, 40.7; HRMS(EI^+) Calcd for $\text{C}_{28}\text{H}_{28}\text{N}_2\text{Si}$ ($[\text{M}]^+$) 420.2016, Found 420.2024.

Silafluorene 146c



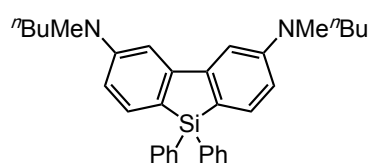
146c was obtained as white solid (106.9 mg, 90%). ^1H NMR (400 MHz, CDCl_3) δ 7.65 (dd, $J = 7.8, 1.4$ Hz, 4H), 7.58 (d, $J = 7.8$ Hz, 2H), 7.40–7.23 (m, 6H), 7.07 (d, $J = 2.3$ Hz, 2H), 6.54 (dd, $J = 7.8, 2.3$ Hz, 2H), 3.42 (t, $J = 6.6$ Hz, 8H), 2.02 (quint, $J = 6.6$ Hz, 8H); ^{13}C NMR (100 MHz, CDCl_3) δ 150.7, 150.0, 135.7, 134.6, 129.5, 127.9, 121.7, 112.0, 111.7, 104.5, 47.8, 25.6; HRMS(EI^+) Calcd for $\text{C}_{32}\text{H}_{32}\text{N}_2\text{Si}$ ($[\text{M}]^+$) 472.2329, Found 472.2337.

Silafluorene 146d



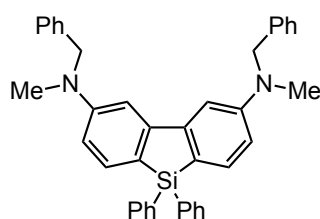
146d was obtained as white solid (101 mg, 81%). ^1H NMR (400 MHz, CDCl_3) δ 7.67 (dd, $J = 6.4, 1.6$ Hz, 4H), 7.64 (d, $J = 7.8$ Hz, 2H), 7.45 (d, $J = 1.8$ Hz, 2H), 7.43–7.28 (m, 6H), 6.90 (dd, $J = 8.0, 2.1$ Hz, 2H), 3.30 (t, $J = 5.5$ Hz, 8H), 1.79 (quin, $J = 5.5$ Hz, 8H), 1.63 (quin, $J = 5.5$ Hz, 4H); ^{13}C NMR (100 MHz, CDCl_3) δ 154.5, 150.4, 135.6, 134.6, 134.5, 129.7, 128.0, 125.7, 115.8, 109.2, 50.5, 26.0, 24.5; HRMS(EI^+) Calcd for $\text{C}_{34}\text{H}_{36}\text{N}_2\text{Si}$ ($[\text{M}]^+$) 500.2642, Found 500.2649.

Silafluorene 146e



146e was obtained as white solid (105 mg, 82%). ^1H NMR (400 MHz, CDCl_3) δ 7.66–7.64 (m, 4H), 7.58 (d, $J = 8.2$ Hz, 2H), 7.36–7.29 (m, 6H), 7.20 (d, $J = 1.8$ Hz, 2H), 6.66 (dd, $J = 8.0, 2.1$ Hz, 2H), 3.42 (t, $J = 7.5$ Hz, 4H), 3.05 (s, 6H), 1.63 (q, $J = 7.5$ Hz, 4H), 1.40 (q, $J = 7.5$ Hz, 4H), 0.99 (t, $J = 7.3$ Hz, 6H); ^{13}C NMR (100 MHz, CDCl_3) δ 151.4, 150.7, 135.6, 135.2, 134.6, 129.5, 127.9, 121.8, 111.7, 104.5, 52.6, 38.6, 29.1, 20.5, 14.2; HRMS (EI^+) Calcd for $\text{C}_{34}\text{H}_{40}\text{N}_2\text{Si}$ ($[\text{M}]^+$) 504.2955, Found 504.2959.

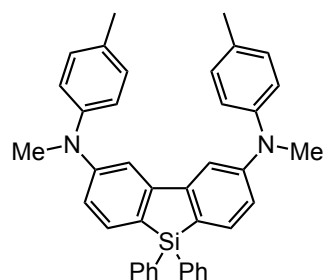
Silafluorene 146f



146f was obtained as white solid (111 mg, 78%). ^1H NMR (400 MHz, CDCl_3) δ 7.64 (dd, $J = 7.8, 1.4$ Hz, 4H), 7.57 (d, $J = 8.2$ Hz, 2H), 7.37–7.23 (m, 16H), 7.15 (d, $J = 2.5$ Hz, 2H), 6.69 (dd, $J = 7.8, 2.3$ Hz, 2H), 4.59 (s, 4H), 3.11 (s, 6H); ^{13}C NMR (100 MHz, CDCl_3) δ 151.9, 150.5, 139.2, 135.6, 135.0, 134.7, 129.6, 128.8, 127.9, 127.1,

126.9, 122.8, 112.2, 105.1, 56.9, 38.9; HRMS(FAB⁺) Calcd for C₄₀H₃₆N₂Si ([M]⁺) 572.2642, Found 572.2649.

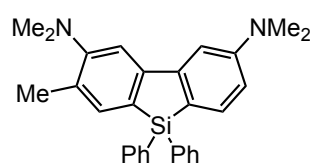
Silafluorene 146g



572.2648.

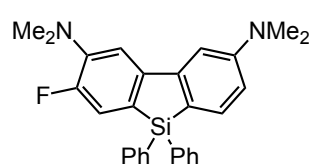
146g was obtained as white solid (48.6 mg, 34%). ¹H NMR (400 MHz, CDCl₃) δ 7.67–7.65 (m, 4H), 7.57 (d, *J* = 7.8 Hz, 2H), 7.38–7.30 (m, 8H), 7.13 (d, *J* = 8.2 Hz, 4H), 7.05 (dd, *J* = 6.4, 1.8 Hz, 4H), 6.81 (dd, *J* = 8.0, 2.1 Hz, 2H), 3.35 (s, 6H), 2.34 (s, 6H); ¹³C NMR (100 MHz, CDCl₃) δ 151.6, 150.3, 146.2, 135.6, 134.5, 134.3, 132.8, 130.0, 129.8, 128.0, 126.0, 123.4, 117.3, 110.0, 40.4, 20.9; HRMS(EI⁺) Calcd for C₄₀H₃₆N₂Si ([M]⁺) 572.2642, Found

Silafluorene 146h



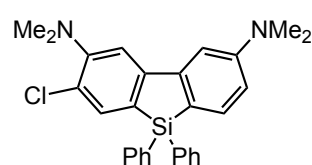
General procedure using *N*³,*N*³,*N*^{3'},*N*^{3'},4-pentamethyl-[1,1'-biphenyl]-3,3'-diamine (63.6 mg, 0.250 mmol) and diphenylsilane (138 mg, 0.750 mmol) at 100 °C for 24 h. The desired compound **146h** was obtained as white powder (91.0 mg, 84%). ¹H NMR (400 MHz, CDCl₃) δ 7.66–7.64 (m, 4H), 7.60 (d, *J* = 8.2 Hz, 1H), 7.51 (d, *J* = 3.7 Hz, 2H), 7.37–7.29 (m, 6H), 7.20 (d, *J* = 1.8 Hz, 1H), 6.68 (dd, *J* = 7.8, 2.3 Hz, 1H), 3.08 (s, 6H), 2.80 (s, 6H), 2.33 (s, 3H); ¹³C NMR (100 MHz, CDCl₃) δ 155.1, 152.7, 150.6, 148.1, 136.5, 135.6, 134.7, 134.5, 131.4, 130.2, 129.7, 128.0, 121.5, 111.9, 110.8, 104.8, 44.1, 40.6, 18.8; HRMS (EI⁺) Calcd for C₂₉H₃₀N₂Si ([M]⁺) 434.2173, Found 434.2179.

Silafluorene 146i



General procedure using 4-fluoro-*N*³,*N*³,*N*^{3'},*N*^{3'}-tetramethyl-[1,1'-biphenyl]-3,3'-diamine (64.6 mg, 0.250 mmol) and diphenylsilane (138 mg, 0.750 mmol) at 100 °C for 24 h. The desired compound **146i** was obtained as white powder (104 mg, 95%). ¹H NMR (400 MHz, CDCl₃) δ 7.65–7.62 (m, 4H), 7.60 (d, *J* = 7.8 Hz, 1H), 7.39–7.31 (m, 8H), 7.14 (d, *J* = 2.3 Hz, 1H), 6.68 (dd, *J* = 8.2, 2.3 Hz, 1H), 3.08 (s, 6H), 2.96 (s, 6H); ¹³C NMR (100 MHz, CDCl₃) δ 155.3 (*J*_{C-F} = 247.6 Hz), 152.8, 149.8, 145.7 (*J*_{C-F} = 1.9 Hz), 142.6 (*J*_{C-F} = 9.6 Hz), 135.6, 134.8, 133.9, 129.9, 129.1 (*J*_{C-F} = 5.8 Hz), 128.1, 121.4, 120.7 (*J*_{C-F} = 20.2 Hz), 111.8, 110.9 (*J*_{C-F} = 2.9 Hz), 104.9, 42.9 (*J*_{C-F} = 3.8 Hz), 40.6; HRMS (EI⁺) Calcd for C₂₈H₂₇FN₂Si ([M]⁺) 438.1922, Found 438.1929.

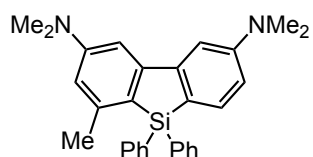
Silafluorene 146j



General procedure using 4-chloro-*N*³,*N*³,*N*^{3'},*N*^{3'}-tetramethyl-[1,1'-biphenyl]-3,3'-diamine (68.7 mg, 0.250 mmol) and diphenylsilane (138 mg, 0.750 mmol) at 100 °C for 24 h. The desired compound **146j** was obtained as a white powder (111 mg, 97%). ¹H NMR (400 MHz, CDCl₃) δ 7.67–7.61 (m, 6H), 7.54 (s, 1H), 7.40–7.32 (m, 6H), 7.17 (d, *J* = 2.3 Hz, 1H),

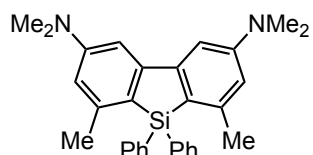
6.72 (dd, $J = 8.2, 2.3$ Hz, 1H), 3.09 (s, 6H), 2.93 (s, 6H); ^{13}C NMR (100 MHz, CDCl_3) δ 152.8, 152.4, 149.5, 148.9, 135.6, 135.5, 134.9, 133.6, 131.9, 130.0, 128.1, 127.8, 121.3, 112.6, 112.4, 105.0, 43.9, 40.6; HRMS (EI^+) Calcd for $\text{C}_{28}\text{H}_{27}\text{ClN}_2\text{Si}$ ($[\text{M}]^+$) 454.1627, Found 454.1630.

Silafluorene 146k



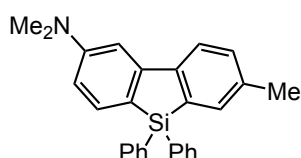
General procedure using $N^3,N^3,N^{3'},N^{3'},5$ -pentamethyl-[1,1'-biphenyl]-3,3'-diamine (63.6 mg, 0.250 mmol) and diphenylsilane (138 mg, 0.750 mmol) at 100 °C for 24 h. The desired compound **146k** was obtained as a white powder (96 mg, 88%). ^1H NMR (400 MHz, CDCl_3) δ 7.67–7.65 (m, 4H), 7.50 (d, $J = 7.8$ Hz, 1H), 7.39–7.29 (m, 6H), 7.23 (d, $J = 2.3$ Hz, 1H), 7.12 (d, $J = 1.8$ Hz, 1H), 6.67 (dd, $J = 8.0, 2.5$ Hz, 1H), 6.49 (d, $J = 1.6$ Hz, 1H), 3.07 (s, 6H), 3.06 (s, 6H), 2.33 (s, 3H); ^{13}C NMR (100 MHz, CDCl_3) δ 153.3, 152.6, 150.8, 150.6, 144.7, 136.0, 134.4, 129.6, 128.0, 123.3, 122.5, 112.9, 112.3, 105.2, 102.9, 40.7, 24.0 (one carbon is missing); HRMS (EI^+) Calcd for $\text{C}_{29}\text{H}_{30}\text{N}_2\text{Si}$ ($[\text{M}]^+$) 434.2173, Found 434.2181.

Silafluorene 146l



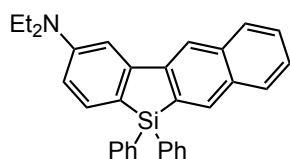
General procedure using $N^3,N^3,N^{3'},N^{3'},5,5'$ -hexamethyl-[1,1'-biphenyl]-3,3'-diamine (67.1 mg, 0.25 mmol) and diphenylsilane (138 mg, 0.75 mmol) at 100 °C for 24 h. The desired compound **146l** was obtained as a white powder (58.4 mg, 52%). ^1H NMR (400 MHz, CDCl_3) δ 7.68 (d, $J = 6.4$ Hz, 4H), 7.37–7.30 (m, 6H), 7.11 (d, $J = 1.8$ Hz, 2H), 6.46 (d, $J = 1.6$ Hz, 2H), 3.05 (s, 12H), 2.24 (s, 6H); ^{13}C NMR (100 MHz, CDCl_3) δ 153.2, 150.9, 144.6, 136.2, 133.6, 129.6, 127.9, 122.8, 112.9, 103.0, 40.8, 23.7; HRMS (EI^+) Calcd for $\text{C}_{30}\text{H}_{32}\text{N}_2\text{Si}$ ($[\text{M}]^+$) 448.2329, Found 448.2333.

Silafluorene 146m



146m was obtained as white solid (39 mg, 40%). ^1H NMR (400 MHz, CDCl_3) δ 7.77 (d, $J = 7.8$ Hz, 1H), 7.67–7.61 (m, 5H), 7.56 (s, 1H), 7.41–7.31 (m, 6H), 7.27–7.23 (m, 2H), 6.69 (dd, $J = 7.8, 2.3$ Hz, 1H), 3.07 (s, 6H), 2.37 (s, 3H); ^{13}C NMR (100 MHz, CDCl_3) δ 152.8, 150.4, 146.6, 137.6, 137.3, 135.6, 134.9, 134.5, 134.1, 131.2, 129.9, 128.1, 120.8, 111.9, 105.0, 40.6, 21.5 (one carbon is missing); HRMS(EI^+) Calcd for $\text{C}_{27}\text{H}_{25}\text{NSi}$ ($[\text{M}]^+$) 391.1751, Found 391.1753.

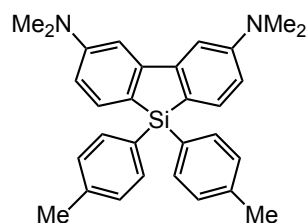
Silafluorene 146n



General procedure using N,N -diethyl-3-(naphthalen-2-yl)aniline (68.9 mg, 0.250 mmol) and diphenylsilane (138 mg, 0.750 mmol) at 140 °C. The desired compound **146n** was obtained as white powder (60.4 mg, 53%). ^1H NMR (600 MHz, CDCl_3) δ 8.08 (d, $J = 8.2$ Hz, 1H), 8.02 (d, $J = 8.9$ Hz, 1H), 7.91 (d, $J = 7.6$ Hz, 1H), 7.88 (d, $J = 7.6$ Hz, 1H), 7.75 (d, $J = 7.6$ Hz, 4H), 7.62 (d, $J = 7.6$ Hz, 1H), 7.39–7.42 (m, 4H), 7.36 (d, $J = 6.9$ Hz, 4H), 6.68 (d, $J = 8.2$ Hz, 1H), 3.49 (q, $J = 6.0$ Hz, 4H), 1.27 (t, $J = 6.0$ Hz, 6H); ^{13}C NMR (150 MHz, CDCl_3) δ 150.5, 150.1,

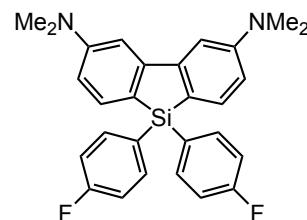
148.8, 137.0, 136.0, 135.5, 134.9, 133.8, 133.3, 131.3, 129.9, 129.6, 128.8, 128.2, 126.8, 125.5, 120.1, 119.9, 111.3, 104.9, 44.5, 12.9; HRMS (FAB⁺) Calcd for C₃₂H₂₉NSi ([M]⁺) 455.2064, Found 455.2068.

Silafluorene 146r



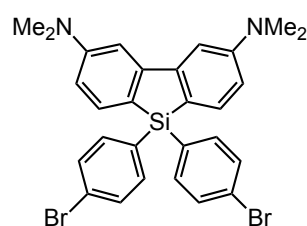
General procedure using *N,N,N',N'*-tetramethyl-1,1'-biphenyl-3,3'-diamine **144b** (60.1 mg, 0.250 mmol) and di-*p*-tolylsilane (159 mg, 0.750 mmol) at 140 °C. The desired compound **146r** was obtained as yellowish powder (81.9 mg, 73%). ¹H NMR (600 MHz, CDCl₃) δ 7.59 (d, *J* = 8.4 Hz, 2H), 7.55 (d, *J* = 7.8 Hz, 4H), 7.25 (d, *J* = 1.2 Hz, 2H), 7.15 (d, *J* = 5.2 Hz, 4H), 6.70 (dd, *J* = 4.8, 1.2 Hz, 2H), 3.08 (s, 12H), 2.34 (s, 6H); ¹³C NMR (150 MHz, CDCl₃) δ 152.5, 150.5, 139.5, 135.7, 134.5, 131.3, 128.8, 123.3, 112.3, 105.1, 40.8, 21.7; HRMS (FAB⁺) Calcd for C₃₀H₃₂N₂Si ([M]⁺) 448.2329, Found 448.2334.

Silafluorene 146s



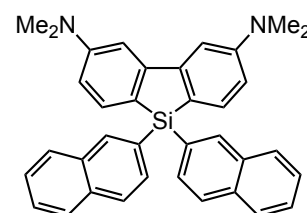
General procedure using *N,N,N',N'*-tetramethyl-1,1'-biphenyl-3,3'-diamine **144b** (60.1 mg, 0.250 mmol) and di-*p*-fluorophenylsilane (165 mg, 0.750 mmol) at 140 °C. The desired compound **146s** was obtained as a yellowish white powder (99.3 mg, 87%). ¹H NMR (400 MHz, CDCl₃) δ 7.69–7.58 (m, 6H), 7.30 (d, *J* = 2.2 Hz, 2H), 7.04 (dd, *J* = 8.4, 8.2 Hz, 4H), 6.72 (dd, *J* = 8.2, 2.2, 2H), 3.09 (s, 12H); ¹³C NMR (100 MHz, CDCl₃) δ 164.3 (*J*_{C-F} = 247 Hz), 152.7, 150.5, 137.5 (*J*_{C-F} = 6.8 Hz), 134.4, 130.2 (*J*_{C-F} = 3.9 Hz), 122.0, 115.2 (*J*_{C-F} = 20.2 Hz), 112.2, 105.0, 40.6; HRMS (FAB⁺) Calcd for C₂₈H₂₆F₂N₂Si ([M]⁺) 456.1828, Found 456.1834.

Silafluorene 146t



General procedure using *N,N,N',N'*-tetramethyl-1,1'-biphenyl-3,3'-diamine **144b** (60.1 mg, 0.250 mmol) and di-*p*-bromophenylsilane (257 mg, 0.750 mmol) at 140 °C. The desired compound **146t** was obtained as white powder (131 mg, 91%). ¹H NMR (600 MHz, CDCl₃) δ 7.58 (d, *J* = 8.2 Hz, 2H), 7.52–7.47 (m, 8H), 7.26 (d, *J* = 2.4 Hz, 2H), 6.72 (dd, *J* = 8.2, 2.4 Hz, 2H), 3.10 (s, 12H); ¹³C NMR (150 MHz, CDCl₃) δ 152.8, 150.6, 137.1, 134.4, 133.4, 131.2, 124.8, 121.2, 112.2, 105.0, 40.6; HRMS (FAB⁺) Calcd for C₂₈H₂₆Br₂N₂Si ([M]⁺) 576.0227, Found 576.0233.

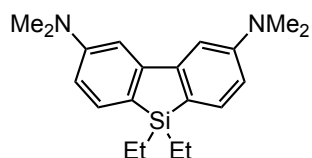
Silafluorene 146u



General Procedure using *N,N,N',N'*-tetramethyl-1,1'-biphenyl-3,3'-diamine **144b** (60.1 mg, 0.250 mmol) and di(naphthalen-2-yl)silane (213 mg, 0.750 mmol) with higher temperature at 140 °C. The desired compound **146u** was obtained as a colorless crystal (105 mg, 81%). ¹H NMR (600 MHz, CDCl₃) δ 8.21 (s, 2H), 7.81–7.71 (m, 10H),

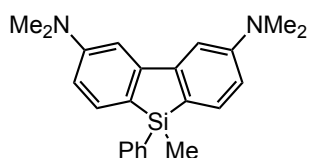
7.49–7.41 (m, 4H), 7.29 (d, $J = 2.3$ Hz, 2H), 6.74 (dd, $J = 8.2, 2.3$ Hz, 2H), 3.09 (s, 12H); ^{13}C NMR (150 MHz, CDCl_3) δ 152.7, 150.7, 136.7, 134.7, 134.2, 133.1, 132.4, 131.6, 128.4, 127.8, 127.2, 126.6, 125.9, 122.6, 112.3, 105.1, 40.7; HRMS (FAB $^+$) Calcd for $\text{C}_{36}\text{H}_{32}\text{N}_2\text{Si}$ ($[\text{M}]^+$) 520.2329, Found 520.2336.

Silafluorene 146v



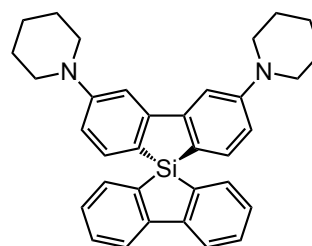
146v was obtained as white solid (70.0 mg, 84%). ^1H NMR (400 MHz, CDCl_3) δ 7.48 (d, $J = 8.2$ Hz, 2H), 7.22 (d, $J = 2.3$ Hz, 2H), 6.69 (dd, $J = 8.2, 2.3$ Hz, 2H), 3.07 (s, 12H), 1.02–0.98 (m, 6H), 0.91–0.87 (m, 4H); ^{13}C NMR (100 MHz, CDCl_3) δ 152.2, 150.3, 133.8, 124.4, 111.8, 105.0, 40.8, 7.9, 4.6; HRMS(EI $^+$) Calcd for $\text{C}_{20}\text{H}_{28}\text{N}_2\text{Si}$ ($[\text{M}]^+$) 324.2016, Found 324.2020.

Silafluorene 146w



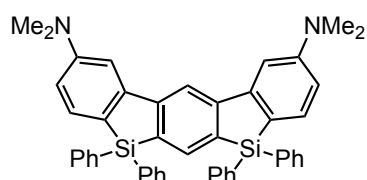
146w was obtained as white solid (71.7 mg, 80%). ^1H NMR (600 MHz, CDCl_3) δ 7.57 (dd, $J = 7.5, 1.6$ Hz, 2H), 7.50 (d, $J = 8.2$ Hz, 2H), 7.32–7.26 (m, 3H), 7.23 (d, $J = 2.3$ Hz, 2H), 6.69 (dd, $J = 8.2, 2.3$ Hz, 2H), 3.07 (s, 12H), 0.67 (s, 3H); ^{13}C NMR (100 MHz, CDCl_3) δ 152.5, 150.2, 137.0, 134.6, 134.0, 129.4, 127.9, 124.4, 112.2, 105.0, 40.8, -4.3; HRMS (EI $^+$) Calcd for $\text{C}_{23}\text{H}_{26}\text{N}_2\text{Si}$ ($[\text{M}]^+$) 358.1860, Found 358.1863.

Spirosilabifluorene 148



The spiro-silabifluorene **148** was synthesized according to the general procedure using 3,3'-di(piperidin-1-yl)-1,1'-biphenyl **144d** (60.1 mg, 0.250 mmol) and 5*H*-dibenzo[*b,d*]silole (137 mg, 0.750 mmol) at 100 °C. The desired compound **148** was obtained as white solid (52.0 mg, 42%). ^1H NMR (400 MHz, CDCl_3) δ 7.89 (d, $J = 7.8$ Hz, 2H), 7.47–7.39 (m, 6H), 7.25–7.16 (m, 4H), 6.76 (dd, $J = 8.0, 2.1$ Hz, 2H), 3.30 (*t*, $J = 5.5$ Hz, 8H), 1.77–1.56 (m, 12H); ^{13}C NMR (100 MHz, CDCl_3) δ 154.8, 151.6, 149.8, 134.9, 134.5, 134.4, 130.9, 127.7, 121.7, 120.8, 115.6, 108.8, 50.3, 26.0, 24.5; HRMS(EI $^+$) Calcd for $\text{C}_{34}\text{H}_{34}\text{N}_2\text{Si}$ ($[\text{M}]^+$) 498.2486, Found 498.2489.

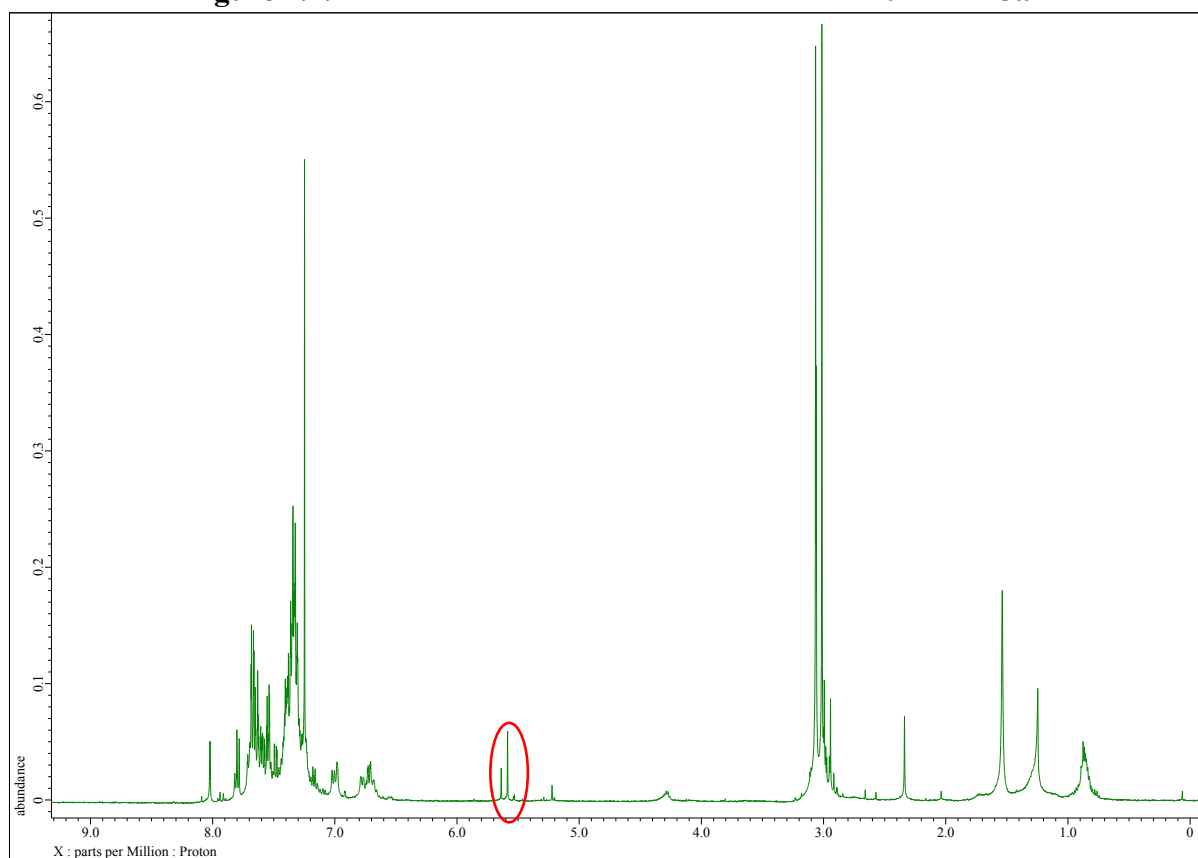
Silicon-bridged terphenyl compound 150



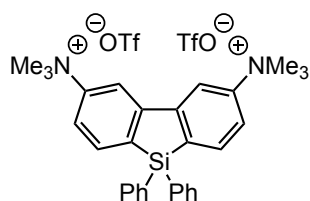
The silicon-bridged terphenyl compound **150** was synthesized according to general procedure using $N^3, N^3, N^{3'}, N^{3'}$ -tetramethyl-[1,1':3',1''-terphenyl]-3,3''-diamine (79.0 mg, 0.250 mmol) and diphenylsilane (276 mg, 1.50 mmol, 6 equiv) at 100 °C. After 24 h, the reaction mixture was cooled to room temperature then 1.0 mol% of $\text{RhCl}_2(\text{PPh}_3)_3$ was added. The reaction mixture was heated to 140 °C, stirred for 24 h. The silicon-bridged terphenyl compound **150** was obtained as white solid (47.0 mg, 28%). ^1H NMR (400 MHz, CDCl_3) δ 8.30 (s, 1H), 8.15 (s, 1H), 7.68–7.64 (m, 10H), 7.42–7.29 (m, 14H), 6.76 (dd, $J = 8.2, 2.3$ Hz, 2H), 3.12 (s, 12H); ^{13}C NMR (100 MHz,

CDCl₃) δ 152.9, 151.8, 150.3, 139.3, 136.8, 135.8, 134.9, 134.1, 129.9, 128.1, 122.0, 113.2, 112.7, 105.5, 40.76; HRMS(EI⁺) Calcd for C₄₆H₄₀N₂Si₂ ([M]⁺) 676.2725, Found 676.2733.

Figure 2.1. Crude ¹H NMR of the reaction between **149** and **145a**.

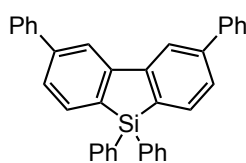


Silafluorene **151**



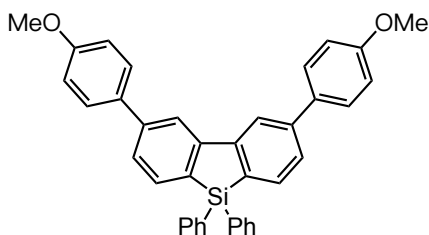
To a dry round bottom flask equipped with a magnetic stir bar was charged **146b** (1.09 g, 2.60 mmol, 1.0 equiv) and CH₂Cl₂ (17 mL). To the resultant stirring solution was added dropwise MeOTf (939 mg, 5.70 mmol, 2.2 equiv) at room temperature. The solution was stirred at room temperature for 2 h. The reaction mixture was concentrated to remove CH₂Cl₂ and the residue was treated with Et₂O (20 mL). The resultant solid was filtered, washed with Et₂O and hexane, and dried under vacuum to give **151** as white solid (1.89 g, 97%). ¹H NMR (400 MHz, Acetone-*d*₆) δ 8.96 (d, *J* = 2.5 Hz, 2H), 8.28 (d, *J* = 8.2 Hz, 2H), 8.13 (dd, *J* = 8.2, 2.5 Hz, 2H), 7.71 (dd, *J* = 7.6, 1.4 Hz, 4H), 7.57–7.49 (m, 2H), 7.45 (t, *J* = 7.6 Hz, 4H), 3.98 (s, 18H); ¹³C NMR (100 MHz, Acetone-*d*₆) δ 151.4, 150.3, 139.9, 136.5, 136.1, 135.1, 131.8, 130.9, 129.3, 122.0 (q, *J* = 8.2, 321.1 Hz), 121.1, 115.7, 57.8; HRMS(FAB⁺) Calcd for C₃₁H₃₄F₃N₂O₃SSi⁺ ([M-OTf]⁺) 599.2006, Found 599.2012.

Silafluorene 152



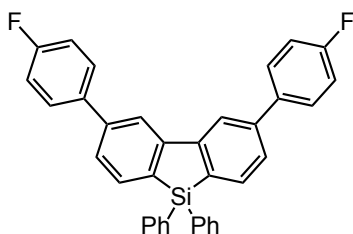
Compound **152** was synthesized according to the reported method.^[80] To a dry Schlenk flask equipped with a magnetic stir bar was added the compound **151** (150 mg, 0.200 mmol, 1.0 equiv) and PdCl₂(PPh₃)₂ (2.8 mg, 0.0040 mmol, 2.0 mol%). The flask was sealed with a rubber septum, evacuated/filled with nitrogen. THF (0.4 mL) was added via syringe, and the resultant slurry was stirred for 5 min. Then phenylmagnesium bromide (0.5 M solution in THF, 0.88 mL, 0.44 mmol, 2.2 equiv) was added dropwise at room temperature. After 1 h, the reaction mixture was quenched with water (1 mL) and 6N HCl (3 mL), extracted with Et₂O. The organic extract was dried over Na₂SO₄, filtered, and concentrated. The crude product was purified by chromatography on silica gel (eluent: hexane/ethyl acetate = 100:0 to 20:1) to give the compound **152** as white solid (93.2 mg, 96% yield). ¹H NMR (400 MHz, CDCl₃) δ 8.22 (s, 2H), 7.92 (d, *J* = 7.3 Hz, 2H), 7.80–7.71 (m, 8H), 7.61 (d, *J* = 7.3 Hz, 2H), 7.57–7.37 (m, 12H); ¹³C NMR (100 MHz, CDCl₃) δ 149.4, 144.0, 141.5, 135.7, 135.1, 134.5, 132.7, 130.3, 129.0, 128.3, 127.8, 127.5, 127.2, 120.3; HRMS(EI⁺) Calcd for C₃₆H₂₆Si ([M]⁺) 486.1798, Found 486.1804.

Silafluorene 153



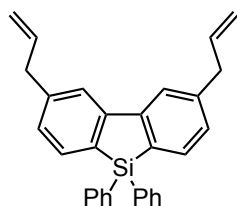
The same method as **152**. The reaction was carried out using 0.15 mmol of **151**. (4-methoxyphenyl)magnesium bromide (1.0 M solution in THF, 0.33 mL, 0.33 mmol, 2.2 equiv) were used. The crude product was purified by chromatography on silica gel (eluent: hexane/dichloromethane = 5:1 to 2:1) to give the compound **153** as white solid (43.2 mg, 53% yield). ¹H NMR (400 MHz, CDCl₃) δ 8.12 (d, *J* = 1.4 Hz, 2H), 7.84 (d, *J* = 7.3 Hz, 2H), 7.72–7.70 (m, 4H), 7.63 (dt, *J* = 9.3, 2.5 Hz, 4H), 7.52 (dd, *J* = 7.3, 1.4 Hz, 2H), 7.45–7.35 (m, 6H), 7.02 (dt, *J* = 9.6, 2.5 Hz, 4H), 3.88 (s, 6H); ¹³C NMR (150 MHz, CDCl₃) δ 159.6, 149.5, 143.6, 135.7, 134.5, 134.0, 133.0, 130.3, 128.5, 128.3, 126.8, 119.8, 114.4, 55.5 (one carbon is missing); HRMS(EI⁺) Calcd for C₃₈H₃₀O₂Si ([M]⁺) 546.2010, Found 546.2012.

Silafluorene 154



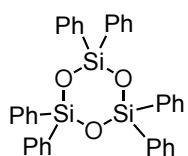
The same method as **152**. The reaction was carried out using 0.15 mmol of **151**. (4-fluorophenyl)magnesium bromide (0.5 M solution in THF, 1.2 mL, 0.60 mmol, 4.0 equiv) were used. The crude product was purified by chromatography on silica gel (eluent: hexane/dichloromethane = 5:1) to give the compound **154** as white solid (55.3 mg, 71% yield). ¹H NMR (400 MHz, CDCl₃) δ 8.10 (d, *J* = 1.1 Hz, 2H), 7.86 (d, *J* = 7.8 Hz, 2H), 7.70 (dd, *J* = 7.8, 1.4 Hz, 4H), 7.66–7.63 (m, 4H), 7.51 (dd, *J* = 7.5, 1.6 Hz, 2H), 7.44–7.36 (m, 6H), 7.20–7.15 (m, 4H); ¹³C NMR (150 MHz, CDCl₃) δ 162.8 (¹*J*_{C-F} = 245.6 Hz), 149.3, 143.1, 137.6 (⁴*J*_{C-F} = 2.9 Hz), 135.7, 135.3, 134.6, 132.6, 130.4, 129.1 (³*J*_{C-F} = 8.6 Hz), 128.4, 127.1, 120.1, 115.9 (²*J*_{C-F} = 21.5 Hz); HRMS(EI⁺) Calcd for C₃₆H₂₄F₂Si ([M]⁺) 522.1610, Found 522.1616.

Silafluorene 155



The same method as **152**. The reaction was carried out using 0.15 mmol of **151**. Allylmagnesium bromide (1.0 M solution in THF, 1.2 mL, 0.33 mmol, 2.2 equiv) were used. The crude product was purified by chromatography on silica gel (eluent: hexane/ethyl acetate = 50:1) to give the corresponding silafluorene **155** as white solid (27.6 mg, 34% yield). ^1H NMR (400 MHz, CDCl_3) δ 7.71–7.69 (m, 4H), 7.65–7.63 (m, 4H), 7.42–7.31 (m, 6H), 7.15 (dd, $J = 7.3, 1.4$ Hz, 2H), 6.08–5.98 (m, 2H), 5.19–5.11 (m, 4H), 3.48 (d, $J = 6.9$ Hz, 4H); ^{13}C NMR (100 MHz, CDCl_3) δ 149.3, 143.0, 137.4, 135.6, 134.2, 133.9, 133.2, 130.1, 128.4, 128.2, 121.7, 116.3, 40.8; HRMS(EI $^+$) Calcd for $\text{C}_{30}\text{H}_{26}\text{Si}$ ($[\text{M}]^+$) 414.1798, Found 414.1803.

The byproduct of the reaction between dimethoxy-biphenyl **144p** (45.1 mg 0.200 mmol, 1.0 equiv) and dihydrodiphenylsilane **145a** (111 mg, 0.600 mmol, 3.0 equiv) was obtained by recrystallization from the dichloromethane/ethanol solution as a white solid (56 mg).



Spectral Data: ^1H NMR (400 MHz, CDCl_3) δ 7.46 (d, $J = 7.8$ Hz, 12H), 7.33 (t, $J = 7.3$ Hz, 6H), 7.16 (dd, $J = 7.5, 7.5$ Hz, 12H); ^{13}C NMR (100 MHz, CDCl_3) δ 134.6, 134.5, 130.1, 127.7.

Based on the spectral data of the compound, one possible structure is Hexaphenylcyclotrisiloxane, the cyclic trimerization product of H_2SiPh_2 with H_2O .^[76b]

Figure 2.2. Mass Spectrum of the byproduct (EI $^+$).

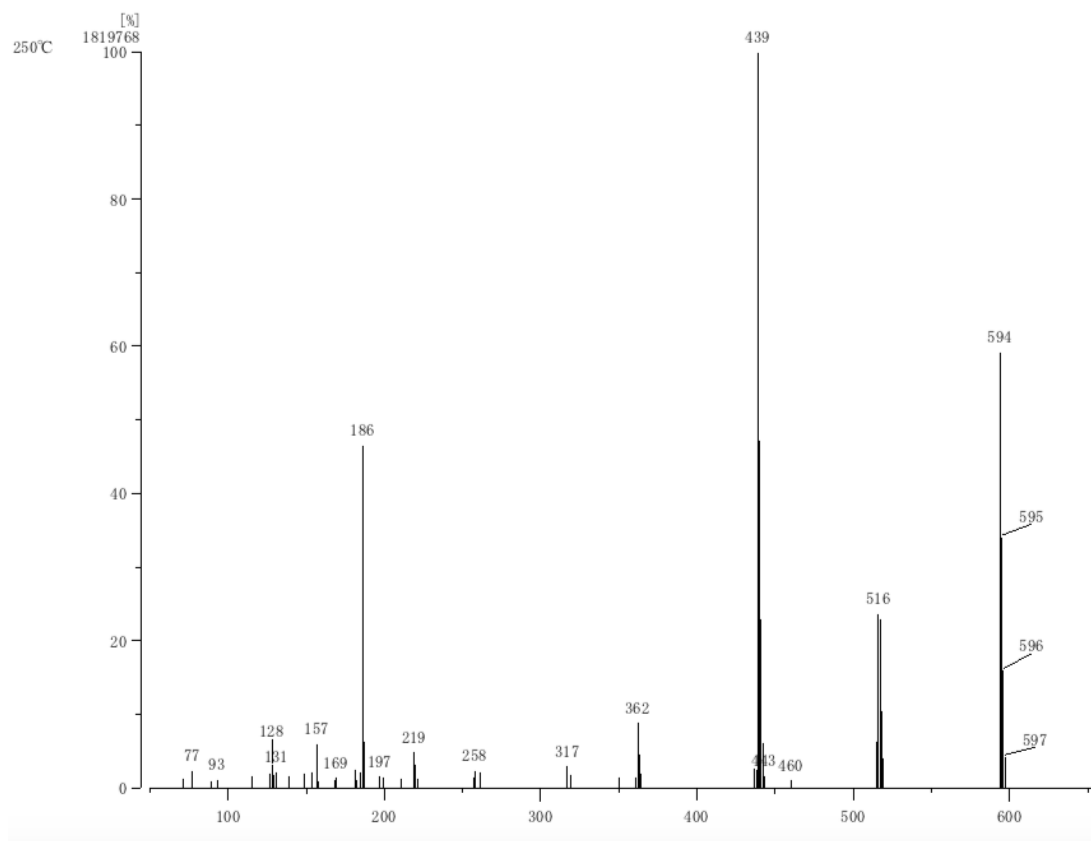
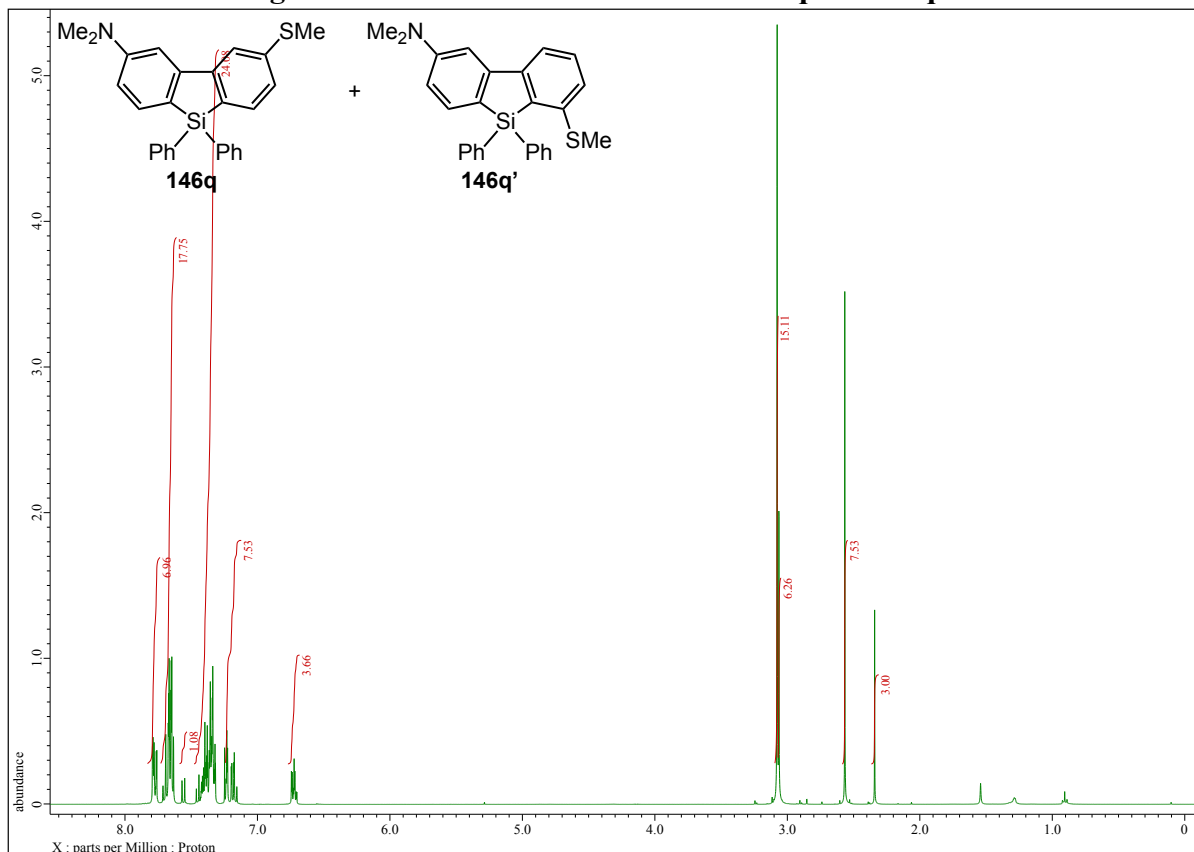


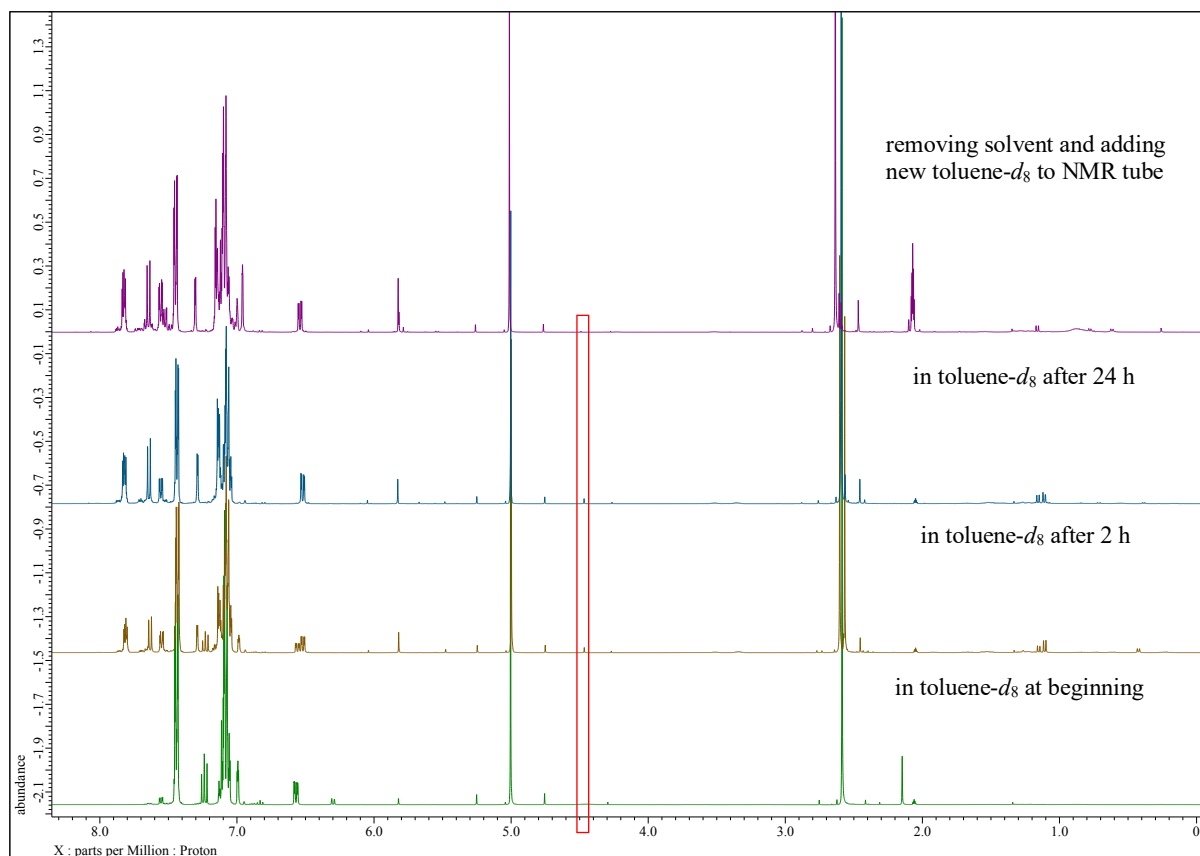
Figure 2.3. ^1H NMR of the mixture of **146q** and **146q'**.



2.4.4 Experiment for Detecting By-product H_2

To detect the by-product H_2 , ^1H NMR experiment was conducted.^[34] Biphenyl **144b** (60.5 mg, 0.250 mmol, 1.0 equiv) and tris(pentafluorophenyl)borane ($\text{B}(\text{C}_6\text{F}_5)_3$, 6.4 mg, 0.013 mmol, 5.0 mol%) was added to a NMR tube with a J. Young valve. The NMR tube was closed and filled with nitrogen. Toluene- d_8 (0.50 mL) was added via syringe. 2,6-Lutidine (2.2 μL , 2.0 mg, 0.019 mmol, 7.5 mol%) and diphenylsilane **145a** (0.14 mL, 138 mg, 0.750 mmol, 3.0 equiv) were then added to the mixture. The ^1H NMR spectrum of the reaction mixture was recorded. Then, the NMR tube was placed into an oil bath (100 $^\circ\text{C}$). After 2 h, the mixture was checked by ^1H NMR spectroscopy again. After completion of the reaction (24 h), ^1H NMR of the resulted mixture was detected. Finally, the solvent and the possible H_2 by-product were removed under reduced pressure and the residue was dissolved in toluene- d_8 again. In comparison, the resulting mixture was subjected to ^1H NMR spectroscopy again. As shown in figure 2.4, the proton signal of H_2 was observed at 4.49 ppm.

Figure 2.4. Observation of signal of H₂ by ¹H NMR.



Chapter 3

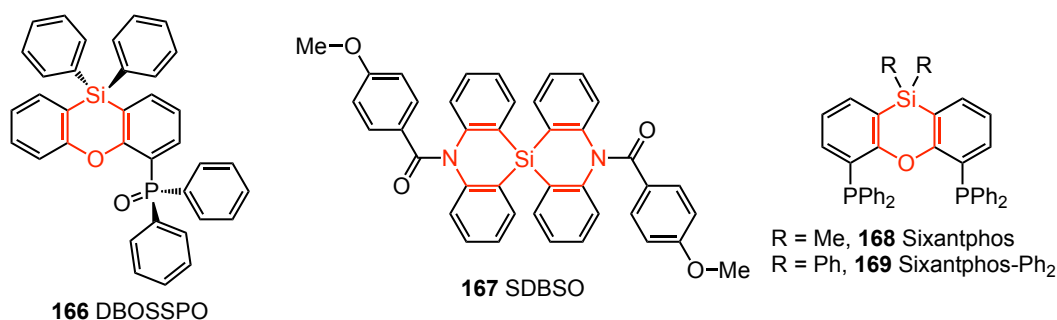
Synthesis of Six-membered Silacycles by Borane-catalyzed Double Sila-Friedel–Crafts Reaction

In this chapter, I introduced a catalytic preparation method of six-membered silacyclic compounds such as phenoxasilins and phenothiasilins. A borane-catalyzed double sila-Friedel–Crafts reaction of amino groups-substituted diaryl ethers and dihydrosilanes successfully proceeded to afford phenoxasilin derivatives in moderate to excellent yields. Under the optimal conditions, phenothiasilins were also obtained from the corresponding diaryl thioethers and dihydrosilanes. In addition, I investigated the gram-scale synthesis of bis(dimethylamino)phenoxasilin and the conversions of its amino groups.

3.1 Introduction

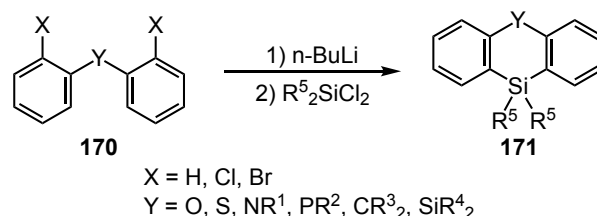
The silicon-bridged six-membered biarys (phenazasilines, phenoxasilins, phenothiasilins), benefitting from both Si and a heteroatom in a fused six-membered ring, are important in organosilicon chemistry, and have fascinating applications as organic electronic materials (**166** and **167**),^[94] ligands (**168** and **169**),^[95] and reagents (Scheme 3.1).^[96] Although a variety of methods have been developed for the preparation of siloles over the last 10 years, preparative methods for the six-membered silacyclic ring system remain relatively unexplored. Thus, the development of novel approaches to construct six-membered silacyclic skeletons is demanded.

Scheme 3.1. Examples of six-membered silacycle-containing functional molecules.



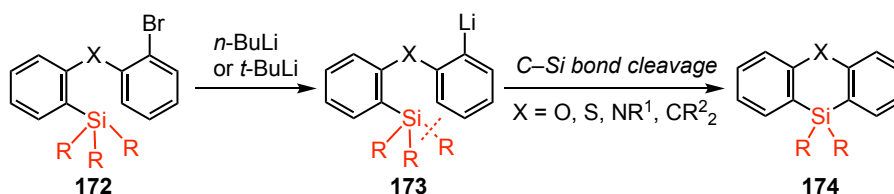
These six-membered silacycles are generally prepared by the reaction between dichlorosilane reagents and heteroatom-bridged dilithiated diaryl compounds **170**, such as dilithiated diaryl ethers and dilithiated diaryl thioethers (Scheme 3.2).^[50]

Scheme 3.2. Classical synthetic route for six-membered silacycles.



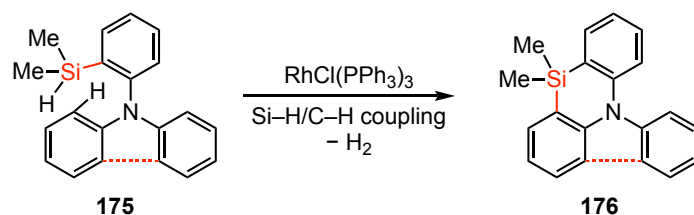
An intramolecular nucleophilic substitution at the silicon atom using organolithium reagents **173** via the cleavage of an inert C–Si bond has been developed for the synthesis of six-membered silacycles **174** (Scheme 3.3).^[51]

Scheme 3.3. Intramolecular S_N-Si leading to six-membered silacycles.



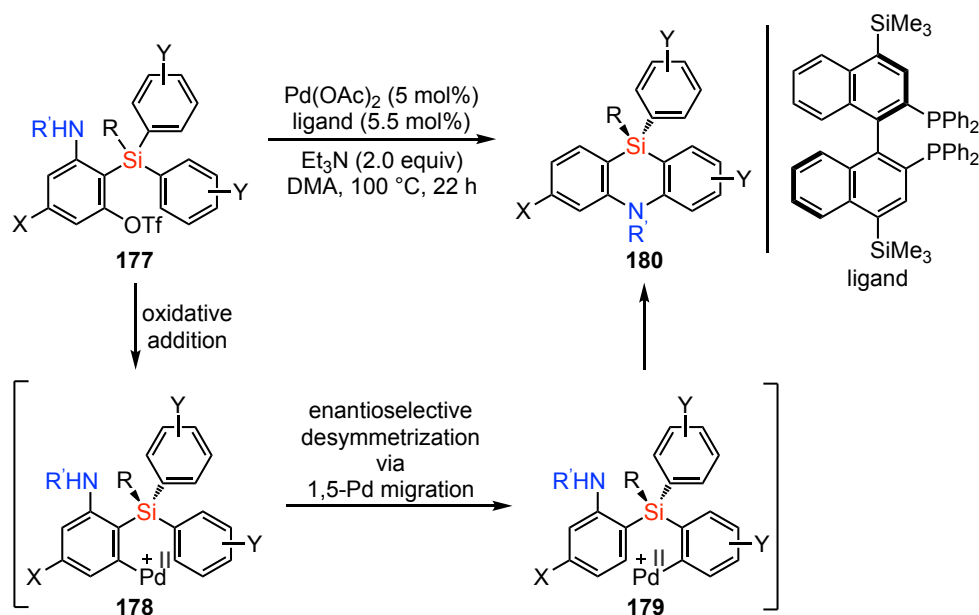
In addition, catalytic reaction systems were also developed as efficient synthetic strategies. The rhodium-catalyzed synthesis of phenazasilines biarylhydrosilanes **176** was presented by Huang's group (Scheme 3.4).^[48b] This method offered opportunities for preparing π -extended phenazasilines with enhanced optoelectronic properties for device applications in organic electronics.

Scheme 3.4. Rhodium-catalyzed synthesis of phenazasilines from biarylhydrosilanes.



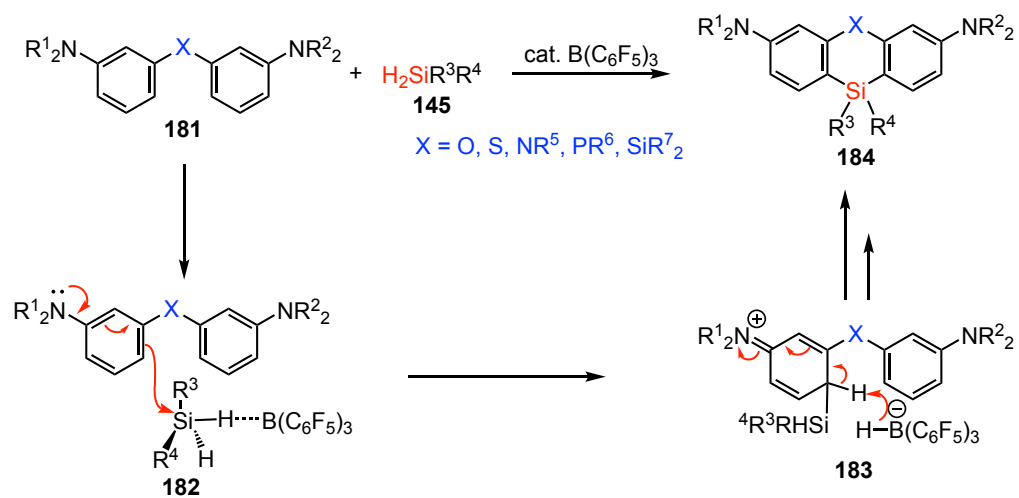
Shintani and Nozaki *et al.* developed a palladium-catalyzed asymmetric synthesis of 5,10-dihydrophenazasilines **180** with silicon-stereogenic center. The reaction proceeded via an unprecedented enantioselective 1,5-palladium migration. High enantioselectivity was achieved by employing 4,4'-bis(trimethylsilyl)-(*R*)-Binap as the chiral ligand, and a series of mechanistic investigations were carried out to probe the catalytic cycle of this process (Scheme 3.5).^[97]

Scheme 3.5. Palladium-catalyzed asymmetric synthesis of 5,10-dihydrophenazasilines with silicon-stereogenic center via an unprecedented enantioselective 1,5-palladium migration.



Based on the double sila-Friedel–Crafts reactions for the synthesis of silafluorene derivatives described in Chapter 2,^[70] I envisaged that the catalytic reaction of heteroatom-bridged amino-diaryls with dihydrosilanes for the preparation of six-membered silacycles is feasible (Scheme 3.6). I hypothesized that the desired silacyclic compounds will be formed through the ion-pair intermediate **183**.

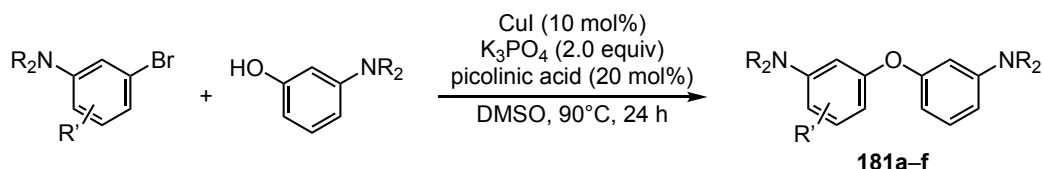
Scheme 3.6. Borane-catalyzed double sila-Friedel–Crafts reaction for the synthesis of six-membered silacyclic compounds.



3.2 Results and Discussion

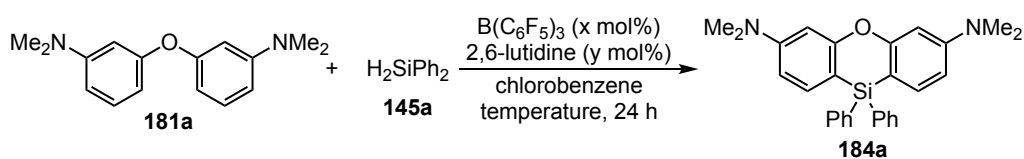
First, the reaction of diaryl ether **181a** and diphenyldihydrosilane **145a** was investigated (Table 3.1). The diaryl ethers **181a** was prepared according to a reported procedure: that is, CuI-catalyzed O-arylation of aminophenol using picolinic acid as the ligand (Scheme 3.7).^[98]

Scheme 3.7. Synthesis of diaryl ethers **181a–f**.



Under the optimal condition used for the synthesis of silafluorene derivatives in Chapter 2, that is, $(B(C_6F_5)_3)$ (5.0 mol%) and 2,6-lutidine (7.5 mol%) in chlorobenzene at $100^\circ C$, the desired phenoxasilin **184a** was obtained in 60% yield (entry 1). The structure of phenoxasilin **184a** was determined by 1H and ^{13}C NMR spectroscopy, HRMS spectrometry and single crystal X-ray crystallography. When the reaction temperature was increased to $140^\circ C$, the yield of **184a** was improved to 88% (entry 2). 3.0 mol% of the catalyst effectively promoted the reaction (entry 3), while the yield of **184a** decreased in the case of 1.5 mol% of the catalyst (entry 4). Finally, it was found that the reaction in the absence of 2,6-lutidine gave the best result with the yield of 99% (entry 5). This reaction proceeded with excellent yield, even without using a base, probably due to the enhanced nucleophilicity and basicity of **181a** compared to biphenyl **144**, which arise from the conjugation of oxygen atom.

Table 3.1. Optimization of reaction conditions for the synthesis of phenoxalin **184a**.

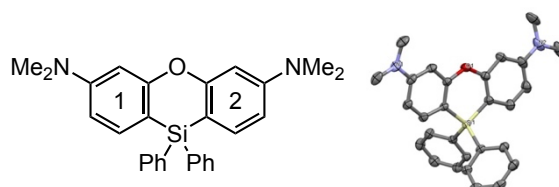


entry ^a	x (mol%)	y (mol%)	temp (°C)	yield (%)
1	5.0	7.5	100	60
2	5.0	7.5	140	88
3	3.0	7.5	140	97
4	1.5	7.5	140	87
5	3.0	0	140	99

^a**181a** (0.25 mmol), **145a** (0.75 mmol), chlorobenzene (0.4 mL).

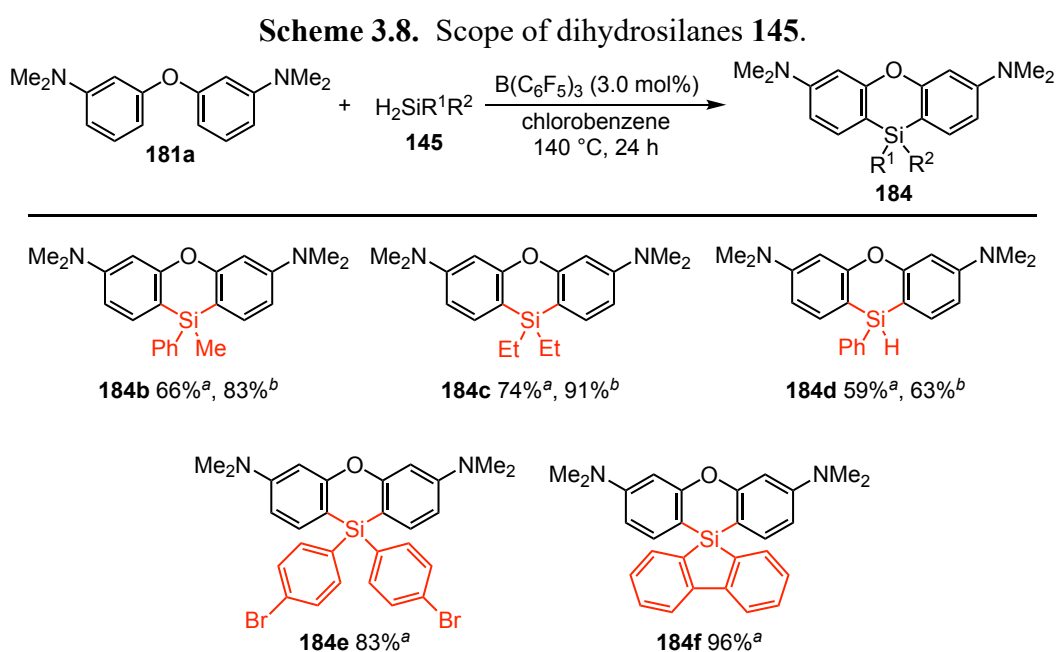
The X-ray single crystal structure analysis revealed that the compound **184a** has the rigid structure with low bent angles ($< 4^\circ$) between the planes of two phenyl groups (numbered as 1 and 2) around the O atom (Figure 3.1). This structure is more flat than the reported π -extended phenazasilines with the angles $< 11^\circ$.^[48b]

Figure 3.1. Single crystal X-ray structure of **184a** in the solid state. Displacement ellipsoids are drawn at the 50% probability level. All hydrogen atoms are omitted for clarity.



The scope of the dihydrosilanes **145** was then investigated (Scheme 3.8). The reactions between phenylmethylsilyl dihydrosilane **145b** and diethylsilyl dihydrosilane **145c** gave the corresponding phenoxasilins **184b** and **184c** with 66 and 74% yields, respectively. When a catalytic amount of 2,6-lutidine was used, the yields of **184b** and **184c** were improved to 83 and 91%, probably because of the enhancement of the deprotonation step by 2,6-lutidine.^[30] The reaction of phenylsilyl dihydrosilane **145d** gave the phenoxasilin product **184d** in 59% and 63% yield, respectively. In this reaction, the substrate was consumed completely, and no product other than **184d** was obtained after the purification by column chromatography on silica gel. The

possible deoxygenation of diaryl ether **181a** with Ph_3SiH as the reductant catalyzed by $\text{B}(\text{C}_6\text{F}_5)_3$ occurred.^[99] Phenoxasilin **184e** was obtained from di(4-bromo-phenyl)dihydrosilane **145e** in 83% yield without loss of the bromine atom. Additionally, 9,9-dihydro-5-silafluorene **145f** can be used for the preparation of spiro-type phenoxasilin **184f** which was obtained in 96% yield. This spiro-structure was reported as partial structures of emission materials in organic electronic devices.^[100]

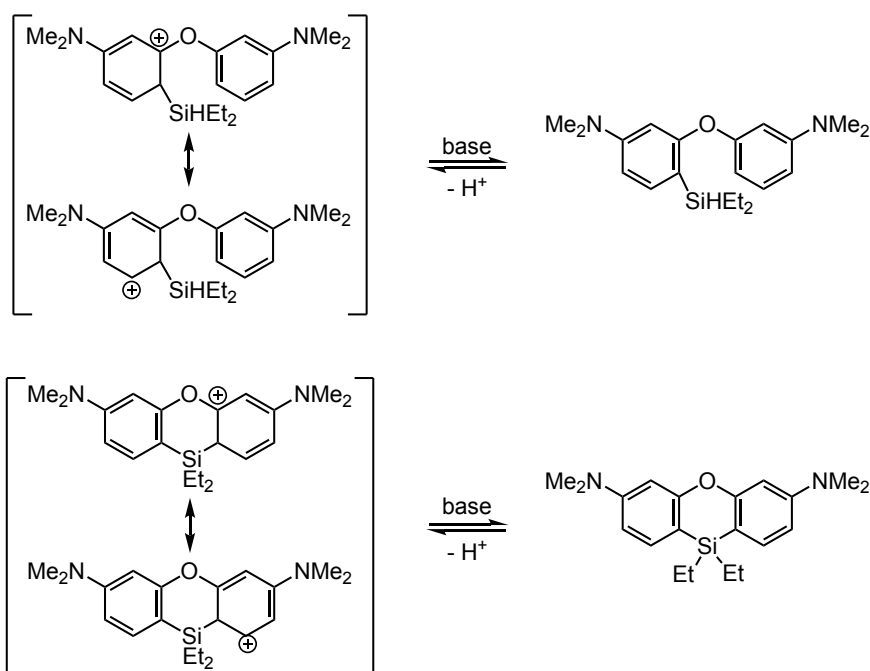


^a**181a** (1.0 equiv), **145** (3.0 equiv), $\text{B}(\text{C}_6\text{F}_5)_3$ (3.0 mol%), 140 °C, 24 h.

^b**181a** (1.0 equiv), **145** (3.0 equiv), $\text{B}(\text{C}_6\text{F}_5)_3$ (3.0 mol%), 2,6-lutidine (7.5 mol%), 140 °C, 24 h.

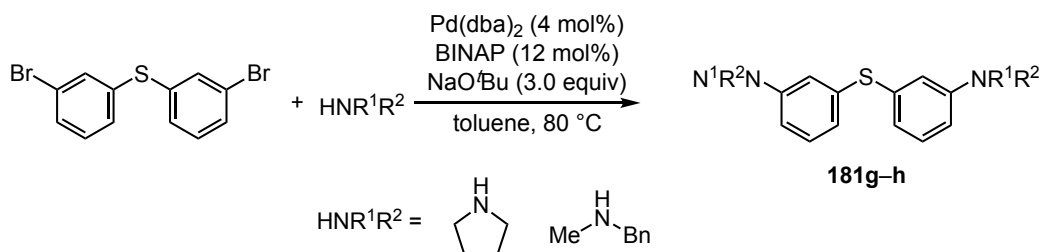
Compared to diaryldihydrosilane and arylhydrosilane, the efficiency of 2,6-lutidine was more significant in the case of phenylmethylidihydrosilane and diethyldihydrosilane. These results can be rationalized by the stability of the silicenium ion by β -silicon effect of the alkyl group (Scheme 3.9).^[101]

Scheme 3.9. Stabilization by β -silicon effect and the deprotonation with base.



Subsequently, I investigated the scope of biaryl ethers and biaryl thioethers using dihydrodiphenylsilane **145a** (Scheme 3.11). Biaryl ethers **181b–f** were synthesized following the same method as described for **181a** (Scheme 3.7).^[98] Biaryl thioethers **181g–h** were synthesized by Pd/BINAP-catalyzed amination of bis(3-bromophenyl)sulfan (Scheme 3.10).^[74]

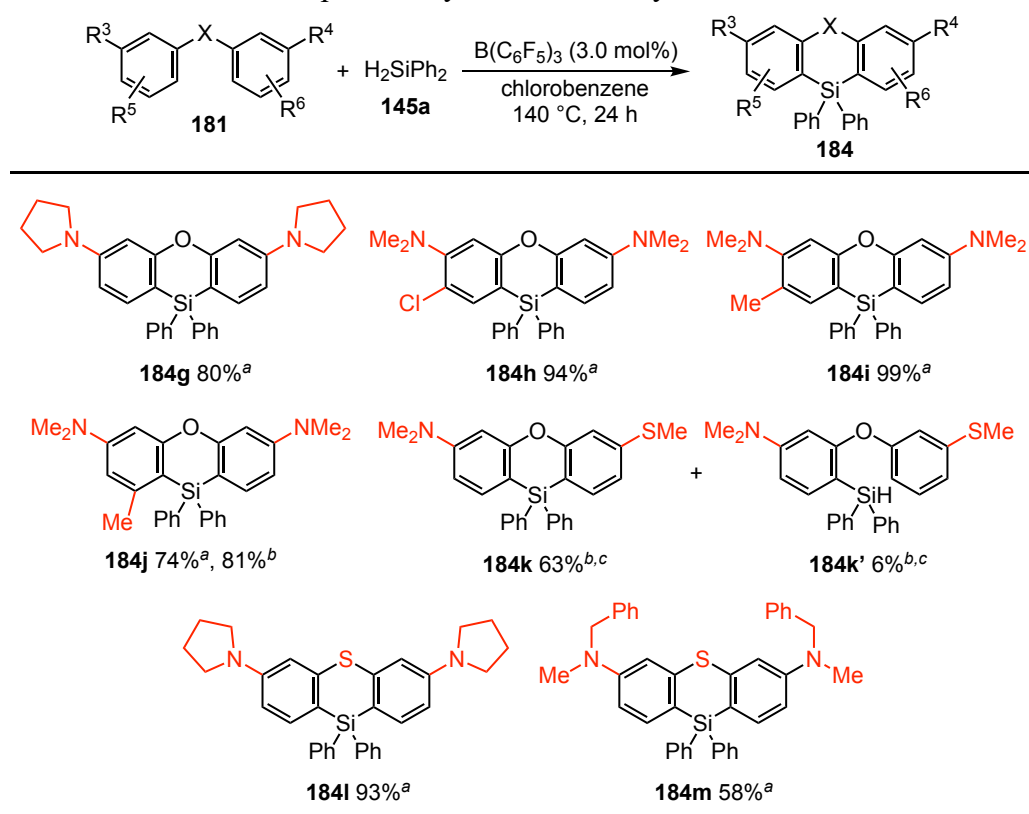
Scheme 3.10. Synthesis of biaryl thioethers **181g–h**.



Pyrrolidine-substituted phenoxasilin **184g** was formed in 80% yield from diaryl ether **181b**. The chloro-substituted diaryl ether was transformed into phenoxasilin **184h** in 94% yield without influence of the chlorine atom. The methyl-substituted phenoxasilins **184i** and **184j** were obtained in good yields despite the steric effect of the methyl group. The biaryl ether bearing one of SMe group instead of NMe₂ group **181k** gave a mixture of the desired

phenoxasilin **184k** and the uncyclized hydrosilane **184k'** via a single sila-Friedel–Crafts reaction in 35% yield with 2,6-lutidine (**184k**:**184k'** = 63:37). This result was rationalized as the weaker electron-donating ability of the SMe group compared to that of NMe₂. Upon increasing the reaction temperature to 180 °C, the ratio of cyclized compound **184k** improved and the mixture of **184k** and **184k'** was obtained in 68% yield (**184k**:**184k'** = 92:8). Diaryl thioether **181g** was also converted to phenothiasilin **184i** in 93% yield. The reaction system was applied to *N*-(benzyl)methylamin-substituted diaryl thioether **181h**, and phenothiasilin **184m** was obtained in 58% yield. The moderate conversion of the benzylmethylamino diaryl thioether **181h** compared to diaryl thioether **181g** is possibly due to the decreased electron density at the benzene rings.

Scheme 3.11. Scope of diaryl ether and diaryl thioether derivatives.



^a**181** (1.0 equiv), **145a** (3.0 equiv), $\text{B}(\text{C}_6\text{F}_5)_3$ (3.0 mol%), 140 °C, 24 h.

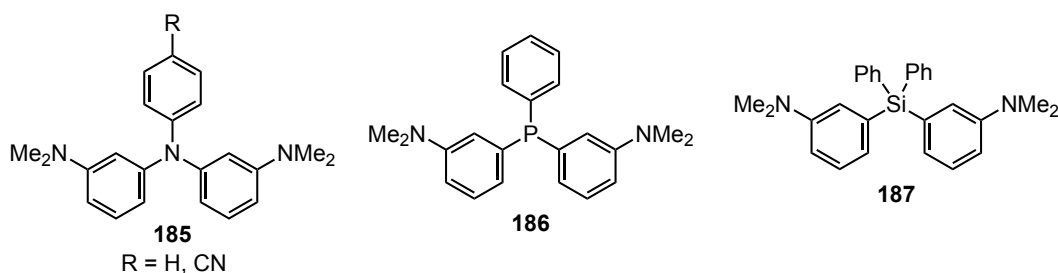
^b**181** (1.0 equiv), **145a** (3.0 equiv), $\text{B}(\text{C}_6\text{F}_5)_3$ (3.0 mol%), 2,6-lutidine (7.5 mol%), 140 °C, 24 h.

^c180 °C.

This reaction system was not applicable to sila-Friedel–Crafts reaction of triaryl amine **185**, triaryl phosphine **186**, and tetraaryl silane **187** (Scheme 3.12). Triaryl amines **185** as a substrate,

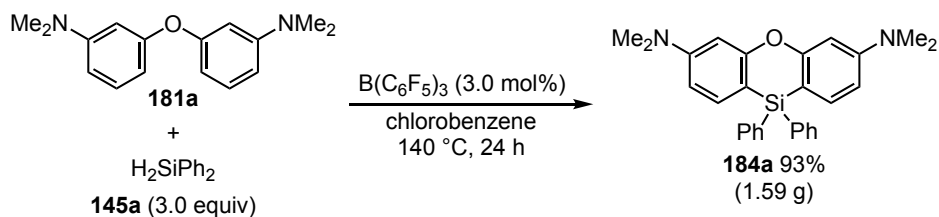
some uncertain structures other than the desired sila-Friedel–Crafts products were obtained. In addition, triaryl phosphine **186** and tetraaryl silane **187** were recovered completely after the reactions. These results are probably due to the low electron density in **186** and **187** compared with diaryl ether **181a**, or in other side, the steric hinderance of the phenyl groups on the P and Si atoms.

Scheme 3.12. Other substrates.



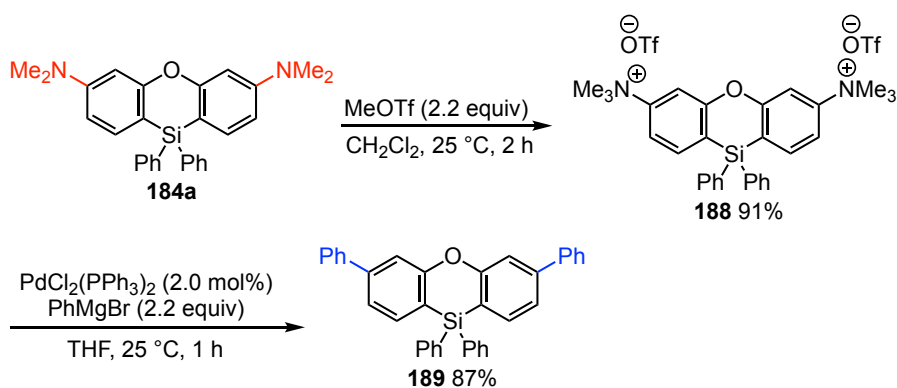
The gram-scale synthesis of phenoxasilin **184a** was conducted (Scheme 3.13). The reaction of 1.00 g of diaryl ether **181a** with 2.16 g of dihydrodiphenylsilane **145a** in the presence of a catalytic amount of $B(C_6F_5)_3$ afforded 1.59 g of phenoxasilin **184a** in 93% yield, which is comparable to the yield in 0.250 mmol scale reaction of **181a** with **145a** (99%), demonstrating the practicability of this protocol.

Scheme 3.13. Gram-scale synthesis of **184a**.



Besides, the amino groups of phenoxasilin **184a** was converted to phenyl groups via the cross-coupling reaction (Scheme 3.14).^[80] Preparation of the ammonium salt **188** by the treatment of **184a** with MeOTf, which followed by the sequential palladium-catalyzed cross-coupling reaction with the Grignard reagent (PhMgBr), afforded the desired diphenylated phenoxasilin **189** in 87% yield.

Scheme 3.14. Transformation of the amino groups in **184a**.



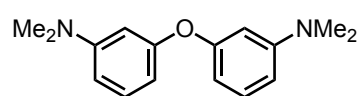
3.3 Conclusion

In conclusion, I have developed the catalytic preparation method of phenoxasilin and phenothiasilin derivatives from diaryl ethers and diaryl thioether via double sila-Friedel–Crafts reaction. This is the first example of the synthesis of the silicon-containing six-membered cyclic compounds by direct reactions between diaryl ethers or diaryl thioether and dihydrosilanes. The reaction system can be used for the gram-scale synthesis of phenoxasilins. Moreover, the transformation of the amino groups in the phenoxasilin product were also demonstrated. I hope that the reaction system will be useful for developing high-performance multi-heteroatom modified aromatic molecules for organic optoelectronics.

3.4 Experimental Section

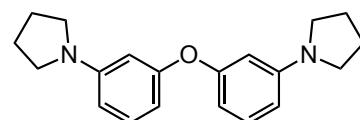
3.4.1 Synthesis and Characterization of Substrates

3,3'-Oxybis(*N,N*-dimethylaniline) (**181a**)



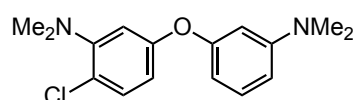
Compound **181a** was synthesized according to the reported method.^[98] To a mixture of 3-(dimethylamino)phenol (987 mg, 7.20 mmol, 1.2 equiv), CuI (114 mg, 0.600 mmol, 10 mol%), 2-picolinic acid (148 mg, 1.20 mmol, 20 mol%) and K₃PO₄ (2.55 g, 12.0 mmol, 2.0 equiv) in DMSO (15 mL) at room temperature was added 3-bromo-*N,N*-dimethylaniline (**S1**, 1.20 g, 6.00 mmol, 1.0 equiv) and the mixture was stirred vigorously at 90 °C for 24 h. The reaction mixture was cooled to room temperature, filtered with Celite and washed with EtOAc (50 mL). The filtrate was diluted with EtOAc (50 mL) and washed with brine (3 × 50 mL). The aqueous layers were extracted with EtOAc (2 × 50 mL). The combined organic layers were dried over Na₂SO₄ and the solvent removed in vacuo. Purification by column chromatography (eluent: hexane/EtOAc 20:1 to 10:1) gave compound **181a** as white solid (1.14 g, 76% yield). ¹H NMR (400 MHz, CDCl₃) δ 7.15 (dd, *J* = 8.0, 8.0 Hz, 2H), 6.44–6.48 (m, 4H), 6.35 (dd, *J* = 8.0, 1.6 Hz, 2H), 2.93 (s, 12H); ¹³C NMR (100 MHz, CDCl₃) δ 158.5, 152.2, 129.9, 107.5, 106.9, 103.5, 40.7; HRMS(EI⁺) Calcd for C₁₆H₂₀N₂O ([M]⁺) 256.1570, Found 256.1578.

1,1'-[Oxybis(3,1-phenylene)]dipyrrolidine (**181b**)



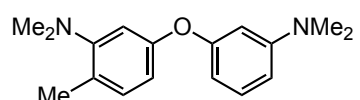
Compound **181b** was obtained in 56% yield (355 mg, 1.12 mmol) following the same method as described for **181a** by the reaction between 1-(3-bromophenyl)pyrrolidine^[102] (452 mg, 2.00 mmol) and 3-(pyrrolidin-1-yl)phenol (392 mg, 2.40 mmol). ¹H NMR (400 MHz, CDCl₃) δ 7.13 (dd, *J* = 8.2, 8.2 Hz, 2H), 6.28–6.31 (m, 6H), 3.23–3.27 (m, 8H), 1.96–2.00 (m, 8H); ¹³C NMR (100 MHz, CDCl₃) δ 158.5, 149.4, 129.9, 106.7, 105.8, 102.5, 47.8, 25.6; HRMS(EI⁺) Calcd for C₂₀H₂₄N₂O ([M]⁺) 308.1883, Found 308.1890.

2-Chloro-5-(3-(dimethylamino)phenoxy)-*N,N*-dimethylaniline (**181c**)



Compound **181c** was obtained in 62% yield (449 mg, 1.55 mmol) following the same method as described for **181a** by the reaction between **S4** (586 mg, 2.50 mmol) and 3-(dimethylamino)phenol (412 mg, 3.00 mmol). ¹H NMR (400 MHz, CDCl₃) δ 7.24 (d, *J* = 8.7 Hz, 1H), 7.17 (dd, *J* = 8.2, 8.2 Hz, 1H), 6.78 (d, *J* = 2.7 Hz, 1H), 6.56 (dd, *J* = 8.7, 2.7 Hz, 1H), 6.49 (dd, *J* = 8.5, 2.5 Hz, 1H), 6.39 (dd, *J* = 2.3, 2.3 Hz, 1H), 6.32 (dd, *J* = 8.0, 2.1 Hz, 1H), 2.93 (s, 6H), 2.79 (s, 6H); ¹³C NMR (100 MHz, CDCl₃) δ 157.9, 156.9, 152.2, 151.6, 131.2, 130.1, 121.8, 112.9, 111.0, 108.0, 106.8, 103.4, 43.8, 40.6; HRMS (EI⁺) Calcd for C₁₆H₁₉ClN₂O ([M]⁺) 290.1180, Found 290.1187.

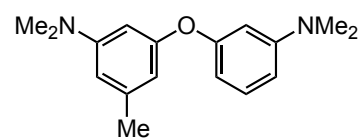
5-(3-(Dimethylamino)phenoxy)-*N,N*,2-trimethylaniline (**181d**)



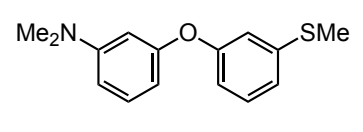
Compound **181d** was obtained in 52% yield (354 mg, 1.31 mmol) following the same method as described for **181a** by the reaction

between 3-bromo-*N,N*,6-trimethylaniline (535 mg, 2.50 mmol) and 3-(dimethylamino)phenol (412 mg, 3.00 mmol). ¹H NMR (400 MHz, CDCl₃) δ 7.15 (dd, *J* = 8.2, 8.2 Hz, 1H), 7.07 (d, *J* = 8.2 Hz, 1H), 6.76 (d, *J* = 2.7 Hz, 1H), 6.58 (dd, *J* = 8.2, 2.7 Hz, 1H), 6.46 (dd, *J* = 8.0, 2.1 Hz, 1H), 6.41 (dd, *J* = 2.3, 2.3 Hz, 1H), 6.31 (dd, *J* = 7.8, 1.8 Hz, 1H), 2.93 (s, 6H), 2.67 (s, 6H), 2.28 (s, 3H); ¹³C NMR (100 MHz, CDCl₃) δ 158.7, 155.8, 154.0, 152.2, 131.8, 130.0, 126.6, 112.7, 109.9, 107.4, 106.4, 103.1, 44.2, 40.7, 18.1; HRMS (EI⁺) Calcd for C₁₇H₂₂N₂O ([M]⁺) 270.1727, Found 270.1732.

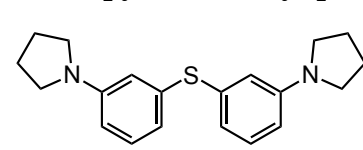
3-(3-(Dimethylamino)phenoxy)-*N,N*,5-trimethylaniline (181e)

 Compound **181e** was obtained in 54% yield (369 mg, 1.36 mmol) following the same method as described for **181a** by the reaction between **S6** (535 mg, 2.50 mmol) and 3-(dimethylamino)phenol (412 mg, 3.00 mmol). ¹H NMR (400 MHz, CDCl₃) δ 7.15 (dd, *J* = 8.0, 8.0 Hz, 1H), 6.44–6.48 (m, 2H), 6.35 (dd, *J* = 8.0, 1.1 Hz, 1H), 6.27 (dd, *J* = 2.3, 2.3 Hz, 2H), 6.19 (s, 1H), 2.93 (s, 6H), 2.91 (s, 6H), 2.26 (s, 3H); ¹³C NMR (100 MHz, CDCl₃) δ 158.4, 158.4, 152.1, 152.0, 140.0, 129.9, 108.3, 107.8, 107.5, 107.0, 103.6, 100.8, 40.8, 40.7, 22.1; HRMS (EI⁺) Calcd for C₁₇H₂₂N₂O ([M]⁺) 270.1727, Found 270.1729.

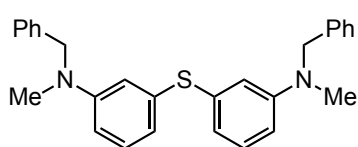
N,N-Dimethyl-3-(3-(methylthio)phenoxy)aniline (181f)

 Compound **181f** was obtained in 44% yield (285 mg, 1.10 mmol) following the same method as described for **181a** by the reaction between 3-bromo-*N,N*-dimethylaniline (508 mg, 2.50 mmol) and 3-(methylthio)phenol (412 mg, 3.00 mmol). ¹H NMR (400 MHz, CDCl₃) δ 7.15–7.23 (m, 2H), 6.91–6.96 (m, 2H), 6.76 (dd, *J* = 8.2, 1.1 Hz, 1H), 6.49 (dd, *J* = 8.0, 2.1 Hz, 1H), 6.41 (dd, *J* = 2.3, 2.3 Hz, 1H), 6.33 (dd, *J* = 8.2, 1.8 Hz, 1H), 2.93 (s, 6H), 2.45 (s, 3H); ¹³C NMR (100 MHz, CDCl₃) δ 158.2, 157.8, 152.2, 140.2, 130.1, 129.9, 120.8, 116.4, 115.2, 108.0, 107.1, 103.7, 40.6, 15.7; HRMS (EI⁺) Calcd for C₁₅H₁₇NOS ([M]⁺) 259.1025, Found 259.1032.

Bis(3-(pyrrolidin-1-yl)phenyl)sulfane (181g)

 Compound **181g** was synthesized according to a reported method.^[74] A Schlenk flask was charged with bis(3-bromophenyl)sulfane^[103] (313 mg, 0.910 mmol, 1.00 equiv), pyrrolidine (226 μL, 2.73 mmol, 3.0 equiv), NaO^tBu (262 mg, 2.73 mmol, 3.0 equiv), Pd(dba)₂ (21.6 mg, 80.0 μmol, 4.00 mol %), BINAP (67.0 mg, 110 μmol, 12.0 mol %), and toluene (1.0 mL) under N₂. The flask was immersed in an oil bath and heated to 80 °C with stirring overnight. The mixture was cooled to room temperature, filtered over Celite, and concentrated. The crude product was then purified by column chromatography (eluent: hexane) on silica gel to give **181g** as white solid (173 mg, 59%). ¹H NMR (400 MHz, CDCl₃) δ 7.12 (dd, *J* = 7.8, 7.8 Hz, 2H), 6.62–6.64 (m, 4H), 6.42–6.44 (m, 2H), 3.22–3.25 (m, 8H), 1.96–1.99 (m, 8H); ¹³C NMR (100 MHz, CDCl₃) δ 148.4, 136.6, 129.7, 118.0, 114.0, 110.4, 47.7, 25.6; HRMS (EI⁺) Calcd for C₂₀H₂₄N₂S ([M]⁺) 324.1655, Found 324.1660.

3,3'-Thiobis(*N*-benzyl-*N*-methylaniline) (**181h**)

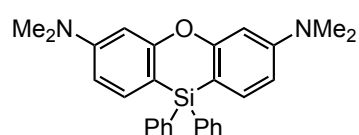


Compound **181h** was obtained in 71% yield following the same method as described for **181g** by the reaction between bis(3-bromophenyl)sulfan^[103] (258 mg, 0.750 mmol) and benzylmethylamine (218 mg, 1.80 mmol). ¹H NMR (400 MHz, CDCl₃) δ 7.29 (dd, *J* = 7.3, 7.3 Hz, 4H), 7.16–7.25 (m, 6H), 7.10 (dd, *J* = 8.0, 8.0 Hz, 2H), 6.76 (dd, *J* = 2.1, 2.1 Hz, 2H), 6.66 (d, *J* = 7.8 Hz, 2H), 6.59 (dd, *J* = 8.5, 2.5 Hz, 2H), 4.48 (s, 4H), 2.97 (s, 6H); ¹³C NMR (100 MHz, CDCl₃) δ 150.3, 138.8, 136.5, 129.8, 128.7, 127.0, 126.8, 119.1, 114.5, 111.1, 56.6, 38.7; HRMS (EI⁺) Calcd for C₂₈H₂₈N₂S ([M]⁺) 424.1968, Found 424.1971.

3.4.2 General Procedure for the Borane-catalyzed Double Sila-Friedel – Crafts Reaction and Spectral Data of Six-membered Silacycles **184**^[34,70]

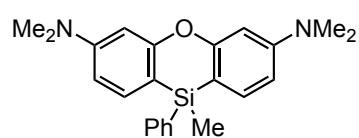
A test tube with a screw cap equipped with a magnetic stirring bar was charged diaryl ether **181a** (64.1 mg, 0.250 mmol, 1.00 equiv) and tris(pentafluorophenyl)borane (B(C₆F₅)₃, 3.80 mg, 0.00750 mmol, 3.0 mol%). The tube was evacuated and filled with nitrogen. Chlorobenzene (0.40 mL) was added via syringe. Diphenylsilane **145a** (0.140 mL, 0.750 mmol, 3.0 equiv) was then added to the mixture (if necessary, 2,6-lutidine (2.20 μL, 0.0190 mmol, 7.5 mol %) was also added). The test tube was closed with a screw cap and the reaction mixture was stirred at 140 °C (oil bath) for 24 h. After completion of the reaction, the mixture was cooled to room temperature. Dichloromethane (10 mL) were added. The crude product was purified by column chromatography on silica gel (eluent: hexane/EtOAc 25:1) to give compound **184a** as white solid (106 mg, 97% yield).

Phenoxasilin **184a**



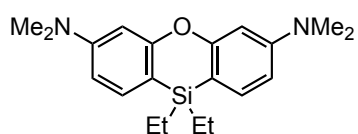
¹H NMR (400 MHz, CDCl₃) δ 7.58 (dd, *J* = 7.8, 1.4 Hz, 4H), 7.28–7.38 (m, 8H), 6.52–6.54 (m, 4H), 2.98 (s, 12H); ¹³C NMR (100 MHz, CDCl₃) δ 162.1, 153.2, 136.09, 136.06, 135.9, 129.4, 127.9, 108.3, 102.3, 100.6, 40.3; HRMS (EI⁺) Calcd for C₂₈H₂₈N₂OSi ([M]⁺) 436.1965, Found 436.1972.

Phenoxasilin **184b**



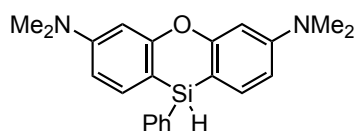
Compound **184b** was obtained as white solid (62.5 mg, 83%) from diaryl ether **181a** (51.3 mg, 0.200 mmol) with 2,6-lutidine. ¹H NMR (400 MHz, CDCl₃) δ 7.52–7.54 (m, 2H), 7.29–7.31 (m, 5H), 6.54 (d, *J* = 2.5 Hz, 1H), 6.50–6.52 (m, 3H), 2.99 (s, 12H), 0.70 (s, 3H); ¹³C NMR (100 MHz, CDCl₃) δ 161.7, 153.1, 138.6, 135.3, 134.8, 129.2, 127.9, 108.2, 104.0, 100.6, 40.4, -2.0; HRMS (EI⁺) Calcd for C₂₃H₂₆N₂OSi ([M]⁺) 374.1809, Found 374.1811.

Phenoxasilin **184c**



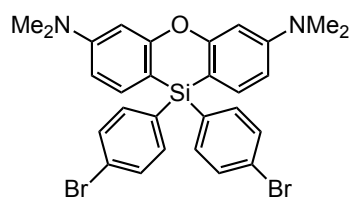
Compound **184c** was obtained as white solid (77.2 mg, 91%) from diaryl ether **181a** (64.1 mg, 0.250 mmol) with 2,6-lutidine. ^1H NMR (400 MHz, CDCl_3) δ 7.32 (d, J = 8.2 Hz, 2H), 6.54 (dd, J = 8.0, 2.1 Hz, 2H), 6.47 (d, J = 2.3 Hz, 2H), 2.99 (s, 12H), 0.85–0.90 (m, 10H); ^{13}C NMR (100 MHz, CDCl_3) δ 162.0, 152.8, 134.8, 107.8, 103.5, 100.7, 40.4, 7.8, 6.6; HRMS (EI^+) Calcd for $\text{C}_{20}\text{H}_{28}\text{N}_2\text{OSi}$ ($[\text{M}]^+$) 340.1965, Found 340.1974.

Phenoxasilin **184d**



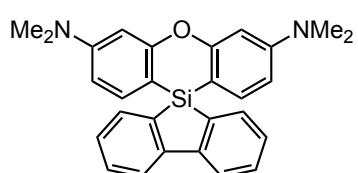
Compound **184d** was obtained as white solid (56.6 mg, 63%) from diaryl ether **181a** (64.8 mg, 0.253 mmol) with 2,6-lutidine. ^1H NMR (400 MHz, CDCl_3) δ 7.60 (dd, J = 7.5, 1.6 Hz, 2H), 7.28–7.38 (m, 5H), 6.52 (dd, J = 6.4, 2.3 Hz, 4H), 5.42 (s, 1H), 3.00 (s, 12H); ^{13}C NMR (100 MHz, CDCl_3) δ 161.9, 153.3, 136.3, 136.0, 135.5, 129.8, 128.1, 108.2, 100.6, 100.2, 40.3; HRMS (EI^+) Calcd for $\text{C}_{22}\text{H}_{24}\text{N}_2\text{OSi}$ ($[\text{M}]^+$) 360.1652, Found 360.1656.

Phenoxasilin **184e**



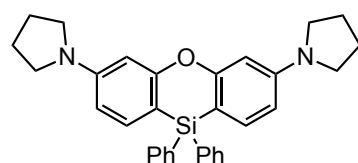
Compound **184e** was obtained as white solid (98.1 mg, 83%) from diaryl ether **181a** (51.3 mg, 0.200 mmol). ^1H NMR (400 MHz, CDCl_3) δ 7.40–7.47 (m, 8H), 7.30 (dd, J = 4.1 Hz, 2H), 6.51–6.55 (m, 4H), 3.00 (s, 12H); ^{13}C NMR (100 MHz, CDCl_3) δ 162.1, 153.3, 137.4, 135.7, 134.6, 131.2, 124.7, 108.4, 100.9, 100.6, 40.3; HRMS (EI^+) Calcd for $\text{C}_{28}\text{H}_{26}\text{Br}_2\text{N}_2\text{OSi}$ ($[\text{M}]^+$) 592.0176, Found 592.1083.

Phenoxasilin **184f**



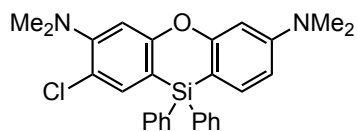
Compound **184f** was obtained as white solid (83.9 mg, 96%) from diaryl ether **181a** (51.3 mg, 0.200 mmol). ^1H NMR (400 MHz, CDCl_3) δ 7.89 (d, J = 7.3 Hz, 2H), 7.43–7.47 (m, 4H), 7.19 (dd, J = 7.3, 7.3 Hz, 2H), 6.99 (d, J = 8.2 Hz, 2H), 6.58 (d, J = 2.3 Hz, 2H), 6.39 (dd, J = 8.2, 2.3 Hz, 2H), 2.99 (s, 12H); ^{13}C NMR (100 MHz, CDCl_3) δ 163.2, 153.6, 148.9, 137.5, 135.9, 134.5, 130.9, 127.9, 120.7, 108.1, 100.6, 99.4, 40.3; HRMS (EI^+) Calcd for $\text{C}_{28}\text{H}_{26}\text{N}_2\text{OSi}$ ($[\text{M}]^+$) 434.1809, Found 434.1814.

Phenoxasilin **184g**



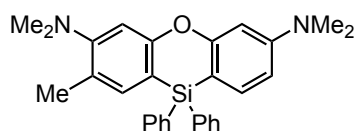
Compound **184g** was obtained as white solid (78.1 mg, 80%) from diaryl ether **181b** (61.7 mg, 0.200 mmol). ^1H NMR (400 MHz, CD_2Cl_2) δ 7.55 (dd, J = 8.0, 1.6 Hz, 4H), 7.30–7.39 (m, 8H), 6.40 (dd, J = 8.2, 2.3 Hz, 2H), 6.34 (d, J = 2.3 Hz, 2H), 3.30–3.33 (m, 8H), 1.99–2.02 (m, 8H); ^{13}C NMR (100 MHz, CD_2Cl_2) δ 162.2, 151.0, 136.7, 136.1, 135.9, 129.6, 128.0, 108.4, 101.1, 99.9, 47.9, 25.8; HRMS (EI^+) Calcd for $\text{C}_{32}\text{H}_{32}\text{N}_2\text{OSi}$ ($[\text{M}]^+$) 488.2278, Found 488.2284.

Phenoxasilin **184h**



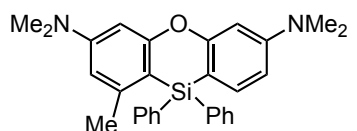
Compound **184h** was obtained as white solid (92.6 mg, 94%) from diaryl ether **181c** (61.1 mg, 0.210 mmol). ^1H NMR (400 MHz, CDCl_3) δ 7.57 (d, $J = 6.4$ Hz, 4H), 7.33–7.44 (m, 8H), 6.89 (s, 1H), 6.52–6.57 (m, 2H), 3.01 (s, 6H), 2.86 (s, 6H); ^{13}C NMR (100 MHz, CDCl_3) δ 161.8, 160.0, 153.3, 153.1, 136.3, 136.1, 136.0, 134.9, 129.9, 128.1, 122.0, 111.0, 109.7, 108.7, 101.2, 100.4, 43.7, 40.3; HRMS (EI^+) Calcd for $\text{C}_{28}\text{H}_{27}\text{ClN}_2\text{OSi}$ ($[\text{M}]^+$) 470.1576, Found 470.1582.

Phenoxasilin **184i**



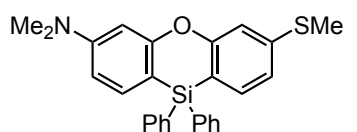
Compound **184i** was obtained as white solid (95.2 mg, 99%) from diaryl ether **181d** (54.1 mg, 0.200 mmol). ^1H NMR (400 MHz, CD_2Cl_2) δ 7.56 (dd, $J = 8.0, 1.6$ Hz, 4H), 7.32–7.39 (m, 7H), 7.26 (s, 1H), 6.82 (s, 1H), 6.56 (dd, $J = 8.2, 2.3$ Hz, 1H), 6.50 (d, $J = 2.3$ Hz, 1H), 2.99 (s, 6H), 2.74 (s, 6H), 2.24 (s, 3H); ^{13}C NMR (100 MHz, CD_2Cl_2) δ 162.2, 160.0, 156.4, 153.7, 137.2, 136.1, 136.0, 135.9, 129.9, 128.2, 126.4, 108.7, 108.6, 107.6, 101.6, 100.5, 43.9, 40.3, 18.3; HRMS (EI^+) Calcd for $\text{C}_{29}\text{H}_{30}\text{N}_2\text{OSi}$ ($[\text{M}]^+$) 450.2122, Found 450.2127.

Phenoxasilin **184j**



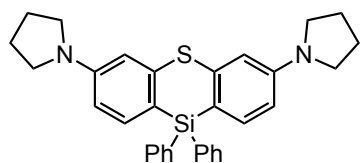
Compound **184j** was obtained as white solid (72.5 mg, 81%) from diaryl ether **181e** (54.1 mg, 0.200 mmol) with 2,6-lutidine. ^1H NMR (400 MHz, CDCl_3) δ 7.63 (dd, $J = 7.8, 1.8$ Hz, 4H), 7.30–7.35 (m, 6H), 7.24 (d, $J = 4.3$ Hz, 1H), 6.43–6.48 (m, 3H), 6.36 (d, $J = 2.3$ Hz, 1H), 3.00 (s, 6H), 2.96 (s, 6H), 2.17 (s, 3H); ^{13}C NMR (100 MHz, CDCl_3) δ 162.7, 161.4, 153.1, 153.0, 146.1, 136.3, 136.1, 136.0, 129.3, 127.9, 109.4, 108.3, 103.6, 101.5, 100.0, 98.8, 40.3, 40.2, 24.7; HRMS (EI^+) Calcd for $\text{C}_{29}\text{H}_{30}\text{N}_2\text{OSi}$ ($[\text{M}]^+$) 450.2122, Found 450.2126.

Phenoxasilin **184k**



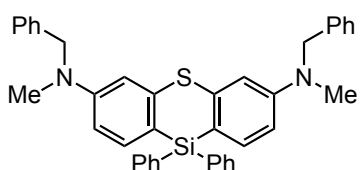
The mixture of **184k** and the hydrosilane **184k'** produced via a single sila-Friedel–Crafts reaction was obtained as white solid (60.1 mg, 68% yield of **184k** and **184k'** (**184k**:**184k'** = 92:8)) from diaryl ether **181f** (52.0 mg, 0.200 mmol). ^1H NMR (400 MHz, CDCl_3) δ 7.64 (dd, $J = 7.8, 1.4$ Hz, 4H), 7.38–7.50 (m, 8H), 7.14 (d, $J = 1.1$ Hz, 1H), 7.04 (dd, $J = 8.0, 1.6$ Hz, 1H), 6.62 (td, $J = 8.9, 2.3$ Hz, 2H), 3.08 (s, 6H), 2.58 (s, 3H); ^{13}C NMR (100 MHz, CDCl_3) δ 161.8, 161.0, 153.3, 142.7, 136.0, 135.9, 135.5, 135.1, 129.8, 128.0, 120.6, 114.6, 112.6, 108.6, 101.5, 100.6, 40.3, 15.1; HRMS (EI^+) Calcd for $\text{C}_{27}\text{H}_{25}\text{NOSSi}$ ($[\text{M}]^+$) 439.1421, Found 439.1427.

Phenothiasiline **184l**



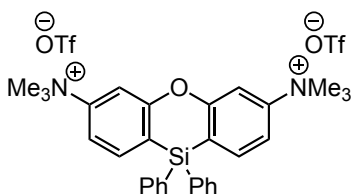
Compound **184l** was obtained as white solid (46.9 mg, 93%) from diaryl ether **181g** (32.6 mg, 0.100 mmol). ^1H NMR (400 MHz, CD_2Cl_2) δ 7.46 (dd, $J = 8.0, 1.6$ Hz, 4H), 7.31–7.41 (m, 6H), 7.21 (d, $J = 8.2$ Hz, 2H), 6.67 (d, $J = 2.3$ Hz, 2H), 6.44 (dd, $J = 8.2, 2.3$ Hz, 2H), 3.27–3.30 (m, 8H), 1.97–2.00 (m, 8H); ^{13}C NMR (100 MHz, CD_2Cl_2) δ 149.0, 144.2, 136.8, 136.3, 135.2, 129.7, 128.1, 115.7, 110.2, 109.8, 47.7, 25.7; HRMS (EI^+) Calcd for $\text{C}_{32}\text{H}_{32}\text{N}_2\text{SSi}$ ($[\text{M}]^+$) 504.2050, Found 504.2057.

Phenothiasiline **184m**



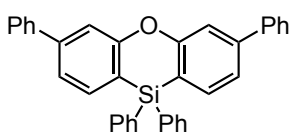
Compound **184m** was obtained as white solid (70.4 mg, 58%) from diaryl ether **181h** (85.5 mg, 0.200 mmol). ^1H NMR (400 MHz, CDCl_3) δ 7.50 (dd, $J = 8.0, 1.6$ Hz, 4H), 7.29–7.40 (m, 11H), 7.18–7.25 (m, 7H), 6.88 (d, $J = 2.3$ Hz, 2H), 6.59 (dd, $J = 8.2, 2.3$ Hz, 2H), 4.54 (s, 4H), 3.03 (s, 6H); ^{13}C NMR (100 MHz, CDCl_3) δ 150.5, 144.3, 138.6, 136.8, 136.3, 134.4, 129.6, 128.8, 127.9, 127.1, 126.7, 117.6, 110.3, 56.1, 38.5 (one carbon is missing); HRMS (EI^+) Calcd for $\text{C}_{40}\text{H}_{36}\text{N}_2\text{SSi}$ ($[\text{M}]^+$) 604.2363, Found 604.2370.

Ammonium Salt **188**



A dry round-bottomed flask equipped with a magnetic stirring bar was charged with **184a** (175 mg, 0.400 mmol, 1.00 equiv) and CH_2Cl_2 (5 mL). To the resultant stirring solution was added dropwise MeOTf (144 mg, 0.880 mmol, 2.20 equiv) at room temperature. The solution was stirred at room temperature for 2 h. The reaction mixture was concentrated to remove CH_2Cl_2 and the residue was treated with Et_2O (20 mL). The resultant solid was filtered, washed with Et_2O and hexane, and dried under vacuum to give **188** as white solid (279 mg, 91%). ^1H NMR (400 MHz, $\text{DMSO}-d_6$) δ 7.96 (d, $J = 8.2$ Hz, 2H), 7.84–7.90 (m, 4H), 7.40–7.57 (m, 12H), 3.66 (s, 18H); ^{13}C NMR (150 MHz, $\text{DMSO}-d_6$) δ 159.3, 150.2, 137.5, 135.4, 131.3, 130.9, 128.6, 120.7 (q, $J = 322$ Hz), 117.6, 116.0, 110.8, 56.3; HRMS (FAB^+) Calcd for $\text{C}_{31}\text{H}_{34}\text{F}_3\text{N}_2\text{O}_4\text{SSi}$ ($[\text{M}^-\text{OTf}]^+$) 615.1961, Found 615.1962.

Phenoxasilin **189**



Compound **189** was synthesized according to a reported method. To a dry Schlenk flask equipped with a magnetic stirring bar was added compound **188** (153 mg, 0.200 mmol, 1.0 equiv) and $\text{PdCl}_2(\text{PPh}_3)_2$ (2.8 mg, 0.0040 mmol, 2.0 mol %). The flask was sealed with a rubber septum, evacuated/filled with nitrogen. THF (1.5 mL) was added via syringe, and the resultant slurry was stirred for 5 min. Then phenylmagnesium bromide (0.5 M solution in THF, 0.88 mL, 0.44 mmol, 2.2 equiv) was added dropwise at room temperature. After 1 h, the reaction mixture was quenched with water (1.0 mL) and 6 M HCl (3 mL), then extracted with Et_2O . The organic

extract was dried over Na₂SO₄, filtered, and concentrated. The crude product was purified by chromatography on silica gel (eluent: hexane/EtOAc 50:1) to give compound **189** as white solid (87.2 mg, 87% yield). ¹H NMR (400 MHz, CDCl₃) δ 7.63–7.68 (m, 10H), 7.53 (d, *J* = 1.4 Hz, 2H), 7.37–7.49 (m, 14H); ¹³C NMR (100 MHz, CDCl₃) δ 160.9, 144.9, 140.5, 136.1, 136.0, 134.1, 130.2, 129.0, 128.3, 128.0, 127.4, 121.9, 116.8, 114.7; HRMS(EI⁺) Calcd for C₃₆H₂₆OSi ([M]⁺) 502.1747, Found 502.1755.

Chapter 4

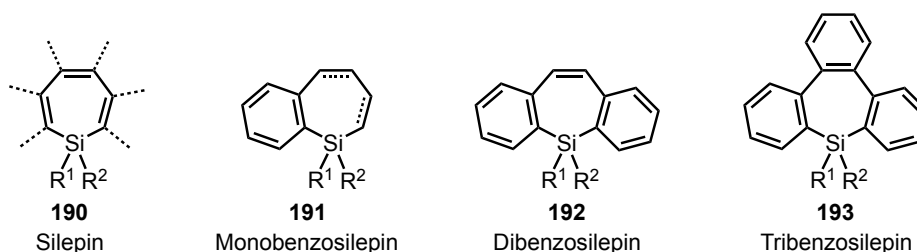
Facile Synthesis of Tribenzosilepins from Terphenyls and Dihydrosilanes by Double Sila-Friedel–Crafts Reaction

In this chapter, I described the synthesis of tribenzosilepins from terphenyls and dihydrosilanes using a double sila-Friedel–Crafts reaction. Tribenzosilepin derivatives with different substituents were formed in moderate to high yield. The synthesis of bidirectional silepin was successfully achieved using the reaction system. Moreover, the amino groups of tribenzosilepin derivatives can be transformed into aryl groups, and the backbone π -system in tribenzosilepin can be extended. Additionally, optical properties of selected tribenzosilepins were investigated.

4.1 Introduction

In organic electronics and photonics, silicon-containing cyclic compounds have fascinating potential applications prospects.^[62c,64b,94] In the past several decades, the syntheses and photoluminescence properties of five/six-membered silacycles have been widely explored.^[5,50f,64a,65,70,97,104] Furthermore, silepin (silacycloheptatriene) **190** and benzene-ring-fused silepins including monobenzosilepin **191**, dibenzosilepin **192**, and tribenzosilepin **193**, also exhibit attractive structural features (Scheme 4.1).

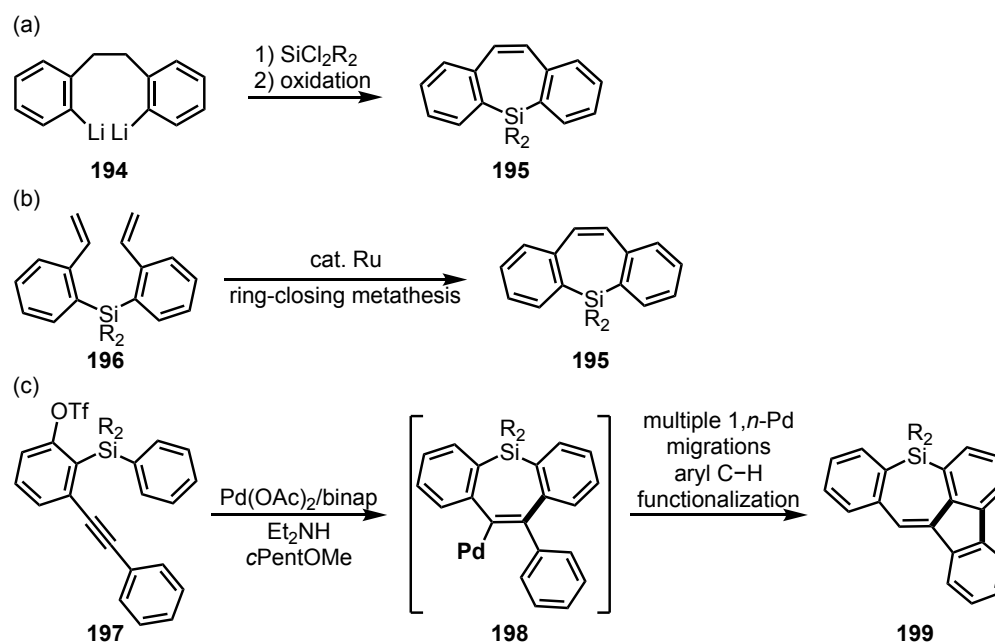
Scheme 4.1. Structures of silepin derivatives.



The synthetic methods and optical properties of silepins^[96b,105] and dibenzosilepins^[52] have been researched. Some dibenzosilepins show strong blue fluorescence (quantum yield up to

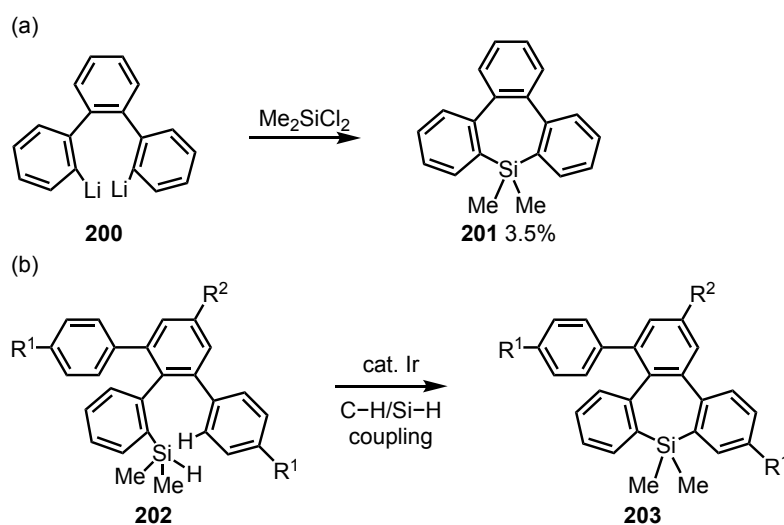
0.93).^[52i,k] Generally, they were prepared by the reaction between the bis(2-lithioaryl)ethene **194** and dichlorosilanes with the following oxidation (Scheme 4.2a). Besides, ruthenium-catalyzed ring-closing metathesis of bis(2-vinylphenyl)silanes **196** (Scheme 4.2b)^[52j] and palladium-catalyzed protocols (Scheme 4.2c)^[52k] have been reported for the synthesis of dibenzosilolepines. The synthesis of monobenzosilolepin derivatives have been developed by several methods.^[106]

Scheme 4.2. Synthetic approaches of dibenzosilolepin derivatives.



Conversely, the synthesis of tribenzosilolepins have not been widely studied. A conventional reaction between dilithiated terphenyl **200** and dimethyldichlorosilane lead to the formation of tribenzosilolepin **201** in very low yield (Scheme 4.3a).^[53] The iridium-catalyzed intramolecular reaction of 2',6'-diaryl-2-(hydrosilyl)biphenyl **202** through dehydrogenative C–H/Si–H coupling have been developed recently (Scheme 4.3b).^[54] However, practical synthetic methods of tribenzosilolepin derivatives with improved yield based on C–H silylation are still desired.

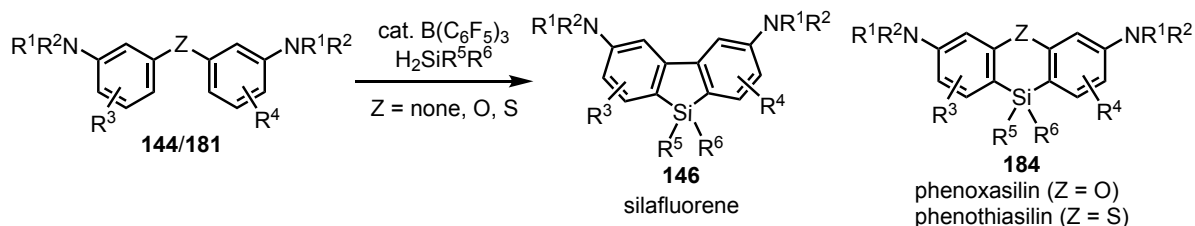
Scheme 4.3. Synthetic methods of tribenzosilepin.



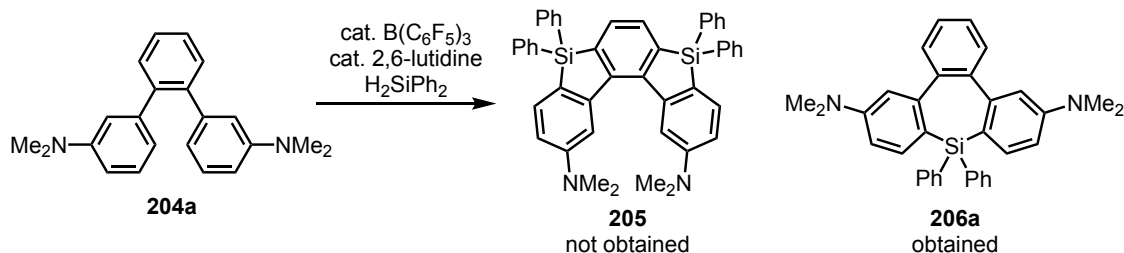
Electrophilic silylation is a fundamental pathway for the transformation of the C–H bond into a C–Si bond in order to synthesize organosilicon compounds.^[55] Electron-deficient borane can effectively activate Si–H bond^[107] and catalyze the sila-Friedel–Crafts reaction between hydrosilanes and electron-rich aromatic rings.^[31,32,34,39,69] $\text{B}(\text{C}_6\text{F}_5)_3$ -catalyzed intra- and intermolecular sila-Friedel–Crafts reactions are useful for the synthesis of silacycles, such as dibenzosilole and silafluorene derivatives.^[30] As mentioned in Chapters 2 and 3, I developed $\text{B}(\text{C}_6\text{F}_5)_3$ -catalyzed double sila-Friedel–Crafts reaction for the simple synthesis of silafluorene, phenoxasilin, and phenothiasilin derivatives (Scheme 4.4a).^[70,104f] During the study of the silafluorene synthesis using the diamino-substituted *o*-terphenyl **204a** and diphenyldihydrosilane (**145a**), the desired bidirectional silafluorene **205** was not obtained. However, the tribenzosilepin **206a** was formed. Hence, the result inspired me to start the development of the new synthetic method of tribenzosilepins.

Scheme 4.4. Double sila-Friedel–Crafts reaction for synthesis of silacyclic compounds.

a) Chapter 2, 3: Synthesis of five- and six-membered silacyclic compounds



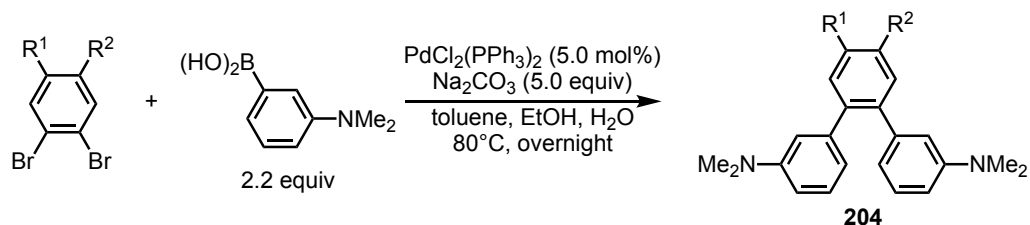
b) Preliminary result



4.2 Results and Discussion

Terphenyls **204** were synthesized by the Suzuki-Miyaura cross-coupling reaction of substituted 1,2-dibromobenzenes with (3-(dimethylamino)phenyl)boronic acid (Scheme 4.5).^[75]

Scheme 4.5. Synthesis of substrates **204**.

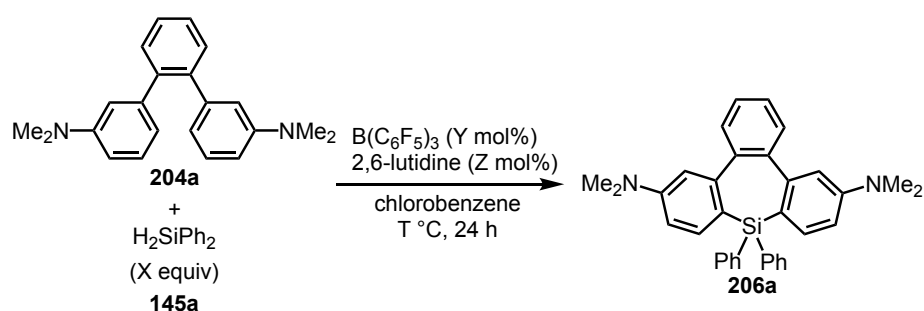


I firstly optimized the reaction conditions by tuning the reaction temperature and the loading amounts of dihydrosilane **145a**, the borane catalyst, and 2,6-lutidine (Table 4.1). The desired reaction proceeded under the reaction conditions (100 °C, 6.0 equivalents of **145a**, 5.0 mol% of $\text{B(C}_6\text{F}_5)_3$, and 7.5 mol% of 2,6-lutidine) to afford the tribenzosilolepin **206a** in 87% yield (entry 1). Upon decreasing the equivalent of **145a** from 6 to 1.5 equiv, the yield of **206a** remained at approximately 80% (entries 1–3). Although the yield of **206a** maintained when $\text{B(C}_6\text{F}_5)_3$ was reduced to 3.0 mol% (entry 4), the yield of **206a** significantly dropped to 63% using 1.0 mol%

of $B(C_6F_5)_3$ (entry 5). In addition, the yield decreased to 52% at 80 °C (entry 6). In the absence of 2,6-lutidine, **206a** was obtained in 68% yield (entry 7). By comparing the results in entries 4 and 7, the base slightly accelerated the deprotonation step with the improvement of the yield from 68% to 80%.

Based on the above results, the following experiments were carried out using the reaction conditions shown in entry 4.

Table 4.1. Optimization of reaction conditions for synthesis of **206a** from diaminoterphenyl **204a** and dihydrodiphenylsilane **145a**.



entry	X (equiv)	Y (mol%)	Z (mol%)	T (°C)	yield (%)
1	6.0	5.0	7.5	100	87
2	3.0	5.0	7.5	100	84
3	1.5	5.0	7.5	100	81
4	1.5	3.0	7.5	100	80
5	1.5	1.0	7.5	100	63
6	1.5	3.0	7.5	80	52
7	1.5	3.0	0	100	68

Single crystals of **206a** were obtained from its dichloromethane/ethanol solution by the slow evaporation of the solvent. The single-crystal X-ray diffraction analysis of **206a** in solid-state was shown in Figure 4.1. It revealed that the upper benzene ring, along with the seven-membered ring in **206a**, formed a saddle-shaped upward conformation, while the two other benzene rings constructed a downward conformation. The benzene moieties connected to the silicon atom are in two distinct structural environments because of the twisted conformation of the silepin skeleton.

Figure 4.1. Single crystal X-ray structure of **206a** in the solid state. Displacement ellipsoids are drawn at the 50% probability level. All hydrogen atoms are omitted for clarity.



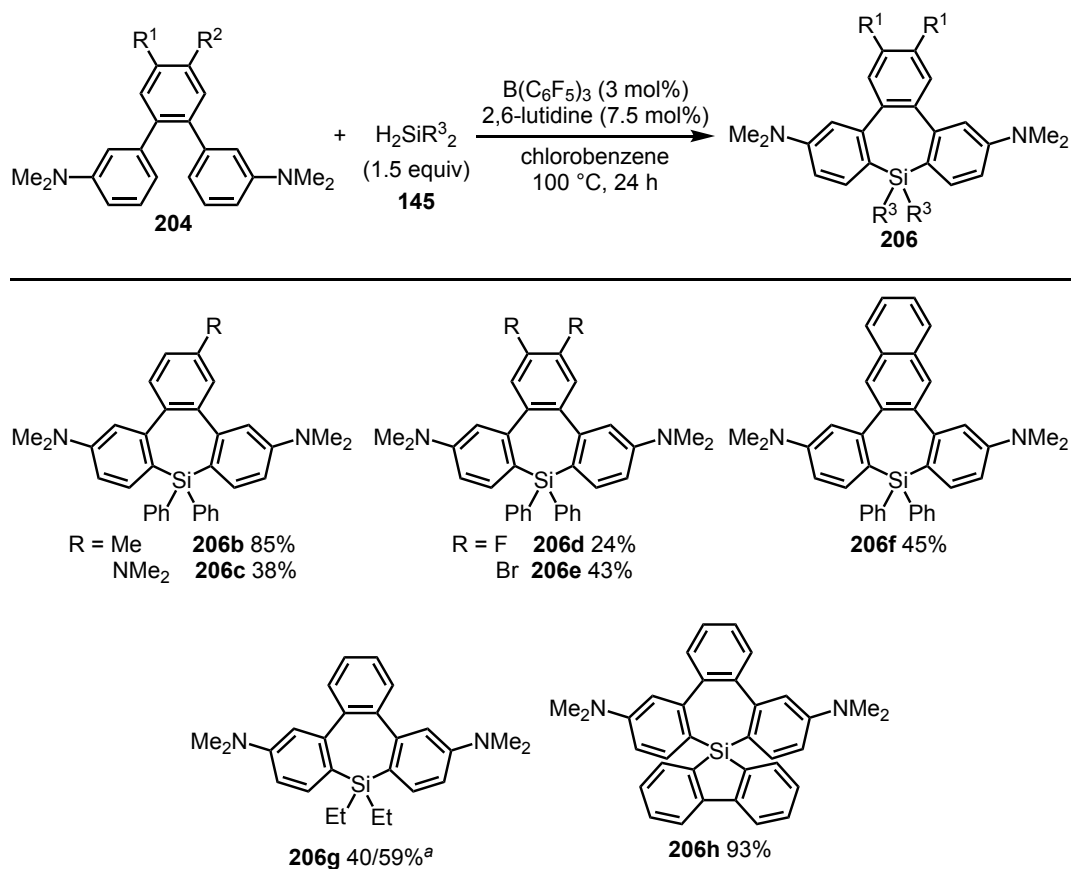
The optimized reaction conditions were applied for the synthesis of other silepin derivatives (Scheme 4.6). Methyl- or dimethylamino-substituted terphenyl **204b** and **204c** gave the corresponding silepins **206b** and **206c** in 85% and 38% yields, respectively. 43% of substrate **204c** was recovered after purification by flash column chromatography. Difluoro-substituted silepin **206d** was obtained in 24% yield with the recovery of **204d** in 60%. Dibromo-substituted terphenyl **204e** was transformed to **206e** without losing any bromine atoms and can be converted to other functional groups using a wide variety of transformations, such as coupling reactions. In the case of **204e**, the recovery of the substrate is 46%. The low conversion of **204d** and **204e** is mainly due to the decreased electron density at the phenyl ring derived from the inductive effect of halogen.

The formation of five-membered cyclic products were not detected during the double sila-Friedel–Crafts reaction for the synthesis of tribenzosilepin derivative **206a–e**. It is due to the low electron density of the central benzene ring, demonstrated that the double sila-Friedel–Crafts reaction needs electron rich arenes as substrates.

The reaction of the naphthalene-substituted substrate **204f** also proceeded successfully and afforded **206f** in 45% yield. In this reaction, substrate **204f** was not recovered and byproducts were formed (the structures could not be determined). The synthesis of tribenzosilepins is sensitive to the substituents on the central benzene ring. Dihydrodiethylsilane **145c** gave **206g** in 40% yield. Considering about the low boiling point of dihydrodiethylsilane (56 °C), I increased the amount of dihydrodiethylsilane to 3.0 equivalents, as a result, the yield was improved to 59% (recovery of **204a** is 24%). The reaction of **204a** with dihydrosilafluorene **145f** resulted in the formation of the corresponding silepin **206h**, having the spiro-structure, in

93% yield. This is the first example of a 5-silaspiro[4.6] structure being described using the current route of synthesis.

Scheme 4.6. Substrate Scope.



^a H_2SiEt_2 (3 equiv).

In the ^1H and ^{13}C NMR spectra, the two aryl or ethyl groups on the silicon atom were observed independently at room temperature. These findings suggest that the two substituents exist in distinct environments in solution and that boat-to-boat ring inversions via the planar conformation was not observed by NMR at ambient temperature.^[53]

The structure of **206g** in the solid state was confirmed by single crystal X-ray structure analysis (Figure 4.2). To investigate the detail assignment of the two ethyl groups of **206g**, heteronuclear multiple quantum coherence (HMQC) and heteronuclear single quantum correlation (HSQC) of **206g** were measured. The results revealed that the protons (H^1 and H^2) of one of the ethyl groups were observed at the higher field than H_3 and H_4 by the ring current

effect of the central benzene ring (Figure 4.3a). Additionally, the two ethyl groups of **206g** appeared independently in the ^1H NMR spectrum at 25 °C, 60 °C, and 100 °C in toluene- d_8 (Figure 4.3). Even though the shift of peaks was observed, the inversion of **206g** was not detected, even at 100 °C.

Figure 4.2. Single crystal X-ray structure of **206g** in the solid state. All hydrogen atoms are omitted for clarity.

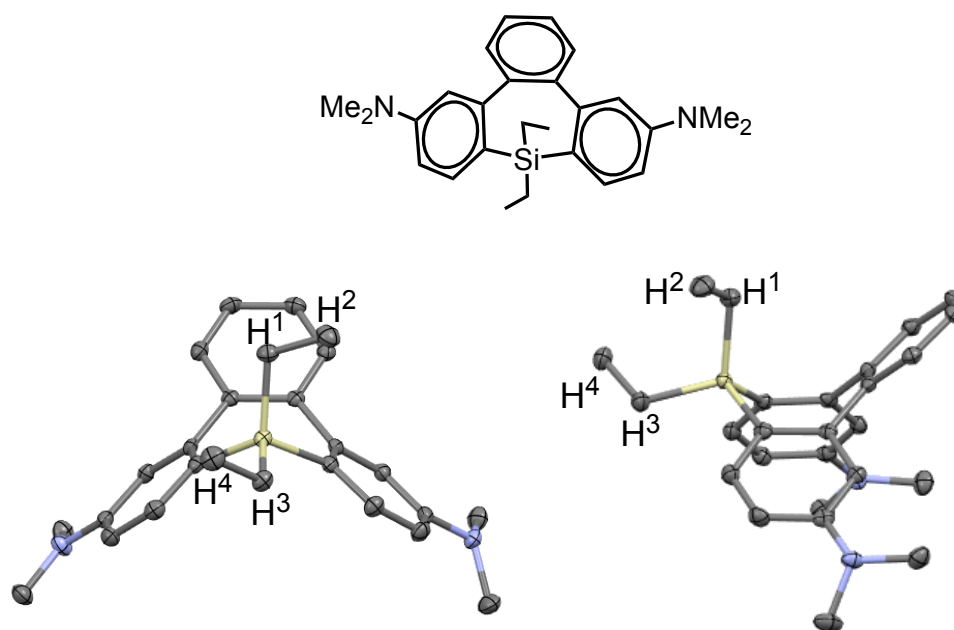
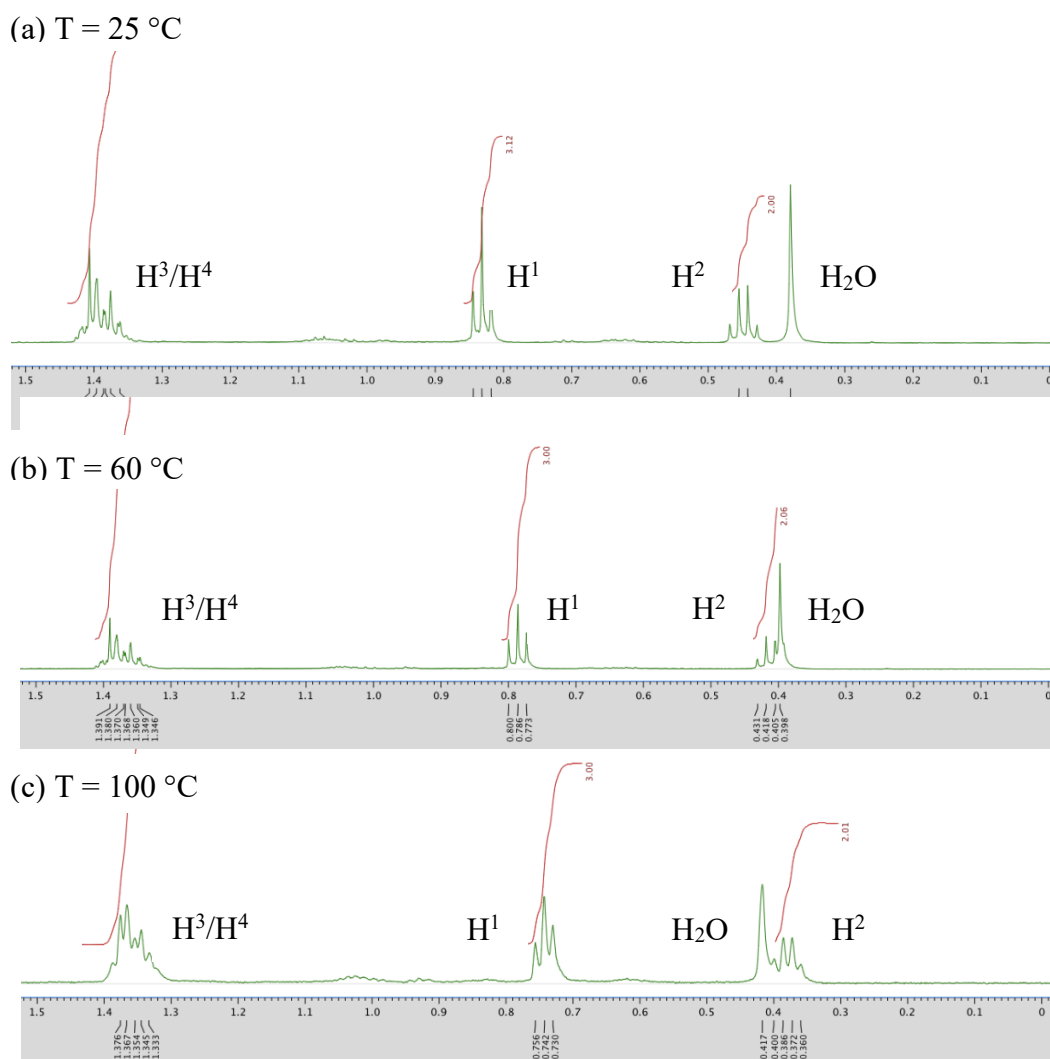


Figure 4.3. Variable temperature ^1H NMR of **206g** in toluene- d_8 .



The quadruple Friedel–Crafts silylation of tetraphenyl benzene **207** was investigated under the optimal reaction conditions (Scheme 4.7). Substrate **207** was synthesized by Suzuki–Miyaura cross-coupling reaction of 1,2,4,5-tetrabromobenzene with (3-(dimethylamino)phenyl boronic acid (experimental section).^[75] As a result, disilepin **209** was successfully obtained in 85% yield.

Based on the result of the non-inversion of the silepin ring as described above, I considered that the formation of *cis*- or *trans*-stereoisomers related to the two silicon atoms of the corresponding bidirectional **209** was possible (Scheme 4.7). The solid structure of **209** was revealed by single-crystal X-ray crystallography, which confirmed it to be the *trans*-isomer (Figure 4.4). The selective formation of the *trans*-isomer is probably due to the steric repulsion

of the two phenyl groups on the two silicon atoms during the second intramolecular silylation step, which hampered the formation of the *cis* isomer.

Scheme 4.7. Synthesis of bidirectional silepin **212**.

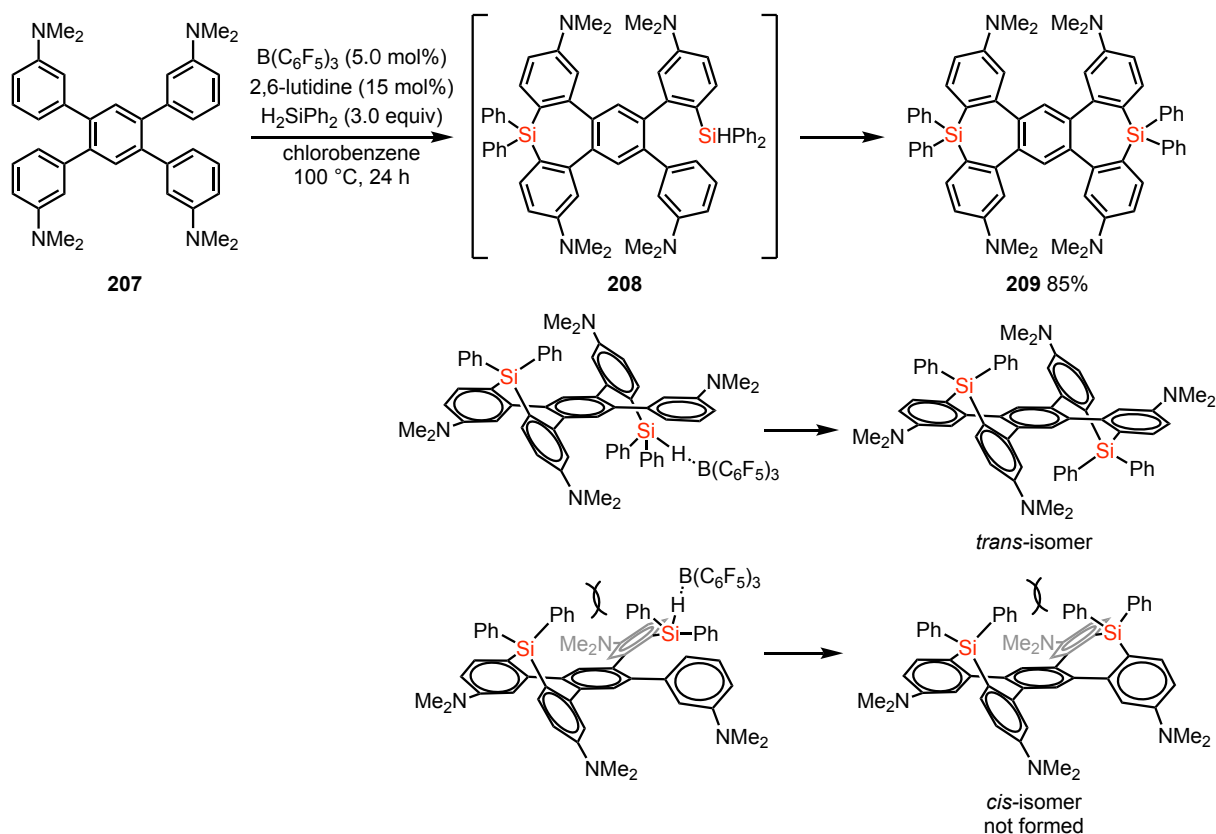
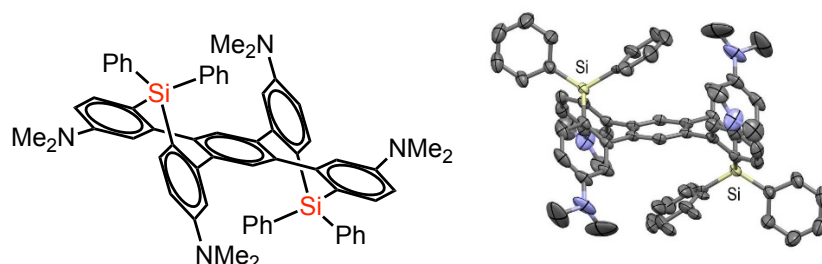


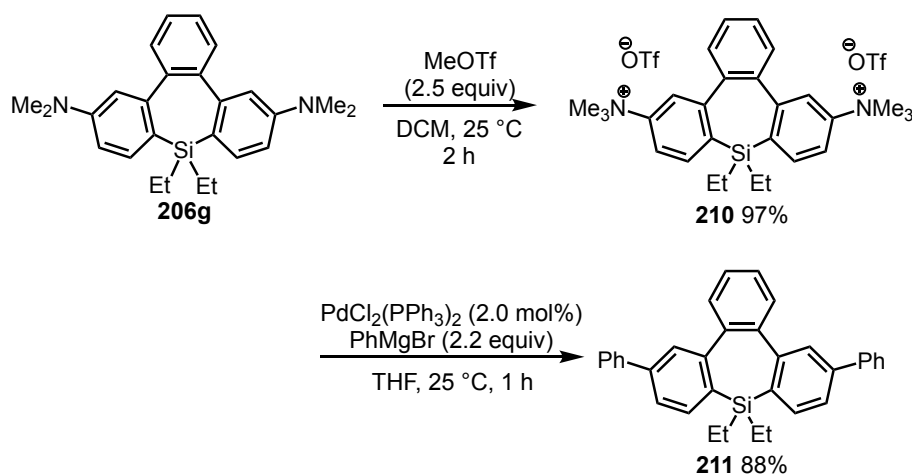
Figure 4.4. Single crystal X-Ray structure of **209** in the solid state. Displacement ellipsoids are drawn at the 50% probability level. All hydrogen atoms are omitted for clarity.



The amino groups of tribenzosilepin can be transformed to other substituents via cross-coupling reactions between aryltrimethylammonium triflates and aryl Grignard reagents (Scheme 4.8).^[80] Firstly, the amino groups of **206g** were converted to their corresponding

triflate salts **210**. Thereafter, the reaction of **210** with phenyl Grignard reagent using a catalytic amount of $\text{PdCl}_2(\text{PPh}_3)_2$ afforded the corresponding cross-coupling product **211** in 88% yield.

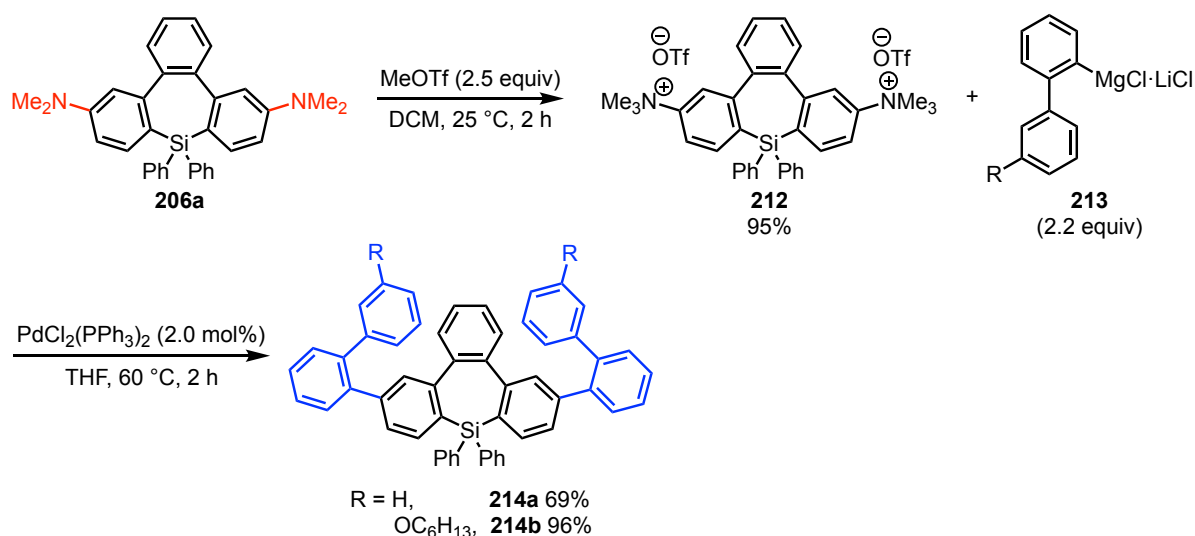
Scheme 4.8. Conversions of amino groups on silepin **206g**.



Curved π -conjugated molecules exhibit attractive optical and electrochemical properties.^[108] Considering the saddle structure of the obtained tribenzosilepin derivatives, I planned to construct silicon-embedded curved π -conjugated molecules.

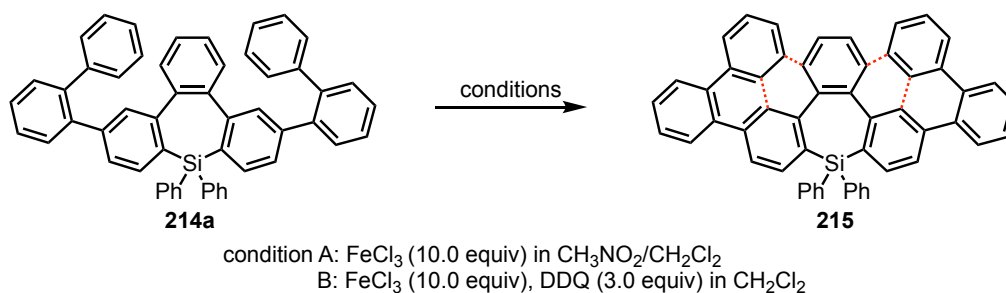
The π -conjugated system of tribenzosilepin can be enlarged through conversions of amino groups of silepins to aryl groups and a sequential oxidative cyclization. Firstly, the amino groups of **206a** were converted to **214** through the cross-coupling reaction between triflate salts **212** and biphenyl Turbo Grignard reagents using a catalytic amount of $\text{PdCl}_2(\text{PPh}_3)_2$ at 60°C afforded the corresponding products **214a** and **214b** in 69% and 96% yield, respectively (Scheme 4.9).^[80]

Scheme 4.9. Conversions of amino groups on silepin **206a**.



I then investigated cyclization reaction of **214a** using FeCl_3 system.^[109] However, the desired reaction did not proceed, and the substrate was recovered completely. The conditions using FeCl_3/DDQ afforded products with very poor solubility that I couldn't confirm the structure (Scheme 4.10).^[110]

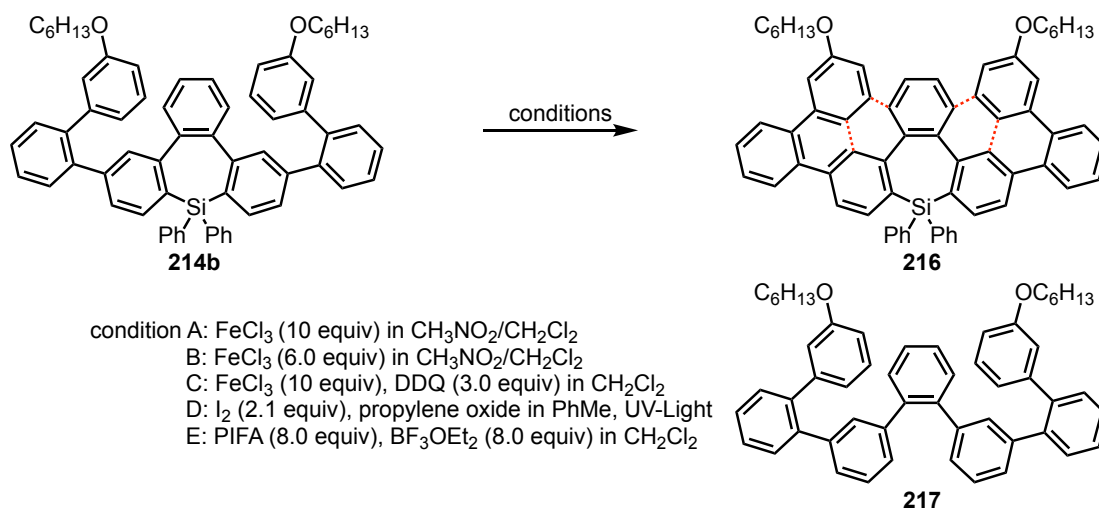
Scheme 4.10. Attempt on enlargement of π -conjugated system from **214a**.



To enhance the solubility and the reactivity, biphenyl bearing $-\text{OC}_6\text{H}_{13}$ groups, which have high solubility and electron donating ability, was adopted. Although I investigated several Scholl reaction conditions (Scheme 4.11), desired π -extended compound **216** was not obtained. Using 10 or 6 equivalents of FeCl_3 (conditions A and B), afforded the desilylated product **217**.^[111] In the reaction system using FeCl_3/DDQ (condition C), it was uncertain that the

reaction product was obtained.^[110] The reactions using I₂ and propylene oxide (condition D)^[112] or [bis(trifluoroacetoxy)iodo]benzene (PIFA) and BF₃OEt₂ (condition E),^[113] did not proceed.

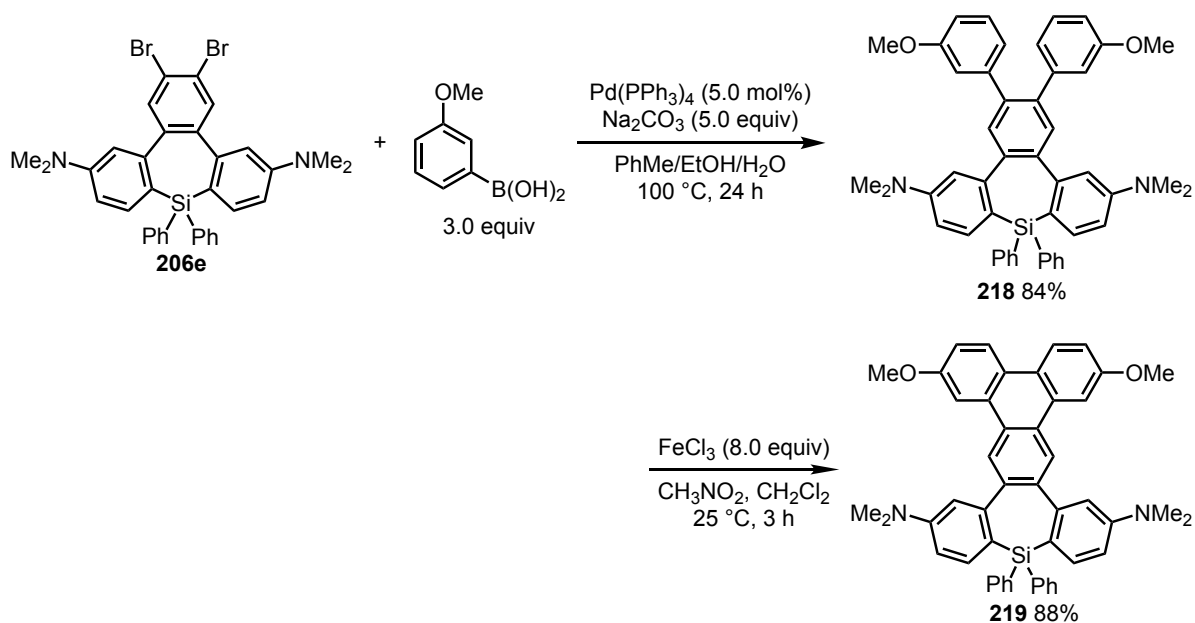
Scheme 4.11. Attempt on enlargement of π -conjugated system from **214b**.



Based on the above results for preparing the curved π -conjugated molecules, I tried to extend the π -system of the aromatics at the backbone.

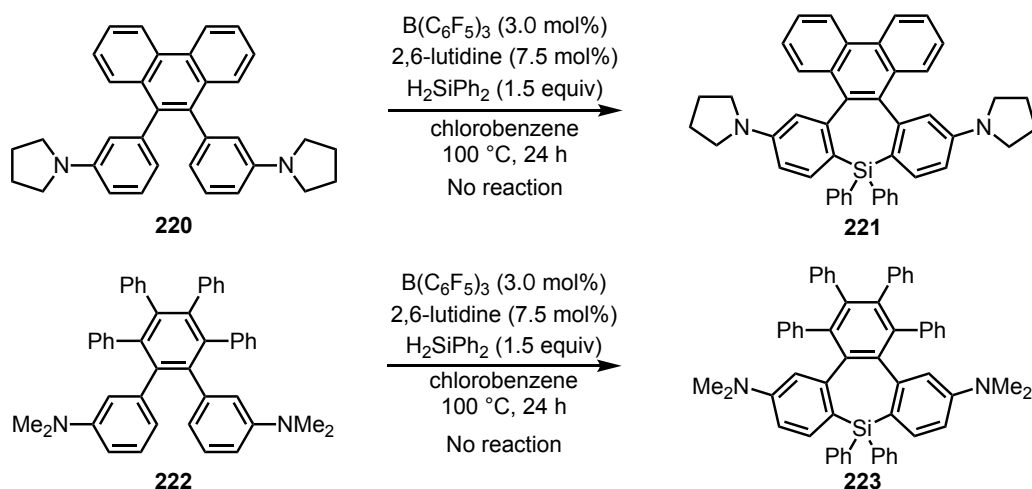
Finally, the π -conjugated system of **206e** was extended by a cross-coupling reaction and a successive Scholl reaction (Scheme 4.12). The Suzuki–Miyaura cross-coupling reaction of **206e** with 3-methoxyphenylboronic acid afforded **218** in 84% yield.^[114] The backbone π -system in **218** was further extended by a Scholl-type reaction using FeCl₃ as an oxidant to give **219** in 88% yield without the loss of the SiPh₂ and dimethyl amino groups.^[111] The structure of **219** was confirmed by ¹H and ¹³C NMR spectroscopy, high-resolution mass spectrometry, and X-ray single crystallography.

Scheme 4.12. Extension of the backbone π -system from **206e**.



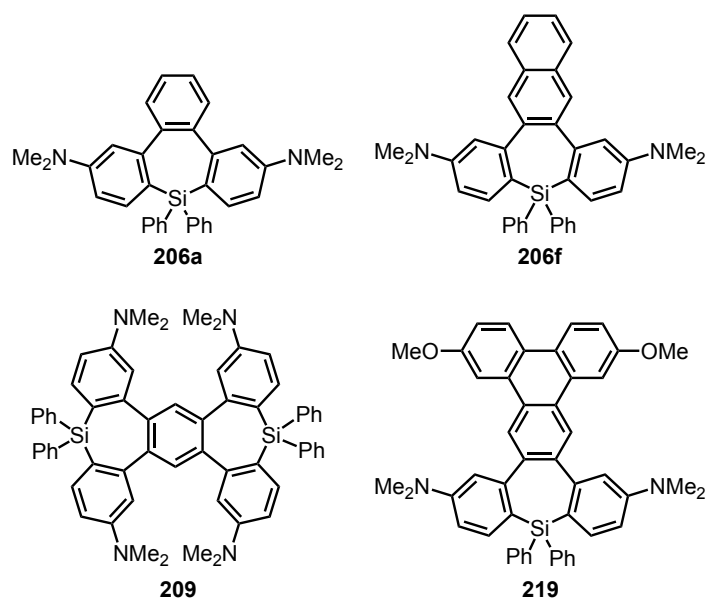
Extension of the π -conjugated system of substrates **220** and **222** was also investigated (Scheme 4.13). There was no reaction proceed with the two substrates, the compound **220** and **222** were recovered after the reaction. These results are mainly due to the structure rigidity of the phenanthrene framework in **220** and the steric hinderance with the phenyl groups on the backbone in **222**.

Scheme 4.13. Other substrates



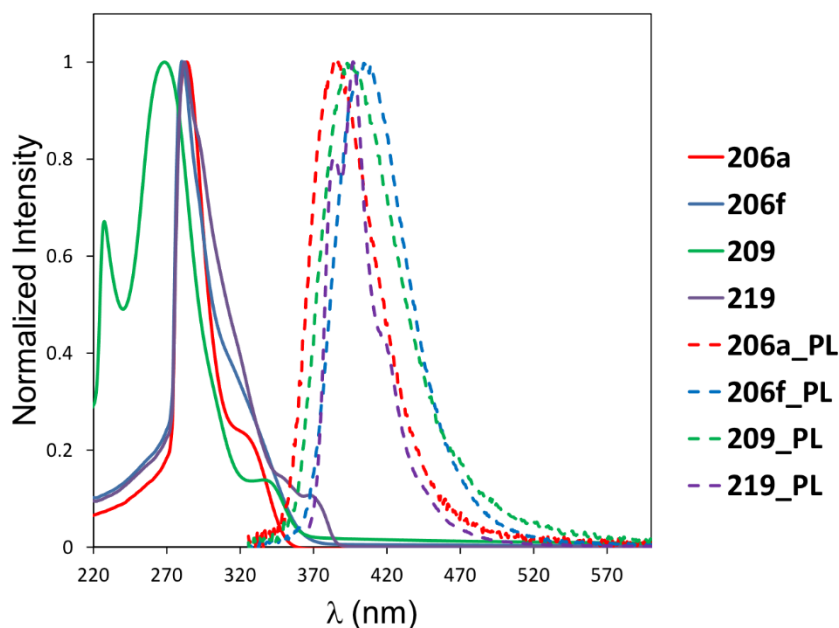
The optical properties of **206a**, **206f**, **209**, and **219** were studied by UV/Vis absorption and photoluminescence spectroscopy (Table 4.2, Figure 4.5). In the absorption spectra, the λ_{max} of the silepins appeared in the range of 269–284 nm. Photoluminescence spectroscopy indicated that the silepins emitted violet-blue fluorescence. The emission peaks of **209** and **219** were slightly red-shifted (10 nm) compared to that of **206a**, while **206f** with the direct extension of the π -conjugated system have a red-shifted of 19 nm. From **206a** to **206f**, the red-shift PL band clearly supports the extended π -system by the introduction of a naphthyl group. There was only a small difference of quantum yields between **206a**, **206f**, and **209**. While silepin **219** exhibited threefold improvement of photoluminescence quantum yield compared to **206a**.

Table 4.2. Optical properties of **206a**, **206f**, **209** and **219**.



Entry	λ_{max} (nm)	λ_{em} (nm)	Φ_{F}
206a	284	387	0.11
206f	280	406	0.16
209	269	395	0.14
219	282	397	0.37

Figure 4.5. UV absorption (solid line) and photoluminescence (dot line) spectra of **206a**, **206f**, **209**, and **219** in toluene (5.0×10^{-5} M).



4.3 Conclusion

In conclusion, I have developed a facile synthetic method for the synthesis of tribenzosilepin derivatives. The double sila-Friedel–Crafts reaction between amino group-containing terphenyls and dihydrosilanes afforded tribenzosilepins bearing electron-withdrawing or -donating groups on the backbone in good yields. This is a rare example of the synthesis of tribenzosilepin derivatives and the first example of the direct synthesis from terphenyls and dihydrosilanes. The rigid structures of resulting tribenzosilepins at ambient temperature were confirmed by their NMR spectra in solution. The reaction of the bidirectional substrate stereoselectively formed the *trans*-disilepin. In addition, the extension of π -conjugate systems of the silepin derivatives and the transformation of amino groups to other aromatic substituents were achieved. I hope that the provided synthesis will prove useful for the synthesis of novel π -conjugated systems.

4.4 Experimental Section

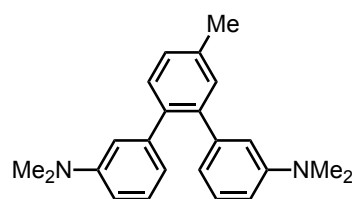
4.4.1 Synthesis and Characterization of Substrates

*N*³,*N*³,*N*^{3''},*N*^{3''}-Tetramethyl-[1,1':2',1''-terphenyl]-3,3''-diamine (**204a**)



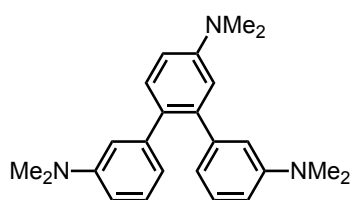
Compound **204a** was synthesized by Suzuki-Miyaura coupling reaction.^[75] A mixture of (3-(dimethylamino)phenyl)boronic acid (0.550 g, 8.80 mmol, 2.2 equiv), 1,2-dibromobenzene (0.940 g, 4.00 mmol, 1.0 equiv), Na₂CO₃ (2.10 g, 20.0 mmol, 5.0 equiv) and PdCl₂(PPh₃)₂ (0.140 mg, 0.200 mmol, 5.0 mol%) in a mixture of toluene (30 mL), water (4.0 mL) and ethanol (8.0 mL) was heated to 80 °C under nitrogen atmosphere. After the completion of the reaction monitored by TLC, the mixture was cooled to room temperature, then diluted with water and EtOAc. The aqueous layer was extracted with EtOAc (3 × 50 mL). The combined organic phases were dried over MgSO₄ and concentrated under reduced pressure. The crude product was then purified further by column chromatography (eluent: hexane/ethyl acetate = 15:1) on silica gel to give **204a** (0.970 g, 76%) as colorless oil. ¹H NMR (400 MHz, CDCl₃): δ 7.47 (dd, *J* = 5.5, 3.7 Hz, 2H), 7.38–7.41 (m, 2H), 7.11 (dd, *J* = 8.0, 8.0 Hz, 2H), 6.58–6.61 (m, 4H), 6.53 (s, 2H), 2.76 (s, 12H); ¹³C NMR (100 MHz, CDCl₃): δ 150.4, 142.5, 141.5, 130.5, 128.6, 127.3, 118.7, 115.4, 111.3, 40.9; HRMS(EI⁺) Calcd for C₂₂H₂₄N₂ ([M]⁺) 316.1934, Found 316.1939.

*N*³,*N*³,*N*^{3''},*N*^{3''},4'-Pentamethyl-[1,1':2',1''-terphenyl]-3,3''-diamine (**204b**)



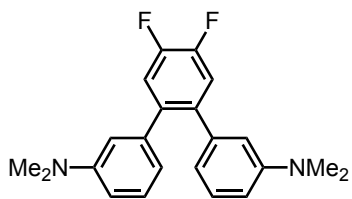
The same method as **204a**. A mixture of (3-(dimethylamino)phenyl)boronic acid (0.730 g, 4.40 mmol, 2.2 equiv), 1,2-dibromo-4-methylbenzene (0.500 g, 2.00 mmol, 1.0 equiv), Na₂CO₃ (1.10 g, 10.0 mmol, 5.0 equiv) and Pd(PPh₃)₄ (120 mg, 0.100 mmol, 5.0 mol%) in a mixture of toluene (20 mL), water (3.0 mL) and ethanol (6.0 mL) was heated to 80 °C under nitrogen atmosphere. After the completion of the reaction monitored by TLC, the mixture was cooled to room temperature, then diluted with water and EtOAc. The aqueous layer was extracted with EtOAc (3 × 30 mL). The combined organic phases were dried over MgSO₄ and concentrated under reduced pressure. The crude product was then purified further by column chromatography (eluent: hexane/ethyl acetate = 20:1) on silica gel to give **204b** (0.48 g, 68%) as colorless oil. ¹H NMR (400 MHz, CDCl₃): δ 7.37 (d, *J* = 7.8 Hz, 1H), 7.29 (s, 1H), 7.21 (dd, *J* = 7.8, 1.8 Hz, 1H), 7.07–7.12 (m, 2H), 6.57–6.60 (m, 4H), 6.51–6.53 (m, 2H), 2.76 (s, 6H), 2.75 (s, 6H), 2.43 (s, 3H); ¹³C NMR (100 MHz, CDCl₃): δ 150.39, 150.37, 142.6, 142.4, 141.3, 138.7, 137.0, 131.2, 130.4, 128.5, 128.0, 118.8, 118.7, 115.5, 115.4, 111.3, 111.1, 40.9, 21.3; HRMS(EI⁺) Calcd for C₂₃H₂₆N₂ ([M]⁺) 330.2091, Found 330.2097.

*N*³,*N*³,*N*^{3''},*N*^{3''},*N*⁴,*N*⁴-Hexamethyl-[1,1':2',1'-terphenyl]-3,3',4'-triamine (**204c**)



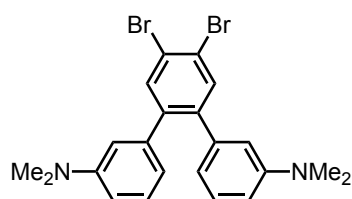
The same method as **204a**. A mixture of (3-(dimethylamino)phenyl)boronic acid (0.623 g, 3.75 mmol, 2.5 equiv), 3,4-dibromo-*N,N*-dimethylaniline (0.426 g, 1.5 mmol, 1.0 equiv), Na₂CO₃ (0.812 g, 7.5 mmol, 5.0 equiv) and PdCl₂(PPh₃)₂ (57.8 mg, 0.075 mmol, 5.0 mol%) in a mixture of toluene (14 mL), degassed water (2.0 mL) and ethanol (2.0 mL) was heated to 80 °C under nitrogen. After the completion of the reaction monitored by TLC (12 h), the mixture was cooled to room temperature, then diluted with water and EtOAc. The aqueous layer was extracted with EtOAc (3 × 30 mL). The combined organic phases were dried over Na₂SO₄ and concentrated under reduced pressure. The crude product was then purified further by column chromatography (eluent: hexane/ethyl acetate = 10:1) on silica gel to give **204c** (471 mg, 87%) as yellowish solid. ¹H NMR (400 MHz, CDCl₃): δ 7.40 (d, *J* = 8.7 Hz, 1H), 7.09–7.17 (m, 2H), 6.86 (d, *J* = 2.3 Hz, 1H), 6.83 (dd, *J* = 8.5, 3.0 Hz, 1H), 6.60–6.70 (m, 5H), 6.53–6.54 (m, 1H), 3.03 (s, 6H), 2.79 (s, 6H), 2.76 (s, 6H); ¹³C NMR (100 MHz, CDCl₃): δ 150.2, 150.1, 149.8, 143.4, 142.6, 142.1, 131.2, 130.0, 128.6, 128.5, 119.2, 118.9, 115.9, 115.6, 114.7, 111.7, 111.4, 110.9, 41.11, 41.00, 40.85; HRMS(EI⁺) Calcd for C₂₄H₂₉N₃ ([M]⁺) 359.2356, Found 359.2361.

4',5'-Difluoro-*N*³,*N*³,*N*^{3''},*N*^{3''}-tetramethyl-[1,1':2',1''-terphenyl]-3,3''-diamine (**204d**)



The same method as **204a**. A mixture of (3-(dimethylamino)phenyl)boronic acid (0.500 g, 3.00 mmol, 3.0 equiv), 1,2-dibromo-4,5-difluorobenzene (0.278 g, 1.00 mmol, 1.0 equiv), Na₂CO₃ (0.546 g, 5.20 mmol, 5.0 equiv) and PdCl₂(PPh₃)₂ (37.0 mg, 0.050 mmol, 5.0 mol%) in a mixture of toluene (10 mL), degassed water (1.5 mL) and ethanol (1.5 mL) was heated to 80 °C under nitrogen. After the completion of the reaction monitored by TLC, the mixture was cooled to room temperature, then diluted with water and EtOAc. The aqueous layer was extracted with EtOAc (3 × 30 mL). The combined organic phases were dried over Na₂SO₄ and concentrated under reduced pressure. The crude product was then purified further by column chromatography (eluent: hexane/ethyl acetate = 20:1) on silica gel to give **204d** (198 mg, 56%) as colorless oil. ¹H NMR (400 MHz, CD₂Cl₂): δ 7.25–7.30 (m, 2H), 7.10 (dd, *J* = 7.6, 8.4 Hz, 2H), 6.64 (dd, *J* = 8.2, 2.3 Hz, 2H), 6.54 (d, *J* = 7.3 Hz, 2H), 6.48–6.49 (m, 2H), 2.78 (s, 12H); ¹³C NMR (100 MHz, CD₂Cl₂): δ 150.6, 149.4 (dd, *J* = 248.5, 14.4 Hz), 141.0, 138.6 (dd, *J* = 7.3, 5.6 Hz), 129.0, 119.2 (dd, *J* = 15.8, 10.1 Hz), 118.6, 115.2, 111.9, 40.9; HRMS(EI⁺) Calcd for C₂₂H₂₂F₂N₂ ([M]⁺) 352.1746, Found 352.1752.

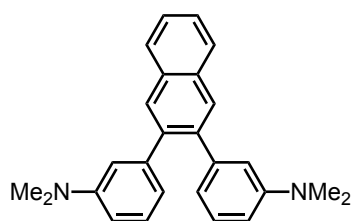
4',5'-Dibromo-*N*³,*N*³,*N*^{3''},*N*^{3''}-tetramethyl-[1,1':2',1''-terphenyl]-3,3''-diamine (**204e**)



The same method as **204a**. A mixture of (3-(dimethylamino)phenyl)boronic acid (0.18 g, 1.1 mmol, 2.2 equiv), 1,2-dibromo-4,5-diodobenzene (0.240 g, 0.50 mmol, 1.0 equiv), Na₂CO₃ (0.270 g, 2.5 mmol, 5.0 equiv) and PdCl₂(PPh₃)₂

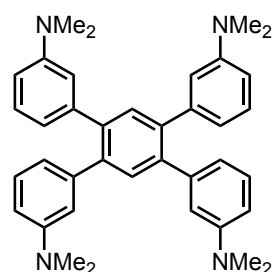
(18.0 mg, 0.0250 mmol, 5.0 mol%) in a mixture of toluene (10 mL), degassed water (2.0 mL) and ethanol (4.0 mL) was heated to 50 °C under nitrogen. After the completion of the reaction monitored by TLC, the mixture was cooled to room temperature, then diluted with water and EtOAc. The aqueous layer was extracted with EtOAc (3 × 20 mL). The combined organic phases were dried over MgSO₄ and concentrated under reduced pressure. The crude product was then purified further by column chromatography (eluent: hexane/ethyl acetate = 20:1) on silica gel to give **204e** (203 mg, 85%) as colorless oil. ¹H NMR (400 MHz, CDCl₃): δ 7.70 (s, 2H), 7.11 (dd, *J* = 8.0, 8.0 Hz, 2H), 6.59 (d, *J* = 7.7 Hz, 4H), 6.45 (s, 2H), 2.77 (s, 12H); ¹³C NMR (100 MHz, CDCl₃): δ 150.3, 142.1, 140.2, 135.1, 128.9, 123.3, 118.5, 114.8, 112.0, 40.9; HRMS(EI⁺) Calcd for C₂₂H₂₂Br₂N₂ ([M]⁺) 472.0144, Found 472.0149.

3,3'-(Naphthalene-2,3-diyl)bis(*N,N*-dimethylaniline) (**204f**)



The same method as **204a**. A mixture of (3-(dimethylamino)phenyl)boronic acid (0.550 g, 3.30 mmol, 2.2 equiv), naphthalene-2,3-diyl bis(trifluoromethanesulfonate) (0.640 g, 1.50 mmol, 1.0 equiv), Na₂CO₃ (0.800 g, 7.50 mmol, 5.0 equiv) and PdCl₂(PPh₃)₂ (53.0 mg, 0.0750 mmol, 5.0 mol%) in a mixture of toluene (15 mL), water (2.0 mL) and ethanol (4.0 mL) was heated to 80 °C under nitrogen. After completion of the reaction monitored by TLC, the mixture was cooled to room temperature, then diluted with water and EtOAc. The aqueous layer was extracted with EtOAc (3 × 20 mL). The combined organic phases were dried over MgSO₄ and concentrated under reduced pressure. The crude product was then purified further by column chromatography (eluent: hexane/ethyl acetate = 15:1) on silica gel to give **204f** (0.59 g, quant) as a white solid. ¹H NMR (400 MHz, CDCl₃): δ 7.93 (s, 2H), 7.88 (dd, *J* = 6.4, 3.2 Hz, 2H), 7.49 (dd, *J* = 6.0, 3.2 Hz, 2H), 7.14 (dd, *J* = 8.0, 8.0 Hz, 2H), 6.69 (d, *J* = 7.8 Hz, 2H), 6.60–6.64 (m, 4H), 2.78 (s, 12H); ¹³C NMR (100 MHz, CDCl₃): δ 150.4, 142.4, 140.1, 132.7, 129.1, 128.6, 127.8, 126.2, 118.8, 115.5, 111.4, 40.9; HRMS(EI⁺) Calcd for C₂₆H₂₆N₂ ([M]⁺) 366.2091, Found 366.2094.

4',5'-Bis(3-(dimethylamino)phenyl)-*N*³,*N*³,*N*^{3''},*N*^{3''}-tetramethyl-[1,1':2',1''-terphenyl]-3,3''-diamine (**207**)



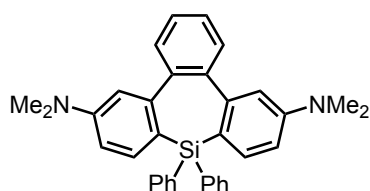
The same method as **204a**. A mixture of (3-(dimethylamino)phenyl)boronic acid (1.50 g, 9.00 mmol, 4.5 equiv), 1,2,4,5-tetrabromobenzene (0.790 g, 2.00 mmol, 1.0 equiv), Na₂CO₃ (2.10 g, 20.0 mmol, 10 equiv) and PdCl₂(PPh₃)₂ (0.14 g, 0.2 mmol, 10 mol%) in a mixture of toluene (25 mL), water (3.0 mL) and ethanol (6.0 mL) was heated to 80 °C under nitrogen. After the completion of the reaction monitored by TLC, the mixture was cooled to room temperature, then diluted with water and EtOAc. The aqueous layer was extracted with EtOAc (3 × 30 mL). The combined organic phases were dried over MgSO₄ and concentrated under reduced pressure. The crude product was then purified further by column chromatography (eluent: dichloromethane/hexane = 5:1) on silica gel to give **207** (0.43 g, 39%) as yellow powder. ¹H

NMR (400 MHz, CDCl₃): δ 7.64 (s, 2H), 7.11 (dd, J = 8.0, 8.0 Hz, 4H), 6.60–6.66 (m, 12H), 2.78 (s, 24H); ¹³C NMR (100 MHz, CDCl₃): δ 150.5, 142.1, 140.3, 132.5, 128.6, 118.8, 115.2, 111.2, 40.9; HRMS(EI⁺) Calcd for C₃₈H₄₂N₄ ([M]⁺) 554.3404, Found 554.3409.

4.4.2 General Procedure for Synthesis of Silepin Derivatives by a Borane Catalyst^[34,70]

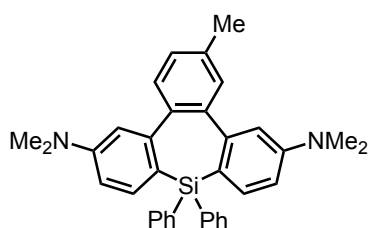
To a test tube with a screw cap equipped with a magnetic stir bar was charged triphenyl **204a** (63.0 mg, 0.200 mmol, 1.0 equiv) and tris(pentafluorophenyl)borane (B(C₆F₅)₃, 3.10 mg, 0.00600 mmol, 3.0 mol%). The test tube was evacuated and filled with nitrogen. Chlorobenzene (0.40 mL) was added via syringe. Diphenylsilane **145a** (55.3 μ L, 0.30 mmol, 1.5 equiv) and 2,6-lutidine (1.70 μ L, 0.0150 mmol, 7.5 mol%) were then added to the mixture. The test tube was closed with a cap. The reaction mixture was stirred at 100 °C (oil bath) for 24 h. After the completion of the reaction, the mixture was cooled to room temperature. The desired silepin **206a** was obtained by column chromatography (eluent: hexane/ethyl acetate = 20:1) on silica gel in 80% isolated yield.

*N*⁶,*N*⁶,*N*¹²,*N*¹²-Tetramethyl-9,9-diphenyl-9*H*-tribenzo[*b,d,f*]silepin-6,12-diamine (**206a**)



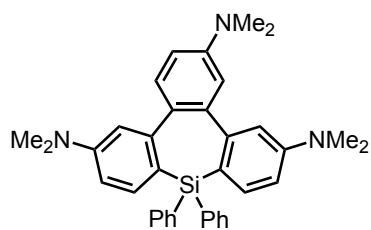
206a was obtained as a white solid (80 mg, 80%). ¹H NMR (400 MHz, CDCl₃): δ 7.56 (dd, J = 7.9, 1.7 Hz, 2H), 7.41–7.49 (m, 3H), 7.28 (d, J = 8.2 Hz, 2H), 7.17–7.22 (m, 4H), 7.06–7.11 (m, 3H), 6.99 (dd, J = 7.4, 7.4 Hz, 2H), 6.82 (d, J = 2.3 Hz, 2H), 6.62 (dd, J = 8.2, 2.3 Hz, 2H), 2.96 (s, 12H); ¹³C NMR (100 MHz, CDCl₃): δ 151.6, 148.7, 142.0, 137.9, 135.3, 134.8, 134.2, 133.0, 131.9, 129.6, 128.5, 127.8, 126.9, 126.7, 125.3, 114.9, 110.2, 40.4; HRMS(EI⁺) Calcd for C₃₄H₃₂N₂Si ([M]⁺) 496.2329, Found 496.2333.

*N*⁶,*N*⁶,*N*¹²,*N*¹²,2-Pentamethyl-9,9-diphenyl-9*H*-tribenzo[*b,d,f*]silepin-6,12-diamine (**206b**)



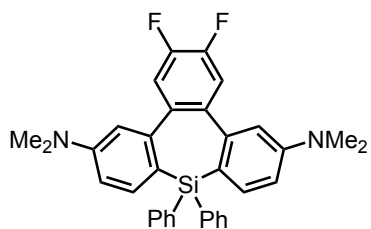
206b was obtained as a white solid (87 mg, 85%). ¹H NMR (400 MHz, CDCl₃): δ 7.56 (dd, J = 8.0, 1.6 Hz, 2H), 7.40–7.48 (m, 3H), 7.25–7.27 (m, 2H), 7.17 (dd, J = 7.8, 1.4 Hz, 2H), 7.07–7.12 (m, 2H), 6.97–7.03 (m, 3H), 6.88 (dd, J = 7.8, 1.8 Hz, 1H), 6.81 (dd, J = 9.4, 2.5 Hz, 2H), 6.59–6.63 (m, 2H), 2.96 (s, 6H), 2.94 (s, 6H), 2.22 (s, 3H); ¹³C NMR (100 MHz, CDCl₃): δ 151.59, 151.56, 148.8, 148.7, 141.8, 139.2, 137.9, 136.2, 135.4, 134.8, 134.7, 134.3, 133.1, 132.4, 131.9, 129.6, 128.4, 127.8, 127.4, 126.8, 125.3, 125.2, 119.6, 114.8, 110.2, 110.1, 40.5, 40.4, 21.0; HRMS(EI⁺) Calcd for C₃₅H₃₄N₂Si ([M]⁺) 510.2486, Found 510.2490.

***N*²,*N*²,*N*⁶,*N*⁶,*N*¹²,*N*¹²-Hexamethyl-9,9-diphenyl-9*H*-tribenzo[*b,d,f*]silepin-2,6,12-triamine (206c)**



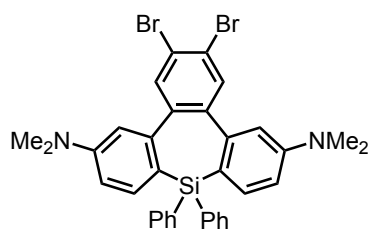
206c was obtained as a white solid (51 mg, 38%). ¹H NMR (400 MHz, CD₂Cl₂): δ 7.50–7.53 (m, 2H), 7.46–7.49 (m, 1H), 7.41–7.45 (m, 2H), 7.21 (dd, *J* = 8.2, 1.8 Hz, 2H), 7.17–7.19 (m, 2H), 7.12–7.16 (m, 1H), 7.02–7.06 (m, 3H), 6.84 (d, *J* = 2.3 Hz, 1H), 6.76 (s, 1H), 6.64 (dd, *J* = 8.5, 2.5 Hz, 1H), 6.56–6.61 (m, 3H), 2.96 (s, 6H), 2.95 (s, 6H), 2.85 (s, 6H); ¹³C NMR (100 MHz, CDCl₃): δ 151.6, 151.5, 149.4, 149.2, 148.9, 142.5, 137.9, 135.4, 134.7, 134.6, 134.5, 133.3, 132.8, 129.5, 128.4, 127.8, 126.8, 125.3, 125.2, 116.4, 114.9, 114.7, 112.4, 110.2, 109.7, 41.2, 40.5(2C) (one carbon is missing); HRMS(EI⁺) Calcd for C₃₆H₃₇N₃Si ([M]⁺) 539.2751, Found 539.2757.

2,3-Difluoro-*N*⁶,*N*⁶,*N*¹²,*N*¹²-tetramethyl-9,9-diphenyl-9*H*-tribenzo[*b,d,f*]silepine-6,12-diamine (206d)



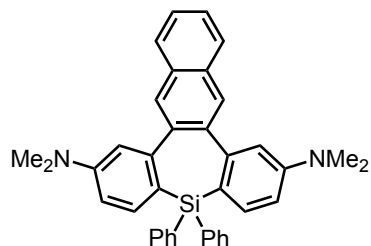
206d was obtained as a white solid (31 mg, 24%). ¹H NMR (600 MHz, CDCl₃): δ 7.55–7.57 (m, 2H), 7.48–7.52 (m, 1H), 7.44–7.46 (m, 2H), 7.30 (d, *J* = 8.2 Hz, 2H), 7.18–7.21 (m, 3H), 7.01–7.09 (m, 4H), 6.74 (br, 2H), 6.65 (br, 2H), 2.97 (s, 12H); ¹³C NMR (150 MHz, CDCl₃): δ 151.5, 148.3 (dd, *J* = 250.0, 14.4 Hz), 146.7, 139.0, 137.8, 135.3, 135.0, 133.8, 132.4, 129.8, 129.0, 127.9, 127.1, 125.11, 120.13 (dd, *J* = 9.4, 7.9 Hz), 114.5 (d, *J* = 7.8 Hz), 110.6 (d, *J* = 5.6 Hz), 40.4; HRMS(EI⁺) Calcd for C₃₄H₃₀F₂N₂Si ([M]⁺) 532.2141, Found 532.2144.

2,3-Dibromo-*N*⁶,*N*⁶,*N*¹²,*N*¹²-tetramethyl-9,9-diphenyl-9*H*-tribenzo[*b,d,f*]silepine-6,12-diamine (206e)



206e was obtained as a white solid (56 mg, 43%). ¹H NMR (400 MHz, CDCl₃) δ 7.57 (dd, *J* = 8.0, 1.6 Hz, 2H), 7.48–7.54 (m, 2H), 7.42–7.46 (m, 2H), 7.41 (s, 2H), 7.26–7.28 (m, 2H), 7.15–7.20 (m, 2H), 7.06 (dd, *J* = 7.6, 7.6 Hz, 2H), 6.72 (d, *J* = 2.3 Hz, 2H), 6.63 (dd, *J* = 8.5, 2.5 Hz, 2H), 2.96 (s, 12H); ¹³C NMR (100 MHz, CDCl₃): δ 151.6, 146.2, 142.7, 137.8, 136.2, 135.4, 134.9, 133.6, 132.1, 129.9, 129.0, 128.0, 127.0, 125.4, 122.3, 114.2, 110.8, 40.4. HRMS(EI⁺) Calcd for C₃₄H₃₀Br₂N₂Si ([M]⁺) 652.0540, Found 652.0547.

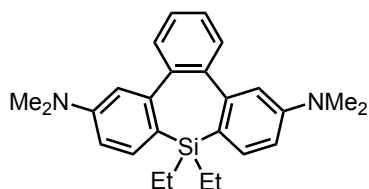
***N*⁷,*N*⁷,*N*¹³,*N*¹³-Tetramethyl-10,10-diphenyl-10*H*-dibenzo[*b,f*]naphtho-[2,3-*d*]silepin-7,13-diamine (206f)**



206f was obtained as a white solid (49 mg, 45%). ¹H NMR (400 MHz, CDCl₃) δ 7.67–7.70 (m, 4H), 7.57 (dd, *J* = 8.0, 1.6 Hz, 2H), 7.42–7.49 (m, 3H), 7.37 (q, *J* = 3.2 Hz, 2H), 7.31 (d, *J* = 8.2 Hz, 2H), 7.16 (dd, *J* = 7.8, 1.4 Hz, 2H), 6.94 (d, *J* = 2.3 Hz, 2H), 6.77–6.84 (m, 3H), 6.64 (dd, *J* = 8.2, 2.7 Hz, 2H), 2.98 (s, 12H);

^{13}C NMR (100 MHz, CDCl_3): δ 151.7, 148.9, 140.9, 137.9, 135.3, 134.9, 133.9, 132.9, 132.0, 130.7, 129.6, 128.4, 127.8, 127.4, 126.6, 125.8, 125.3, 115.3, 110.1, 40.5; HRMS(EI^+) Calcd for $\text{C}_{38}\text{H}_{34}\text{N}_2\text{Si}$ ($[\text{M}]^+$) 546.2486, Found 546.2492.

9,9-Diethyl- N^6,N^6,N^{12},N^{12} -tetramethyl-9*H*-tribenzo[*b,d,f*]silepin-6,12-diamine (**206g**)



206g was obtained as a white solid (47 mg, 59%). ^1H NMR (400 MHz, CDCl_3): δ 7.44–7.48 (m, 2H), 7.38–7.41 (m, 2H), 7.31 (d, $J = 8.2$ Hz, 2H), 6.77 (d, $J = 2.3$ Hz, 2H), 6.64 (dd, $J = 8.2, 2.7$ Hz, 2H), 2.93 (s, 12H), 1.28 (m, 5H), 0.59 (t, $J = 8.0$ Hz, 3H), 0.14 (q, $J = 7.9$ Hz, 2H); ^{13}C NMR (100 MHz, CDCl_3): δ 151.2, 147.7, 142.4, 132.4, 131.7, 127.5, 127.0, 114.9, 110.6, 40.5, 8.1, 7.8, 2.5, 1.0; HRMS(EI^+) Calcd for $\text{C}_{26}\text{H}_{32}\text{N}_2\text{Si}$ ($[\text{M}]^+$) 400.2329, Found 400.2334.

Figure 4.6. HMQC spectrum of **206g**.

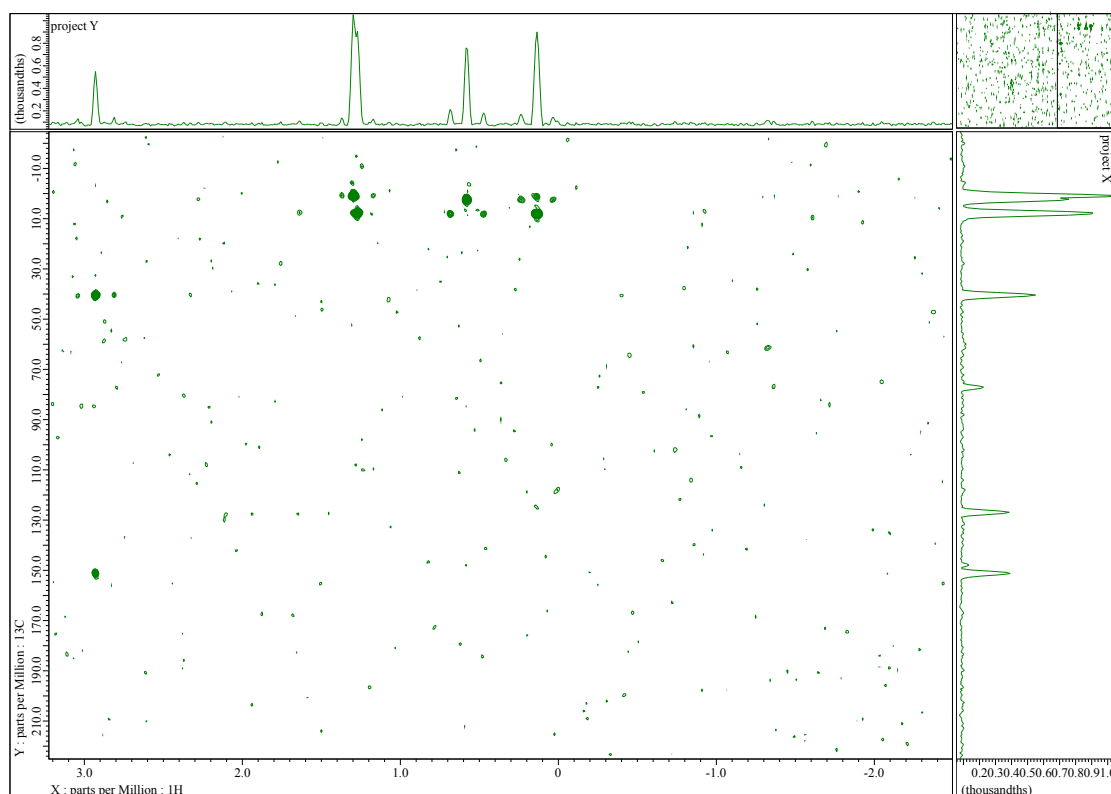
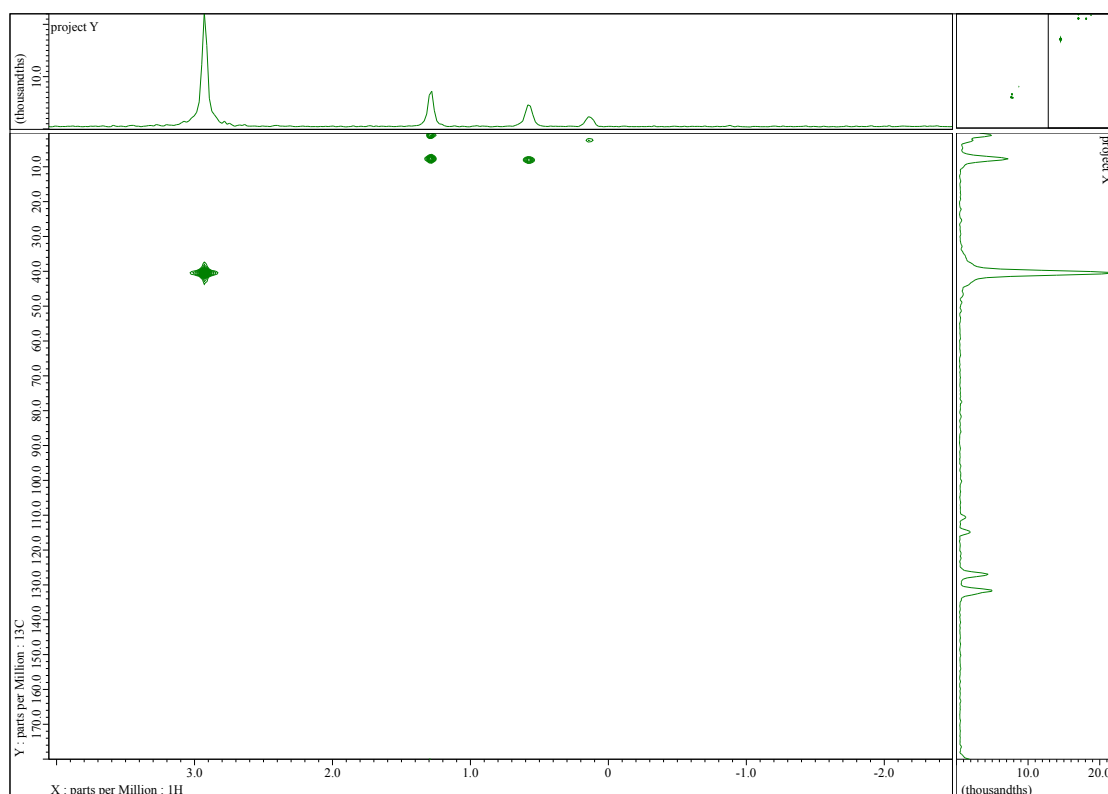
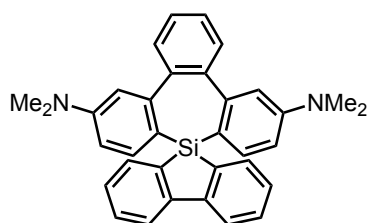


Figure 4.7. HSQC spectrum of **206g**.

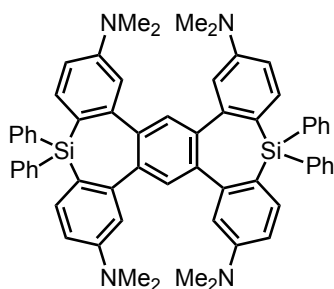


***N*⁶,*N*⁶,*N*¹²,*N*¹²-Tetramethylspiro[dibenzo[*b,d*]silole-5,9'-tribenzo[*b,d,f*]silepin]-6',12'-diamine (206h)**



206h was obtained as a white solid (92 mg, 93%). ¹H NMR (400 MHz, CDCl₃) δ 7.96 (d, *J* = 6.9 Hz, 1H), 7.91 (d, *J* = 7.8 Hz, 1H), 7.71 (d, *J* = 7.8 Hz, 1H), 7.55–7.64 (m, 5H), 7.46 (dd, *J* = 7.2, 7.2 Hz, 1H), 7.34 (d, *J* = 8.2 Hz, 2H), 7.18–7.22 (m, 1H), 6.88 (d, *J* = 2.1 Hz, 2H), 6.80 (dd, *J* = 7.4, 7.4 Hz, 1H), 6.56 (dd, *J* = 8.5, 2.5 Hz, 2H), 5.64 (d, *J* = 6.9 Hz, 1H), 2.93 (s, 12H); ¹³C NMR (100 MHz, CDCl₃): δ 151.9, 150.1, 148.0, 147.6, 142.3, 137.2, 135.6, 133.5, 133.3, 133.2, 133.0, 131.0, 130.0, 127.7, 127.6, 127.3, 125.0, 121.5, 120.6, 114.8, 110.7, 40.5. HRMS(EI⁺) Calcd for C₃₄H₃₀N₂Si ([M]⁺) 494.2173, Found 494.2173.

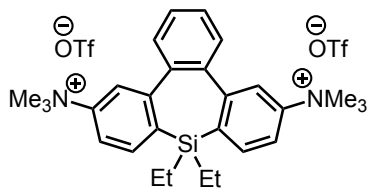
(*N*⁶,*N*⁶,*N*¹²,*N*¹²-Tetramethyl-9,9-diphenyl-9*H*-6,12-diamine)tribenzo[*b,d,f*]bissilepin (209)



209 was obtained as a white solid (78 mg, 85%, 0.10 mmol scale). ¹H NMR (400 MHz, CDCl₃): δ 7.62 (dd, *J* = 7.8, 1.4 Hz, 4H), 7.44–7.50 (m, 6H), 7.27–7.30 (m, 8H), 6.99–7.05 (m, 6H), 6.84 (s, 2H), 6.59 (dd, *J* = 8.2, 2.7 Hz, 4H), 6.44 (d, *J* = 2.3 Hz, 4H), 2.94 (s, 24H); ¹³C NMR (100 MHz, CDCl₃): δ 151.4, 148.4, 140.0, 137.8, 135.7, 134.8, 134.3, 134.1, 132.7, 129.7, 128.5, 127.9, 126.4, 125.4,

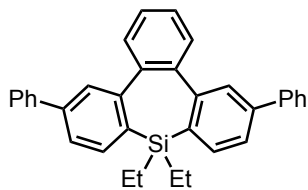
114.6, 110.0, 40.4; HRMS(FAB⁺) Calcd for C₆₂H₅₈N₄Si ([M+H]⁺) 915.4273, Found 915.4277.

9,9-Diethyl-*N*⁶,*N*⁶,*N*⁶,*N*¹²,*N*¹²,*N*¹²-hexamethyl-9*H*-tribenzo[*b,d,f*]silepin-6,12-diaminium triflate (**210**)



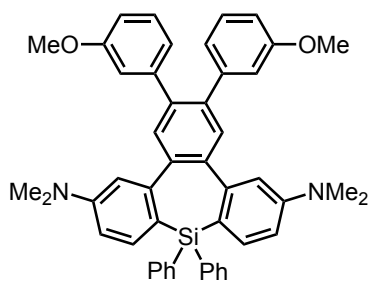
The compound **210** was prepared according to the procedure in the previous literature.^[12] In a dry two neck round bottom flask equipped with a magnetic stir bar was charged the compound **206g** (200.3 mg, 0.50 mmol, 1.0 equiv) and CH₂Cl₂ (5.0 mL). To the resultant stirring solution was added dropwise MeOTf (206 mg, 1.25 mmol, 2.5 equiv) at room temperature. The solution was stirred at room temperature for 2 h. The reaction mixture was concentrated to remove CH₂Cl₂ and the residue was treated with Et₂O (20 mL). The resultant solid was filtered, washed with Et₂O and hexane, and then dried under vacuum to give silepin **210** as a white solid (333 mg, 91%). ¹H NMR (400 MHz, DMSO-*d*₆): δ 7.88–7.92 (m, 4H), 7.60–7.69 (m, 6H), 3.59 (s, 18H), 1.45 (q, *J* = 7.8 Hz, 2H), 1.28 (t, *J* = 7.5 Hz, 3H), 0.52 (t, *J* = 8.0 Hz, 3H), 0.14 (q, *J* = 7.9 Hz, 2H); ¹³C NMR (100 MHz, CDCl₃): δ 148.6, 147.2, 141.3, 139.2, 133.4, 132.4, 128.8, 121.9, 120.8 (q, *J* = 321 Hz), 118.6, 56.4, 7.6, 7.1, 0.44, -0.07; HRMS(FAB⁺) Calcd for C₂₉H₃₈F₃N₂O₃SSi⁺ ([M-OTf⁻]⁺) 579.2319, Found 579.2326.

9,9-Diethyl-6,12-diphenyl-9*H*-tribenzo[*b,d,f*]silepin (**211**)



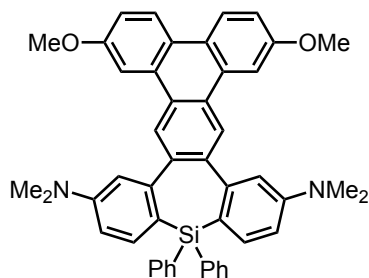
To a dry 20 mL Schlenk flask equipped with a magnetic stir bar was added the compound **210** (0.150 g, 0.20 mmol, 1.0 equiv) and PdCl₂(PPh₃)₂ (2.80 mg, 0.00400 mmol, 2.0 mol%). The flask was sealed with a rubber septum, evacuated/filled with nitrogen. THF (2.0 mL) was added via syringe, and the resultant slurry was stirred for 5 min at room temperature. Then phenylmagnesium bromide (0.5 M solution in THF, 0.88 mL, 0.440 mmol, 2.2 equiv) was added dropwise. After 1 h, the reaction mixture was quenched with water (1 mL) and 1N HCl (5 mL), and then extracted with Et₂O. The organic extract was dried over MgSO₄, filtered, and concentrated. The crude product was purified by chromatography on silica gel (eluent: hexane/ethyl acetate = 100:0 to 20:1) to give the compound **211** as white powder (82 mg, 88% yield). ¹H NMR (400 MHz, CDCl₃): δ 7.66 (d, *J* = 1.8 Hz, 2H), 7.57–7.60 (m, 6H), 7.49–7.53 (m, 4H), 7.40–7.48 (m, 6H), 7.31–7.35 (m, 2H), 1.37–1.46 (m, 5H), 0.65 (t, *J* = 7.8 Hz, 3H), 0.27 (q, *J* = 7.9 Hz, 2H); ¹³C NMR (100 MHz, CDCl₃): δ 147.1, 142.2, 141.5, 141.1, 139.1, 132.2, 131.9, 129.2, 128.9, 127.5, 127.3, 125.2, 8.1, 7.6, 1.6, 1.0 (one carbon is missing); HRMS(EI⁺) Calcd for C₃₄H₃₀Si ([M]⁺) 466.2111, Found 466.2118.

2,3-Bis(3-methoxyphenyl)-*N*⁶,*N*⁶,*N*¹²,*N*¹²-tetramethyl-9,9-diphenyl-9*H*-tribenzo[*b,d,f*]silepin-6,12-diamine (**218**)



Compound **215** was synthesized by Suzuki-Miyaura coupling reaction.^[114] A mixture of **206e** (156.0 mg, 0.24 mmol, 1.0 equiv), (3-methoxyphenyl)boronic acid (110 mg, 0.72 mmol, 3.0 equiv), Na₂CO₃ (127 mg, 1.2 mmol, 5.0 equiv) and Pd(PPh₃)₄ (14.0 mg, 0.012 mmol, 5.0 mol%) in a mixture of toluene (3 mL), water (0.75 mL) and ethanol (0.75 mL) was heated to 80 °C under nitrogen. After the completion of the reaction monitored by TLC, the mixture was cooled to room temperature, then diluted with water and EtOAc. The aqueous layer was extracted with EtOAc (3 × 20 mL). The combined organic phases were dried over Na₂SO₄ and concentrated under reduced pressure. The crude product was then purified further by column chromatography (eluent: hexane/ethyl acetate = 10:1) on silica gel to give **218** (142 mg, 84%) as white solid. ¹H NMR (400 MHz, CDCl₃): δ 7.62–7.64 (m, 2H), 7.45–7.53 (m, 3H), 7.34 (d, *J* = 6.9 Hz, 2H), 7.08–7.22 (m, 8H), 7.03 (dd, *J* = 7.2, 7.2 Hz, 2H), 6.90 (s, 1H), 6.60–6.74 (m, 6H), 6.48–6.51 (m, 2H), 3.63 (s, 6H), 2.96 (s, 12H); ¹³C NMR (100 MHz, CDCl₃): δ 159.1, 151.7, 148.0, 142.7, 141.4, 138.4, 137.8, 135.6, 134.5, 133.8, 132.5, 129.7, 128.8, 128.3, 127.9, 126.8, 125.74, 125.65, 122.3, 115.2, 114.4, 112.5, 110.4, 55.2, 40.4; HRMS(EI⁺) Calcd for C₄₈H₄₄N₂O₂Si ([M]⁺) 708.3167, Found 708.3171.

3,17-Dimethoxy-*N*⁷,*N*⁷,*N*¹³,*N*¹³-tetramethyl-10,10-diphenyl-10*H*-dibenzo[*b,f*]triphenylene[2,3-*d*]silepin-7,13-diamine (**219**)



Compound **219** was synthesized according to the reported procedure.^[111] Silepin **218** (142 mg, 0.2 mmol, 1.0 equiv) was dissolved in dry dichloromethane (6.0 mL) and cooled to 0 °C in an ice/water bath under a nitrogen atmosphere. A solution of iron (III) chloride (250 mg, 1.54 mmol, 8.0 equiv) in nitromethane (1.0 mL) was added dropwise to the above solution at 0 °C and the mixture was stirred for 3 h at room temperature. To the resulting mixture was added methanol (10 mL) followed by water (10 mL) and dichloromethane (20 mL). The organic layer was separated and dried over anhydrous Na₂SO₄ and evaporated to produce a brown oil. The purification of the crude product by column chromatography using hexanes as eluent afforded **219** (122.8 mg, 88%) as white solid. ¹H NMR (400 MHz, CD₂Cl₂): δ 8.44 (d, *J* = 8.7 Hz, 2H), 8.38 (s, 2H), 7.95 (d, *J* = 2.7 Hz, 2H), 7.44–7.57 (m, 5H), 7.32–7.35 (m, 3H), 7.19–7.26 (m, 4H), 7.02 (s, 1H), 6.74–6.84 (m, 5H), 3.98 (s, 6H), 3.02 (s, 12H); ¹³C NMR (100 MHz, CD₂Cl₂): δ 158.7, 152.0, 148.8, 141.6, 138.1, 135.5, 135.1, 134.1, 132.8, 130.12, 130.06, 128.9, 128.6, 128.2, 127.1, 126.8, 124.7, 124.2, 116.2, 115.6, 110.7, 106.2, 55.9, 40.7 (one carbon is missing); HRMS(EI⁺) Calcd for C₄₈H₄₂N₂O₂Si ([M]⁺) 706.3010, Found 706.3018.

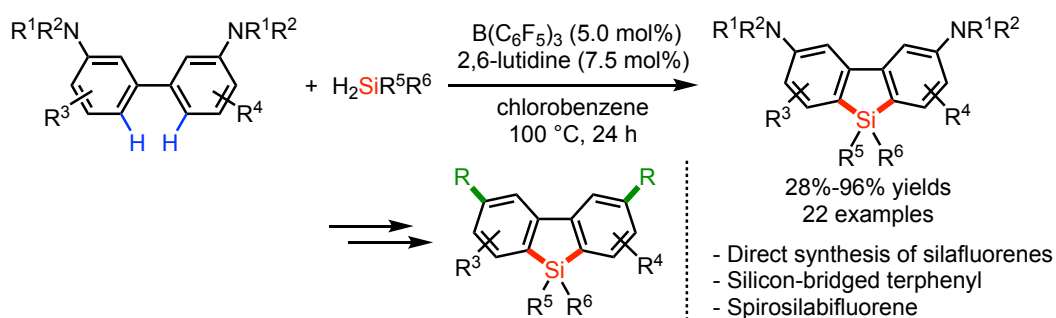
Chapter 5

Conclusion

In Chapter 1, the general introduction of C(sp²)-H silylation and its application is described. I mainly focused on the transition metal-catalyzed C(sp²)-H silylation and C(sp²)-H silylation by electrophilic aromatic substitution reactions along with some of the reaction mechanisms.

In Chapter 2, the Lewis acid (B(C₆F₅)₃) catalyzed direct synthesis of silafluorene derivatives from biphenyls and dihydrosilanes via a double sila-Friedel-Crafts reaction was disclosed. The synthesized silafluorene derivatives with 22 examples, including multi-substituted derivatives, spiro-silabifluorenes, and silicon-bridged terphenyl derivatives, were obtained in good to excellent yields (28–96%). Additionally, conversions of the amino groups of the silafluorene derivatives were also illustrated. However, the transformations of the amino groups are limited to aryl and allyl groups. I hope that novel π -conjugated molecules based on the synthesis of silafluorene derivatives can be obtained through the versatile transformations of the amino groups in the future.

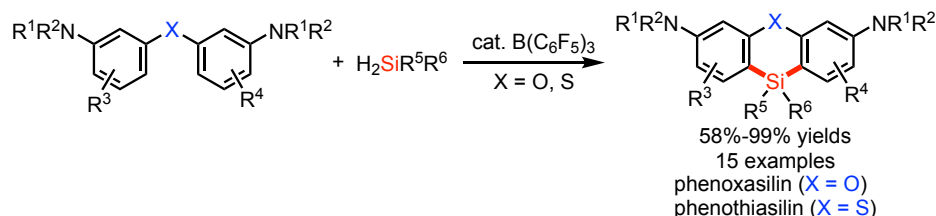
Scheme 5.1. Lewis acid-catalyzed synthesis of silafluorene derivatives from biphenyls and dihydrosilanes via a double sila-Friedel-Crafts reaction.



In Chapter 3, the application of the catalytic synthesis of silafluorenes in Chapter 2 to the six-membered silacyclic compounds was described. With the optimal reaction conditions, phenoxasilin and phenothiasilin derivatives were obtained with 15 examples in moderate to excellent yields (58–99%). The amino groups were converted to aryl groups. Hopefully, the

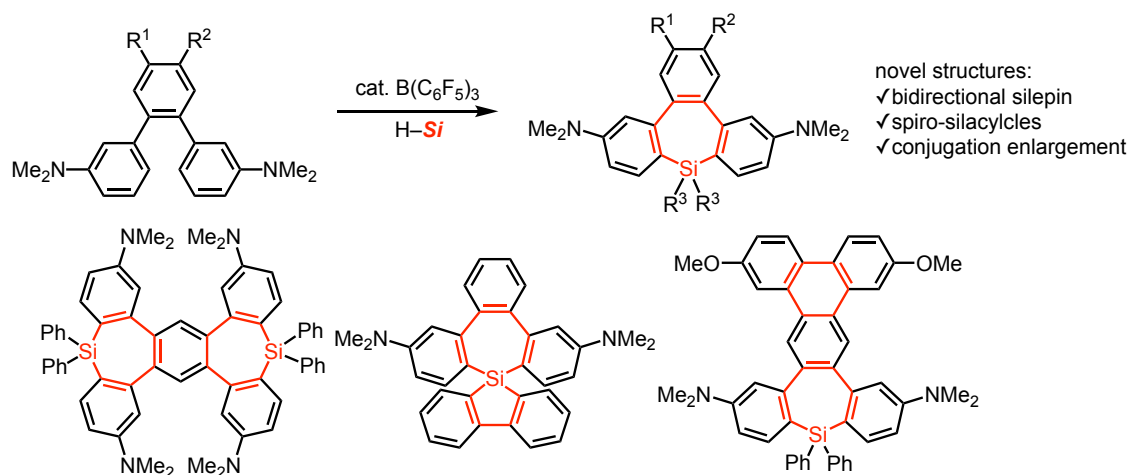
synthetic methods can produce the promising phenazasilines and six-membered silacycles with heteroatom P or Si.

Scheme 5.2. Synthesis of six-membered silacycles by borane-catalyzed double silylation-Friedel–Crafts reaction.



In Chapter 4, the double silylation-Friedel–Crafts reaction for the synthesis of tribenzosilepin derivatives using amino group-containing terphenyls and dihydrosilanes was developed. The structure rigidity of the tribenzosilepins in solution at an ambient temperature was supported by X-ray crystallography and (variable temperature) NMR spectra. A bidirectional silylation occurred under this catalytic system, which afforded a disilepin compound with the stereoselective formation of *trans*-isomer. Besides, the enlargement of π -conjugate systems of the silepin skeleton was also realized. The optical properties of some synthesized tribenzosilepins were investigated. It is hoped that construction of the silicon-embedded π -extension systems could be realized through the synthesis of tribenzosilepin derivatives.

Scheme 5.3. Facile synthesis of tribenzosilepins from terphenyls and dihydrosilanes by double silylation-Friedel–Crafts reaction.



In conclusions, borane-catalyzed double sila-Friedel–Crafts reactions for the synthesis of silacycles (silafluorene, phenoxasilin, phenothiasilin and tribenzosilepins) from the electron rich arene or heteroarene (diamino-substituted biphenyls, biaryls, and terphenyls) with hydrosilanes was achieved. This is the first example of the synthesis of silacycles from biaryl substrates and dihydrosilanes directly. This reaction system offers an efficient and convenient way for the construction of silacycles, which have been traditionally synthesized by the reaction between dilithiated intermediates and dichlorosilanes or intramolecular silylation from silyl substituted biaryls. However, the reaction system needs electron rich arenes or heteroarenes as substrates, and the electron-donating group was limited to amino groups. This is the limitation of the sila-Friedel–Crafts reaction.

I investigated transformations of the electron-rich amino groups by palladium-catalyzed cross-coupling reaction between ammonium triflate and Grignard reagent, and nickel-catalyzed borylation and C–N bond reduction. Among them, only the cross-coupling reaction proceeded. Desilylation was the problematic point to construct various π -conjugated molecules in some reactions.

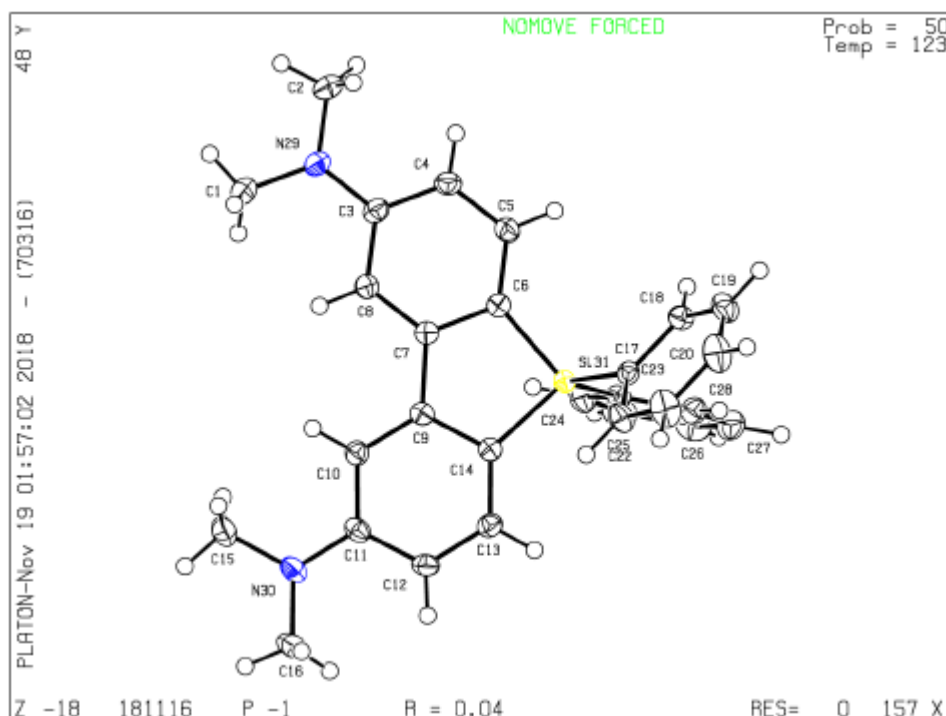
Based on these research projects, I believe that the protocols should enrich the chemistry of silicon-containing planar and curved π -conjugated molecules in the near future.

Supporting Information

X-ray Structures

S.1 X-ray Structure of Compound 146b

Single crystals of $C_{28}H_{28}N_2Si$, 4,6-bis(dimethylamino)-9,9-diphenyl-9*H*-9-silafluorene **146b**, were recrystallized from hot toluene solution. A suitable crystal was selected, and their X-ray diffraction was collected on a XtaLAB AFC10 (RCD3): fixedchi single diffractometer with graphite monochromated Mo- $K\alpha$ radiation ($\lambda = 0.71070\text{\AA}$). The crystal was kept at 123 K during data collection. The data were collected using ω scan in the θ range of $4.752 \leq \theta \leq 62.052$ deg. The data were corrected for Lorentz and polarization effects. The structures were solved by direct methods,^[115] and expanded using Fourier techniques.^[116] Hydrogen atoms were refined using the riding model. The final cycle of full-matrix least-squares refinement on F2 was based on 19804 observed reflections and 6081 variable parameters. Neutral atom scattering factors were taken from Cromer and Waber.^[117] All calculations were performed using the Olex-2 crystallographic software package except for refinement,^[118] which was performed using SHELXL-97.5 Details^[119] of final refinement as well as the bond lengths and angles are summarized in the supporting information, and the numbering scheme employed is also shown in the supporting information, which were drawn with ORTEP at 50% probability ellipsoid.



Crystal structure determination of 146b

Crystal Data for **146b** ($M = 420.61$ g/mol): triclinic, space group $P-1$ (no. 2), $a = 9.4768(4)$ \AA , $b = 10.9099(4)$ \AA , $c = 13.1313(5)$ \AA , $\alpha = 113.798(3)^\circ$, $\beta = 91.992(4)^\circ$, $\gamma = 112.004(4)^\circ$, $V = 1123.73(8)$ \AA^3 , $Z = 2$, $T = 123$ K, $\mu(\text{Mo } K\alpha) = 0.123$ mm^{-1} , $D_{\text{calc}} = 1.243$ g/cm^3 , 19804 reflections measured ($4.752^\circ \leq 2\theta \leq 62.052^\circ$), 6081 unique ($R_{\text{int}} = 0.0303$,

$R_{\text{sigma}} = 0.0328$) which were used in all calculations. The final R_1 was 0.0402 ($I > 2\sigma(I)$) and wR_2 was 0.1100 (all data).

Table S.1. Crystal data and structure refinement for **146b**.

Identification code	146b
Empirical formula	$\text{C}_{28}\text{H}_{28}\text{N}_2\text{Si}$
Formula weight	420.61
Temperature/K	123
Crystal system	triclinic
Space group	$P-1$
$a/\text{\AA}$	9.4768(4)
$b/\text{\AA}$	10.9099(4)
$c/\text{\AA}$	13.1313(5)
$\alpha/^\circ$	113.798(3)
$\beta/^\circ$	91.992(4)
$\gamma/^\circ$	112.004(4)
Volume/ \AA^3	1123.73(8)
Z	2
$D_{\text{calc}}/\text{g/cm}^3$	1.243
μ/mm^{-1}	0.123
$F(000)$	448.0
Crystal size/ mm^3	$0.359 \times 0.274 \times 0.133$
Radiation	Mo $K\alpha$ ($\lambda = 0.71073$)
2θ range for data collection/ $^\circ$	4.752 to 62.052
Index ranges	$-13 \leq h \leq 12, -15 \leq k \leq 15, -18 \leq l \leq 18$
Reflections collected	19804
Independent reflections	6081 [$R_{\text{int}} = 0.0303, R_{\text{sigma}} = 0.0328$]
Data/restraints/parameters	6081/0/284
Goodness-of-fit on F^2	1.085

Final R indexes [$I \geq 2\sigma(I)$]	$R_1 = 0.0402$, $wR_2 = 0.1060$
Final R indexes [all data]	$R_1 = 0.0467$, $wR_2 = 0.1100$
Largest diff. peak/hole / $e \text{ \AA}^{-3}$	0.34/-0.27

Table S.2. Fractional Atomic Coordinates ($\times 10^4$) and Equivalent Isotropic Displacement Parameters ($\text{\AA}^2 \times 10^3$) for **146b**. U_{eq} is defined as 1/3 of of the trace of the orthogonalised U_{ij} tensor.

Atom	x	y	z	$U(\text{eq})$
Si31	2484.7(3)	8754.1(3)	2548.1(3)	16.61(9)
C14	1136.7(13)	8151.3(12)	1210.4(9)	17.8(2)
C9	-187.8(13)	6850.7(12)	997.0(9)	17.4(2)
N29	-2303.6(13)	3266.8(12)	2600.7(9)	28.0(2)
C6	1196.8(13)	7135.5(12)	2736.5(10)	18.7(2)
C23	2711.5(13)	10575.8(13)	3697.0(9)	18.9(2)
N30	-2728.2(13)	6366.3(12)	-1463.7(9)	27.1(2)
C7	-144.1(13)	6267.4(12)	1842.0(9)	17.7(2)
C17	4449.0(13)	8795.5(12)	2384.8(10)	18.1(2)
C27	4234.8(17)	13169.4(14)	4997.2(11)	29.7(3)
C3	-1140.1(14)	4507.2(13)	2609.9(10)	21.6(2)
C18	5509.8(14)	9046.6(13)	3294.6(10)	21.9(2)
C10	-1434.2(14)	6225.0(12)	85.9(10)	20.1(2)
C13	1157.8(14)	8767.0(13)	461.4(10)	21.3(2)
C11	-1422.7(14)	6894.3(13)	-633.7(10)	21.0(2)
C5	1352.5(14)	6636.2(13)	3535.6(10)	22.2(2)
C16	-2604.7(18)	6854.3(16)	-2339.3(11)	32.2(3)
C12	-76.3(15)	8160.4(13)	-443.3(10)	22.9(2)
C8	-1292.2(14)	4981.2(13)	1780.4(10)	20.6(2)
C25	1478.3(17)	12090.9(16)	4839.9(12)	33.4(3)
C28	4134.7(14)	11817.8(13)	4194.3(10)	23.2(2)

C22	4867.9(14)	8468.2(14)	1331.8(10)	25.1(3)
C4	221.4(15)	5348.7(14)	3477.1(10)	23.4(2)
C26	2903.9(18)	13305.5(15)	5313.7(11)	31.7(3)
C2	-1909.3(17)	2556.5(16)	3212.9(13)	35.1(3)
C19	6927.1(15)	8977.2(15)	3156.1(12)	28.4(3)
C1	-3662.4(16)	2360.0(15)	1680.9(12)	31.5(3)
C20	7317.2(16)	8661.3(16)	2101.0(12)	33.6(3)
C24	1384.6(15)	10741.8(15)	4045.0(11)	27.3(3)
C21	6291.4(16)	8406.7(17)	1189.9(12)	33.7(3)
C15	-4033.7(17)	4992.7(15)	-1701.5(13)	34.5(3)

Table S.3. Anisotropic Displacement Parameters ($\text{\AA}^2 \times 10^3$) for **146b**. The Anisotropic displacement factor exponent takes the form: $-2\pi^2[h^2a^*2U_{11}+2hka^*b^*U_{12}+\dots]$.

Atom	U_{11}	U_{22}	U_{33}	U_{23}	U_{13}	U_{12}
Si31	16.06(15)	16.55(15)	16.44(15)	7.01(12)	2.91(11)	6.63(12)
C14	18.7(5)	17.3(5)	17.8(5)	7.0(4)	4.2(4)	8.9(4)
C9	19.5(5)	17.3(5)	16.9(5)	6.7(4)	4.5(4)	10.2(4)
N29	30.0(6)	23.6(5)	25.7(5)	14.4(4)	2.7(4)	3.3(4)
C6	18.9(5)	18.6(5)	18.6(5)	8.1(4)	4.8(4)	8.2(4)
C23	21.0(5)	20.3(5)	16.6(5)	8.1(4)	3.3(4)	10.1(4)
N30	28.3(5)	27.4(5)	21.9(5)	10.8(4)	-3.3(4)	9.3(5)
C7	19.4(5)	17.6(5)	17.3(5)	7.5(4)	5.2(4)	9.3(4)
C17	17.9(5)	14.9(5)	20.0(5)	6.8(4)	3.1(4)	6.7(4)
C27	36.5(7)	19.4(6)	25.8(6)	7.1(5)	4.0(5)	8.2(5)
C3	24.8(6)	18.9(5)	20.2(5)	9.2(4)	7.3(5)	7.9(5)
C18	22.6(6)	22.4(6)	21.9(5)	10.8(5)	3.5(4)	9.9(5)
C10	20.9(5)	17.4(5)	20.0(5)	7.0(4)	2.5(4)	7.8(4)
C13	23.1(6)	18.5(5)	22.6(6)	10.0(4)	5.2(5)	8.3(5)

C11	25.3(6)	20.3(5)	16.6(5)	5.3(4)	1.4(4)	12.4(5)
C5	22.3(6)	24.0(6)	18.6(5)	9.4(5)	2.7(4)	8.5(5)
C16	42.1(8)	30.7(7)	23.4(6)	12.0(5)	-3.3(6)	16.2(6)
C12	30.4(6)	21.6(6)	20.7(5)	11.7(5)	4.4(5)	12.8(5)
C8	21.2(5)	19.4(5)	18.9(5)	7.9(4)	2.8(4)	7.2(5)
C25	37.9(7)	40.0(8)	30.3(7)	12.4(6)	11.5(6)	27.8(7)
C28	23.9(6)	21.2(6)	23.0(6)	9.0(5)	5.5(5)	9.0(5)
C22	23.0(6)	29.7(6)	18.8(5)	6.9(5)	2.9(5)	11.9(5)
C4	28.4(6)	24.6(6)	19.2(5)	12.5(5)	5.9(5)	10.4(5)
C26	50.3(8)	25.5(6)	21.7(6)	6.4(5)	7.8(6)	23.2(6)
C2	36.3(7)	31.9(7)	36.0(7)	24.2(6)	4.2(6)	3.9(6)
C19	24.3(6)	28.7(6)	31.1(7)	10.8(5)	-0.8(5)	13.7(5)
C1	30.3(7)	26.2(6)	30.5(7)	15.7(5)	2.1(5)	1.7(5)
C20	22.8(6)	36.3(7)	36.2(7)	6.6(6)	5.9(5)	17.8(6)
C24	22.6(6)	29.7(6)	26.8(6)	8.5(5)	3.5(5)	13.1(5)
C21	28.4(7)	40.2(8)	25.1(6)	5.1(6)	9.4(5)	17.3(6)
C15	32.9(7)	26.2(7)	33.3(7)	10.8(6)	-10.2(6)	5.9(6)

Table S.4. Bond Lengths for **146b**.

Atom	Atom	Length/Å	Atom	Atom	Length/Å
Si31	C14	1.8526(12)	C7	C8	1.3848(16)
Si31	C6	1.8514(12)	C17	C18	1.3997(16)
Si31	C23	1.8735(12)	C17	C22	1.3939(16)
Si31	C17	1.8671(12)	C27	C28	1.3887(17)
C14	C9	1.4098(16)	C27	C26	1.383(2)
C14	C13	1.3941(16)	C3	C8	1.4052(16)
C9	C7	1.4913(15)	C3	C4	1.4038(17)
C9	C10	1.3896(16)	C18	C19	1.3874(17)

N29	C3	1.3838(15)	C10	C11	1.4065(16)
N29	C2	1.4440(17)	C13	C12	1.3806(17)
N29	C1	1.4383(17)	C11	C12	1.4060(17)
C6	C7	1.4100(16)	C5	C4	1.3809(17)
C6	C5	1.3893(16)	C25	C26	1.379(2)
C23	C28	1.3917(17)	C25	C24	1.3855(18)
C23	C24	1.4024(16)	C22	C21	1.3908(18)
N30	C11	1.3841(15)	C19	C20	1.386(2)
N30	C16	1.4407(17)	C20	C21	1.379(2)
N30	C15	1.4423(17)			

Table S.5. Bond Angles for **146b**.

Atom	Atom	Atom	Angle/°	Atom	Atom	Atom	Angle/°
C14	Si31	C23	112.68(5)	C8	C7	C6	121.09(10)
C14	Si31	C17	115.18(5)	C18	C17	Si31	121.14(9)
C6	Si31	C14	91.83(5)	C22	C17	Si31	121.21(9)
C6	Si31	C23	113.97(5)	C22	C17	C18	117.48(10)
C6	Si31	C17	112.72(5)	C26	C27	C28	120.11(12)
C17	Si31	C23	109.63(5)	N29	C3	C8	121.68(11)
C9	C14	Si31	109.49(8)	N29	C3	C4	120.13(11)
C13	C14	Si31	132.95(9)	C4	C3	C8	118.18(11)
C13	C14	C9	117.45(10)	C19	C18	C17	121.34(11)
C14	C9	C7	114.59(10)	C9	C10	C11	120.74(11)
C10	C9	C14	121.09(10)	C12	C13	C14	122.01(11)
C10	C9	C7	124.28(10)	N30	C11	C10	120.83(11)
C3	N29	C2	118.79(11)	N30	C11	C12	121.15(11)
C3	N29	C1	120.18(11)	C12	C11	C10	117.93(11)
C1	N29	C2	116.47(11)	C4	C5	C6	121.51(11)

C7	C6	Si31	109.64(8)	C13	C12	C11	120.66(11)
C5	C6	Si31	132.42(9)	C7	C8	C3	120.49(11)
C5	C6	C7	117.88(10)	C26	C25	C24	119.87(12)
C28	C23	Si31	123.28(9)	C27	C28	C23	121.32(12)
C28	C23	C24	117.32(11)	C21	C22	C17	121.42(12)
C24	C23	Si31	119.32(9)	C5	C4	C3	120.80(11)
C11	N30	C16	119.94(11)	C25	C26	C27	119.85(12)
C11	N30	C15	119.43(11)	C20	C19	C18	119.88(12)
C16	N30	C15	117.13(11)	C21	C20	C19	119.93(12)
C6	C7	C9	114.39(10)	C25	C24	C23	121.52(12)
C8	C7	C9	124.51(10)	C20	C21	C22	119.94(12)

Table S.6. Hydrogen Atom Coordinates ($\text{\AA}\times 10^4$) and Isotropic Displacement Parameters ($\text{\AA}^2\times 10^3$) for **146b**.

Atom	x	y	z	U(eq)
H8AA	5198.41	13984.42	5322.58	36
H0BA	5259.54	9264.35	4006.49	26
H1BA	-2285.6	5353.83	-49.46	24
H2BA	2029.71	9612.02	574.57	26
H4BA	2238.74	7181.53	4123.26	27
HA	-2157.99	7915.9	-1991.95	48
HB	-3623.34	6462.62	-2799.43	48
HC	-1950.45	6509.41	-2809.85	48
H5BA	-16.43	8593.65	-931.66	27
H6BA	-2170.35	4427.08	1185.58	25
H7BA	581.74	12177.51	5053.62	40
H8BA	5036.72	11741.11	3984.74	28
H9BA	4180.65	8286.92	710.7	30
H0CA	363.25	5035.29	4018.69	28

H1CA	2969.87	14213.68	5844.78	38
H2CA	-995.82	2414.84	3019.64	53
H2CB	-2762.59	1614.23	3007.51	53
H2CC	-1707.46	3168.23	4018.5	53
H3CA	7614.15	9142.5	3770.2	34
H4CA	-4077.6	2976.74	1552.27	47
H4CB	-4435.61	1672.27	1875.98	47
H4CC	-3381.07	1825.71	1000.68	47
H5CA	8269.64	8620.92	2007.47	40
H6CA	419.51	9927.44	3735.15	33
H7CA	6551.43	8194.21	481.32	40
H8CA	-3707.71	4204.17	-1962.63	52
H8CB	-4850.85	4789.2	-2280.89	52
H8CC	-4411.7	5070.41	-1019.4	52

S.2 X-ray Structure of Compound **184a**

A suitable crystal of C₂₈H₂₈N₂Si, phenoxasilin **184a** was selected, and its X-ray diffraction data were collected on a Rigaku Saturn70 CCD area detector with graphite monochromated Mo K α radiation ($\lambda = 0.71070$ Å). The crystal was kept at 123 K during data collection. The data were collected using ω scan in the θ range of $3.154 \leq 2\theta \leq 62.02$ deg. The data were corrected for Lorentz and polarization effects. The structures were solved by direct methods,^[115] and expanded using Fourier techniques.^[116] Hydrogen atoms were refined using the riding model. The final cycle of full-matrix least-squares refinement on F² was based on 14757 observed reflections and 585 variable parameters. Neutral atom scattering factors were taken from Cromer and Waber.^[117] All calculations were performed using the Olex-2 crystallographic software package except for refinement,^[118] which was performed using SHELXL-97.5 Details^[119] of final refinement as well as the bond lengths and angles are summarized in the following Tables together with the numbering scheme employed, which were drawn with ORTEP at 50% probability ellipsoid.

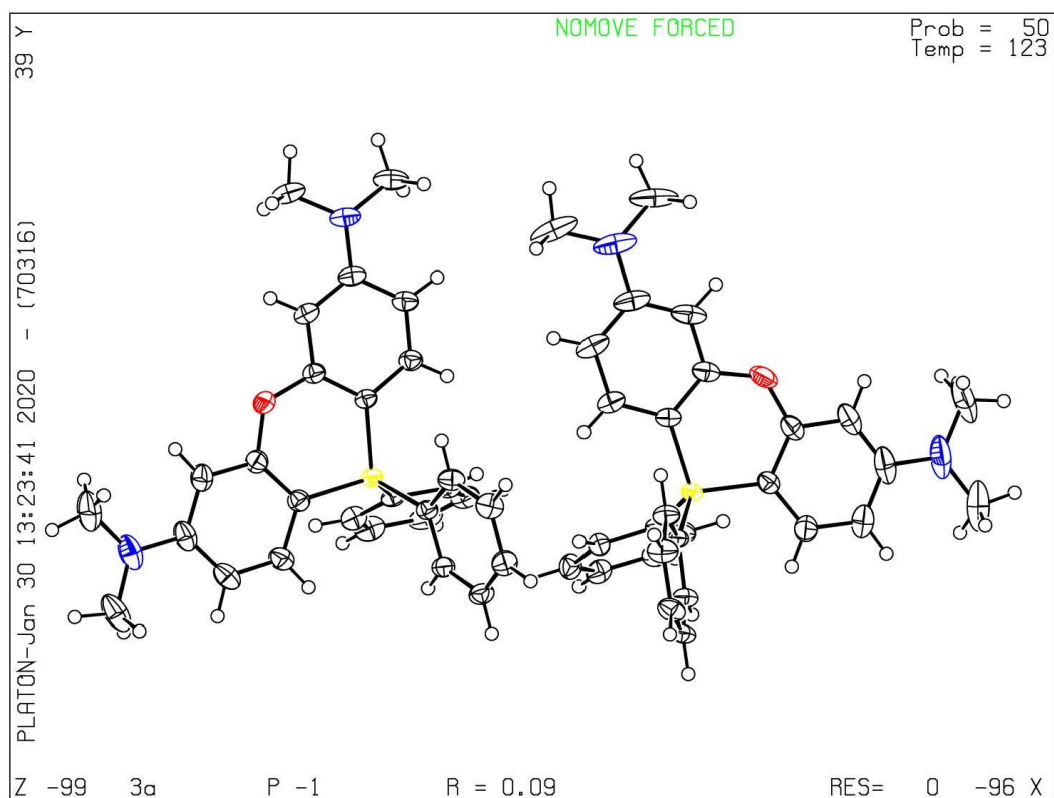


Table S.7. Crystal data and structure refinement for **184a**.

Identification code	184a
Empirical formula	C ₂₈ H ₂₈ N ₂ O ₂ Si
Formula weight	436.61
Temperature/K	123
Crystal system	triclinic
Space group	<i>P</i> -1
<i>a</i> /Å	12.4645(5)
<i>b</i> /Å	12.9987(5)
<i>c</i> /Å	16.7305(5)
α /°	83.723(3)
β /°	73.112(3)
γ /°	86.634(3)
Volume/Å ³	2577.23(17)
<i>Z</i>	5
<i>D</i> _{calc} g/cm ³	1.407
μ /mm ⁻¹	0.140
<i>F</i> (000)	1160.0
Crystal size/mm ³	0.4 × 0.25 × 0.24

Radiation	Mo K α ($\lambda = 0.71073$)
2θ range for data collection/ $^\circ$	3.154 to 62.02
Index ranges	$-17 \leq h \leq 17$, $-18 \leq k \leq 18$, $-24 \leq l \leq 23$
Reflections collected	45536
Independent reflections	14757 [$R_{\text{int}} = 0.0927$, $R_{\text{sigma}} = 0.0651$]
Data/restraints/parameters	14757/0/585
Goodness-of-fit on F^2	1.054
Final R indexes [$I \geq 2\sigma(I)$]	$R_1 = 0.0867$, $wR_2 = 0.2276$
Final R indexes [all data]	$R_1 = 0.1064$, $wR_2 = 0.2547$
Largest diff. peak/hole / e \AA^{-3}	0.51/-1.08

Table S.8. Fractional Atomic Coordinates ($\times 10^4$) and Equivalent Isotropic Displacement Parameters ($\text{\AA}^2 \times 10^3$) for **184a**. U_{eq} is defined as 1/3 of of the trace of the orthogonalised U_{ij} tensor.

Atom	x	y	z	$U(\text{eq})$
Si2	6530.7(5)	4007.1(4)	7117.8(3)	21.50(14)
Si1	8719.6(5)	2527.8(4)	2672.9(3)	21.71(14)
O1	11029.7(14)	1998.7(13)	1340.2(10)	34.1(4)
O2	7428.1(17)	2711.6(14)	8522.2(11)	40.4(4)
C51	6730.7(17)	5400.9(14)	6699.4(12)	21.8(4)
N1	12675.5(18)	-218.4(16)	3117.5(15)	39.5(5)
C1	9944.8(17)	1755.6(15)	2834.2(13)	23.5(4)
C17	7427.0(17)	1732.0(14)	2994.8(13)	24.0(4)
C24	8381.0(17)	3676.4(14)	3299.1(12)	22.8(4)
C37	7873.9(18)	3284.4(16)	7010.6(14)	26.7(4)
C45	5624.9(17)	3434.2(14)	6569.2(12)	22.3(4)
C56	5809.0(19)	6018.2(16)	6611.0(14)	27.8(4)
C46	5879.7(18)	3579.4(16)	5695.5(13)	27.1(4)
C23	7378.2(18)	4241.0(16)	3353.6(13)	26.9(4)
C6	10878.2(18)	1574.7(16)	2161.6(13)	26.0(4)
C22	6902.8(18)	1463.2(15)	3845.6(14)	27.9(4)
C52	7751.7(19)	5882.2(16)	6542.7(15)	30.2(4)
C55	5885(2)	7082.6(17)	6402.3(15)	31.6(5)
C50	4726.4(18)	2809.5(15)	7008.2(13)	27.1(4)
N2	10325(2)	3775(2)	-1080.2(14)	51.7(6)
C48	4383(2)	2477.3(17)	5718.0(15)	32.1(5)
C29	5880.9(19)	3834.9(16)	8255.9(13)	27.9(4)
C9	9185.4(18)	2892.1(16)	1534.4(13)	27.1(4)
C49	4108(2)	2331.2(16)	6583.2(15)	31.5(5)

C3	10854.9(19)	593.9(16)	3723.1(15)	30.2(4)
C25	9120(2)	4032.6(17)	3690.1(15)	31.3(4)
C2	9982.0(18)	1241.9(16)	3610.8(14)	27.8(4)
C38	8120(2)	2743.3(16)	7705.0(15)	31.1(5)
C10	10245.3(19)	2608.7(16)	1045.0(13)	28.7(4)
C47	5269(2)	3106.1(18)	5272.4(14)	32.2(5)
C28	7124(2)	5137.1(17)	3767.0(15)	32.0(5)
C21	6001(2)	804.1(17)	4110.2(16)	34.5(5)
C4	11787.0(19)	418.3(16)	3026.9(16)	30.9(4)
C18	7002(2)	1325.2(18)	2413.7(16)	32.3(5)
C42	8699.1(19)	3204.9(18)	6232.4(16)	33.3(5)
C53	7839(2)	6950.9(18)	6319.7(17)	37.0(5)
C11	10649(2)	2910.9(19)	191.2(15)	35.3(5)
C30	4828(2)	4270.9(19)	8653.9(15)	36.7(5)
C54	6896(2)	7547.1(17)	6260.7(15)	33.9(5)
C14	8521(2)	3506.8(19)	1098.8(15)	35.2(5)
C12	9959(2)	3509.4(19)	-231.5(15)	38.6(5)
C19	6088(2)	672.5(19)	2673.1(18)	38.4(5)
C34	6393(2)	3204.2(17)	8780.3(14)	32.2(5)
C20	5592(2)	410.8(17)	3521.4(19)	38.5(6)
N4	10900(2)	1522.0(19)	6790(2)	58.8(8)
C5	11782.2(19)	923.9(17)	2245.5(15)	31.4(5)
C26	8875(2)	4925.6(18)	4106.6(16)	36.1(5)
C7	12614(2)	-805.5(19)	3916(2)	42.6(6)
N3	4280(3)	3160(3)	10849.8(15)	70.9(9)
C27	7878(2)	5477.0(17)	4142.7(15)	35.0(5)
C41	9687(2)	2625.9(19)	6146(2)	41.8(6)
C40	9912(2)	2089.6(18)	6857(2)	43.0(6)
C39	9115(2)	2155.8(18)	7637(2)	42.5(6)
C33	5884(3)	3004(2)	9639.2(15)	43.8(6)
C13	8885(2)	3809(2)	249.7(16)	40.6(6)
C31	4297(3)	4075(2)	9502.8(16)	45.4(6)
C8	13515(2)	-523(2)	2379(2)	44.1(6)
C32	4822(3)	3411(2)	10011.2(15)	48.6(7)
C16	9653(3)	4481(2)	-1486.0(18)	56.6(8)
C15	11473(3)	3553(3)	-1553.0(18)	61.2(9)
C44	11596(2)	1277(2)	5974(3)	68.6(12)
C43	11038(3)	853(2)	7510(3)	68.1(11)
C35	3200(4)	3645(3)	11236(2)	74.4(12)

C36 4867(5) 2539(4) 11371(2) 87.2(15)

Table S.9. Anisotropic Displacement Parameters ($\text{\AA}^2 \times 10^3$) for **184a**. The Anisotropic displacement factor exponent takes the form: $-2\pi^2[h^2a^*U_{11}+2hka^*b^*U_{12}+\dots]$.

Atom	U ₁₁	U ₂₂	U ₃₃	U ₂₃	U ₁₃	U ₁₂
Si2	22.7(3)	19.3(2)	23.4(3)	0.06(18)	-9.3(2)	1.88(19)
Si1	18.9(3)	19.4(2)	25.5(3)	0.40(19)	-5.4(2)	0.54(19)
O1	27.7(8)	40.6(9)	28.0(8)	0.3(6)	-1.3(6)	6.9(7)
O2	51.2(11)	38.2(9)	37.4(9)	3.1(7)	-25.6(8)	7.7(8)
C51	22.8(9)	20.6(8)	23.3(8)	-2.3(6)	-9.3(7)	3.0(7)
N1	32.3(11)	32.4(10)	54.6(13)	-1.3(9)	-17.0(10)	11.2(8)
C1	21.7(9)	20.2(8)	27.8(9)	-1.4(7)	-6.5(7)	1.1(7)
C17	22.1(9)	16.8(8)	32.1(10)	-0.8(7)	-7.1(8)	1.7(7)
C24	22.0(9)	19.0(8)	25.3(9)	2.3(6)	-4.9(7)	-0.8(7)
C37	23.6(10)	22.7(9)	36.3(10)	-1.2(7)	-13.5(8)	1.1(7)
C45	22.4(9)	18.8(8)	26.3(9)	-1.1(7)	-9.2(7)	2.8(7)
C56	28.5(10)	22.5(9)	35.9(10)	-2.6(7)	-15.6(9)	3.0(8)
C46	26.6(10)	29.1(10)	25.8(9)	-2.2(7)	-7.5(8)	-2.7(8)
C23	24.4(10)	25.9(9)	29.1(9)	-0.2(7)	-7.3(8)	2.0(8)
C6	22.4(10)	25.7(9)	29.4(10)	-1.4(7)	-6.9(8)	0.6(7)
C22	25.9(10)	21.3(9)	33.8(10)	2.3(7)	-6.0(8)	0.2(7)
C52	27.5(11)	23.9(9)	39.6(11)	0.6(8)	-11.8(9)	0.2(8)
C55	38.3(12)	25.0(9)	37.6(11)	-3.3(8)	-21.6(10)	7.4(8)
C50	30.1(11)	21.9(9)	28.7(9)	1.3(7)	-9.0(8)	-0.7(8)
N2	70.3(17)	53.9(14)	27.3(10)	8.4(9)	-10.2(11)	-14.6(13)
C48	31.8(11)	28.2(10)	39.9(12)	-12.4(9)	-12.9(9)	0.4(8)
C29	32.8(11)	25.4(9)	26.9(9)	-0.4(7)	-11.4(8)	-1.5(8)
C9	27.6(10)	24.9(9)	27.4(9)	0.4(7)	-6.8(8)	-0.7(8)
C49	31.5(11)	21.5(9)	41.7(12)	-1.9(8)	-10.5(9)	-3.7(8)
C3	27.7(11)	24.9(9)	37.9(11)	2.6(8)	-11.8(9)	1.3(8)
C25	29.3(11)	27.1(10)	40.5(12)	-2.2(8)	-15.2(9)	-0.7(8)
C2	25.5(10)	25.1(9)	31.2(10)	1.7(7)	-7.2(8)	0.6(8)
C38	34.5(12)	23.3(9)	41.6(12)	-2.3(8)	-21.2(10)	1.5(8)
C10	30.8(11)	25.7(9)	27.8(10)	-0.5(7)	-6.1(8)	-1.2(8)
C47	34.1(12)	34.8(11)	29.7(10)	-9.3(8)	-9.8(9)	-1.1(9)
C28	32.2(11)	25.6(9)	36.5(11)	-2.2(8)	-8.8(9)	6.3(8)
C21	27.4(11)	24.1(10)	45.4(13)	6.7(9)	-3.9(9)	-1.2(8)
C4	27.6(11)	20.9(9)	45.7(12)	-2.9(8)	-13.9(9)	3.6(8)
C18	29.6(11)	29.7(10)	39.4(11)	-6.5(9)	-11.2(9)	-1.5(8)

C42	24.0(10)	28.0(10)	45.9(13)	-3.7(9)	-7.5(9)	2.6(8)
C53	34.4(12)	25.5(10)	51.8(14)	2.9(9)	-15.0(11)	-5.5(9)
C11	37.2(13)	37.5(12)	27.5(10)	-1.1(9)	-3.5(9)	-4.1(10)
C30	40.9(13)	36.8(12)	30.3(11)	-4.6(9)	-7.0(10)	2.1(10)
C54	45.4(14)	20.7(9)	40.0(12)	0.9(8)	-20.4(10)	-1.1(9)
C14	37.9(13)	33.4(11)	33.3(11)	4.0(9)	-12.1(10)	2.3(9)
C12	53.6(16)	34.8(11)	26.7(10)	3.4(8)	-11.1(10)	-10.0(11)
C19	31.9(12)	32.4(11)	55.8(15)	-11.8(10)	-17.3(11)	-1.6(9)
C34	46.2(13)	27.2(10)	27.4(10)	-1.3(8)	-17.5(9)	-2.5(9)
C20	26.8(11)	18.8(9)	67.6(17)	-0.3(10)	-10.7(11)	-2.6(8)
N4	39.6(13)	32.6(11)	111(2)	-10.8(13)	-33.2(15)	13.4(10)
C5	24.7(10)	29.4(10)	38.0(11)	-4.8(8)	-6.4(9)	5.5(8)
C26	40.3(13)	28.8(10)	43.7(13)	-5.5(9)	-17.9(11)	-3.6(9)
C7	38.2(13)	24.4(10)	69.7(18)	5.2(11)	-26.3(13)	1.5(9)
N3	105(3)	72.3(19)	23.2(11)	-3.5(11)	1.4(13)	-12.0(18)
C27	44.6(14)	22.3(9)	37.9(11)	-5.0(8)	-11.2(10)	1.2(9)
C41	27.8(12)	29.0(11)	66.3(17)	-11.4(11)	-8.8(11)	5.5(9)
C40	30.8(12)	24.0(10)	80(2)	-10.0(11)	-24.5(13)	5.4(9)
C39	48.0(15)	23.6(10)	69.1(18)	-3.1(10)	-39.2(14)	5.4(10)
C33	70.0(19)	38.6(12)	25.9(11)	1.7(9)	-19.3(12)	-7.2(12)
C13	51.2(15)	37.4(12)	34.6(12)	8.2(9)	-18.4(11)	-3.7(11)
C31	49.9(16)	48.7(15)	31.7(12)	-9.1(10)	0.1(11)	-5.5(12)
C8	30.5(12)	32.3(12)	69.0(18)	-7.4(11)	-14.9(12)	10.9(10)
C32	77(2)	43.8(14)	24.0(11)	-4.2(9)	-8.9(12)	-18.1(14)
C16	95(3)	42.9(14)	37.4(13)	11.1(11)	-29.3(15)	-22.8(16)
C15	80(2)	65(2)	28.2(12)	4.1(12)	1.0(14)	-18.9(18)
C44	27.4(14)	34.5(14)	139(4)	-18.5(18)	-15.0(18)	9.1(11)
C43	53.2(19)	32.8(13)	134(4)	-3.2(17)	-57(2)	13.6(13)
C35	99(3)	81(2)	33.2(14)	-19.0(15)	9.5(16)	-41(2)
C36	146(4)	87(3)	25.1(14)	7.3(15)	-22(2)	-16(3)

Table S.10. Bond Lengths for **184a**.

Atom	Atom	Length/Å	Atom	Atom	Length/Å
Si2	C51	1.873(2)	N2	C16	1.452(4)
Si2	C37	1.843(2)	N2	C15	1.450(5)
Si2	C45	1.877(2)	C48	C49	1.381(3)
Si2	C29	1.834(2)	C48	C47	1.392(3)
Si1	C1	1.847(2)	C29	C30	1.405(3)
Si1	C17	1.878(2)	C29	C34	1.398(3)

Si1	C24	1.875(2)	C9	C10	1.390(3)
Si1	C9	1.839(2)	C9	C14	1.414(3)
O1	C6	1.387(3)	C3	C2	1.380(3)
O1	C10	1.390(3)	C3	C4	1.414(3)
O2	C38	1.386(3)	C25	C26	1.392(3)
O2	C34	1.379(3)	C38	C39	1.401(3)
C51	C56	1.396(3)	C10	C11	1.390(3)
C51	C52	1.394(3)	C28	C27	1.388(3)
N1	C4	1.377(3)	C21	C20	1.388(4)
N1	C7	1.448(4)	C4	C5	1.399(3)
N1	C8	1.444(4)	C18	C19	1.397(3)
C1	C6	1.393(3)	C42	C41	1.384(3)
C1	C2	1.406(3)	C53	C54	1.391(3)
C17	C22	1.398(3)	C11	C12	1.414(4)
C17	C18	1.396(3)	C30	C31	1.383(3)
C24	C23	1.396(3)	C14	C13	1.379(3)
C24	C25	1.399(3)	C12	C13	1.405(4)
C37	C38	1.393(3)	C19	C20	1.386(4)
C37	C42	1.415(3)	C34	C33	1.394(3)
C45	C46	1.397(3)	N4	C40	1.380(3)
C45	C50	1.397(3)	N4	C44	1.447(5)
C56	C55	1.391(3)	N4	C43	1.452(5)
C46	C47	1.387(3)	C26	C27	1.387(4)
C23	C28	1.393(3)	N3	C32	1.381(3)
C6	C5	1.400(3)	N3	C35	1.453(6)
C22	C21	1.391(3)	N3	C36	1.447(6)
C52	C53	1.401(3)	C41	C40	1.403(4)
C55	C54	1.376(3)	C40	C39	1.399(4)
C50	C49	1.399(3)	C33	C32	1.389(5)
N2	C12	1.370(3)	C31	C32	1.412(4)

Table S.11. Bond Angles for **184a**.

Atom Atom Atom Angle/°				Atom Atom Atom Angle/°			
C51	Si2	C45	107.90(8)	C10	C9	C14	115.2(2)
C37	Si2	C51	112.34(9)	C14	C9	Si1	123.13(17)
C37	Si2	C45	112.36(9)	C48	C49	C50	119.9(2)
C29	Si2	C51	112.83(9)	C2	C3	C4	119.6(2)
C29	Si2	C37	101.74(10)	C26	C25	C24	121.3(2)
C29	Si2	C45	109.65(10)	C3	C2	C1	124.2(2)

C1	Si1	C17	111.15(9)	O2	C38	C37	125.0(2)
C1	Si1	C24	112.77(9)	O2	C38	C39	112.8(2)
C24	Si1	C17	106.55(9)	C37	C38	C39	122.2(2)
C9	Si1	C1	101.39(10)	O1	C10	C9	124.88(19)
C9	Si1	C17	112.21(10)	C11	C10	O1	111.7(2)
C9	Si1	C24	112.88(9)	C11	C10	C9	123.4(2)
C6	O1	C10	125.60(17)	C46	C47	C48	120.1(2)
C34	O2	C38	125.89(17)	C27	C28	C23	119.5(2)
C56	C51	Si2	119.61(15)	C20	C21	C22	119.8(2)
C52	C51	Si2	122.45(15)	N1	C4	C3	121.1(2)
C52	C51	C56	117.66(18)	N1	C4	C5	121.2(2)
C4	N1	C7	120.0(2)	C5	C4	C3	117.7(2)
C4	N1	C8	119.4(2)	C17	C18	C19	121.2(2)
C8	N1	C7	118.4(2)	C41	C42	C37	123.4(2)
C6	C1	Si1	121.07(15)	C54	C53	C52	119.9(2)
C6	C1	C2	114.90(18)	C10	C11	C12	120.2(2)
C2	C1	Si1	123.84(16)	C31	C30	C29	123.3(2)
C22	C17	Si1	119.78(16)	C55	C54	C53	120.0(2)
C18	C17	Si1	122.53(17)	C13	C14	C9	123.2(2)
C18	C17	C22	117.52(19)	N2	C12	C11	121.0(3)
C23	C24	Si1	119.73(15)	N2	C12	C13	121.5(3)
C23	C24	C25	117.51(19)	C13	C12	C11	117.5(2)
C25	C24	Si1	122.69(16)	C20	C19	C18	120.0(2)
C38	C37	Si2	121.02(18)	O2	C34	C29	125.1(2)
C38	C37	C42	115.6(2)	O2	C34	C33	112.6(2)
C42	C37	Si2	123.38(16)	C33	C34	C29	122.3(2)
C46	C45	Si2	120.02(15)	C19	C20	C21	119.8(2)
C46	C45	C50	118.19(18)	C40	N4	C44	119.8(3)
C50	C45	Si2	121.70(15)	C40	N4	C43	119.5(3)
C55	C56	C51	121.8(2)	C44	N4	C43	116.7(3)
C47	C46	C45	121.0(2)	C4	C5	C6	120.7(2)
C28	C23	C24	121.7(2)	C27	C26	C25	119.9(2)
O1	C6	C1	125.17(18)	C32	N3	C35	120.2(3)
O1	C6	C5	111.95(18)	C32	N3	C36	119.5(4)
C1	C6	C5	122.9(2)	C36	N3	C35	119.6(3)
C21	C22	C17	121.7(2)	C26	C27	C28	120.1(2)
C51	C52	C53	120.9(2)	C42	C41	C40	119.8(3)
C54	C55	C56	119.8(2)	N4	C40	C41	120.9(3)
C45	C50	C49	120.9(2)	N4	C40	C39	120.8(3)

C12	N2	C16	120.0(3)	C39	C40	C41	118.2(2)
C12	N2	C15	120.8(3)	C40	C39	C38	120.8(2)
C15	N2	C16	117.9(2)	C32	C33	C34	120.9(3)
C49	C48	C47	119.9(2)	C14	C13	C12	120.5(2)
C30	C29	Si2	123.26(17)	C30	C31	C32	119.7(3)
C34	C29	Si2	121.04(18)	N3	C32	C33	121.3(3)
C34	C29	C30	115.6(2)	N3	C32	C31	120.6(3)
C10	C9	Si1	121.66(16)	C33	C32	C31	118.1(2)

Table S.12. Hydrogen Atom Coordinates ($\text{\AA} \times 10^4$) and Isotropic Displacement Parameters ($\text{\AA}^2 \times 10^3$) for **184a**.

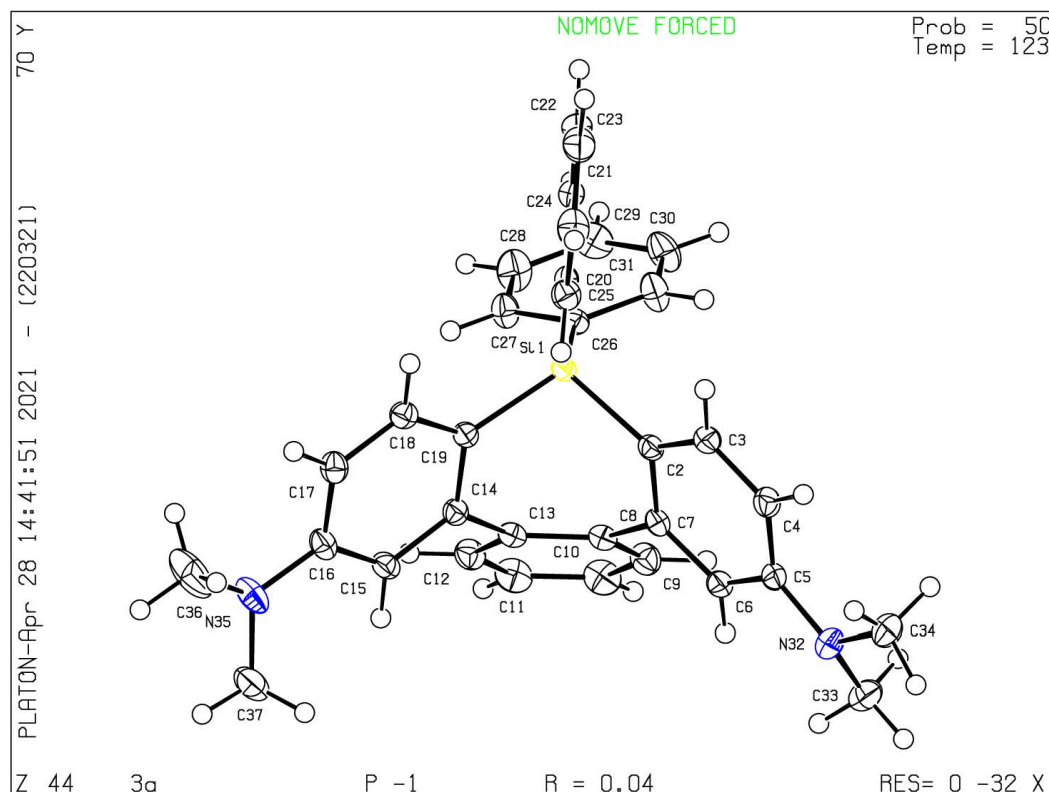
Atom	<i>x</i>	<i>y</i>	<i>z</i>	U(eq)
H56	5111.06	5702.83	6695.78	33
H46	6481.14	4009.13	5386.1	33
H23	6855.91	4007.99	3102.21	32
H22	7169.12	1737.76	4253.66	34
H52	8396.72	5480.11	6587.81	36
H55	5241.54	7487.2	6357.63	38
H50	4532.5	2708.08	7603.33	32
H48	3968.16	2149.05	5427.64	38
H49	3500.5	1906.54	6889.17	38
H3	10829.66	267.98	4264.69	36
H25	9803.18	3657.42	3670.91	38
H2	9366.56	1347.69	4088.93	33
H47	5454.63	3211.3	4677.67	39
H28	6439.22	5512.44	3791.52	38
H21	5667.07	623.64	4692.2	41
H18	7341.16	1495.39	1830.93	39
H42	8568.18	3568.06	5743.57	40
H53	8541.3	7268.41	6208.83	44
H11	11390.45	2714.77	-109.38	42
H30	4461.87	4722.62	8323.54	44
H54	6950.32	8274.42	6122.72	41
H14	7789.94	3721.77	1405.64	42
H19	5806.87	408.09	2268.32	46
H20	4973.14	-36.37	3699.07	46
H5	12399.08	824.55	1766.83	38
H26	9389.66	5156.76	4365.72	43
H7A	12589.19	-329.06	4336.91	64

H7B	13276.3	-1268.53	3857.21	64
H7C	11935.83	-1215.98	4094.56	64
H27	7710.88	6088.08	4424.85	42
H41	10210.12	2591.64	5608.26	50
H39	9251.17	1797.93	8125.99	51
H33	6268.14	2583.29	9974.83	53
H13	8404.9	4223.61	-11.95	49
H31	3583.19	4386.27	9742.44	54
H8A	13149.16	-820.2	2015.16	66
H8B	14033.34	-1040	2545.97	66
H8C	13932	84.72	2073.84	66
H16A	8915.97	4187.44	-1396.59	85
H16B	10031.32	4585.94	-2089.16	85
H16C	9557.23	5147.06	-1246.03	85
H15A	11985.19	3916.98	-1341.13	92
H15B	11579.92	3785.05	-2147.45	92
H15C	11631.46	2805.45	-1489.86	92
H44A	11158.44	899.79	5705.89	103
H44B	12243.24	847.17	6038.64	103
H44C	11857.21	1919.68	5623.54	103
H43A	10931.82	1262.46	7986.55	102
H43B	11793.65	535	7370.48	102
H43C	10481.31	309.86	7657.83	102
H35A	3288.76	4389.5	11231.68	112
H35B	2909.11	3338.95	11816.63	112
H35C	2673.2	3531.92	10920.76	112
H36A	5080.35	1864.32	11153.01	131
H36B	4375.32	2440.29	11947.44	131
H36C	5542.07	2893.25	11366.13	131

S.3 X-ray Structure of Compound 206a

A single crystal of N^6, N^6, N^{12}, N^{12} -tetramethyl-9,9-diphenyl-9*H*-tribenzo[*b,d,f*]silepin-6,12-diamine ($C_{34}H_{32}N_2Si$) (**206a**) was prepared by recrystallization from the dichloromethane/ethanol solution. A suitable crystal was selected, and the X-ray diffraction was collected on an Rigaku AFC HyPix-6000 diffractometer: fixed-chi single diffractometer with graphite monochromated Mo- $K\alpha$ radiation ($\lambda = 0.71073\text{\AA}$). The crystal was kept at 123 K during data collection. The data were collected using ω scan in the θ range of $5.182 \leq 2\theta \leq 54.964$ deg. The data were corrected for Lorentz and polarization effects. The structures were solved by direct methods,^[115] and expanded using Fourier techniques.^[116] Hydrogen atoms were refined using the riding model. The final cycle of full-matrix least-squares refinement on F^2

was based on 12122 observed reflections. Neutral atom scattering factors were taken from Cromer and Waber.^[117] All calculations were performed using the Olex-2 crystallographic software package except for refinement,^[118] which was performed using version 2018/3 of ShelXL (Sheldrick, 2015) of final refinement as well as the bond lengths and angles are summarized in the supporting information, and the numbering scheme employed is also shown in the supporting information, which were drawn with ORTEP at 50% probability ellipsoid.



Crystal structure determination of 206a

$C_{34}H_{32}N_2Si$ ($M = 496.70$ g/mol): triclinic, space group $P-1$ (no. 2), $a = 9.8113(2)$ Å, $b = 12.0833(4)$ Å, $c = 12.1527(3)$ Å, $\alpha = 82.005(2)^\circ$, $\beta = 82.769(2)^\circ$, $\gamma = 71.726(3)^\circ$, $V = 1349.59(7)$ Å³, $Z = 2$, $T = 123$ K, $\mu(\text{Mo K}\alpha) = 0.113$ mm⁻¹, $D_{\text{calc}} = 1.222$ g/cm³, 20753 reflections measured ($5.182^\circ \leq 2\theta \leq 54.964^\circ$), 6188 unique ($R_{\text{int}} = 0.0182$, $R_{\text{sigma}} = 0.0186$) which were used in all calculations. The final R_1 was 0.0353 ($I > 2\sigma(I)$) and wR_2 was 0.0950 (all data).

Table S.13. Crystal data and structure refinement for 206a

Empirical formula	$C_{34}H_{32}N_2Si$
Formula weight	496.70
Temperature/K	123
Crystal system	triclinic
Space group	$P-1$
$a/\text{Å}$	9.8113(2)
$b/\text{Å}$	12.0833(4)

$c/\text{\AA}$	12.1527(3)
$a/^\circ$	82.005(2)
$\beta/^\circ$	82.769(2)
$\gamma/^\circ$	71.726(3)
Volume/ \AA^3	1349.59(7)
Z	2
$D_{\text{calc}} \text{ g/cm}^3$	1.222
μ/mm^{-1}	0.113
$F(000)$	528.0
Crystal size/ mm^3	$0.5 \times 0.4 \times 0.4$
Radiation	Mo $K\alpha$ ($\lambda = 0.71073$)
2θ range for data collection/ $^\circ$	5.182 to 54.964
Index ranges	$-12 \leq h \leq 12, -15 \leq k \leq 14, -15 \leq l \leq 15$
Reflections collected	20753
Independent reflections	6188 [$R_{\text{int}} = 0.0182, R_{\text{sigma}} = 0.0186$]
Data/restraints/parameters	6188/0/338
Goodness-of-fit on F^2	1.046
Final R indexes [$I \geq 2\sigma(I)$]	$R_1 = 0.0353, wR_2 = 0.0929$
Final R indexes [all data]	$R_1 = 0.0386, wR_2 = 0.0950$
Largest diff. peak/hole / $e \text{ \AA}^{-3}$	0.38/-0.28

Table S.14. Fractional Atomic Coordinates ($\times 10^4$) and Equivalent Isotropic Displacement Parameters ($\text{\AA}^2 \times 10^3$) for **206a**. U_{eq} is defined as 1/3 of the trace of the orthogonalised U_{ij} tensor.

Atom	x	y	z	U_{eq}
Si1	6746.1(3)	4082.5(2)	3022.0(2)	15.30(8)
N32	11465.1(11)	1937.6(9)	-515.6(9)	26.6(2)
N35	8314.5(13)	-68.4(9)	6567.6(9)	30.0(2)
C20	7029.9(12)	5405.3(9)	3484.1(9)	17.8(2)
C26	4883.4(11)	4513.4(9)	2574.3(9)	17.9(2)
C7	8141.1(12)	2482.0(9)	1431.8(9)	17.7(2)
C8	7011.7(12)	1886.3(9)	1781.1(9)	18.8(2)
C3	9206.9(12)	4003.2(10)	1450.1(9)	20.3(2)
C19	7128.2(11)	2837.7(9)	4133.0(9)	16.5(2)
C2	8114.9(11)	3511.9(9)	1865.8(9)	17.4(2)
C14	7166.2(11)	1711.9(9)	3916.4(9)	17.6(2)
C18	7532.4(12)	2941.6(10)	5166.1(9)	19.4(2)
C25	8366.9(13)	5387.4(10)	3786.8(10)	22.4(2)
C13	6603.6(12)	1516.7(9)	2893.4(9)	18.5(2)
C5	10334.4(12)	2493.6(10)	228.9(9)	20.7(2)

Atom	<i>x</i>	<i>y</i>	<i>z</i>	<i>U</i> _{eq}
C16	7975.8(12)	874.7(10)	5762.2(10)	21.5(2)
C6	9214.0(12)	2010.9(10)	609.5(9)	19.8(2)
C12	5566.1(13)	921.9(10)	3079.1(10)	23.7(2)
C15	7597.7(12)	755.1(10)	4718.0(9)	20.2(2)
C17	7945.3(12)	1998.9(10)	5967.5(9)	21.8(2)
C9	6348.0(13)	1646.5(11)	923.6(10)	24.9(2)
C27	3764.2(13)	4231.7(11)	3251.6(10)	24.2(2)
C4	10303.8(12)	3515.1(10)	662.0(9)	21.9(2)
C21	5911.2(13)	6460.5(10)	3508.5(9)	21.5(2)
C11	4931.1(14)	692.6(11)	2219.5(11)	28.3(3)
C31	4559.1(14)	5186.6(12)	1556.7(11)	29.1(3)
C24	8587.4(15)	6390.4(12)	4066.4(10)	29.2(3)
C30	3164.7(15)	5577.2(12)	1236.7(11)	33.2(3)
C22	6119.5(15)	7460.8(11)	3808.1(10)	28.8(3)
C29	2068.0(14)	5302.7(12)	1931.0(12)	30.9(3)
C10	5323.4(14)	1063.3(11)	1131.7(11)	29.3(3)
C34	12557.5(14)	2507.1(12)	-920.4(11)	30.7(3)
C23	7459.8(17)	7424.0(12)	4069.9(11)	32.7(3)
C37	8686.9(16)	-1254.7(11)	6268.7(12)	33.8(3)
C33	11149.0(16)	1297.2(12)	-1324.4(11)	34.4(3)
C28	2369.8(14)	4620.0(13)	2931.6(12)	32.8(3)
C36	8741(2)	73.1(15)	7609.9(14)	52.4(5)

Table S.15. Anisotropic Displacement Parameters ($\times 10^4$) for **206a**. The anisotropic displacement factor exponent takes the form: $-2\pi^2[h^2a^{*2}U_{11}+2hka^*b^*U_{12}+\dots]$.

Atom	<i>U</i> ₁₁	<i>U</i> ₂₂	<i>U</i> ₃₃	<i>U</i> ₂₃	<i>U</i> ₁₃	<i>U</i> ₁₂
Si1	13.78(14)	13.97(14)	17.33(14)	0.08(10)	-0.89(10)	-3.94(11)
N32	27.4(5)	26.1(5)	23.0(5)	-4.2(4)	6.6(4)	-5.9(4)
N35	36.4(6)	24.3(5)	29.0(5)	9.5(4)	-13.3(5)	-9.9(5)
C20	19.3(5)	17.2(5)	16.6(5)	-0.7(4)	1.7(4)	-6.8(4)
C26	16.4(5)	16.7(5)	20.0(5)	-1.1(4)	-2.5(4)	-4.3(4)
C7	19.1(5)	17.0(5)	16.1(5)	2.2(4)	-4.2(4)	-4.7(4)
C8	19.5(5)	15.2(5)	21.2(5)	-1.1(4)	-3.3(4)	-4.5(4)
C3	21.7(5)	17.7(5)	21.0(5)	-1.0(4)	-0.3(4)	-6.4(4)
C19	13.2(5)	16.6(5)	18.2(5)	0.2(4)	-0.4(4)	-3.6(4)
C2	16.9(5)	15.9(5)	17.7(5)	1.0(4)	-2.0(4)	-3.5(4)
C14	15.3(5)	18.2(5)	18.4(5)	-0.4(4)	0.2(4)	-5.2(4)
C18	17.7(5)	19.1(5)	21.2(5)	-2.0(4)	-1.0(4)	-5.5(4)
C25	21.9(5)	22.9(6)	23.1(5)	-1.4(4)	-1.5(4)	-8.3(4)
C13	18.3(5)	14.7(5)	22.0(5)	-0.9(4)	-2.4(4)	-4.3(4)

Atom	U ₁₁	U ₂₂	U ₃₃	U ₂₃	U ₁₃	U ₁₂
C5	21.8(5)	19.3(5)	16.6(5)	1.6(4)	-0.1(4)	-1.8(4)
C16	18.2(5)	21.9(5)	22.4(5)	4.7(4)	-3.4(4)	-5.7(4)
C6	24.4(5)	16.8(5)	17.2(5)	-0.5(4)	-2.9(4)	-4.7(4)
C12	23.0(6)	22.0(6)	27.2(6)	-0.8(4)	-0.9(4)	-9.6(5)
C15	20.4(5)	16.1(5)	23.2(5)	0.9(4)	-1.0(4)	-6.0(4)
C17	20.8(5)	25.7(6)	18.9(5)	0.1(4)	-4.3(4)	-7.4(4)
C9	29.3(6)	24.5(6)	22.5(5)	-0.9(4)	-6.2(5)	-9.5(5)
C27	20.3(5)	29.7(6)	21.8(5)	3.2(5)	-2.7(4)	-8.8(5)
C4	20.8(5)	22.1(5)	22.0(5)	0.7(4)	1.7(4)	-7.9(4)
C21	23.1(5)	19.8(5)	19.2(5)	-1.1(4)	2.8(4)	-5.2(4)
C11	25.3(6)	26.7(6)	37.9(7)	-3.3(5)	-4.9(5)	-14.1(5)
C31	24.5(6)	34.9(7)	26.1(6)	9.4(5)	-4.5(5)	-10.8(5)
C24	35.2(7)	34.9(7)	25.3(6)	-2.5(5)	-3.4(5)	-21.6(6)
C30	31.5(7)	35.0(7)	30.8(7)	10.6(5)	-14.6(5)	-8.1(6)
C22	39.7(7)	18.1(5)	25.0(6)	-4.3(4)	4.2(5)	-5.2(5)
C29	20.6(6)	33.2(7)	39.5(7)	-0.2(5)	-13.0(5)	-6.5(5)
C10	31.6(7)	29.0(6)	32.3(6)	-4.1(5)	-11.5(5)	-12.7(5)
C34	25.7(6)	31.7(7)	28.7(6)	-2.4(5)	8.2(5)	-4.5(5)
C23	53.9(8)	25.0(6)	25.8(6)	-5.8(5)	0.6(6)	-21.6(6)
C37	35.1(7)	23.2(6)	37.9(7)	8.4(5)	-5.1(6)	-5.6(5)
C33	43.6(8)	27.2(6)	30.2(7)	-9.9(5)	10.0(6)	-9.7(6)
C28	19.5(6)	45.0(8)	35.0(7)	2.6(6)	-2.7(5)	-14.0(6)
C36	82.5(13)	39.8(8)	42.2(9)	17.3(7)	-40.1(9)	-24.8(9)

Table S.16. Bond Lengths in Å for **206a**.

Atom	Atom	Length/Å	Atom	Atom	Length/Å
Si1	C20	1.8749(11)	C19	C14	1.4095(15)
Si1	C26	1.8660(11)	C19	C18	1.3964(15)
Si1	C19	1.8534(11)	C14	C13	1.4972(15)
Si1	C2	1.8620(11)	C14	C15	1.3959(15)
N32	C5	1.3963(14)	C18	C17	1.3825(16)
N32	C34	1.4492(17)	C25	C24	1.3887(17)
N32	C33	1.4491(17)	C13	C12	1.3999(16)
N35	C16	1.3788(15)	C5	C6	1.4005(16)
N35	C37	1.4503(18)	C5	C4	1.3982(16)
N35	C36	1.4308(18)	C16	C15	1.4042(16)
C20	C25	1.3994(16)	C16	C17	1.4055(17)
C20	C21	1.3986(15)	C12	C11	1.3815(17)
C26	C27	1.3885(16)	C9	C10	1.3790(18)
C26	C31	1.3961(16)	C27	C28	1.3870(17)

Atom Atom Length/Å			Atom Atom Length/Å		
C7	C8	1.4909(15)	C21	C22	1.3898(17)
C7	C2	1.4095(15)	C11	C10	1.3827(19)
C7	C6	1.3959(15)	C31	C30	1.3870(18)
C8	C13	1.4124(15)	C24	C23	1.385(2)
C8	C9	1.4025(16)	C30	C29	1.377(2)
C3	C2	1.3909(15)	C22	C23	1.377(2)
C3	C4	1.3867(16)	C29	C28	1.3803(19)

Table S.17. Bond Angles in ° for **206a**.

Atom Atom Atom Angle/°				Atom Atom Atom Angle/°			
C26	Si1	C20	108.00(5)	C19	C14	C13	121.94(9)
C19	Si1	C20	110.70(5)	C15	C14	C19	120.09(10)
C19	Si1	C26	113.96(5)	C15	C14	C13	117.63(10)
C19	Si1	C2	102.46(5)	C17	C18	C19	122.79(10)
C2	Si1	C20	110.54(5)	C24	C25	C20	121.20(11)
C2	Si1	C26	111.14(5)	C8	C13	C14	126.09(10)
C5	N32	C34	118.13(10)	C12	C13	C8	118.14(10)
C5	N32	C33	117.96(11)	C12	C13	C14	115.76(10)
C34	N32	C33	114.26(10)	N32	C5	C6	120.66(11)
C16	N35	C37	120.39(11)	N32	C5	C4	121.87(11)
C16	N35	C36	119.76(11)	C4	C5	C6	117.41(10)
C36	N35	C37	117.02(11)	N35	C16	C15	121.11(11)
C25	C20	Si1	121.70(8)	N35	C16	C17	121.39(11)
C21	C20	Si1	120.73(9)	C15	C16	C17	117.46(10)
C21	C20	C25	117.55(10)	C7	C6	C5	122.13(10)
C27	C26	Si1	121.89(8)	C11	C12	C13	122.47(11)
C27	C26	C31	117.73(10)	C14	C15	C16	122.03(10)
C31	C26	Si1	120.31(9)	C18	C17	C16	120.28(11)
C2	C7	C8	122.35(10)	C10	C9	C8	122.30(11)
C6	C7	C8	117.43(10)	C28	C27	C26	120.97(11)
C6	C7	C2	120.17(10)	C3	C4	C5	120.19(11)
C13	C8	C7	125.16(10)	C22	C21	C20	121.43(12)
C9	C8	C7	116.51(10)	C12	C11	C10	119.31(11)
C9	C8	C13	118.30(10)	C30	C31	C26	121.35(11)
C4	C3	C2	123.11(11)	C23	C24	C25	119.69(12)
C14	C19	Si1	120.37(8)	C29	C30	C31	119.86(12)
C18	C19	Si1	121.97(8)	C23	C22	C21	119.62(12)
C18	C19	C14	117.33(10)	C30	C29	C28	119.72(11)

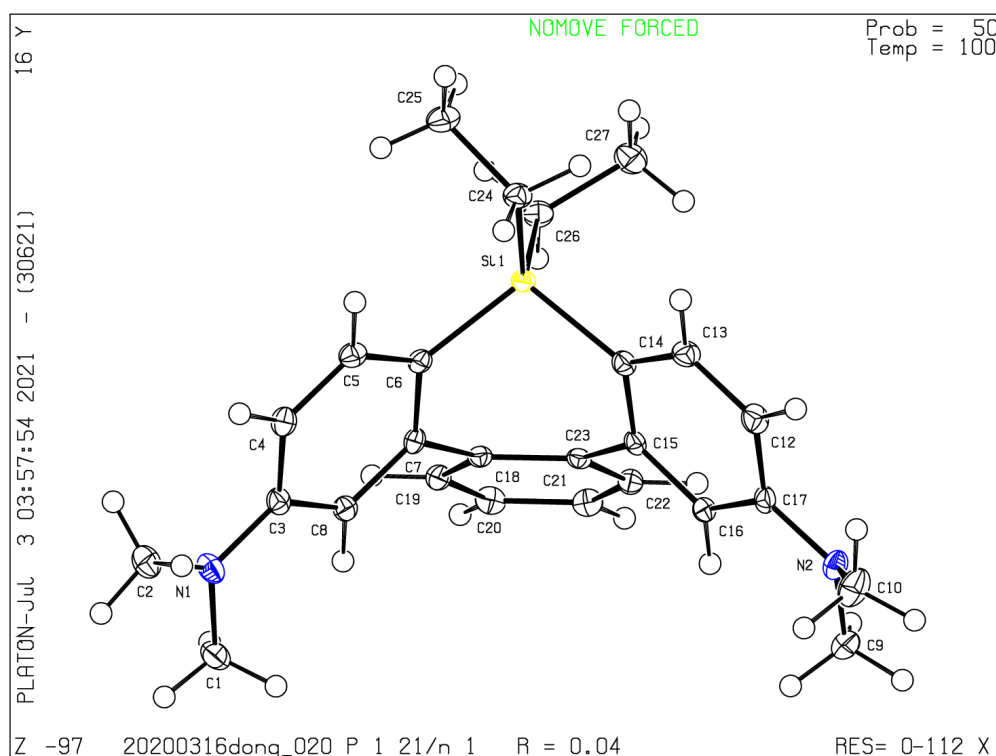
Atom	Atom	Atom	Angle/°	Atom	Atom	Atom	Angle/°
C7	C2	Si1	119.79(8)	C9	C10	C11	119.48(11)
C3	C2	Si1	123.12(8)	C22	C23	C24	120.46(12)
C3	C2	C7	116.90(10)	C29	C28	C27	120.35(12)

Table S.18. Hydrogen Fractional Atomic Coordinates ($\times 10^4$) and Equivalent Isotropic Displacement Parameters ($\text{\AA}^2 \times 10^3$) for **206a**. U_{eq} is defined as 1/3 of the trace of the orthogonalised U_{ij} .

Atom	<i>x</i>	<i>y</i>	<i>z</i>	U_{eq}
H3	9200.95	4706.5	1718.87	24
H18	7523.37	3691.84	5325.11	23
H25	9137.88	4676.2	3801.25	27
H6	9183.29	1341.19	297.92	24
H12	5288.16	666.27	3824.19	28
H15	7636.83	-0.3	4552.04	24
H17	8209.49	2111.52	6659.83	26
H9	6613.57	1894.49	173.21	30
H27	3956.41	3766.04	3944.31	29
H4	11036.64	3875.75	415.71	26
H21	4988.93	6494.24	3316.18	26
H11	4232.26	284.48	2374.26	34
H31	5308.94	5381.13	1073.6	35
H24	9507.53	6367.58	4254.32	35
H30	2966.37	6033.07	540.11	40
H22	5341.98	8165.96	3832.21	35
H29	1108.05	5582	1722.13	37
H10	4890.54	917.43	532.39	35
H34A	12137.35	3220.33	-1408.03	46
H34B	13352.48	1973.73	-1340.48	46
H34C	12921.35	2712.44	-286.53	46
H23	7611.67	8112.52	4254.17	39
H37A	7821.38	-1403.79	6082.64	51
H37B	9087.39	-1811.08	6899.26	51
H37C	9403.74	-1350.86	5622.21	51
H33A	10783.27	667.66	-933.96	52
H33B	12029.83	959.25	-1795.32	52
H33C	10420.04	1831.6	-1790.82	52
H28	1618.32	4415	3403.61	39
H36A	9695.99	188.35	7492.92	79
H36B	8776.52	-629.15	8131.4	79
H36C	8042.37	757.1	7919.15	79

S.4 X-ray Structure of Compound 206g

Single crystals of $C_{26}H_{32}N_2Si$, 9,9-diethyl- N^6,N^6,N^{12},N^{12} -tetramethyl-9*H*-tribenzo[*b,d,f*]silepin-6,12-diamine (**206g**) were prepared by recrystallization from the dichloromethane/ethanol solution. A suitable crystal was selected, and the X-ray diffraction was collected on a XtaLAB AFC10 (RCD3): fixed-chi single diffractometer. The crystal was kept at 100 K during data collection. The data were collected using ω scan in the θ range of $5.148 \leq \theta \leq 54.964$ deg. The data were corrected for Lorentz and polarization effects. The structures were solved by direct methods,^[115] and expanded using Fourier techniques.^[116] Hydrogen atoms were refined using the riding model. The final cycle of full-matrix least-squares refinement on F^2 was based on 12122 observed reflections. Neutral atom scattering factors were taken from Cromer and Waber.^[117] All calculations were performed using the Olex-2 crystallographic software package except for refinement,^[118] which was performed using version 2018/3 of ShelXL (Sheldrick, 2015) of final refinement as well as the bond lengths and angles are summarized in the supporting information, and the numbering scheme employed is also shown in the supporting information, which were drawn with ORTEP at 50% probability ellipsoid.



Crystal structure determination of 206g

$C_{26}H_{32}N_2Si$ ($M = 400.62$ g/mol): monoclinic, space group $P2_1/n$ (no. 14), $a = 8.6133(2)$ Å, $b = 16.3209(5)$ Å, $c = 15.8387(5)$ Å, $\beta = 96.685(3)^\circ$, $V = 2211.42(11)$ Å³, $Z = 4$, $T = 100$ K, $\mu(\text{Mo K}\alpha) = 0.121$ mm⁻¹, $D_{\text{calc}} = 1.203$ g/cm³, 19729 reflections measured ($5.148^\circ \leq 2\theta \leq 54.964^\circ$),

5071 unique ($R_{\text{int}} = 0.0368$, $R_{\text{sigma}} = 0.0345$) which were used in all calculations. The final R_1 was 0.0362 ($I > 2\sigma(I)$) and wR_2 was 0.0975 (all data).

Table S.19. Crystal data and structure refinement for **206g**.

Empirical formula	$\text{C}_{26}\text{H}_{32}\text{N}_2\text{Si}$
Formula weight	400.62
Temperature/K	100
Crystal system	monoclinic
Space group	$P2_1/n$
$a/\text{\AA}$	8.6133(2)
$b/\text{\AA}$	16.3209(5)
$c/\text{\AA}$	15.8387(5)
$\alpha/^\circ$	90
$\beta/^\circ$	96.685(3)
$\gamma/^\circ$	90
Volume/ \AA^3	2211.42(11)
Z	4
$D_{\text{calc}} \text{ g/cm}^3$	1.203
μ/mm^{-1}	0.121
$F(000)$	864.0
Crystal size/ mm^3	$0.197 \times 0.149 \times 0.136$
Radiation	Mo $K\alpha$ ($\lambda = 0.71073$)
2θ range for data collection/ $^\circ$	5.148 to 54.964
Index ranges	$-11 \leq h \leq 11$, $-16 \leq k \leq 21$, $-20 \leq l \leq 20$
Reflections collected	19729
Independent reflections	5071 [$R_{\text{int}} = 0.0368$, $R_{\text{sigma}} = 0.0345$]
Data/restraints/parameters	5071/0/268
Goodness-of-fit on F^2	1.066
Final R indexes [$I \geq 2\sigma(I)$]	$R_1 = 0.0362$, $wR_2 = 0.0944$
Final R indexes [all data]	$R_1 = 0.0419$, $wR_2 = 0.0975$
Largest diff. peak/hole / $e \text{ \AA}^{-3}$	0.33/-0.29

Table S.20. Fractional Atomic Coordinates ($\times 10^4$) and Equivalent Isotropic Displacement Parameters ($\text{\AA}^2 \times 10^3$) for **206g**. U_{eq} is defined as 1/3 of of the trace of the orthogonalised U_{ij} tensor.

Atom	x	y	z	$U(\text{eq})$
Si1	8864.6(4)	4027.0(2)	7537.8(2)	11.38(9)
N2	4500.1(12)	6250.4(6)	9280.7(6)	15.4(2)
N1	4470.6(12)	3821.3(7)	4248.3(6)	17.2(2)

Table S.20. Fractional Atomic Coordinates ($\times 10^4$) and Equivalent Isotropic Displacement Parameters ($\text{\AA}^2 \times 10^3$) for **206g**. U_{eq} is defined as 1/3 of the trace of the orthogonalised U_{IJ} tensor.

Atom	<i>x</i>	<i>y</i>	<i>z</i>	U(eq)
C6	7613.1(13)	3857.9(7)	6510.9(7)	12.4(2)
C7	6096.7(13)	3532.0(7)	6495.8(7)	11.9(2)
C15	6060.5(13)	4411.6(7)	8258.2(7)	11.5(2)
C18	5506.2(13)	3164.1(7)	7260.0(7)	11.5(2)
C14	7578.6(13)	4669.3(7)	8141.5(7)	13.0(2)
C16	5046.5(13)	4941.6(7)	8623.6(7)	12.7(2)
C5	8015.8(14)	4168.0(7)	5740.8(8)	14.7(2)
C4	7010.1(14)	4161.1(8)	4994.1(8)	15.2(2)
C19	4837.4(13)	2382.9(7)	7156.3(8)	14.2(2)
C3	5494.2(14)	3837.4(7)	4980.4(7)	13.8(2)
C22	4768.1(13)	3159.0(7)	8685.3(7)	13.9(2)
C23	5475.3(13)	3563.9(7)	8049.4(7)	11.6(2)
C13	8016.3(14)	5458.2(8)	8426.5(8)	15.7(2)
C8	5073.6(13)	3520.6(7)	5746.5(7)	13.2(2)
C24	10640.9(14)	4625.8(8)	7338.4(8)	15.8(2)
C17	5498.1(14)	5731.2(7)	8895.2(7)	13.4(2)
C20	4142.9(14)	1997.5(8)	7791.7(8)	15.9(2)
C12	7027.6(14)	5980.0(8)	8795.3(8)	16.7(3)
C2	4903.4(15)	4191.5(8)	3481.7(8)	19.6(3)
C21	4107.4(14)	2388.9(8)	8565.4(8)	16.1(2)
C26	9502.4(14)	3084.2(8)	8156.2(8)	16.4(2)
C27	10375.1(15)	3296.1(9)	9029.9(8)	22.1(3)
C9	2956.0(15)	5951.8(8)	9403.5(8)	19.5(3)
C1	2855.1(14)	3592.1(9)	4281.9(8)	19.8(3)
C25	11851.7(14)	4124.5(8)	6922.8(9)	20.1(3)
C10	4517.6(17)	7117.8(8)	9073.2(9)	24.0(3)

Table S.21. Anisotropic Displacement Parameters ($\text{\AA}^2 \times 10^3$) for **206g**. The Anisotropic displacement factor exponent takes the form: $-2\pi^2[h^2a^*U_{11}+2hka^*b^*U_{12}+\dots]$.

Atom	U_{11}	U_{22}	U_{33}	U_{23}	U_{13}	U_{12}
Si1	10.05(15)	10.87(17)	13.03(16)	-0.61(12)	0.49(11)	0.14(11)
N2	19.0(5)	12.2(5)	15.5(5)	-1.8(4)	3.8(4)	2.3(4)
N1	17.8(5)	20.8(6)	12.3(5)	1.5(4)	-0.7(4)	-4.0(4)

C6	12.5(5)	10.5(5)	14.2(5)	-1.7(4)	1.5(4)	1.9(4)
C7	14.5(5)	8.5(5)	12.9(5)	-2.7(4)	2.6(4)	1.2(4)
C15	13.5(5)	11.4(5)	8.9(5)	0.5(4)	-1.0(4)	0.6(4)
C18	9.9(5)	11.6(5)	12.9(5)	0.2(4)	0.8(4)	1.5(4)
C14	14.0(5)	12.8(6)	11.7(5)	0.0(4)	-0.6(4)	0.7(4)
C16	13.1(5)	14.1(6)	10.6(5)	0.4(4)	0.9(4)	0.8(4)
C5	12.7(5)	13.8(6)	18.0(6)	-0.4(5)	2.9(4)	-0.3(4)
C4	17.9(6)	14.5(6)	13.6(6)	0.5(4)	3.7(4)	-0.5(5)
C19	14.0(5)	12.9(6)	15.4(6)	-2.0(4)	0.8(4)	1.1(4)
C3	16.8(6)	10.3(5)	13.8(5)	-1.9(4)	0.0(4)	0.9(4)
C22	14.4(5)	14.2(6)	13.0(5)	0.2(4)	0.9(4)	1.8(4)
C23	9.7(5)	11.6(5)	12.8(5)	0.2(4)	-1.0(4)	1.4(4)
C13	13.5(5)	15.0(6)	18.4(6)	-1.5(5)	0.6(4)	-1.7(5)
C8	12.8(5)	11.8(6)	14.8(6)	-2.6(4)	1.6(4)	-1.4(4)
C24	12.9(5)	15.0(6)	19.3(6)	-1.6(5)	0.8(4)	-1.0(5)
C17	17.6(6)	13.8(6)	8.7(5)	-0.1(4)	0.8(4)	2.8(5)
C20	16.4(5)	10.4(6)	20.5(6)	0.7(5)	0.3(4)	-1.5(4)
C12	19.1(6)	12.0(6)	18.5(6)	-3.4(5)	-0.1(5)	-1.9(5)
C2	22.9(6)	21.8(7)	13.6(6)	3.1(5)	0.2(5)	-1.4(5)
C21	16.0(5)	15.7(6)	17.0(6)	4.1(5)	3.1(4)	0.2(5)
C26	15.7(5)	14.9(6)	18.5(6)	1.8(5)	1.3(4)	1.5(5)
C27	22.3(6)	24.6(7)	18.6(6)	3.9(5)	-0.8(5)	3.5(5)
C9	17.6(6)	20.7(7)	20.7(6)	-3.7(5)	4.0(5)	3.5(5)
C1	16.8(6)	24.4(7)	17.1(6)	-1.1(5)	-2.5(5)	-2.2(5)
C25	13.4(6)	22.5(7)	24.9(7)	0.0(5)	3.9(5)	-0.2(5)
C10	34.3(7)	14.6(6)	24.4(7)	1.4(5)	9.4(6)	6.8(5)

Table S.22. Bond Lengths for **206g**.

Atom	Atom	Length/Å	Atom	Atom	Length/Å
Si1	C6	1.8643(12)	C15	C23	1.4963(16)
Si1	C14	1.8672(12)	C18	C19	1.4010(17)
Si1	C24	1.8730(12)	C18	C23	1.4133(16)
Si1	C26	1.8718(13)	C14	C13	1.4016(17)
N2	C17	1.3971(16)	C16	C17	1.3993(17)
N2	C9	1.4507(16)	C5	C4	1.3823(17)
N2	C10	1.4539(17)	C4	C3	1.4063(17)
N1	C3	1.3728(15)	C19	C20	1.3807(17)
N1	C2	1.4435(16)	C3	C8	1.4048(17)
N1	C1	1.4478(16)	C22	C23	1.4017(16)

Table S.22. Bond Lengths for **206g**.

Atom	Atom	Length/Å	Atom	Atom	Length/Å
C6	C7	1.4078(16)	C22	C21	1.3836(17)
C6	C5	1.4010(17)	C13	C12	1.3811(18)
C7	C18	1.4926(16)	C24	C25	1.5330(17)
C7	C8	1.3935(16)	C17	C12	1.4049(17)
C15	C14	1.4061(16)	C20	C21	1.3855(18)
C15	C16	1.4013(16)	C26	C27	1.5354(17)

Table S.23. Bond Angles for **206g**.

Atom	Atom	Atom	Angle/°	Atom	Atom	Atom	Angle/°
C6	Si1	C14	102.28(5)	C15	C14	Si1	121.04(9)
C6	Si1	C24	109.32(5)	C13	C14	Si1	121.82(9)
C6	Si1	C26	116.07(6)	C13	C14	C15	116.86(11)
C14	Si1	C24	109.78(6)	C17	C16	C15	122.09(11)
C14	Si1	C26	110.43(5)	C4	C5	C6	123.23(11)
C26	Si1	C24	108.75(6)	C5	C4	C3	120.30(11)
C17	N2	C9	118.37(10)	C20	C19	C18	122.43(11)
C17	N2	C10	117.95(10)	N1	C3	C4	121.61(11)
C9	N2	C10	113.03(10)	N1	C3	C8	121.18(11)
C3	N1	C2	119.94(10)	C8	C3	C4	117.21(11)
C3	N1	C1	119.96(10)	C21	C22	C23	122.39(11)
C2	N1	C1	118.85(10)	C18	C23	C15	125.58(10)
C7	C6	Si1	120.79(9)	C22	C23	C15	116.13(10)
C5	C6	Si1	121.97(9)	C22	C23	C18	118.20(11)
C5	C6	C7	116.42(10)	C12	C13	C14	123.14(11)
C6	C7	C18	122.77(10)	C7	C8	C3	121.98(11)
C8	C7	C6	120.86(11)	C25	C24	Si1	113.82(9)
C8	C7	C18	116.35(10)	N2	C17	C16	121.99(11)
C14	C15	C23	122.82(10)	N2	C17	C12	120.44(11)
C16	C15	C14	120.23(11)	C16	C17	C12	117.53(11)
C16	C15	C23	116.88(10)	C19	C20	C21	119.38(11)
C19	C18	C7	116.44(10)	C13	C12	C17	120.13(11)
C19	C18	C23	118.30(10)	C22	C21	C20	119.29(11)
C23	C18	C7	125.11(10)	C27	C26	Si1	111.68(9)

Table S.24. Hydrogen Atom Coordinates ($\text{\AA}\times 10^4$) and Isotropic Displacement Parameters ($\text{\AA}^2\times 10^3$) for **206g**.

Atom	x	y	z	U(eq)
H16	4020	4759.16	8688.98	15
H5	9029.93	4394.11	5731.28	18
H4	7344.42	4376.01	4487.88	18
H19	4862.82	2108.04	6629.36	17
H22	4741.34	3423.04	9217.97	17
H13	9042.17	5642.98	8362.92	19
H8	4061.16	3291.75	5754	16
H24A	10310.89	5097.26	6966.87	19
H24B	11140.43	4846.35	7885.97	19
H20	3693.4	1468.88	7699.19	19
H12	7382.33	6508.05	8981.83	20
H2A	5063.87	4780.9	3572.48	29
H2B	4067.62	4103.39	3015.49	29
H2C	5872.49	3941.7	3336.69	29
H21	3634.66	2131.34	9008.84	19
H26A	8574.26	2747.05	8234.4	20
H26B	10194.3	2755.75	7830.57	20
H27A	11343.74	3587.78	8953.97	33
H27B	10625.77	2790.69	9351.12	33
H27C	9712.99	3645.27	9342.26	33
H9A	2333.11	5883.1	8849.67	29
H9B	2441.42	6347.08	9744.72	29
H9C	3050.26	5423.52	9699.18	29
H1A	2805.46	3023.78	4476.5	30
H1B	2275.4	3643.49	3714.15	30
H1C	2390.86	3954.09	4677.79	30
H25A	11384.04	3926.04	6366.68	30
H25B	12188.81	3656.61	7286.46	30
H25C	12756.28	4470.5	6849.53	30
H10A	5601.41	7305.57	9089.68	36
H10B	3992.48	7427.67	9487.71	36
H10C	3970.58	7204.94	8502.42	36

S.5 X-ray Structure of Compound 209

A single crystal of (N^6, N^6, N^{12}, N^{12} -tetramethyl-9,9-diphenyl-9*H*-6,12-diamine) tribenzo[*b,d,f*]bissilepin ($C_{62}H_{58}N_4Si_2$) (**209**) was prepared by recrystallization from the

dichloromethane/ethanol solution. A suitable crystal was selected, and the X-ray diffraction was collected on an Rigaku AFC HyPix-6000 diffractometer: fixed-chi single diffractometer with graphite monochromated Mo K α radiation ($\lambda = 0.71073\text{\AA}$). The crystal was kept at 173 K during data collection. The data were collected using ω scan in the θ range of $4.476 \leq 2\theta \leq 54.966$ deg. The data were corrected for Lorentz and polarization effects. The structures were solved by direct methods,^[115] and expanded using Fourier techniques.^[116] Hydrogen atoms were refined using the riding model. The final cycle of full-matrix least-squares refinement on F^2 was based on 26837 observed reflections. Neutral atom scattering factors were taken from Cromer and Waber.^[117] All calculations were performed using the Olex-2 crystallographic software package except for refinement,^[118] which was performed using version 2018/3 of ShelXL (Sheldrick, 2015) of final refinement as well as the bond lengths and angles are summarized in the supporting information, and the numbering scheme employed is also shown in the supporting information, which were drawn with ORTEP at 50% probability ellipsoid.

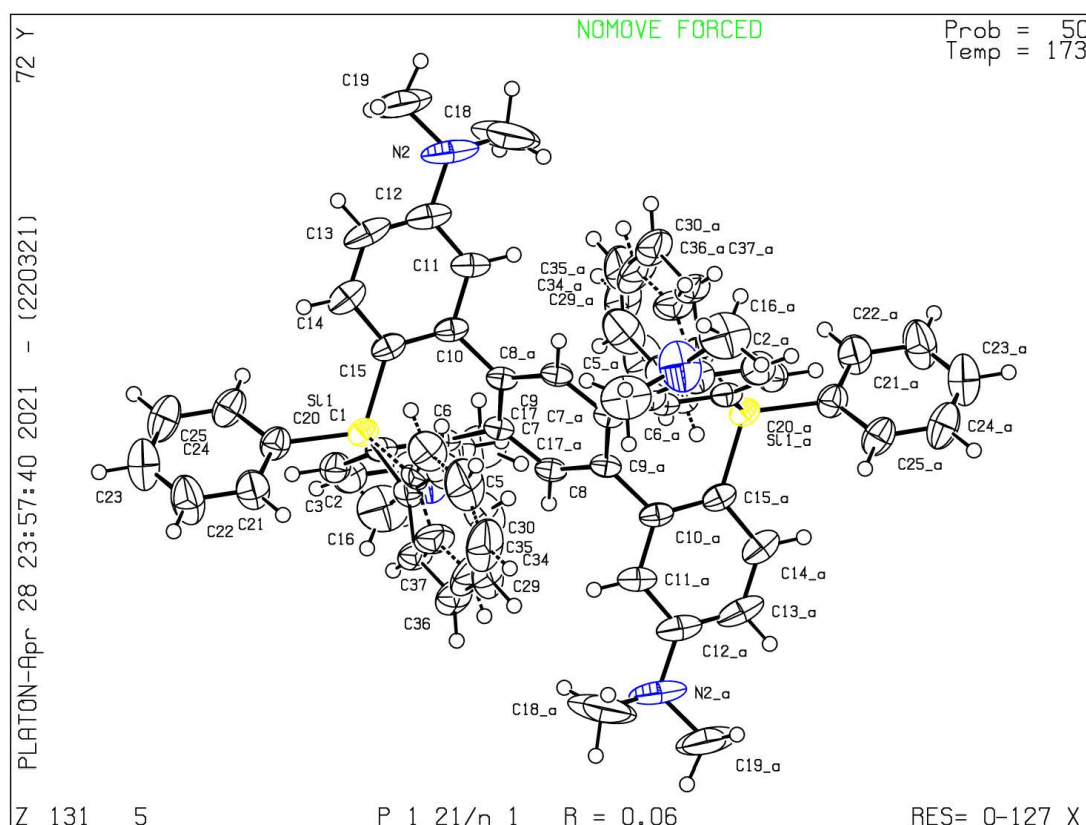


Table S.25. Crystal data and structure refinement for **209**.

Empirical formula	C ₆₂ H ₅₈ N ₄ Si ₂
Formula weight	915.30
Temperature/K	173
Crystal system	monoclinic
Space group	$P2_1/n$
$a/\text{\AA}$	15.3334(8)

$b/\text{\AA}$	11.1613(8)
$c/\text{\AA}$	15.7358(9)
$\alpha/^\circ$	90
$\beta/^\circ$	91.890(5)
$\gamma/^\circ$	90
Volume/ \AA^3	2691.6(3)
Z	50
$D_{\text{calc}} \text{ g/cm}^3$	28.234
μ/mm^{-1}	2.689
$F(000)$	24300.0
Crystal size/ mm^3	$0.24 \times 0.09 \times 0.09$
Radiation	Mo $K\alpha$ ($\lambda = 0.71073$)
2θ range for data collection/ $^\circ$	4.476 to 54.966
Index ranges	$-19 \leq h \leq 19, -14 \leq k \leq 13, -20 \leq l \leq 20$
Reflections collected	26837
Independent reflections	6128 [$R_{\text{int}} = 0.0504, R_{\text{sigma}} = 0.0491$]
Data/restraints/parameters	6128/108/366
Goodness-of-fit on F^2	1.052
Final R indexes [$I \geq 2\sigma(I)$]	$R_1 = 0.0615, wR_2 = 0.1631$
Final R indexes [all data]	$R_1 = 0.0791, wR_2 = 0.1720$
Largest diff. peak/hole / $e \text{\AA}^{-3}$	0.50/-0.27

Table S.26. Fractional Atomic Coordinates ($\times 10^4$) and Equivalent Isotropic Displacement Parameters ($\text{\AA}^2 \times 10^3$) for **209**. U_{eq} is defined as 1/3 of the trace of the orthogonalised U_{ij} tensor.

Atom	x	y	z	$U(\text{eq})$
Si1	5956.9(3)	4776.0(5)	7395.1(4)	36.19(17)
C9	5105.9(11)	5771.0(16)	5709.9(12)	31.5(4)
C7	4686.3(11)	4661.1(16)	5801.7(12)	30.7(4)
C10	5273.0(12)	6668.1(16)	6394.2(13)	34.5(4)
C8	4597.5(12)	3937.8(16)	5088.8(13)	32.0(4)
C6	4326.6(12)	4191.7(16)	6605.8(13)	33.7(4)
C1	4849.4(13)	4082.3(17)	7350.8(13)	36.2(4)
C15	5728.6(13)	6372.9(18)	7147.2(14)	37.9(4)
C5	3475.1(14)	3756.8(19)	6569.8(14)	40.8(5)
C11	5015.6(14)	7847.7(18)	6222.0(16)	44.1(5)
C2	4479.0(15)	3512(2)	8037.9(14)	44.9(5)
N2	4930.8(19)	9946.6(19)	6589(2)	82.1(9)
C20	6461.4(14)	4569(2)	8480.3(14)	43.7(5)

Atom	x	y	z	U(eq)
N1	2281.8(15)	2707(3)	7206.1(17)	76.7(8)
C14	5934.7(15)	7320(2)	7701.7(17)	51.5(6)
C4	3116.9(15)	3176(2)	7266.7(15)	49.2(6)
C12	5203.0(16)	8767(2)	6786.8(19)	55.0(6)
C3	3638.4(17)	3072(2)	8000.4(15)	51.5(6)
C25	6072.3(16)	5018(2)	9204.0(15)	53.6(6)
C13	5677.1(17)	8493(2)	7515(2)	61.1(7)
C21	7227.4(17)	3914(3)	8607.7(16)	60.0(7)
C24	6428.8(19)	4813(3)	10006.9(16)	67.3(8)
C17	1658.8(17)	3185(3)	6612(2)	78.0(9)
C22	7587(2)	3721(4)	9413.4(19)	80.1(10)
C16	1986(2)	1923(3)	7851(2)	87.1(11)
C23	7181(2)	4163(4)	10111.8(18)	78.2(9)
C19	4973(4)	10789(3)	7274(3)	138(2)
C18	4224(4)	10117(3)	5980(4)	152(2)
C28	7873(9)	4662(19)	5616(7)	92(4)
C29	7810(9)	3520(20)	5317(8)	99(4)
C31	6666(8)	3127(12)	6228(10)	64(3)
C27	7328(8)	5034(13)	6243(9)	61(3)
C26	6666(13)	4270(11)	6536(12)	38(2)
C30	7229(10)	2740(20)	5608(11)	96(5)
C36	7028(8)	2188(12)	5856(8)	73(3)
C37	6589(6)	2744(11)	6490(7)	51(2)
C33	7130(8)	4628(13)	6047(8)	60(3)
C35	7510(12)	2820(17)	5317(7)	89(4)
C34	7569(11)	4047(16)	5394(9)	97(5)
C32	6662(11)	3957(13)	6611(11)	40(2)

Table S.27. Anisotropic Displacement Parameters ($\times 10^4$) for **209**. The anisotropic displacement factor exponent takes the form: $-2\pi^2[h^2a^{*2}U_{11}+2hka^*b^*U_{12}+\dots]$.

Atom	U ₁₁	U ₂₂	U ₃₃	U ₂₃	U ₁₃	U ₁₂
Si1	32.2(3)	38.9(3)	38.0(3)	-6.0(2)	8.4(2)	5.8(2)
C9	26.8(8)	24.5(9)	43.3(10)	1.7(8)	5.8(7)	2.3(7)
C7	27.6(9)	24.5(9)	40.2(10)	3.0(7)	5.8(7)	1.7(7)
C10	29.7(9)	26.4(9)	48.4(11)	-4.2(8)	14.9(8)	-1.3(7)
C8	28.7(9)	22.3(8)	45.4(11)	3.3(8)	5.3(8)	-3.3(7)
C6	35.4(9)	22.8(9)	43.6(11)	1.2(8)	12.1(8)	1.0(7)
C1	40.2(10)	26.4(9)	42.6(11)	-1.3(8)	11.3(8)	2.0(8)

Atom	U ₁₁	U ₂₂	U ₃₃	U ₂₃	U ₁₃	U ₁₂
C15	31.4(9)	34.9(10)	48.0(11)	-10.2(9)	11.3(8)	-4.1(8)
C5	38.3(10)	37.1(11)	47.8(12)	2.9(9)	10.5(9)	-6.5(9)
C11	41.3(11)	26.2(10)	65.9(14)	-1.2(9)	17.1(10)	1.4(8)
C2	55.1(13)	41.1(12)	38.9(11)	-0.1(9)	9.1(9)	0.3(10)
N2	84.1(17)	26.5(10)	138(3)	-21.5(13)	38.7(17)	0.2(11)
C20	38.5(11)	53.7(13)	39.4(11)	-5.4(10)	6.6(8)	3.4(10)
N1	54.5(13)	99(2)	77.9(16)	21.8(14)	13.6(12)	-36.7(13)
C14	46.9(12)	51.9(14)	56.5(14)	-20.7(11)	13.1(10)	-11.7(10)
C4	47.1(12)	45.3(13)	56.2(14)	1.8(10)	19.0(10)	-12.2(10)
C12	52.5(13)	29.6(11)	84.7(18)	-11.6(11)	28.5(13)	-4.0(10)
C3	64.8(15)	44.9(13)	45.9(13)	4.3(10)	20.3(11)	-10.9(11)
C25	44.0(12)	71.0(17)	46.3(13)	-15.1(12)	10.7(10)	-1.6(11)
C13	56.8(14)	42.1(13)	86.1(19)	-32.9(13)	29.0(13)	-16.3(11)
C21	51.3(14)	80.4(19)	48.6(14)	2.5(13)	7.1(11)	18.6(13)
C24	63.8(16)	97(2)	42.0(13)	-13.6(14)	13.9(12)	-15.2(16)
C17	42.0(14)	83(2)	110(3)	-3.2(19)	20.3(16)	-12.7(14)
C22	62.2(17)	123(3)	54.8(16)	13.1(17)	-3.5(13)	23.9(18)
C16	75(2)	84(2)	105(3)	12.8(19)	45.3(19)	-29.8(17)
C23	68.2(19)	120(3)	46.5(15)	8.8(17)	-2.8(13)	-6.7(19)
C19	243(6)	36.0(17)	139(4)	-22(2)	72(4)	10(3)
C18	169(5)	45(2)	240(7)	8(3)	-45(5)	43(3)
C28	76(6)	144(10)	60(5)	14(6)	32(4)	41(6)
C29	78(6)	165(13)	55(5)	-21(7)	12(4)	65(7)
C31	67(4)	52(5)	74(7)	-15(5)	2(4)	24(4)
C27	45(5)	79(6)	60(6)	11(4)	23(4)	15(4)
C26	46(4)	37(5)	31(4)	5(4)	0(3)	25(4)
C30	95(8)	124(11)	69(9)	-52(8)	-2(5)	51(7)
C36	69(5)	86(6)	63(5)	-29(4)	-8(3)	45(4)
C37	47(3)	51(5)	55(5)	-15(3)	1(3)	23(3)
C33	50(5)	76(6)	55(5)	10(4)	20(4)	24(4)
C35	105(9)	128(8)	37(4)	-3(5)	17(4)	79(7)
C34	105(9)	123(8)	64(6)	28(6)	48(6)	70(7)
C32	35(3)	49(6)	37(4)	2(5)	4(3)	27(4)

Table S.28. Bond Lengths in Å for **209**.

Atom	Atom	Length/Å	Atom	Atom	Length/Å
Si1	C1	1.866(2)	C20	C21	1.392(3)
Si1	C15	1.855(2)	N1	C4	1.384(3)

Atom Atom Length/Å			Atom Atom Length/Å		
Si1	C20	1.866(2)	N1	C17	1.419(4)
Si1	C26	1.852(17)	N1	C16	1.426(4)
Si1	C32	1.901(16)	C14	C13	1.396(4)
C9	C7	1.406(3)	C4	C3	1.387(4)
C9	C10	1.486(3)	C12	C13	1.371(4)
C9	C8 ¹	1.389(3)	C25	C24	1.379(4)
C7	C8	1.385(3)	C21	C22	1.382(4)
C7	C6	1.492(3)	C24	C23	1.369(5)
C10	C15	1.395(3)	C22	C23	1.372(4)
C10	C11	1.398(3)	C28	C29	1.366(17)
C6	C1	1.404(3)	C28	C27	1.378(13)
C6	C5	1.392(3)	C29	C30	1.335(18)
C1	C2	1.392(3)	C31	C26	1.364(14)
C15	C14	1.400(3)	C31	C30	1.393(15)
C5	C4	1.401(3)	C27	C26	1.414(17)
C11	C12	1.382(3)	C36	C37	1.370(11)
C2	C3	1.379(3)	C36	C35	1.343(15)
N2	C12	1.412(3)	C37	C32	1.370(13)
N2	C19	1.431(5)	C33	C34	1.406(13)
N2	C18	1.435(6)	C33	C32	1.382(15)
C20	C25	1.396(3)	C35	C34	1.378(17)

Table S.29. Bond Angles in ° for **209**.

Atom Atom Atom Angle/°				Atom Atom Atom Angle/°			
C1	Si1	C20	109.41(10)	C21	C20	Si1	121.28(17)
C1	Si1	C32	108.2(6)	C21	C20	C25	116.9(2)
C15	Si1	C1	103.04(9)	C4	N1	C17	120.3(2)
C15	Si1	C20	112.40(10)	C4	N1	C16	119.9(3)
C15	Si1	C32	115.7(5)	C17	N1	C16	118.5(2)
C20	Si1	C32	107.9(6)	C13	C14	C15	121.3(3)
C26	Si1	C1	113.7(6)	N1	C4	C5	120.4(2)
C26	Si1	C15	104.5(4)	N1	C4	C3	122.2(2)
C26	Si1	C20	113.3(6)	C3	C4	C5	117.4(2)
C7	C9	C10	126.00(17)	C11	C12	N2	119.8(3)
C8 ¹	C9	C7	117.63(17)	C13	C12	C11	117.7(2)
C8 ¹	C9	C10	116.36(16)	C13	C12	N2	122.5(2)
C9	C7	C6	125.45(17)	C2	C3	C4	121.2(2)

Atom Atom Atom Angle/°				Atom Atom Atom Angle/°			
C8	C7	C9	117.62(17)	C24	C25	C20	121.4(2)
C8	C7	C6	116.94(16)	C12	C13	C14	121.6(2)
C15	C10	C9	121.71(17)	C22	C21	C20	121.5(2)
C15	C10	C11	121.14(19)	C23	C24	C25	120.4(2)
C11	C10	C9	116.94(19)	C23	C22	C21	120.1(3)
C7	C8	C91	124.75(17)	C24	C23	C22	119.7(3)
C1	C6	C7	121.47(17)	C29	C28	C27	119.4(11)
C5	C6	C7	117.40(18)	C30	C29	C28	122.0(10)
C5	C6	C1	120.84(18)	C26	C31	C30	123.1(12)
C6	C1	Si1	119.29(14)	C28	C27	C26	120.7(11)
C2	C1	Si1	123.71(17)	C31	C26	Si1	123.4(11)
C2	C1	C6	116.89(19)	C31	C26	C27	116.1(13)
C10	C15	Si1	119.42(14)	C27	C26	Si1	120.0(10)
C10	C15	C14	116.6(2)	C29	C30	C31	118.3(12)
C14	C15	Si1	123.85(19)	C35	C36	C37	121.0(9)
C6	C5	C4	121.4(2)	C36	C37	C32	120.6(10)
C12	C11	C10	121.6(2)	C32	C33	C34	119.4(10)
C3	C2	C1	122.3(2)	C36	C35	C34	120.2(8)
C12	N2	C19	116.1(3)	C35	C34	C33	119.4(10)
C12	N2	C18	118.8(3)	C37	C32	Si1	121.4(9)
C19	N2	C18	115.4(4)	C37	C32	C33	119.2(12)
C25	C20	Si1	121.79(18)	C33	C32	Si1	118.3(8)

Table S.30. Hydrogen Fractional Atomic Coordinates ($\times 10^4$) and Equivalent Isotropic Displacement Parameters ($\text{\AA}^2 \times 10^3$) for **209**. U_{eq} is defined as 1/3 of the trace of the orthogonalised U_{ij} .

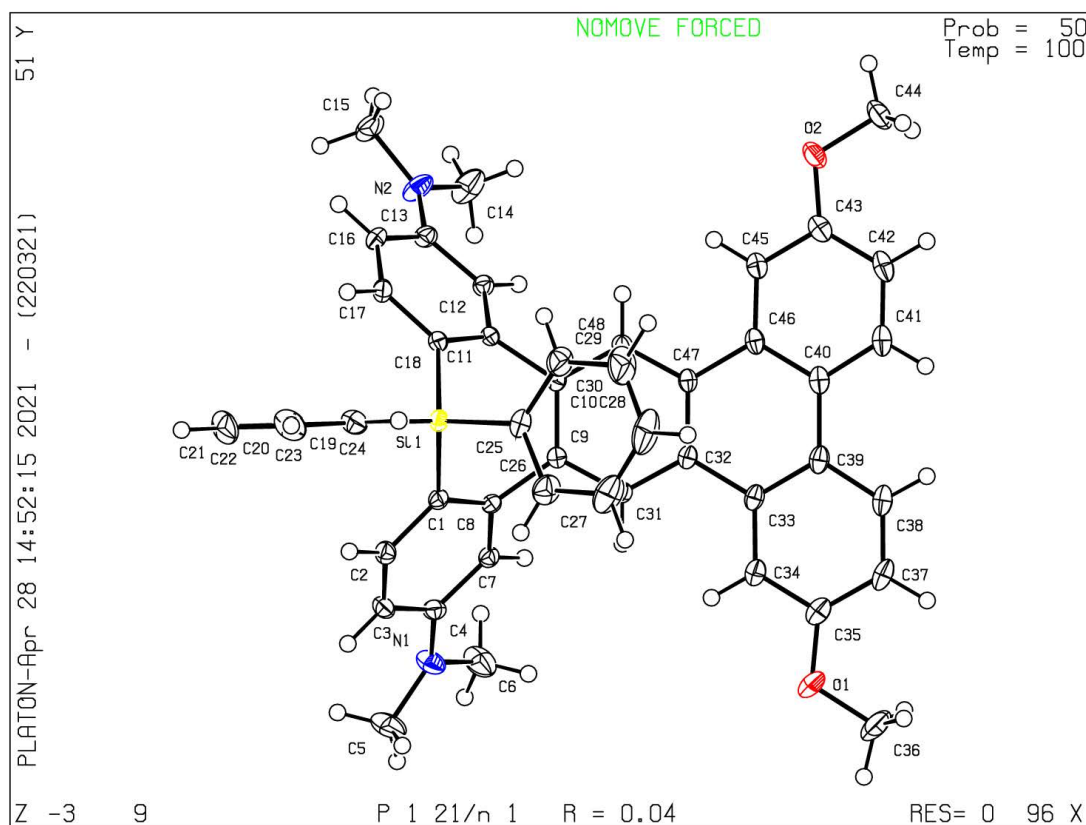
Atom	x	y	z	U(eq)
H8	4313.06	3188.15	5150.62	38
H5	3129.74	3855.61	6062.21	49
H11	4704.64	8020.91	5704.36	53
H2	4817.11	3423.73	8550.89	54
H14	6256.38	7161.12	8215.65	62
H3	3412.28	2690.15	8485.66	62
H25	5550.85	5473.42	9142.14	64
H13	5834.22	9115.89	7901.6	73
H21	7509.86	3593.41	8130	72

Atom	x	y	z	U(eq)
H24	6150.46	5124.67	10489.86	81
H17A	1625.1	4056.1	6684.26	117
H17B	1086.17	2829.3	6707.43	117
H17C	1834.93	3001.27	6033.16	117
H22	8114.65	3281.31	9483.41	96
H16A	2417.79	1286.95	7953.9	131
H16B	1427.69	1566.16	7666.6	131
H16C	1910.51	2376.38	8377.04	131
H23	7422.47	4017.69	10666.2	94
H19A	4633.77	10486.99	7745.85	207
H19B	4730.7	11558.2	7079.57	207
H19C	5581.78	10899.36	7465.95	207
H18A	4402.09	9847.58	5419.23	228
H18B	4069.44	10968.56	5953.65	228
H18C	3717.44	9651.56	6152.45	228
H28	8289.26	5198.5	5393.46	111
H29	8192.23	3262.29	4888.66	119
H31	6263.82	2569.13	6448.24	77
H27	7397.86	5811.46	6480.74	73
H30	7199.21	1942.19	5396.39	116
H36	6990.92	1342.19	5796.84	88
H37	6231.92	2285.18	6849.09	61
H33	7156.14	5475.24	6100.61	72
H35	7810.23	2419.88	4881.45	107
H34	7903.79	4496.73	5008.72	116

S.6 X-ray Structure of Compound 219

A single crystal of 3,17-dimethoxy- N^7, N^7, N^{13}, N^{13} -tetramethyl-10,10-diphenyl-10*H*-dibenzo[*b,f*] triphenyleno[2,3-*d*]silepin-7,13-diamine (C₄₈H₄₂N₂O₂Si) (**219**) was prepared by recrystallization from the dichloromethane/ethanol solution. A suitable crystal was selected, and the X-ray diffraction was collected on an Rigaku AFC HyPix-6000 diffractometer: fixed-chi single diffractometer with graphite monochromated Mo K α radiation ($\lambda = 0.71073\text{\AA}$). The crystal was kept at 100 K during data collection. The data were collected using ω scan in the θ range of $4.038 \leq \theta \leq 54.968$ deg. The data were corrected for Lorentz and polarization effects. The structures were solved by direct methods,^[115] and expanded using Fourier techniques.^[116] Hydrogen atoms were refined using the riding model. The final cycle of full-matrix least-squares refinement on F^2 was based on 44667 observed reflections. Neutral atom scattering factors were taken from Cromer and Waber.^[117] All calculations were performed using the Olex-2 crystallographic software package except for refinement,^[118] which was performed

using version 2018/3 of ShelXL (Sheldrick, 2015) of final refinement as well as the bond lengths and angles are summarized in the supporting information, and the numbering scheme employed is also shown in the supporting information, which were drawn with ORTEP at 50% probability ellipsoid.



Crystal structure determination of 219

$C_{48}H_{42}N_2O_2Si$ ($M = 706.92$ g/mol): monoclinic, space group $P2_1/n$ (no. 14), $a = 9.1920(3)$ Å, $b = 20.3292(6)$ Å, $c = 20.1781(5)$ Å, $\beta = 90.337(2)$, $V = 3770.54(19)$ Å³, $Z = 4$, $T = 100$ K, $\mu(\text{Mo K}\alpha) = 0.105$ mm⁻¹, $D_{\text{calc}} = 1.245$ g/cm³, 44667 reflections measured ($4.038^\circ \leq 2\theta \leq 54.968^\circ$), 8637 unique ($R_{\text{int}} = 0.0329$, $R_{\text{sigma}} = 0.0259$) which were used in all calculations. The final R_1 was 0.0389 ($I > 2\sigma(I)$) and wR_2 was 0.1042 (all data).

Table S.31. Crystal data and structure refinement for 219.

Empirical formula	$C_{48}H_{42}N_2O_2Si$
Formula weight	706.92
Temperature/K	100
Crystal system	monoclinic
Space group	$P2_1/n$
$a/\text{Å}$	9.1920(3)
$b/\text{Å}$	20.3292(6)
$c/\text{Å}$	20.1781(5)

$\alpha/^\circ$	90
$\beta/^\circ$	90.337(2)
$\gamma/^\circ$	90
Volume/ \AA^3	3770.54(19)
Z	4
D _{calc} g/cm ³	1.245
μ/mm^{-1}	0.105
F(000)	1496.0
Crystal size/mm ³	0.305 × 0.19 × 0.109
Radiation	Mo K α ($\lambda = 0.71073$)
2 θ range for data collection/ $^\circ$	4.038 to 54.968
Index ranges	-11 ≤ h ≤ 11, -26 ≤ k ≤ 23, -26 ≤ l ≤ 25
Reflections collected	44667
Independent reflections	8637 [$R_{\text{int}} = 0.0329$, $R_{\text{sigma}} = 0.0259$]
Data/restraints/parameters	8637/0/484
Goodness-of-fit on F ²	1.051
Final R indexes [$I \geq 2\sigma(I)$]	$R_1 = 0.0389$, $wR_2 = 0.0998$
Final R indexes [all data]	$R_1 = 0.0470$, $wR_2 = 0.1042$
Largest diff. peak/hole / e \AA^{-3}	0.36/-0.35

Table S.32. Fractional Atomic Coordinates ($\times 10^4$) and Equivalent Isotropic Displacement Parameters ($\text{\AA}^2 \times 10^3$) for **219**. U_{eq} is defined as 1/3 of the trace of the orthogonalised U_{ij} tensor.

Atom	x	y	z	$U(\text{eq})$
Si1	3302.1(3)	6608.3(2)	4351.2(2)	13.65(8)
O1	6425.3(12)	9918.6(5)	2082.7(5)	32.3(2)
O2	7101.2(11)	9552.2(5)	6931.9(5)	25.3(2)
N1	-473.9(13)	7942.2(6)	2263.8(6)	25.2(3)
N2	-399.6(14)	7621.3(6)	6615.2(6)	27.4(3)
C1	2249.2(13)	7004.4(6)	3668.2(6)	14.8(2)
C2	1543.4(13)	6655.6(6)	3162.4(6)	17.5(2)
C3	683.3(14)	6959.4(6)	2689.5(6)	19.6(3)
C4	436.8(13)	7641.2(6)	2714.9(6)	17.5(2)
C5	-829.5(19)	7594.0(8)	1663.2(7)	35.5(4)
C6	-793.8(19)	8630.9(8)	2317.0(8)	35.9(4)
C7	1158.8(13)	8002.0(6)	3214.1(6)	15.8(2)
C8	2063.6(12)	7692.9(6)	3673.2(6)	14.0(2)
C9	2979.3(12)	8112.7(6)	4114.1(6)	13.8(2)
C10	3027.3(12)	8072.8(6)	4813.2(6)	13.5(2)

Atom	<i>x</i>	<i>y</i>	<i>z</i>	U(eq)
C11	2159.8(12)	7590.3(6)	5206.6(6)	14.0(2)
C12	1252.8(13)	7822.7(6)	5701.4(6)	15.8(2)
C13	539.3(13)	7390.2(6)	6137.8(6)	18.1(2)
C14	-675(2)	8307.8(8)	6677.6(9)	37.8(4)
C15	-823.8(17)	7190.6(7)	7148.5(7)	30.0(3)
C16	817.7(14)	6714.6(6)	6071.3(6)	18.8(3)
C17	1691.4(13)	6487.8(6)	5563.1(6)	17.2(2)
C18	2370.9(13)	6908.6(6)	5111.3(6)	14.7(2)
C19	3090.3(14)	5695.3(6)	4282.6(6)	17.6(2)
C20	1695.0(15)	5416.4(7)	4266.8(7)	24.4(3)
C21	1497.6(18)	4743.8(7)	4200.6(8)	32.3(3)
C22	2689.6(19)	4333.3(7)	4150.8(8)	34.8(4)
C23	4077.7(18)	4594.3(7)	4169.8(7)	31.2(3)
C24	4274.4(15)	5271.0(7)	4235.9(6)	21.8(3)
C25	5250.8(13)	6862.2(6)	4312.3(6)	18.4(2)
C26	5926.8(16)	6942.4(8)	3698.1(8)	29.0(3)
C27	7349.7(17)	7156.2(9)	3649.4(9)	39.6(4)
C28	8137.8(17)	7291.0(9)	4219.2(10)	43.6(4)
C29	7493.2(18)	7224.1(9)	4832.9(10)	42.8(4)
C30	6059.4(15)	7013.6(8)	4877.4(8)	29.0(3)
C31	3899.1(13)	8555.3(6)	3804.3(6)	15.1(2)
C32	4911.4(13)	8945.4(6)	4143.2(6)	15.2(2)
C33	5889.1(13)	9387.8(6)	3784.3(6)	17.1(2)
C34	5786.2(14)	9459.1(6)	3096.4(7)	20.8(3)
C35	6644.0(15)	9899.2(7)	2754.5(7)	24.0(3)
C36	7149(2)	10423.0(10)	1724.4(8)	43.1(4)
C37	7646.1(15)	10283.4(7)	3102.2(7)	27.6(3)
C38	7777.6(15)	10207.5(7)	3780.2(7)	24.8(3)
C39	6919.6(13)	9763.8(6)	4142.1(7)	19.0(3)
C40	7028.5(13)	9700.1(6)	4863.3(6)	18.2(2)
C41	8067.3(14)	10049.9(6)	5235.4(7)	22.2(3)
C42	8144.5(14)	10013.9(6)	5918.1(7)	23.1(3)
C43	7152.4(14)	9620.0(6)	6255.1(7)	20.8(3)
C44	8008.1(17)	9972.6(7)	7317.5(8)	30.7(3)
C45	6131.1(14)	9260.3(6)	5904.1(6)	19.3(3)
C46	6048.8(13)	9289.5(6)	5210.5(6)	16.7(2)
C47	4967.2(13)	8905.7(6)	4838.8(6)	15.0(2)
C48	3987.9(13)	8479.4(6)	5154.8(6)	15.0(2)

Table S.33. Anisotropic Displacement Parameters ($\times 10^4$) for **219**. The anisotropic displacement factor exponent takes the form: $-2\pi^2[h^2a^2U_{11}+2hka^2b^2U_{12}+\dots]$.

Atom	U ₁₁	U ₂₂	U ₃₃	U ₂₃	U ₁₃	U ₁₂
Si1	12.79(16)	12.87(16)	15.30(16)	-0.46(12)	1.57(11)	-1.09(11)
O1	36.0(6)	35.9(6)	25.2(5)	10.4(4)	6.7(4)	-11.5(5)
O2	29.7(5)	21.9(5)	24.3(5)	-2.8(4)	-10.2(4)	-5.1(4)
N1	29.0(6)	25.9(6)	20.5(5)	-2.5(5)	-9.1(5)	3.9(5)
N2	34.9(7)	22.7(6)	24.9(6)	4.3(5)	16.8(5)	4.7(5)
C1	13.6(6)	16.2(6)	14.6(5)	-0.6(4)	3.0(4)	-1.4(4)
C2	18.1(6)	15.7(6)	18.8(6)	-2.8(5)	3.2(5)	-1.1(5)
C3	20.1(6)	22.2(6)	16.6(6)	-4.8(5)	-0.4(5)	-3.8(5)
C4	15.2(6)	23.4(6)	14.0(5)	0.5(5)	0.3(4)	-0.8(5)
C5	42.7(9)	39.9(9)	23.8(7)	-2.8(6)	-16.2(6)	5.9(7)
C6	45.1(9)	26.7(8)	35.6(8)	1.5(6)	-21.2(7)	5.1(7)
C7	16.2(6)	15.7(6)	15.4(5)	-0.3(4)	2.6(4)	-1.1(4)
C8	13.1(5)	16.8(6)	12.3(5)	-0.6(4)	3.2(4)	-2.1(4)
C9	12.7(5)	13.2(5)	15.5(5)	-1.0(4)	0.7(4)	0.4(4)
C10	13.2(5)	11.9(5)	15.4(5)	0.2(4)	1.7(4)	0.3(4)
C11	12.7(5)	16.6(6)	12.8(5)	0.6(4)	-1.7(4)	-2.9(4)
C12	17.0(6)	14.6(6)	15.8(6)	0.1(4)	0.7(4)	0.0(4)
C13	16.7(6)	21.5(6)	16.2(6)	-0.1(5)	3.1(4)	-0.7(5)
C14	47.8(10)	24.5(8)	41.5(9)	-0.1(7)	27.8(8)	5.3(7)
C15	37.0(8)	28.1(7)	25.2(7)	0.9(6)	16.9(6)	-3.3(6)
C16	20.1(6)	18.9(6)	17.4(6)	3.0(5)	3.9(5)	-4.4(5)
C17	17.3(6)	14.9(6)	19.6(6)	0.1(5)	0.8(5)	-3.0(4)
C18	13.3(5)	16.2(6)	14.5(5)	-0.3(4)	-1.0(4)	-1.7(4)
C19	21.6(6)	15.7(6)	15.5(6)	-0.6(5)	0.8(5)	-0.9(5)
C20	24.7(7)	19.3(6)	29.2(7)	-1.4(5)	1.2(5)	-3.6(5)
C21	36.0(8)	21.8(7)	39.0(8)	0.5(6)	-5.9(6)	-10.4(6)
C22	51.2(10)	14.2(7)	38.8(8)	-1.5(6)	-13.0(7)	-2.9(6)
C23	40.5(9)	20.1(7)	33.0(8)	-4.7(6)	-10.0(6)	9.6(6)
C24	25.9(7)	20.0(6)	19.5(6)	-1.6(5)	-3.0(5)	2.3(5)
C25	14.2(6)	14.3(6)	26.8(7)	2.5(5)	3.0(5)	1.5(4)
C26	22.7(7)	32.4(8)	31.9(8)	-1.6(6)	8.9(6)	-0.9(6)
C27	24.8(8)	42.1(9)	52.1(10)	5.6(8)	17.9(7)	-1.5(7)
C28	15.2(7)	41.3(10)	74.4(13)	13.9(9)	6.2(7)	-5.0(6)
C29	23.5(8)	48.8(10)	56.0(11)	11.6(8)	-14.6(7)	-11.0(7)
C30	20.4(7)	34.4(8)	32.0(8)	8.2(6)	-4.3(5)	-4.5(6)

Atom	U ₁₁	U ₂₂	U ₃₃	U ₂₃	U ₁₃	U ₁₂
C31	15.6(6)	14.3(6)	15.3(5)	-0.2(4)	2.3(4)	0.2(4)
C32	13.4(6)	12.4(5)	19.8(6)	0.5(5)	2.4(4)	0.4(4)
C33	14.2(6)	13.4(6)	23.9(6)	1.0(5)	4.0(5)	0.3(4)
C34	18.7(6)	18.6(6)	25.1(6)	1.3(5)	3.3(5)	-3.3(5)
C35	23.0(7)	22.7(7)	26.4(7)	4.9(5)	6.5(5)	-0.5(5)
C36	43.2(10)	51.3(11)	34.8(9)	20.1(8)	5.9(7)	-17.1(8)
C37	23.0(7)	24.5(7)	35.3(8)	6.4(6)	8.3(6)	-7.6(5)
C38	18.5(6)	21.3(7)	34.7(7)	1.5(6)	2.2(5)	-6.4(5)
C39	14.0(6)	15.1(6)	28.0(7)	0.2(5)	3.3(5)	-0.5(4)
C40	13.7(6)	13.8(6)	27.2(6)	-1.3(5)	-0.5(5)	0.5(4)
C41	15.4(6)	16.5(6)	34.6(7)	-1.2(5)	-0.6(5)	-2.5(5)
C42	17.7(6)	17.2(6)	34.3(7)	-4.2(5)	-8.1(5)	-0.8(5)
C43	20.5(6)	16.6(6)	25.3(6)	-2.6(5)	-6.3(5)	2.7(5)
C44	36.3(8)	25.1(7)	30.5(7)	-4.2(6)	-14.0(6)	-7.1(6)
C45	18.1(6)	15.7(6)	24.1(6)	-0.8(5)	-2.9(5)	-1.3(5)
C46	13.9(6)	12.2(6)	24.1(6)	-1.7(5)	-1.8(5)	0.8(4)
C47	13.5(5)	11.9(6)	19.5(6)	-0.7(4)	-0.4(4)	-0.2(4)
C48	16.2(6)	13.8(6)	15.0(5)	-0.7(4)	-0.3(4)	0

Table S.34. Bond Lengths in Å for **219**.

Atom	Atom	Length/Å	Atom	Atom	Length/Å
Si1	C1	1.8625(12)	C19	C20	1.4024(18)
Si1	C18	1.8637(12)	C19	C24	1.3924(18)
Si1	C19	1.8711(13)	C20	C21	1.386(2)
Si1	C25	1.8662(13)	C21	C22	1.381(2)
O1	C35	1.3698(17)	C22	C23	1.382(2)
O1	C36	1.4222(17)	C23	C24	1.394(2)
O2	C43	1.3736(16)	C25	C26	1.3992(19)
O2	C44	1.4224(16)	C25	C30	1.3918(19)
N1	C4	1.3764(16)	C26	C27	1.382(2)
N1	C5	1.4394(18)	C27	C28	1.383(3)
N1	C6	1.4349(19)	C28	C29	1.383(3)
N2	C13	1.3797(16)	C29	C30	1.389(2)
N2	C14	1.4241(19)	C31	C32	1.3983(17)
N2	C15	1.4428(17)	C32	C33	1.4659(16)
C1	C2	1.3990(17)	C32	C47	1.4064(17)
C1	C8	1.4100(17)	C33	C34	1.3982(18)
C2	C3	1.3813(18)	C33	C39	1.4124(18)

Atom Atom Length/Å			Atom Atom Length/Å		
C3	C4	1.4056(18)	C34	C35	1.3801(18)
C4	C7	1.4090(17)	C35	C37	1.394(2)
C7	C8	1.3913(17)	C37	C38	1.381(2)
C8	C9	1.4900(16)	C38	C39	1.4054(18)
C9	C10	1.4133(16)	C39	C40	1.4639(18)
C9	C31	1.3861(16)	C40	C41	1.4045(18)
C10	C11	1.4952(16)	C40	C46	1.4164(17)
C10	C48	1.3895(16)	C41	C42	1.381(2)
C11	C12	1.3874(17)	C42	C43	1.394(2)
C11	C18	1.4126(17)	C43	C45	1.3821(17)
C12	C13	1.4092(17)	C45	C46	1.4023(18)
C13	C16	1.4036(18)	C46	C47	1.4667(16)
C16	C17	1.3852(17)	C47	C48	1.4053(16)
C17	C18	1.3999(17)			

Table S.35. Bond Angles in ° for **219**.

Atom Atom Atom Angle/°				Atom Atom Atom Angle/°			
C1	Si1	C18	103.19(5)	C24	C19	C20	117.59(12)
C1	Si1	C19	108.71(6)	C21	C20	C19	121.35(13)
C1	Si1	C25	110.12(6)	C22	C21	C20	119.98(14)
C18	Si1	C19	109.74(5)	C21	C22	C23	119.91(14)
C18	Si1	C25	112.93(6)	C22	C23	C24	120.04(14)
C25	Si1	C19	111.76(6)	C19	C24	C23	121.13(13)
C35	O1	C36	117.22(12)	C26	C25	Si1	120.06(11)
C43	O2	C44	117.39(11)	C30	C25	Si1	122.33(10)
C4	N1	C5	118.20(12)	C30	C25	C26	117.52(13)
C4	N1	C6	120.56(11)	C27	C26	C25	121.67(15)
C6	N1	C5	119.81(12)	C26	C27	C28	119.64(15)
C13	N2	C14	120.53(11)	C29	C28	C27	120.00(14)
C13	N2	C15	119.14(12)	C28	C29	C30	119.99(16)
C14	N2	C15	118.67(12)	C29	C30	C25	121.17(15)
C2	C1	Si1	123.87(9)	C9	C31	C32	123.61(11)
C2	C1	C8	116.91(11)	C31	C32	C33	120.97(11)
C8	C1	Si1	119.10(9)	C31	C32	C47	118.41(11)
C3	C2	C1	122.58(12)	C47	C32	C33	120.63(11)
C2	C3	C4	120.49(11)	C34	C33	C32	121.06(11)
N1	C4	C3	120.78(11)	C34	C33	C39	119.51(11)
N1	C4	C7	121.56(12)	C39	C33	C32	119.39(11)

Atom	Atom	Atom	Angle/°	Atom	Atom	Atom	Angle/°
C3	C4	C7	117.65(11)	C35	C34	C33	121.86(12)
C8	C7	C4	121.20(11)	O1	C35	C34	115.62(12)
C1	C8	C9	120.32(10)	O1	C35	C37	125.08(12)
C7	C8	C1	121.04(11)	C34	C35	C37	119.31(13)
C7	C8	C9	118.18(11)	C38	C37	C35	119.31(12)
C10	C9	C8	125.27(10)	C37	C38	C39	122.69(13)
C31	C9	C8	116.51(10)	C33	C39	C40	120.13(11)
C31	C9	C10	118.15(11)	C38	C39	C33	117.29(12)
C9	C10	C11	123.63(10)	C38	C39	C40	122.55(12)
C48	C10	C9	118.49(11)	C41	C40	C39	121.93(12)
C48	C10	C11	117.79(10)	C41	C40	C46	117.79(12)
C12	C11	C10	118.90(11)	C46	C40	C39	120.26(11)
C12	C11	C18	121.04(11)	C42	C41	C40	122.50(12)
C18	C11	C10	119.81(10)	C41	C42	C43	119.16(12)
C11	C12	C13	121.40(11)	O2	C43	C42	124.69(12)
N2	C13	C12	121.27(12)	O2	C43	C45	115.42(12)
N2	C13	C16	121.01(11)	C45	C43	C42	119.89(12)
C16	C13	C12	117.72(11)	C43	C45	C46	121.44(12)
C17	C16	C13	120.21(11)	C40	C46	C47	119.44(11)
C16	C17	C18	122.79(12)	C45	C46	C40	119.20(11)
C11	C18	Si1	119.84(9)	C45	C46	C47	121.35(11)
C17	C18	Si1	122.99(9)	C32	C47	C46	120.03(11)
C17	C18	C11	116.66(11)	C48	C47	C32	117.94(11)
C20	C19	Si1	119.83(10)	C48	C47	C46	122.01(11)
C24	C19	Si1	122.57(10)	C10	C48	C47	123.27(11)

Table S.36. Hydrogen Fractional Atomic Coordinates ($\times 10^4$) and Equivalent Isotropic Displacement Parameters ($\text{\AA}^2 \times 10^3$) for **219**. U_{eq} is defined as 1/3 of the trace of the orthogonalised U_{ij} .

Atom	x	y	z	U(eq)
H2	1660.25	6191.7	3143.48	21
H3	255.24	6705.51	2344.53	24
H5A	66.87	7438.92	1454.12	53
H5B	-1346.62	7889.46	1358.8	53
H5C	-1450.88	7216.76	1767.7	53
H6A	-1096.61	8731.71	2770.65	54
H6B	-1580.09	8744.67	2007.56	54
H6C	76.79	8886.76	2209.09	54

Atom	x	y	z	U(eq)
H7	1025.36	8464.83	3237.67	19
H12	1109.78	8283.29	5746.92	19
H14A	201.37	8528.97	6843.32	57
H14B	-1475.15	8377.66	6988.87	57
H14C	-942.36	8489.11	6243.64	57
H15A	-1387.88	6821.66	6968.83	45
H15B	-1419.43	7435.16	7465.49	45
H15C	47.77	7022.25	7373.27	45
H16	405.64	6411.84	6375.83	23
H17	1835.47	6027.17	5519.21	21
H20	868.21	5694.37	4302.1	29
H21	542.84	4565.09	4189.55	39
H22	2555.35	3872.32	4103.53	42
H23	4898.33	4312.2	4137.69	37
H24	5232.62	5445.76	4249.42	26
H26	5394.5	6847.41	3304.64	35
H27	7783.75	7210.34	3226.77	48
H28	9122.26	7429.53	4188.99	52
H29	8030.73	7322.2	5224.15	51
H30	5622.98	6972.24	5300.94	35
H31	3838.31	8595.77	3335.93	18
H34	5106.68	9197.06	2857.58	25
H36A	6877.59	10395.76	1254.85	65
H36B	8203.89	10367.56	1771.42	65
H36C	6865.13	10853.41	1900.1	65
H37	8232.58	10594.21	2875.29	33
H38	8476.57	10465.72	4011.4	30
H41	8742.45	10321.51	5008.81	27
H42	8864.68	10254.63	6155.03	28
H44A	7795.25	10432.27	7207.35	46
H44B	9030.69	9877.71	7221.44	46
H44C	7823.29	9897.46	7789.26	46
H45	5470.38	8987.26	6137.72	23
H48	3982.3	8468.65	5625.51	18

References

- [1] (a) Denmark, S. E.; Neuville, L. *Org. Lett.*, **2000**, *2*, 3221–3224; (b) Denmark, S. E.; Wehrli, D. *Org. Lett.*, **2000**, *2*, 565–568.
- [2] (a) Murata, M.; Ishikura, M.; Nagata, M.; Watanabe, S.; Masuda, Y. *Org. Lett.*, **2002**, *4*, 1843–1845; (b) Manoso, A. S.; DeShong, P. *J. Org. Chem.*, **2001**, *66*, 7449–7455; (c) Denmark, S. E.; Smith, R. C.; Chang, W. -T. T.; Muhuhi, J. M. *J. Am. Chem. Soc.*, **2009**, *131*, 3104–3118; (d) Denmark, S. E.; Kallemeyn, J. M. *J. Am. Chem. Soc.*, **2006**, *128*, 15958–15959.
- [3] Gustavson, W. A.; Epstein, P. S.; Curtis, M. D. *Organometallics*, **1982**, *1*, 884–885.
- [4] Cheng, C.; Hartwig, J. F. *Chem. Rev.*, **2015**, *115*, 8946–8975.
- [5] (a) Ureshino, T.; Yoshida, T.; Kuninobu, Y.; Takai, K. *J. Am. Chem. Soc.*, **2010**, *132*, 14324–14326; (b) Kuninobu, Y.; Yamauchi, K.; Tanura, N.; Seiki, T.; Takai, K. *Angew. Chem. Int. Ed.*, **2013**, *52*, 1520–1522.
- [6] (a) Zhang, Q. W.; An, K.; Liu, L. C.; Guo, S. X.; Jiang, C. R.; Guo, H. F.; He, W. *Angew. Chem. Int. Ed.*, **2016**, *55*, 6319–6323; (b) Zhang, Q. W.; An, K.; Liu, L. C.; Zhang, Q.; Guo, H. F.; He, W. *Angew. Chem. Int. Ed.*, **2017**, *56*, 1125–1129.
- [7] (a) Simmons, E. M.; Hartwig, J. F. *J. Am. Chem. Soc.*, **2010**, *132*, 17092–17095; (b) Zhao, W. T.; Lu, Z. Q.; Zheng, H. L.; Xue, X. S.; Zhao, D. B. *ACS Catal.*, **2018**, *8*, 7997–8005.
- [8] Li, Q.; Driess, M.; Hartwig, J. F. *Angew. Chem. Int. Ed.*, **2014**, *53*, 8471–8474.
- [9] Lin, Y.; Jiang, K. Z.; Cao, J.; Zheng, Z. J.; Xu, Z.; Cui, Y. M.; Xu, L. W. *Adv. Synth. Catal.*, **2017**, *359*, 2247–2252.
- [10] Murai, M.; Takeuchi, Y.; Takai, K. *Chem. Lett.*, **2017**, *46*, 1044–1047.
- [11] (a) Williams, N. A.; Uchimarui, Y.; Tanaka, M. *J. Chem. Soc. Chem. Commun.*, **1995**, 1129–1130. (b) Choi, G.; Tsurugi, H.; Mashima, K. *J. Am. Chem. Soc.*, **2013**, *135*, 13149–13161.
- [12] (a) Kakiuchi, F.; Matsumoto, M.; Sonoda, M.; Fukuyama, T.; Chatani, N.; Murai, S.; Furukawa, N.; Seki, Y. *Chem. Lett.*, **2000**, *29*, 750–751. (b) Li, W. G.; Chen, W. Q.; Zhou, B.; Xu, Y. K.; Deng, G. B.; Liang, Y.; Yang, Y. *Org. Lett.*, **2019**, *21*, 2718–2722.
- [13] Kakiuchi, F.; Matsumoto, M.; Tsuchiya, K.; Igi, K.; Hayamizu, T.; Chatani, N.; Murai, S. *J. Organomet. Chem.*, **2003**, *686*, 134–144.
- [14] Wang, H.; Wang, G. H.; Li, P. F. *Org. Chem. Front.*, **2017**, *4*, 1943–1946.
- [15] Oyamada, J.; Nishiura, M.; Hou, Z. M. *Angew. Chem. Int. Ed.*, **2011**, *50*, 10720–10723.
- [16] Ihara, H.; Suginome, M. *J. Am. Chem. Soc.*, **2009**, *131*, 7502–7503.
- [17] Liu, S.; Zhang, S. L.; Lin, Q.; Huang, Y. Q.; Li, B. *Org. Lett.*, **2019**, *21*, 1134–1138.
- [18] Modak, A.; Patra, T.; Chowdhury, R. Raul, S.; Maiti, D. *Organometallics*, **2017**, *36*, 2418–2423.
- [19] Maji, A.; Guin, S.; Feng, S.; Dahiya, A.; Singh, V. K.; Liu, P.; Maiti, D. *Angew. Chem. Int. Ed.*, **2017**, *56*, 14903–14907.
- [20] Cheng, C.; Hartwig, J. F. *Science*, **2014**, *343*, 853–857.
- [21] (a) Cheng, C.; Hartwig, J. F. *J. Am. Chem. Soc.*, **2015**, *137*, 592–595; (b) Karmel, C.; Chen, Z. W.; Hartwig, J. F. *J. Am. Chem. Soc.*, **2019**, *141*, 7063–7072.

- [22] (a) Ihara, H.; Ueda, A.; Suginome, M. *Chem. Lett.*, **2011**, *40*, 916–918; (b) Fang, H. Q.; Hou, W. J.; Liu, G. X.; Huang, Z. *J. Am. Chem. Soc.*, **2017**, *139*, 11601–11609; (c) Luo, Y.; Teng, H. L.; Xue, C.; Nishiura, M.; Hou, Z. M. *ACS Catal.*, **2018**, *8*, 8027–8032.
- [23] Cacace, F.; Crestoni, M. E.; Fornarini, S. *J. Am. Chem. Soc.*, **1992**, *114*, 6776–6784.
- [24] Sollott, G. P.; Peterson, W. R. *J. Am. Chem. Soc.*, **1967**, *89*, 5054–5056.
- [25] Olah, G. A.; Bach, T.; Prakash, G. K. S. *New J. Chem.*, **1991**, *15*, 571–574.
- [26] Frick, U.; Simchen, G. *Synthesis*, **1984**, 929–930.
- [27] (a) Furukawa, S.; Kobayashi, J.; Kawashima, T. *J. Am. Chem. Soc.*, **2009**, *131*, 14192–14193; (b) Furukawa, S.; Kobayashi, J.; Kawashima, T. *Dalton Trans.*, **2010**, *39*, 9329–9336.
- [28] Massey, A. G.; Park, A. J. *J. Organomet. Chem.*, **1966**, *5*, 218–225.
- [29] Parks, D. J.; Piers, W. E. *J. Am. Chem. Soc.*, **1996**, *118*, 9440–9441.
- [30] Curless, L. D.; Ingleson, M. J. *Organometallics*, **2014**, *33*, 7241–7246.
- [31] Curless, L. D.; Clark, E. R.; Dunsford, J. J.; Ingleson, M. J. *Chem. Commun.*, **2014**, *50*, 5270–5272.
- [32] Han, Y. X.; Zhang, S. T.; He, J. G.; Zhang, Y. T. *J. Am. Chem. Soc.*, **2017**, *139*, 7399–7407.
- [33] Han, Y. X.; Zhang, S. T.; He, J. H.; Zhang, Y. T. *ACS Catal.*, **2018**, *8*, 8765–8773.
- [34] Ma, Y. H.; Wang, B. L.; Zhang, L.; Hou, Z. M. *J. Am. Chem. Soc.*, **2016**, *138*, 3663–3666.
- [35] Hesp, K. D.; McDonald, R.; Ferguson, M. J.; Stradiotto, M. *J. Am. Chem. Soc.*, **2008**, *130*, 16394–16406.
- [36] (a) Klare, H. F. T.; Oestreich, M.; Ito, J.; Nishiyama, H.; Ohki, Y.; Tatsumi, K. *J. Am. Chem. Soc.*, **2011**, *133*, 3312–3315; (b) Königs, C. D. F.; Müller, M. F.; Aiguabella, N.; Klare, H. F. T.; Oestreich, M. *Chem. Commun.*, **2013**, *49*, 1506–1508.
- [37] Omann, L.; Oestreich, M. *Angew. Chem. Int. Ed.*, **2015**, *54*, 10276–10279.
- [38] Wübbolt, S.; Oestreich, M. *Angew. Chem. Int. Ed.*, **2015**, *54*, 15876–15879.
- [39] Yin, Q.; Klare, H. F. T.; Oestreich, M. *Angew. Chem. Int. Ed.*, **2016**, *55*, 3204–3207.
- [40] Yonekura, K.; Iketani, Y.; Sekine, M.; Tani, T.; Matsui, F.; Kamakura, D.; Tsuchimoto, T. *Organometallics*, **2017**, *36*, 3234–3249.
- [41] Chen, Q. A.; Klare, H. F. T.; Oestreich, M. *J. Am. Chem. Soc.*, **2016**, *138*, 7868–7871.
- [42] Nakatsuka, S.; Gotoh, H.; Kinoshita, K.; Yasuda, N.; Hatakeyama, T. *Angew. Chem. Int. Ed.*, **2017**, *56*, 5087–5090.
- [43] Kato, K.; Kim, J. O.; Yorimitsu, H.; Kim, D.; Osuka, A. *Chem. Asian J.*, **2016**, *11*, 1738–1746.
- [44] Wang, W. B.; Shao, X. F. *Org. Biomol. Chem.*, **2021**, *19*, 101–122.
- [45] Zhou, D. D.; Gao, Y.; Liu, B. X.; Tan, Q. T.; Xu, B. *Org. Lett.*, **2017**, *19*, 4628–4631.
- [46] (a) Chan, K.; McKiernan, M. J.; Towns, C. R.; Holmes, A. B. *J. Am. Chem. Soc.* **2005**, *127*, 7662–7663; (b) Nakashima, T.; Shimada, M.; Kurihara, Y.; Tsuchiya, M.; Yamanoi, Y.; Nishibori, E.; Sugimoto, K.; Nishihara, H. *J. Organomet. Chem.*, **2016**, *805*, 27–33.
- [47] Sun, J. W.; Baek, J. Y.; Kim, K. H.; Moon, C. K.; Lee, J. H.; Kwon, S. K.; Kim, Y. H.; Kim, J. J. *Chem. Mater.*, **2015**, *27*, 6675–6681.

- [48] (a) Xu, S.; Li, H. H.; Chen, R. F.; Chen, Z. C.; Xu, L. J.; Tang, Y. T.; Huang, W. *Adv. Optical Mater.*, **2018**, *6*, 1701105; (b) Li, H. H.; Wang, Y.; Yuan, K.; Tao, Y.; Chen, R. F.; Zheng, C.; Zhou, X. H.; Li, J. F.; Huang, W. *Chem. Commun.*, **2014**, *50*, 15760–15763.
- [49] (a) Gilman, H.; Gorsich, R. D. *J. Am. Chem. Soc.*, **1955**, *77*, 6380–6381; (b) Corey, J. Y.; Chang, L. S. *J. Organomet. Chem.*, **1986**, *307*, 7–14; (c) Chan, K. L.; McKiernan, M. J.; Towns, C. R.; Holmes, A. B. *J. Am. Chem. Soc.*, **2005**, *127*, 7662–7663.
- [50] (a) Oita, K.; Gilman, H. *J. Am. Chem. Soc.*, **1957**, *79*, 339–342; (b) Gilman, H.; Trepka, W. J. *J. Org. Chem.*, **1962**, *27*, 1418–1422; (c) Belsky, V. K.; Saratov, I. E.; Reikhsfeld, V. O.; Simonenko, A. A. *J. Organomet. Chem.*, **1983**, *258*, 283–289; (d) Corey, J. Y.; Trankler, K. A.; Braddock-Wilking, J.; Rath, N. P. *Organometallics*, **2010**, *29*, 5708–5713; (e) Wittenberg, D.; McNinch, H. A.; Gilman, H. *J. Am. Chem. Soc.*, **1958**, *80*, 5418–5422; (f) McCarthy, W. Z.; Corey, J. Y.; Corey, E. R. *Organometallics*, **1984**, *3*, 255–263; (g) van der Boon, L. J. P.; Hendriks, J. H.; Roolvink, D.; O’Kennedy, S. J.; Lutz, M.; Slootweg, J. C.; Ehlers, A. W.; Lammertsma, K. *Eur. J. Inorg. Chem.*, **2019**, 3318–3328.
- [51] Onoe, M.; Morioka, T.; Tobisu, M.; Chatani, N. *Chem. Lett.*, **2013**, *42*, 238–240.
- [52] (a) Corey, J. Y.; Dueber, M.; Bichlmeir, B. *J. Organomet. Chem.*, **1971**, *26*, 167–173; (b) Barton, T. J.; Volz, W. E.; Johnson, J. L. *J. Org. Chem.*, **1971**, *36*, 3365–3367; (c) Cartledge, F. K.; Mollere, P. D. *J. Organomet. Chem.*, **1971**, *26*, 175–181; (d) Corey, E. R.; Corey, J. Y.; Glick, M. D. *J. Organomet. Chem.*, **1975**, *101*, 177–186; (e) Corey, E. R.; Corey, J. Y.; Glick, M. D. *J. Organomet. Chem.*, **1977**, *129*, 17–25; (f) Lange, L. D.; Corey, J. Y.; Rath, N. P. *Organometallics*, **1991**, *10*, 3189–3196; (g) Corey, J. Y.; Pitts, A. J.; Winter, R. E. K.; Rath, N. P. *J. Organomet. Chem.*, **1995**, *499*, 113–121; (h) Shirani, H.; Janosik, T. *Organometallics*, **2008**, *27*, 3960–3963; (i) Mercier, L. G.; Furukawa, S.; Piers, W. E.; Wakamiya, A.; Yamaguchi, S.; Parvez, M.; Harrington, R. W.; Clegg, W. *Organometallics*, **2011**, *30*, 1719–1729; (j) Matsuda, T.; Sato, S. *J. Org. Chem.*, **2013**, *78*, 3329–3335; (k) Tsuda, T.; Choi, S. M.; Shintani, R. *J. Am. Chem. Soc.*, **2021**, *143*, 1641–1650.
- [53] Corey, J. Y.; Corey, E. R. *Tetrahedron Lett.*, **1972**, 4669–4672.
- [54] Shibata, T.; Uno, N.; Sasaki, T.; Takano, H.; Sato, T.; Kanyiva, K. S. *J. Org. Chem.*, **2018**, *83*, 3426–3432.
- [55] (a) Bähr, S.; Oestreich, M. *Angew. Chem. Int. Ed.*, **2017**, *56*, 52–59; (b) Richter, S. C.; Oestreich, M. *Trends Chem.*, **2020**, *2*, 13–27.
- [56] Rubin, M.; Gevorgyan, V.; Chandrasekhar, S.; Nagendra Babu, B.; Chandrashekar, G.; Shibuya, M. *e-EROS Encyclopaedia of Reagents for Organic Synthesis*, **2019**, *1*, Wiley.
- [57] Laszlo, P.; Teston, M. *J. Am. Chem. Soc.*, **1990**, *112*, 8750–8754.
- [58] Piers, W. E.; Chivers, T. *Chem. Soc. Rev.*, **1997**, *26*, 345–354.
- [59] Weicker, S. A.; Stephan, D. W. *Bull. Chem. Soc. Jpn.*, **2015**, *88*, 1003–1016.
- [60] Larson, J. R.; Melen, R. L. *Inorg. Chem.*, **2017**, *56*, 8627–8643.
- [61] Zhang, H.; Hagihara, S.; Itami, K. *Chem. Eur. J.*, **2015**, *21*, 16796–16800.
- [62] (a) Chen, R. F.; Fan, Q. L.; Liu, S. J.; Zhu, R.; Pu, K. Y.; Huang, W. *Synth. Met.*, **2006**, *156*, 1161–1167; (b) Mouri, K.; Wakamiya, A.; Yamada, H.; Kajiwara, T.; Yamaguchi, S. *Org. Lett.*, **2007**, *9*, 93–96; (c) Sanchez, J. C.; DiPasquale, A. G.; Rheingold, A. L.; Trogler, W. C. *Chem. Mater.*, **2007**, *19*, 6459–6470; (d) Wang, E.; Li, C.; Zhuang, W.; Peng, J.; Cao,

- Y. J. Mater. Chem.*, **2008**, *18*, 797–801; (e) Sanchez, J. C.; Trogler, W. C. *J. Mater. Chem.*, **2008**, *18*, 3143–3156; (f) Mo, Y. Q.; Deng, X. Y.; Jiang, X.; Cui, Q. H. *J. Polym. Sci., Part A: Polym. Chem.*, **2009**, *47*, 3286–3295.
- [63] (a) Beaupre, S.; Boudreault, P. L. T.; Leclerc, M. *Adv. Mater.*, **2010**, *22*, E6–E27; (b) Corey, J. Y. *Adv. Organomet. Chem.*, **2011**, *59*, 1–180; (c) Woo, S. J.; Kim, Y.; Kim, Y. H.; Kwon, S. K.; Kim, J. J. *J. Mater. Chem. C.*, **2019**, *7*, 4191–4198; (d) Liu, X. Y.; Tian, Q. S.; Zhao, D. L.; Ran, Q.; Liao, L. S.; Fan, J. *J. Mater. Chem. C.*, **2018**, *6*, 8144–8151; (e) Matsuo, K.; Yasuda, T. *Chem. Sci.*, **2019**, *10*, 10687–10697.
- [64] (a) Usta, H.; Lu, G.; Facchetti, A.; Marks, T. J. *J. Am. Chem. Soc.*, **2006**, *128*, 9034–9035; (b) Lu, G.; Usta, H.; Risko, C.; Wang, L.; Facchetti, A.; Ratner, M. A.; Marks, T. J. *J. Am. Chem. Soc.*, **2008**, *130*, 7670–7685.
- [65] (a) Hou, J.; Chen, H. Y.; Zhang, S.; Li, G.; Yang, Y. *J. Am. Chem. Soc.*, **2008**, *130*, 16144–16145; (b) Zou, Y.; Gendron, D.; Neagu-Plesu, R.; Leclerc, M. *Macromolecules*, **2009**, *42*, 6361–6365; (c) Li, G. W.; Kang, C.; Gong, X.; Zhang, J. C.; Li, W. W.; Li, C. H.; Dong, H. L.; Hu, W. P.; Bo, Z. *J. Mater. Chem. C*, **2014**, *2*, 5116–5123; (d) Erlik, O.; Unlu, N. A.; Hizalan, G.; Hacıoglu, S. O.; Comez, S.; Yildiz, E. D.; Toppare, L.; Cirpan, A. *Polym. Chem.*, **2015**, *53*, 1541–1547. (e) Wang, E. G.; Wang, L.; Lan, L. F.; Luo, C.; Zhuang, W. L.; Peng, J. B.; Cao, Y. *Appl. Phys. Lett.*, **2008**, *92*, 033307.
- [66] (a) Tobisu, M.; Onoe, M.; Kita, Y.; Chatani, N. *J. Am. Chem. Soc.*, **2009**, *131*, 7506–7507; (b) Liang, Y.; Zhang, S.; Xi, Z. *J. Am. Chem. Soc.*, **2011**, *133*, 9204–9207; (c) Shimizu, M.; Mochida, K.; Hiyama, T. *Angew. Chem. Int. Ed.*, **2008**, *47*, 9760–9764.
- [67] (a) Matsuda, T.; Kadowaki, S.; Goya, T.; Murakami, M. *Org. Lett.*, **2007**, *9*, 133–136; (b) Shimizu, M.; Mochida, K.; Hiyama, T. *Angew. Chem. Int. Ed.*, **2008**, *47*, 9760–9764; (c) Yabusaki, Y.; Ohshima, N.; Kondo, H.; Kusamoto, T.; Yamanoi, Y.; Nishihara, H. *Chem. Eur. J.*, **2010**, *16*, 5581–5585; (d) Breunig, J. M.; Gupta, P.; Das, A.; Tussupbayev, S.; Diefenbach, M.; Bolte, M.; Wagner, M.; Holthausen, M. C.; Lerner, H. W. *Chem. Asian J.*, **2014**, *9*, 3163–3173.
- [68] (a) Xu, L.; Zhang, S.; Li, P. F. *Org. Chem. Front.*, **2015**, *2*, 459–463; (b) Leifert, D.; Studer, A. *Org. Lett.*, **2015**, *17*, 386–389.
- [69] Omann, L.; Oestreich, M. *Organometallics*, **2017**, *36*, 767–776.
- [70] Dong, Y. F.; Takata, Y.; Yoshigoe, Y.; Sekine, K.; Kuninobu, Y. *Chem. Commun.*, **2019**, *55*, 13303–13306.
- [71] Hartwig, J. F.; Kawatsura, M.; Hauck, S. I.; Shaughnessy, K. H.; Alcarzar-Roman, L. *M. J. Org. Chem.*, **1999**, *64*, 5575–5580.
- [72] Hiyama, T.; Oestreich, M. *Organosilicon Chemistry: Novel Approaches and Reactions.*, **2019**, *11*.
- [73] Cahiez, G.; Chaboche, C.; Mahuteau-Betzer, F.; Ahr, M. *Org. Lett.*, **2005**, *7*, 1943–1946.
- [74] Wolfe, J. P.; Buchwald, D. L. *J. Org. Chem.*, **2000**, *65*, 1144–1157.
- [75] Miyaura, N.; Suzuki, A. *Chem. Rev.*, **1995**, *95*, 2457–2483.
- [76] (a) Gevorgyan, V.; Rubin, M.; Benson, S.; Liu, J. X.; Yamamoto, Y. *J. Org. Chem.*, **2000**, *65*, 6179–6186; (b) Fattakhova, D. S.; Jouikov, V. V.; Voronkov, M. G. *J. Organomet. Chem.*, **2000**, *613*, 170–176.

- [77] Lee, S. H.; Jang, B. B.; Kafafi, Z. H. *J. Am. Chem. Soc.*, **2005**, *127*, 9071–9078.
- [78] (a) Furakawa, S.; Kobayashi, J.; Kawashima, T. *Dalton Trans.*, **2010**, *39*, 9329–9336; (b) Li, L.; Xiang, J.; Xu, C. *Org. Lett.*, **2007**, *9*, 4877–4879.
- [79] (a) Shin, H. N.; Kim, C. S.; Cho, Y. J.; Kwon, H. J.; Kim, B. O.; Kim, S. M.; Yoon, S. S. WO 2010114243, *Dow Advanced Display Materials, Ltd*, **2010**; (b) Yang, H. CN 105985367, *EverDisplay Optronics (Shanghai) Limited*, **2016**.
- [80] Reeves, J. T.; Fandrick, D. R.; Tan, Z.; Song, J. J.; Lee, H.; Yee, N. K.; Senanayake, C. H. *Org. Lett.*, **2010**, *12*, 4388–4391.
- [81] Fyfe, J. W. B.; Watson, A. J. B. *Chem*, **2017**, *3*, 31–55.
- [82] Hu, J. F.; Sun, H. Q.; Cai, W. S.; Pu, X. H.; Zhang, Y. M.; Shi, Z. Z. *J. Org. Chem.*, **2016**, *81*, 14–24.
- [83] Yi, Y. Q. Q.; Y, W. C.; Zhai, D. D.; Zhang, X. Y.; Li, S. Q.; Guan, B. T. *Chem, Commun.*, **2016**, *52*, 10894–10897.
- [84] Reiff, A. L.; Garcia-Frutos, E. M.; Gil, J. M.; Anderson, O. P.; Hegedus, L. S. *Inorg. Chem.*, **2005**, *44*, 9162–9174.
- [85] (a) Yang, X.; Wang, C. *Angew. Chem. Int. Ed.*, **2018**, *57*, 923–928; (b) Corey, J. C.; John, C. S.; Ohmsted, M. C.; Chang, L. S. *J. Organomet. Chem.*, **1986**, *304*, 93–105; (c) Kanno, K.; Hirose, S.; Kyushin, S. *Heteroatom Chem.*, **2018**, *29*: e21478.
- [86] Hisaki, I.; Nakagawa, S.; Tohnai, N.; Miyata, M. *Angew. Chem. Int. Ed.*, **2015**, *54*, 3008–3012.
- [87] Krasovskiy, A.; Knochel, P. *Angew. Chem. Int. Ed.*, **2004**, *43*, 3333–3336.
- [88] Zheng, H. X.; Shan, X. H.; Qu, J. P.; Kang, Y. B. *Org. Lett.*, **2017**, *19*, 5114–5117.
- [89] Bartoli, S.; Cipollone, A.; Squarcia, A.; Madami, A.; Fattori, D. *synthesis*, **2009**, *8*, 1305–1308.
- [90] Shen, H.; Zhang, X.; Liu, Q.; Pan, J.; Hu, W.; Xiong, Y.; Zhu, X. *Tetrahedron Lett.*, **2015**, *56*, 5628–5631.
- [91] Pastierik, T.; Šebej, P.; Medalová, J.; Štacko, P.; Klán, P. *J. Org. Chem.*, **2014**, *79*, 3374–3382.
- [92] Yang, S.; Tang, W.; Yang, Z.; Xu, J. *ACS Catal.*, **2018**, *8*, 9320–9326.
- [93] Roy, P. P.; D'Souza, K.; Cuperlovic-Culf, M.; Kienesberger, P. C.; Touaibia, M. *Eur. J. Med. Chem.*, **2016**, *118*, 290–298.
- [94] (a) Li, J.; Ding, D. X.; Wei, Y.; Zhang, J.; Xu, H. *Adv. Opt. Mater.*, **2016**, *4*, 522–528; (b) Liu, X. Y.; Tang, X.; Zhao, Y.; Zhao, D. L.; Fan, J.; Liao, L. S. *J. Mater. Chem. C*, **2018**, *6*, 1023–1030.
- [95] (a) Kranenburg, M.; van der Burgt, Y. E. M.; Kamer, P. C. J.; van Leeuwen, P. W. N. M.; Goubitz, K.; Fraanje, J. *Organometallics*, **1995**, *14*, 3081–3089; (b) van der Veen, L. A.; Keeven, P. H.; Schoemaker, G. C.; Reek, J. N. H.; Kamer, P. C. J.; van Leeuwen, P. W. N. M.; Lutz, M.; Spek, A. L. *Organometallics*, **2000**, *19*, 872–883; (c) Bronger, R. P. J.; Kamer, P. C. J.; van Leeuwen, P. W. N. M. *Organometallics*, **2003**, *22*, 5358–5369; (d) Clayden, J.; Fletcher, S. P.; Senior, J.; Worrall, C. P. *Tetrahedron: Asymmetry*, **2010**, *21*, 1355–1360; (e) Rajesh, K.; Dudle, B.; Blacque, O.; Berke, H. *Adv. Synth. Catal.*, **2011**, *353*, 1479–1484.

- [96] (a) Corey, J. Y.; Corey, E. R.; Chang, V. H. T.; Hauser, M. A.; Leiber, M. A.; Reinsel, T. E.; Riva, M. E. *Organometallics*, **1984**, *3*, 1051–1060; (b) Nakadaira, Y.; Sato, R.; Sakurai, H. *Organometallics*, **1991**, *10*, 435–442; (c) Betson, M. S.; Clayden, J.; Worrall, C. P.; Peace, S. *Angew. Chem. Int. Ed.*, **2006**, *45*, 5803–5807; (d) Braddock-Wilking, J.; Corey, J. Y.; French, L. M.; Choi, E.; Speedie, V. J.; Rutherford, M. F.; Yao, S.; Xu, H.; Rath, N. P. *Organometallics*, **2006**, *25*, 3974–3988.
- [97] Sato, Y.; Takagi, C.; Shintani, R.; Nozaki, K. *Angew. Chem. Int. Ed.*, **2017**, *56*, 9211–9216.
- [98] Fischer, C.; Sparr, C. *Angew. Chem. Int. Ed.*, **2018**, *57*, 2436–2440.
- [99] Fang, H. Q.; Oestreich, M. *Chem. Sci.*, **2020**, *11*, 12604–12615.
- [100] Takuya, U. **2019**, US 20190363263, A1.
- [101] Shimizu, N.; Watanabe, S.; Hayakawa, F.; Yasuhara, S.; Tsuno, Y.; Inazu, T. *Bull. Chem. Soc. Jpn.*, **1994**, *67*, 500–504.
- [102] Bin, X.; Mao-Lin, Li.; Xiao-Dong, Z.; Shou-Fei, Z.; Qi-Lin, Z. *J. Am. Chem. Soc.*, **2015**, *137*, 8700–8703.
- [103] Wu, X. M.; Hu W. Y. *Chin. Chem. Lett.*, **2012**, *23*, 391–394.
- [104] (a) Maier, G.; Mihm, G.; Reisenauer, H. P. *Angew. Chem. Int. Ed. Engl.*, **1980**, *19*, 52–53; (b) Yamaguchi, S.; Endo, T.; Uchida, M.; Izumizawa, T.; Furukawa, K.; Tamao, K. *Chem.–Eur. J.*, **2000**, *6*, 1683–1692; (c) Boydston, A. J.; Yin, Y.; Pagenkopf, B. L. *J. Am. Chem. Soc.*, **2004**, *126*, 3724–3725; (d) Zhan, X.; Risko, C.; Amy, F.; Chan, C.; Zhao, W.; Barlow, S.; Kahn, A.; Bredas, J. L.; Marder, S. R. *J. Am. Chem. Soc.*, **2005**, *127*, 9021–9029; (e) Zhao, Z. J.; He, B. R.; Tang, B. Z. *Chem. Sci.*, **2015**, *6*, 5347–5365; (f) Dong, Y. F.; Sakai, M.; Fuji, K.; Sekine, K.; Kuninobu, Y. *Beilstein J. Org. Chem.*, **2020**, *16*, 409–414; (g) Snantra, S. *ChemistrySelect*, **2020**, *5*, 9034–9058.
- [105] (a) Barton, T. J.; Kippenha, R. C.; Nelson, A. J. *J. Am. Chem. Soc.*, **1974**, *96*, 2272–2273; (b) Sakamoto, H.; Ishikawa, M. *J. Organomet. Chem.*, **1991**, *418*, 305–309; (c) Nishinaga, T.; Izukawa, Y.; Komatsu, K. *J. Phys. Org. Chem.*, **1998**, *11*, 475–477; (d) Kira, M.; Ishida, S.; Iwamoto, T.; Kabuto, C. *J. Am. Chem. Soc.*, **2002**, *124*, 3830–3831.
- [106] (a) Shiratori, S.; Yasuike, S.; Kurita, J.; Tsuchiya, T. *Chem. Pharm. Bull.*, **1994**, *42*, 2441–2448; (b) Ding, B.; Teng, Z.; Keese, R. *J. Org. Chem.*, **2002**, *67*, 8906–8910; (c) Takamoto, K.; Yoshioka, S.; Fujioka, H.; Arisawa, M. *Org. Lett.*, **2018**, *20*, 1773–1776; (d) Leigh, W. J.; Li, X. *J. Am. Chem. Soc.*, **2003**, *125*, 8096–8097.
- [107] Oestreich, M.; Hermeke, J.; Mohr, J. *Chem. Soc. Rev.*, **2015**, *44*, 2202–2220.
- [108] (a) Hiroto, S. *Bull. Chem. Soc. Jpn.*, **2018**, *91*, 829–838; (b) Chaolumen, Murata, M.; Sugano, Y.; Wakamiya, A.; Murata, Y. *Angew. Chem. Int. Ed.*, **2015**, *54*, 9308–9312; (c) Luo, J. Y.; Xu, X. M.; Mao, R. X.; Mao, Q. *J. Am. Chem. Soc.*, **2012**, *134*, 13796–13803.
- [109] Zhu, C. D.; Wang, D.; Wang, D. Y.; Zhao, Y.; Sun, W. Y.; Shi, Z. *Angew. Chem. Int. Ed.*, **2018**, *57*, 8848–8853.
- [110] Baumgärtner, K.; Meza Chinchá, A. L.; Dreuw, A.; Rominger, F.; Mastalerz, M. *Angew. Chem. Int. Ed.*, **2016**, *55*, 15594–15598.
- [111] Wadumethrige, S. H.; Rathore, R. *Org. Lett.*, **2008**, *10*, 5139–5142.
- [112] Hertz, V. M.; Bolte, M.; Lerner, H. W.; Wagner, M. *Angew. Chem. Int. Ed.*, **2015**, *54*, 8800–8804.

- [113] King, B. T.; Kroulik, J.; Robertson, C. R.; Rempala, P.; Hilton, C. L.; Korinek, J. D.; Gortari, L. M. *J. Org. Chem.*, **2007**, *72*, 2279–2288.
- [114] Wei, B. S.; Zhang, D. C.; Chen, Y. H.; Lei, A. W.; Knochel, P. *Angew. Chem. Int. Ed.*, **2019**, *58*, 15631–15635.
- [115] SIR2008: Burla, M. C.; Caliandro, R.; Camalli, M.; Carrozzini, B.; Cascarano, G. L.; De Caro, L.; Giacovazzo, C.; Polidori, G.; Siliqi, D.; Spagna, R. *J. Appl. Crystallogr.*, **2007**, *40*, 609–613.
- [116] DIRDIF99: Beurskens, P. T.; Admiraal, G.; Beurskens, G.; Bosman, W. P.; de Gelder, R.; Israel, R.; Smits, J. M. M. The DIRDIF-99 program system; Technical Report of the Crystallography Laboratory; University of Nijmegen, Nijmegen, The Netherlands, **1999**.
- [117] Cromer, D. T.; Waber, J. T. International Tables for X-ray Crystallography; Kynoch Press: Birmingham, U.K., **1974**, Vol. 4.
- [118] Olex2 program package: Dolomanov, O. V.; Bourhis, L. J.; Gildea, R. J.; Howard, J. A. K.; Puschmann, H. *J. Appl. Cryst.*, **2009**, *42*, 339–341.
- [119] SHELX97: Sheldrick, G. M. *Acta Cryst.*, **2008**, A64, 112.

Publication List

Parts of the present thesis have been published in the following journals

- Chapter 2.** Dong, Y. F.; Takata, Y.; Yoshigoe, Y.; Sekine, K.; Kuninobu, Y.
Lewis Acid-Catalyzed Synthesis of Silafluorene Derivatives from Biphenyls
and Dihydrosilanes via a Double Sila-Friedel–Crafts Reaction
Chem. Commun. **2019**, 55, 13303–13306.
- Chapter 3.** Dong, Y. F.; Sakai, M.; Fuji, K.; Sekine, K.; Kuninobu, Y.
Synthesis of Six-membered Silacycles by Borane-Catalyzed Double Sila-
Friedel–Crafts Reaction
Beilstein J. Org. Chem. **2020**, 16, 409–414.
- Chapter 4.** Dong, Y. F.; Sekine, K.; Kuninobu, Y.
Facile Synthesis of Tribenzosilepins from Terphenyls and Dihydrosilanes by
Electrophilic Double Silylation
Chem. Commun. **2021**, 57, 7007–7010.

Acknowledgments

This thesis would have been absolutely impossible to achieve without the help and support of many people. Here, I would like to express my sincere thanks to every one of them.

First of all, I would like to thank my advisor Professor Yoichiro Kuninobu for giving me the opportunity to study in his group. For three years, he gave me tremendous support, encouragement and patience. Thank you very much!

I am especially thankful to Assistant Professor Dr. Kohei Sekine, for passing on to me a great deal of his knowledge and experience. All his assistance developing me gradually into a professional chemist, helping me towards my next step after graduated school. Each advice and every discussion are very helpful and is deeply appreciated.

I want to thank Mr. Yuta Takata and Dr. Yusuke Yoshigoe for leaving me with the preliminary results on my first project. I also want to thank Mr. Masahiko Sakai, Mr. Kazuto Fuji for helping me on my second project. Thanks to Toshiaki Mori for helping me on the third project. Thanks to all of my colleagues! Thanks to staffs, Ms. Misa Kojima and Mr. Hiroshi Toshima.

I would like to show my sincerest appreciation to Professor Hiroyuki Furuta and Professor Katsuhiko Tomooka for their kind and patient guidance on this thesis.

Besides, I am indebted to the China Scholarship Council (CSC), Japan Society of the Promotion of Science (JSPS).

At last, I want to thank my mom, my sister, my brother, and my friends for being with me and being there for me.